NOTE TO USERS

This reproduction is the best copy available.

UMI®

Reproduced with permission of the copyright owner. Further reproduction prohibited without permission.

DISSERTATION

OSTEOCHONDRAL PROPERTIES AND RELATIONSHIPS IN THE SYNOVIAL JOINT

Submitted by

Chad W. Lewis

Department of Mechanical Engineering

In partial fulfillment of the requirements

For the Degree of Doctor of Philosophy

Colorado State University

Fort Collins, Colorado

Spring 2004

Reproduced with permission of the copyright owner. Further reproduction prohibited without permission.

UMI Number: 3131682

INFORMATION TO USERS

The quality of this reproduction is dependent upon the quality of the copy submitted. Broken or indistinct print, colored or poor quality illustrations and photographs, print bleed-through, substandard margins, and improper alignment can adversely affect reproduction.

In the unlikely event that the author did not send a complete manuscript and there are missing pages, these will be noted. Also, if unauthorized copyright material had to be removed, a note will indicate the deletion.

UMI®

UMI Microform 3131682

Copyright 2004 by ProQuest Information and Learning Company.

All rights reserved. This microform edition is protected against unauthorized copying under Title 17, United States Code.

ProQuest Information and Learning Company
300 North Zeeb Road
P.O. Box 1346
Ann Arbor, MI 48106-1346

Reproduced with permission of the copyright owner. Further reproduction prohibited without permission.

Copyright by Chad W. Lewis 2004

All Rights Reserved

Reproduced with permission of the copyright owner. Further reproduction prohibited without permission.

COLORADO STATE UNIVERSITY

December 10, 2003

WE HEREBY RECOMMEND THAT THE DISSERTATION PREPARED UNDER OUR SUPERVISION BY CHAD W. LEWIS ENTITLED "OSTEOCHONDRAL PROPERTIES AND RELALTIONSHIPS IN THE SYNOVIAL JOINT" BE ACCEPTED AS FULFILLING IN PART REQUIREMENTS FOR THE DEGREE OF DOCTOR OF PHILOSOPHY IN MECHANICAL ENGINEERING.

Committee on Graduate Work

Robert L. Sah

Chris E. Kawcak

Ffed W. Smith

Donna L. Wheeler **Co-Adviser**

Susan P. James **Co-Adviser**

Alan Kirkpatrick **Department Head/Director**

Reproduced with permission of the copyright owner. Further reproduction prohibited without permission.

ABSTRACT OF DISSERTATION

OSTEOCHONDRAL PROPERTIES AND RELATIONSHIPS
IN THE SYNOVIAL JOINT

The overall goal of this study was to examine the relationship between the properties of articular cartilage and its underlying subchondral bone using an equine model. Thus, the objectives of this study were: (1) to determine the structural and mechanical properties of equine cartilage, (2) to determine the bone mineral density of the underlying subchondral bone, (3) to determine the relationship between these cartilage and bone properties in different joint regions, (4) to develop methodology for subchondral bone plate thickness measurement, (5) to develop experimental protocols and novel equipment for loading opposing osteochondral surfaces and to quantify intra-tissue cartilage strains within the loaded samples, and (6) to determine any regional relationships between the cartilage strains and underlying subchondral bone plate thickness and bone mineral density.

This study presents the first comparative body of data on equine structural/material articular cartilage properties and underlying subchondral bone density for the palmar and dorsal aspects of the medial condyle of the 3rd metacarpal bone, medial trochlear ridge, and the medial femoral condyle. A positive correlation between cartilage tensile equilibrium modulus and underlying bone mineral density was discovered.

The measurement of subchondral bone plate thickness is important to the study of osteoarthritis and joint adaptation. A subchondral bone plate thickness measurement

Reproduced with permission of the copyright owner. Further reproduction prohibited without permission.

technique using high-resolution contact radiographs and image processing was developed with minimal systematic error and high repeatability.

The ability to quantify intra-tissue cartilage strains in loaded physiologically opposing surfaces and underlying subchondral bone characteristics should help elucidate the etiology and progression of osteoarthritis. A custom-designed loading system and associated sample preparation procedure were developed and validated to quantify two-dimensional strain fields using video image correlation analysis between two opposing articular cartilage surfaces from the equine metacarpophalangeal joint. The error involved in this process, including the image acquisition system, data analysis, and induced friction, was on the order of 7600 μstrain (0.76%). The present study demonstrated that superficial cartilage strains were larger than deeper cartilage strains, subchondral bone plate thickness and volumetric bone mineral density across the joint regions were positively correlated, and cartilage strain did not correlate with subchondral bone plate thickness or volumetric bone mineral density in the normal equine metacarpophalangeal joint.

Although there are some limitations, testing opposing osteochondral surfaces in compression has tremendous benefits: (1) strain distributions across articular surfaces with complex geometry can be obtained, (2) provides the capability to relate depth-dependent articular cartilage strains with underlying subchondral bone properties or pathology changes, and (3) emulates physiological boundary conditions better than platen loading experiments. The benefits of the current method could be applied to a variety of applications where opposing articular surface loading would be important, such as,

Reproduced with permission of the copyright owner. Further reproduction prohibited without permission.

determining osteochondral implant discontinuities with surrounding host tissue, determining the effects of cartilage and/or bone defects on overlying cartilage strain distributions, and determining the effects of impact loading on strain distributions between articular cartilage strains.

Chad W. Lewis
Mechanical Engineering Department
Colorado State University
Fort Collins, CO 80523
Spring 2004

Reproduced with permission of the copyright owner. Further reproduction prohibited without permission.

ACKNOWLEDGEMENTS

First and foremost, I would like to thank my advisors Dr. Susan James and Dr. Donna Wheeler for their timely advising, support, encouragement, knowledge, and friendship over the years. Without you, this dissertation wouldn't have been possible. I would also like to thank my other thesis committee members, Dr. Chris Kawcak, Dr. Robert Sah, and Dr. Fred Smith. Thanks, Dr. Kawcak, for your invaluable clinical perspective, sharing your subchondral bone knowledge, and your openness to collaborate. Dr. Sah, I sincerely value your inquisitive and genuine advising, wisdom, encouragement, excitement for research and education, and importantly our friendship. Dr. Smith, thank you for your invaluable mechanics knowledge and dedication to the learning process. I would also like to express my gratitude to all my committee members for taking active roles in my learning experience.

Wayne McIlwraith, thank you for your suggestions and generous support over the years. David Frisbie, thank you for your great suggestions and supplying the fresh samples needed for this study. Phil Chapman, thank you for your statistics consultation. Scott Tucker, thanks for your friendship, tremendous assistance over the years, and mechanics insight.

A BIG thanks goes out to Diane Brenak, Liza Eschbach, Katie Ossa, Mae Lee Mable, Tatiana Motta, Brandon Santoni, Amy Lyons, Joel Millets, Steve, Ely Walker, Jen Harmel, Jon, and Joel Helgerson of the Orthopaedic Bioengineering Research Laboratory for all their assistance, support, and friendship.

Reproduced with permission of the copyright owner. Further reproduction prohibited without permission.

Thanks to Heather Colhoun, Mike Karr, Katie Ruggle, Troy Trumble, Sophie Morriset, Megan Knowlton, Erin Duffy, Chelsea Zimmerman, and all the wonderful volunteers of the Orthopaedic Research Laboratory for their tremendous support, assistance, friendship, and their excitement for equine orthopaedics.

To Won Bae, Amanda Williamson, Albert Chen, Michele Temple, Van Wong, Gayle Nugent, Barbara Schumacher, and Tannin Schmidt of the Cartilage Tissue Engineering Laboratory at the University of California – San Diego, thank you for all your assistance, knowledge, advising, friendship, enthusiasm for the pursuit of knowledge, and importantly thanks for the assistance testing cartilage structural and mechanical properties.

Special thanks to David Braley for his ability to teach his invaluable machining, critical, and creative thinking skills. To Dr. Schaffer for making the fabrication processes an instructional and pleasant experience.

A special thanks goes to Simon Turner for introducing me to orthopaedic research. Also, a well deserved thanks goes to, Guy Beauregard, Andy Green, and Carolyn Skurla graduates of the Rocky Mountain Materials Research Laboratory for their early guidance and being great role models.

To Justin Mauck, Rozann Laflin, Markus Anderle, Chris Bilger, Bert Irtenkauf, and John Kisiday, thank you for all the support, friendship, and endless laughs. Of course, an appreciation must go out to caffeine, The Simpsons, and Seinfeld.

Reproduced with permission of the copyright owner. Further reproduction prohibited without permission.

To my family, I sincerely appreciate your unconditional love, support, and understanding. To my brother, Ryan, and sister-in-law, Katie, thanks for all your invaluable motivation and loving support. I want to earnestly thank my mother and father for their absolute love, understanding, emotional support, encouragement, strength, and for putting up with me for the past five years.

To Zoe, my best friend, life partner, and soul mate, words will never come close to describing how I appreciate the loving support, encouragement, empathy, editorial skills, and impetus to grow.

The study was funded with the assistance from the U.S. Department of Education - Graduate Assistance in Areas of National Need, Orthopaedic Bioengineering Research Laboratory Foundation, Cartilage Tissue Engineering Laboratory Foundation, Equine Orthopaedic Research Laboratory Foundation, and the National Science Foundation; their financial assistance is greatly appreciated.

Reproduced with permission of the copyright owner. Further reproduction prohibited without permission.

To Zoe Lewis

&

Don Lewis and Cindy Lewis

Reproduced with permission of the copyright owner. Further reproduction prohibited without permission.

TABLE OF CONTENTS

Reproduced with permission of the copyright owner. Further reproduction prohibited without permission.

Reproduced with permission of the copyright owner. Further reproduction prohibited without permission.

Reproduced with permission of the copyright owner. Further reproduction prohibited without permission.

Reproduced with permission of the copyright owner. Further reproduction prohibited without permission.

Reproduced with permission of the copyright owner. Further reproduction prohibited without permission.

LIST OF TABLES

Reproduced with permission of the copyright owner. Further reproduction prohibited without permission.

LIST OF FIGURES

Reproduced with permission of the copyright owner. Further reproduction prohibited without permission.

Reproduced with permission of the copyright owner. Further reproduction prohibited without permission.

Reproduced with permission of the copyright owner. Further reproduction prohibited without permission.

Reproduced with permission of the copyright owner. Further reproduction prohibited without permission.

Reproduced with permission of the copyright owner. Further reproduction prohibited without permission.

1 GENERAL INTRODUCTION

1.1 Purpose of study

The overall purpose of this dissertation was to examine the relationship between the properties of articular cartilage and its underlying subchondral bone using an equine model. Thus, the objectives of this dissertation were many-fold: (1) to determine the structural and mechanical properties of equine cartilage, (2) to determine the bone mineral density of the underlying subchondral bone, (3) to determine the relationship between these cartilage and bone properties of different joint regions, (4) to develop a method for measuring the thickness of the subchondral bone plate, (5) to develop experimental protocols and novel equipment for loading opposing osteochondral surfaces and quantify the intra-tissue cartilage strains within the loaded samples, and (6) to determine any regional relationships between the cartilage strains and underlying subchondral bone plate thicknesses and bone mineral densities.

1.2 Hypotheses

The purpose and objectives were developed to test the following hypotheses:

H1. Third metacarpal osteochondral structural and material properties will differ

Reproduced with permission of the copyright owner. Further reproduction prohibited without permission.

from those of the stifle (Chapter 2).

H2. Osteochondral structural and material properties will differ within the third metacarpal and stifle (Chapter 2).

H3. Volumetric subarticular bone mineral density will be correlated to overlying articular cartilage structural/material properties (Chapter 2)

H4. The superficial articular cartilage strains will be larger than strains in deeper layers (Chapter 5).

H5. Subchondral bone plate thickness and volumetric bone mineral density will be positively related (Chapter 5).

H6. Articular cartilage strains will be greater over areas of greater subchondral bone thickness and volumetric bone mineral density (Chapter 5).

1.3 Introduction

Subchondral bone has been shown to adapt by becoming thicker and denser in order to absorb larger loads within the joint as a result of repetitive synovial joint loading. The subchondral bone adaptation process may in turn produce greater degeneration within the articular cartilage; therefore, the articular cartilage overlying thick and/or dense subchondral bone may possibly show larger strains, perhaps indicative of degeneration. Presently, the relationship of subchondral bone thickness and density to overlying articular cartilage strain distributions is unknown. The current introduction provides a brief synopsis of representative past studies of articular cartilage, bone, and their involvement in osteoarthritis.

Reproduced with permission of the copyright owner. Further reproduction prohibited without permission.

1.4 Synovial articulation

1.4.1 Gross anatomy

Synovial joint (or diarthrosis) function depends on these main structures: articular cartilage, subchondral bone, cortical bone, cancellous bone, ligaments, fibrous membranes, and the synovial membrane, which maintains synovial fluid between the articular surfaces (Figure 1.1). There are several types of synovial joints: ginglymus, condyloid reciprocal reception, enarthrosis, and artrodia, to name a few [1]. The ginglymus or hinge joint, for example has limited motion in one plane, commonly the sagittal plane (flexion/extension) due to the geometry of the articular surfaces [1]. The primary function of the synovial joint is to provide smooth, nearly frictionless movement during motion.

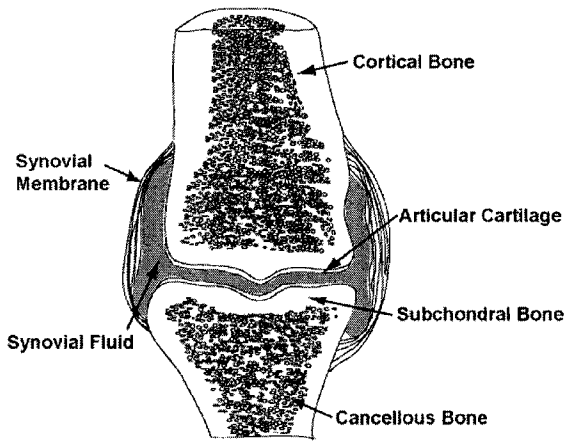

Figure 1.1: Main structures of the synovial joint: synovial membrane, fibrous capsule, ligaments, synovial fluid, articular cartilage, subchondral bone, cortical bone, and cancellous bone. Modified from [2] pg 460.

1.4.2 Cartilage

Cartilage is a connective tissue, which provides protection and support for surrounding structures. There are three types of cartilage: hyaline (articular), fibrocartilage (white), and elastic (yellow). Each cartilage type differs in their proportions

Reproduced with permission of the copyright owner. Further reproduction prohibited without permission.

of extracellular matrix, cell distribution, structure, anatomical location, and function. For example, articular cartilage is primarily composed of cartilage cells (chondrocytes), extracellular matrix (primarily proteoglycan and collagen), and interstitial fluid, which all vary in density with depth. Articular cartilage is predominantly in synovial joints providing load distribution over the articulating bone surfaces of the joint, while providing low friction and wear rate [3]. The functional absence of vascular, nerve, or lymphatic systems in articular cartilage is thought to be due the large cartilage deformations that would make such systems useless [3]. It is well known structural and mechanical properties of cartilage vary during development [4, 5]; therefore, it must be stated that the focus of this dissertation is "adult articular cartilage", and which will be considered synonymous with "cartilage" or "articular cartilage" for the remainder of this dissertation.

1.4.2.1 Cartilage components

1.4.2.1.1 Chondrocytes

Making up <10% of cartilage total volume, chondrocytes, or cartilage cells (10-20μm diameter) provide a balance between the breakdown (catabolism) and production (anabolism) of extracellular matrix macromolecules [3, 6, 7]. Chondrocytes respond to environmental stimuli (e.g. mechanical, chemical, and electrical) by creating and/or breaking down extracellular matrix around them [8-12] to maintain tissue homeostasis. Articular cartilage is avascular which means chondrocytes must receive their nutrients through synovial fluid diffusion facilitated by joint loading [6]. Due to the avascular nature and rare replication of chondrocytes, chondrocyte loss is traumatic to the health of the cartilage [6].

Reproduced with permission of the copyright owner. Further reproduction prohibited without permission.

1.4.2.1.2 Proteoglycans

Fifteen to thirty percent of cartilage wet weight is due to proteoglycans [6]. Proteoglycans have a protein core with one or more polyanionic glycoaminoglycans (GAG) chains (usually chondroitin sulphate or keratin sulphate) covalently attached (Figure 1.2, [3]). Each type of proteoglycan possesses a unique structure and function. One common articular cartilage proteoglycan, aggrecan, comprises the bulk of cartilage proteoglycans having up to 150 GAG chains attached to its core protein [3]. The hydrated aggrecan macromolecules form aggregates which are trapped within an extracellular meshwork of collagen providing articular cartilage with unique biomechanical compressive and chemical properties [10, 13-25]. The polyanionic (high negative charge density) proteoglycans' main function in the extracellular matrix is to provide cartilage with the capability to resist compression – a phenomenon called the Gibbs-Donnan equilibrium induced osmotic pressure [26]. GAG chains have high affinity for water and other ions in the interstitial and synovial fluid producing swelling pressures against the surrounding collagen meshwork. At equilibrium, these pressures increase until the pressure between the surrounding collagen meshwork, proteoglycan colloid, and externally applied compression are equal and opposite [6]. When cartilage is loaded, the sum of the external pressures and collagen forces is temporarily greater than the swelling pressure; thus, causing water to exude from the cartilage. As the water leaves the tissue, the repulsion forces of the polyanionic proteoglycan side chains increase causing subsequent increase in the swelling pressure as water reabsorbs, preventing further cartilage deformation; therefore, the interaction between water and proteoglycans helps resist physiologic loading. Until equilibrium is reached, the cyclic flow of water in and

Reproduced with permission of the copyright owner. Further reproduction prohibited without permission.

out of the cartilage continues. Proteoglycan density or charge density is a function of depth. Studies have found proteoglycan content contributes to cartilage compression properties [19, 22, 27].

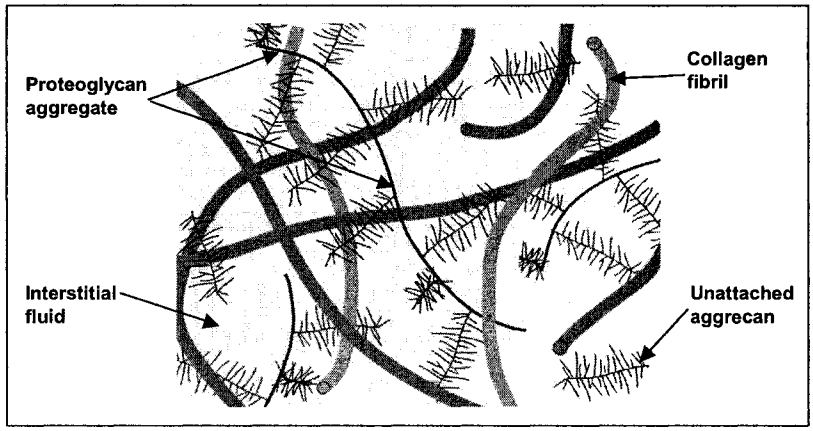

Figure 1.2: Collagen and proteoglycan interaction. [28]

1.4.2.1.3 Collagen

Ten to twenty percent of cartilage wet weight is composed of collagen consisting of three identical alpha-chain peptides wound together to make a right-handed helix [6]. To date, many collagen types have been discovered in cartilage (types II, VI, IX, X, and XI) [29]. Collagen type II is the most common consisting of 90-95% of the collagen present in cartilage. The collagen in the extracellular matrix provides a three-dimensional structural framework entrapping proteoglycans, and maintaining volume, shape, and structural integrity. Past studies have demonstrated that collagen is responsible for the tensile and shear properties of cartilage [18, 30-36].

1.4.2.1.4 Interstitial fluid

Water molecules make up over 65-80% of the wet weight of cartilage and are attracted to the entrapped proteoglycans contributing to cartilage's resilience to compression [37]. Water content (i.e. porosity) is depth-dependent, decreasing from 85%

Reproduced with permission of the copyright owner. Further reproduction prohibited without permission.

at the surface to 60% in the deep layer [37]. Sodium, calcium, chloride, potassium, and other inorganic salts are also present in the interstitial fluid [6].

1.4.2.2 Cartilage organization

The structure/composition of cartilage has been found to vary by species, age, gender, location, and depth from the articular surface [38-40]. These variations in structure and composition contribute to depth-dependent mechanical properties [41-43]. Articular cartilage can be divided into four layers (zones): superficial, middle, deep, and calcified (Figure 1.3). Each layer has unique structure/properties and provides cartilage with its dynamic functional qualities.

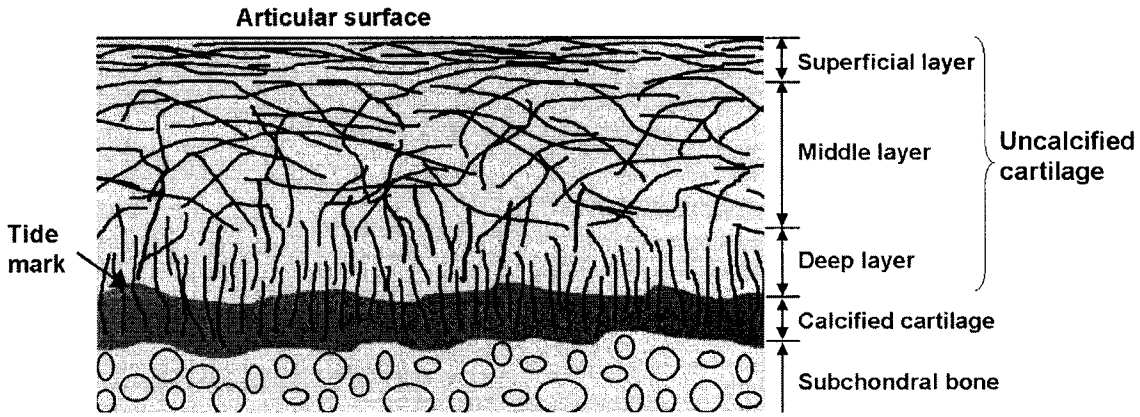

Figure 1.3: Illustration of articular cartilage layers, calcified cartilage, tidemark, and subchondral bone. The depth-dependent collagen orientation is diagramed. Modified from [28]

1.4.2.2.1 Superficial layer

The superficial layer is the thinnest of the layers and contains collagen fibrils aligned parallel to the articular surface. The proteoglycan density is the lowest in this layer, while water concentration has been found to be the highest (Figure 1.3)[6, 37]. Chondrocytes tend to have a flattened ellipsoid shape with major axes parallel with the articular surface [6, 37]. The structural organization of the superficial layer provides

Reproduced with permission of the copyright owner. Further reproduction prohibited without permission.

strength and stiffness to resist applied tensile and shear strains to the articular surface during physiological loading [6, 37]. In addition, the superficial layer acts somewhat like a membrane with low permeability by restricting fluid flow from the tissue, and causing increased interstitial pressure to assist in cartilage compression behavior [44]. The low permeability of this layer limits large macromolecules (e.g. aggrecan) from exiting and other large proteins (e.g. antibodies) from entering the cartilage from the synovial fluid [37].

1.4.2.2.2 Middle layer

The middle layer contains approximately two times the volume of the superficial layer [39]. Chondrocytes in this region are spherical and have a higher density of catabolic organelles than the superficial layer chondrocytes [37, 39]. The middle layer consists of a transition of collagen orientation from parallel to minimal organization relative to the articular surface (Figure 1.3, [45]). The larger diameter of the collagen, along with higher concentrations of proteoglycans, and lower water and collagen concentrations, help differentiate the superficial and middle layer from each other [37, 39].

1.4.2.2.3 Deep layer

Chondrocytes in the deep layer are spheroidal and are often found oriented in columns from the deeper calcified layer [37, 39]. The deep layer collagen fibrils are the largest of all the layers, and are perpendicularly aligned with the articular surface passing through the tidemark into the calcified layer (Figure 1.3). This zone also has the highest concentration of proteoglycans and the lowest concentration of water [37].

Reproduced with permission of the copyright owner. Further reproduction prohibited without permission.

1.4.2.2.4 Calcified layer

Calcified cartilage is a layer of chondrocytes with minimal metabolic activity separated by ossified extracellular matrix (radio-dense), which provides an attachment site for cartilage to bone and intermediate stiffness gradient between the flexible upper cartilage layers and the rigid supportive subchondral bone (Figure 1.3, [46-50]). The tidemark is a basophilic landmark with possible significance in separating uncalcified and calcified cartilage thus creating a mineralization boundary of chondrocytes [6, 39]. Using scanning electron microscopy, Redler et al. found three distinct layers of collagen in the tidemark with transitioning orientations from perpendicular to parallel relative to the articular surface, suggesting that the tidemark acts as a "tether" between the deformable uncalcified and rigid calcified layers [51].

1.4.2.3 Cartilage mechanics

Numerous constitutive relationships have been postulated for articular cartilage relating stress and strain using material properties. A validated model is one that can predict behaviors under various loading conditions using the same material properties. Cartilage models have been proposed using linear elasticity [52-54], viscoelasticity [22, 36, 55-60], porous media [16, 17, 61-66], and physical chemistry principles [10, 13, 67-70]. Using constitutive models, finite element analyses have been used to investigate simple joint contact and possible stress conditions within cartilage at different states of disease [71-80]. Experimental material testing methods such as indentation [38, 63, 81-94], uniaxial tensile testing [5, 18, 30-35, 95-104], confined compression using a porous platen [4, 14, 23, 42, 44, 105-117], unconfined compression with a solid platen [61, 106, 110, 118-125], torsional testing [58, 126], and swelling experiments [14, 18, 26, 34, 127]

Reproduced with permission of the copyright owner. Further reproduction prohibited without permission.

on cartilage samples have been performed to determine the material properties for constitutive models. Cartilage experimental testing methods are also commonly used to determine effects of strain dependent permeability [17, 128], species [38, 85], age[4, 5, 52, 97, 102], joint[38, 83, 86, 90, 117, 129, 130], diet [92], gender[30, 83, 86, 95, 96, 98], loading [10, 88, 131-133], disease state [38, 134-136], biochemical content [4, 5, 19, 30, 34, 81, 99, 137], and structural organization [26, 59, 100, 138, 139] on material properties. From previous and ongoing investigational testing, cartilage is known to have a very intricate composition and structure giving it complex properties such as anisotropy and inhomogeneity. For additional information, Mow and Ratcliffe provide a good overview of cartilage mechanical properties and theory [3].

1.4.2.3.1 Anisotropy

Cartilage anisotropy is primarily seen using uniaxial tensile testing [30, 32, 33, 97]. The tensile equilibrium modulus of cartilage is greater when tested parallel with the splitline pattern (i.e. superficial collagen alignment) compared to perpendicularly. Recently, Wang et. al. investigated anisotropy material properties in compression for bovine cartilage, finding linear orthotropic elasticity to be insufficient for describing cartilage behavior [140].

1.4.2.3.2 Inhomogeneity

Cartilage's biochemical content and structural organization contribute to its inhomogeneity. Uniaxial tensile testing illustrates depth-dependent tensile properties, where the superficial layer has considerably greater properties than deeper layers [31, 35, 97]. Also, compression inhomogeneity has been reported recently using various methods: compression testing cartilage slices from different layers [41, 43, 117, 128, 141] and

Reproduced with permission of the copyright owner. Further reproduction prohibited without permission.

compression testing using chondrocytes as fiducial markers for measuring depth-dependent intra-tissue strains [41-43, 94, 114, 142-144]. For instance, Schinagl et. al. manually tracked fluorescently stained chondrocytes during confined compression and reported the superficial layer equilibrium compression modulus to be significantly smaller than deeper layers indicating that equilibrium compression modulus (as well as strain) was depth-dependent [42, 114]. Lately, less tedious semi-automated chondrocyte tracking methods (i.e. digital image correlation) were adopted showing similar results in confined and unconfined platen loading conditions [43, 123, 143].

Until recently, quantifying strain distributions within articular cartilage focused on compression behavior using an opposing platen, as opposed to another articular surface. Using quantitative electronic speckle pattern interferometry, Erne et al. [144] attempted to quantify articular cartilage intra-tissue strain distributions within unmatched opposing porcine osteochondral medial femoral and medial patellar specimens ($5x5x5mm^3$) under confined compression. Unfortunately, these researchers were only able to capture one-dimensional infinitesimal strain fields and only within the femoral condyle sections (one surface). The boundary conditions are significantly more complex when loading with an opposing articular surface, therefore no constitutive relationships are feasible and strain distributions are the only response. To fully understand deformational changes occurring within articular cartilage during articular loading, two-dimensional strain field quantification of various regions along the width of physiologically matched joint surfaces is needed.

Reproduced with permission of the copyright owner. Further reproduction prohibited without permission.

1.4.3 Subchondral bone plate (ScBP)

Subchondral bone can refer to some or all of the subarticular structures. However, for this study, the subchondral bone plate (ScBP) was defined as the radio-dense layer between the uncalcified articular cartilage and the supportive trabecular system [145]. The subchondral bone plate consists of type-I collagen fibrils interwoven with inorganic calcium and phosphorus crystalline structures (hydroxyapatite) forming haversian systems similar to cortical bone around osteocytes (bone cells) [146]. The less dense underlying trabecular bone supports the ScBP with strut-like structures organized perpendicular to the overlying articular surface [51, 147, 148]. The majority of energy dissipation is provided by the haversion system of the cortical bone and trabeculae system of the cancellous bone [149]. Subchondral bone structure similarities are found across species and unlike cartilage, subchondral bone is highly vascular, and is therefore, highly reactive to remodeling and microfractures [145]. The adaptation of bone morphology to mechanical stress has been thought to transform tissue structure and is controlled by modeling and remodeling processes [150-158]. Modeling consists of independent formation or resorption rates of bone at a given location to withstand physiological demands [156, 158]. Remodeling involves removing and replacing "packets" of bone to repair damaged bone (i.e microfractures) [157, 158]. Bone strain is thought to stimulate these processes (modeling and remodeling), but the actual mechanism is currently unknown [149, 150, 153, 159-172]. The strain magnitude and rate have been found to have significant effects on bone formation, and thus bone geometry [156, 157, 166, 173].

Reproduced with permission of the copyright owner. Further reproduction prohibited without permission.

For example, the ScBP optimally remodels (densification and thickening) according to its stress environment (e.g., induced by exercise and aging) [145, 152, 174-177]. Subchondral bone plate thickness is an indicator of the structural morphology, while bone mineral density is indicative of the mineral content (hydroxyapatite) within a quantized area or volume. A positive relationship between mean trabecular thickness and mineral density of bone has been noted, therefore it is assumed the structural measurement (ScBP thickness, macro-view) may positively correlate with bone mineral density. Increases in structural bone thickness and bone mineral density are noted to increase cortical bone mechanical properties [174, 178-182].

ScBP thickness can be determined using either histological or radiological methods. Radiological methods include radiography and quantitative computed tomography (CT). Conventional radiography is limited to planar views, whereas CT reconstructs multiple planar views into a three-dimensional view. In the horse, Kawcak et al. found CT superior to conventional radiography for diagnosing OA changes (i.e. joint lesions) [183].

The ScBP thickness varies between/within joints and is dependent on joint function [145, 184, 185]. The geometric concavity of the surface (convex/concave) has been noted to have an effect on ScBP thickness as well [177, 186, 187]. The convex shaped surface is found to be much thinner than its concave counterpart due in part to greater tensile stresses acting on the concave surface [186]. Using computer simulations, the concave curvature has been noted to augment joint incongruity, providing a more

Reproduced with permission of the copyright owner. Further reproduction prohibited without permission.

even stress distribution across the joint, while enhancing cartilage nutrition and lubrication [177].

Apparent bone mineral density is commonly determined using conventional radiography, radiographic absorbtiometry (single and dual), quantitative computed tomography, or quantitative ultrasound [188]. Each method has its benefits and limitations. For example, dual energy x-ray absorbtiometry (DEXA), provides a measurement of bone mineral content (g, grams) within an area (cm^2) to give an apparent area bone mineral density (g/cm^2), which is not a true density. Investigators have divided the apparent bone mineral density by the specimen thickness in an attempt to estimate true bone mineral density. Since CT reconstructs a volumetric rendition of the tissue imaged, quantitative CT is capable of quantifying true bone density (g/cm^3).

Bone mineral density (BMD) also varies between/within joints and is routinely found to be greater under areas of predominately-loaded regions [145, 189]. Two factors, age and exercise, have been found to significantly affect the magnitude and distribution of bone mineral density [183, 190-192]. Investigators have drawn conflicting conclusions about the relationship between ScBP thickness and BMD under areas of cartilage degradation [46, 47, 158, 193-204].

1.4.4 Fibrous capsule and ligaments

The interior of the fibrous capsule is lined with the synovial membrane. The ligaments are either intracapsular (collateral) or extrasynovial (cruciates) [146]. These fibrous structures are mainly connective tissue with low cellularity, extracellular type I

Reproduced with permission of the copyright owner. Further reproduction prohibited without permission.

collagen, proteoglycans, noncollagenous proteins, and water to provide joint stability [146].

1.4.5 Synovial fluid/membrane

The synovial fluid consists mostly of blood plasma constituents with high concentrations of hyaluronan making it extremely viscous [146]. Hyaluronan provides non-Newtonian properties to synovial fluid enabling it to withstand high shear stresses and, surprisingly, absorb some joint load energy [146]. Solute diffusion through the synovial membrane via the synovial fluid provides nutrients needed for articular cartilage metabolism [146].

1.5 Osteoarthritis

Osteoarthritis, also known as osteoarthrosis (OA), is a group of non-inflammatory joint disorders leading to cartilage degradation and subchondral sclerosis (densification and thickening) in synovial joints [205]. OA is often classified as being either primary or secondary. Primary OA is generalized and does not have any single precipitating factor, while secondary OA is perpetuated by a specific factor such as joint stresses, congenital abnormalities, and not limited to instability due to trauma. OA is also commonly found in the equine population and unfortunately, joint disease is the most common cause of expenditure of equine athletes [2, 146:Rossdale, 1985 #1568, 158, 199, 206, 207]. Recently, the equine model has been used for OA and cartilage healing studies [208-215].

1.5.1 Some morphological changes in osteoarthritis

There are some common morphological changes, which occur in the human and horse OA condition. Various joint tissues can be affected, including the articular

Reproduced with permission of the copyright owner. Further reproduction prohibited without permission.

cartilage, subchondral bone, trabecular bone, synovial capsule, and ligaments [216]. Most commonly, connective tissue changes related to OA include articular cartilage fibrillation and subchondral bone remodeling [158, 199, 201, 216-219]. The first morphological change is debated, since both articular cartilage and subchondral bone are so physiologically entwined [49, 152, 158, 174, 180, 182, 194, 195, 198, 200, 202, 204, 218, 220-228].

1.5.1.1 Subchondral Bone and Calcified Cartilage

Remodeling of both subchondral bone and calcified cartilage is common in OA. Diagnostically, remodeling may be seen as thickening and/or increased bone mineral density of the ScBP. In addition to the subchondral bone and calcified cartilage remodeling, an increased vasculature within these tissues is also commonly seen [49, 218, 226, 229-233]. According to some investigations, cartilage thinning is also found during OA due to tidemark advancement, producing multiple tidemarks [218, 226, 234]. The number of tidemarks has been discovered to increase with age, signifying a progressing calcification front [235]. The presence of microcracks in calcified cartilage has been suggested to initiate this remodeling and tidemark advancement [50, 218]. In addition to formation, bone resorption is also found to be associated with OA, leading to articular surface collapse, subchondral bone cysts, and/or fragmentation [202, 206, 225, 236].

It has been postulated repetitive joint loading induces microfractures within subchondral bone and calcified cartilage, thereby inducing remodeling (thickening and/or densification) in these tissues [201, 237, 238]. The remodeling causes increases in

Reproduced with permission of the copyright owner. Further reproduction prohibited without permission.

material stiffness of subchondral bone and calcified cartilage leading to greater intra-tissue strains applied within uncalcified cartilage. The greater strains within uncalcified cartilage provoke matrix failure and breakdown (i.e. cartilage degradation). Repetitive loading induced changes during exercise are dependent on exercise duration, exercise type, rest period length, and joint studied [158, 183, 191, 201, 225, 239-242].

Exercise-associated OA is common in human, equine, and canine species [99, 101, 158, 199, 204-207, 227, 234, 243-248]. The equine metacarpophalangeal (MCP) joint is exposed to high mechanical loading and wear, predisposing the joint to osteochondral fragmentation, subchondral bone lesions, articular/subarticular cysts, and articular surface fibrillations and erosion [49, 158, 205-207, 239, 249-251]. An increase in subchondral bone thickness and bone mineral density with exercise has been noted in the equine MCP joint, which may be associated with the high incidence of fractures and articular lesions in this joint [189, 193, 206, 207, 239, 251, 252]. The structural OA manifestations in the equine MCP joint are very similar to the human condition, possibly making the MCP joint an excellent model for the study of OA progression. For more information, the reader is referred to an inclusive review on the role of subchondral bone in both the human and the horse [158].

1.5.1.2 Cartilage

Fibrillation, softening, swelling, discoloration, fissures and ulceration are some common morphological cartilage changes present during OA [253]. Known biochemical changes during OA include: increased water content and decreased proteoglycan and

Reproduced with permission of the copyright owner. Further reproduction prohibited without permission.

collagen organization and content [253]. Cartilage biochemical changes are biochemically and/or mechanically mediated [2, 8, 9, 132, 199, 207, 253-261].

Changes in biochemical and structural properties degrade cartilage's material properties. Changes in the proteoglycan-collagen matrix associated with OA cause decreases in equilibrium compression modulus, shear modulus, tensile stiffness, tensile strength, and increases in permeability [15, 26, 30, 34, 98, 101, 112, 135, 262-264]. Since these properties are dependent on cartilage strain and the disease state, intra-tissue cartilage strain may be correlated with underlying subchondral properties, possibly illustrating early extracellular matrix changes coinciding with subchondral bone properties.

1.6 Conclusion

To fully understand deformational changes occurring within articular cartilage during articular loading and how these changes are related to underlying subchondral bone changes, two-dimensional strain field quantification of various regions along the width of physiologically matched joint surfaces is needed. In the present study, pre-existing and new testing methods are applied to equine osteochondral tissue to investigate cartilage and subchondral bone properties and relationships.

1.7 References

1. Gray, H, *Gray's Anatomy*. Vol. 29th. 1974, Philadelphia: Running Press.

2. McIlwraith, CW, *Diseases of Joints, Tendons, Ligaments, and Related Structures*, in *Adams' Lameness in Horses*, T.S., S., Editor. 2002, Lippincott Williams & Wilkins: Philadelphia. p. 459-644.

Reproduced with permission of the copyright owner. Further reproduction prohibited without permission.

3. Mow, V and Ratcliffe, A, *Structure and function of articular cartilage and meniscus*, in *Basic Orthopaedic Biomechanics*, Mow, V. and Hayes, W., Editors. 1997, Lippincott-Raven: Philadelphia, PA. p. 113-177.

4. Williamson, AK, Chen, AC, and Sah, RL, *Compressive properties and function-composition relationships of developing bovine articular cartilage.* J Orthop Res, 2001. **19**(6): p. 1113-21.

5. Williamson, AK, Chen, AC, Masuda, K, Thonar, EJ, and Sah, RL, *Tensile mechanical properties of bovine articular cartilage: variations with growth and relationships to collagen network components.* Journal of Orthopaedic Research, 2003. **21**: p. 872-880.

6. Mankin, HJ, Mow, VC, Buckwalter, JA, Iannotti, JP, and Ratcliffe, A, *Form and Function of Articular Cartilage*, in *Orthopaedic Basic Science*, Simon, S.R., Editor. 1994, American Academy of Orthopaedic Surgeons. p. 1-44.

7. Guilak, F, Sah, RL, and Setton, LA, *Physical regulation of cartilage metabolism*, in *Basic Orthopaedic Biomechanics*, Mow, V.C. and Hayes, W.C., Editors. 1997, Lippincott-Raven: Philadelphia. p. 179-207.

8. Sah, RL, Kim, YJ, Doong, JY, Grodzinsky, A, Plaas, A, and Sandy, JD, *Biosynthetic response of cartilage explants to dynamic compression.* Journal of Orthopaedic Research, 1989. **7**(5): p. 619-636.

9. Sah, RL and Grodzinsky, AJ, *Biosynthetic response to mechanical and electrical forces*, in *The biology of tooth movement.* 1989, CRC Press: Boca Raton, FL. p. 335-347.

10. Grodzinsky, AJ, Levenston, ME, Jin, M, and Frank, EH, *Cartilage tissue remodeling in response to mechanical forces.* Annu Rev Biomed Eng, 2000. **2**: p. 691-713.

11. Bonassar, LJ, Grodzinsky, AJ, Srinivasan, A, Davila, SG, and Trippel, SB, *Mechanical and physicochemical regulation of the action of insulin-like growth factor-I on articular cartilage.* Arch Biochem Biophys, 2000. **379**(1): p. 57-63.

12. Jin, M, Frank, EH, Quinn, TM, Hunziker, EB, and Grodzinsky, AJ, *Tissue shear deformation stimulates proteoglycan and protein biosynthesis in bovine cartilage explants.* Archives of Biochemistry and Biophysics, 2001. **395**(1): p. 41-48.

13. Maroudas, A, *Biophysical chemistry of cartilaginous tissues with special reference to solute and fluid transport.* Biorheology, 1975. **12**(3-4): p. 233-48.

Reproduced with permission of the copyright owner. Further reproduction prohibited without permission.

14. Eisenberg, SR and Grodzinsky, AJ, *Swelling of articular cartilage and other connective tissues: electromechanochemical forces.* J Orthop Res, 1985. **3**(2): p. 148-59.

15. Maroudas, A, Wachtel, E, Grushko, G, Katz, E, and Weinberg, P, *The effect of osmotic and mechanical pressures on water partitioning in articular cartilage.* ? er Biophysica Acta, 1991. **1073**: p. 285-294.

16. Mow, V, Kuei, S, Lai, W, and Armstrong, C, *Biphasic creep and stress relaxation of articular cartilage in compression: Theory and Experiments.* Journal of Biomechanical Engineering, 1980. **102**: p. 73-84.

17. Lai, WM, Mow, VC, and Roth, V, *Effects of nonlinear strain-dependent permeability and rate of compression on the stress behavior of articular cartilage.* Journal of Biomechanical Engineering, 1981. **103**: p. 61-66.

18. Grodzinsky, AJ, Roth, V, Myers, E, Grossman, WD, and Mow, VC, *The significance of electromechanical and osmotic forces in the nonequilibrium swelling behavior of articular cartilage in tension.* J Biomech Eng, 1981. **103**(4): p. 221-31.

19. Armstrong, CG and Mow, VC, *Variations in the intrinsic mechanical properties of human articular cartilage with age, degeneration, and water content.* Journal of Bone & Joint Surgery - American Volume, 1982. **64**(1): p. 88-94.

20. Mow, V, Atheshian, G, Lai, W, and Gu, W, *Effects of fixed charges on the stress relaxation behavior of hydrated soft tissues in a confined compression problem.* Int. J. Solids Structures, 1998. **35**(34-35): p. 4945-4962.

21. Mow, VC and Guo, XE, *Mechano-electrochemical properties of articular cartilage: their inhomogeneities and anisotropies.* Annu Rev Biomed Eng, 2002. **4**: p. 175-209.

22. Lee, RC, Frank, EH, Grodzinsky, AJ, and Roylance, DK, *Oscillatory compressional behavior of articular cartilage and its associated electromechanical properties.* J Biomech Eng, 1981. **103**(4): p. 280-92.

23. Frank, E and Grodzinsky, A, *Cartilage electromechanics - II. a continuum model of cartilage electrokinetics and correlation with experiments.* J. Biomechanics, 1987. **20**(6): p. 629-639.

24. Frank, E and Grodzinsky, A, *Cartilage electromechanics - I. electrokinetic transduction and the effects of electrolyte pH and ionic strength.* Journal of Biomechanics, 1987. **20**(6): p. 615-627.

Reproduced with permission of the copyright owner. Further reproduction prohibited without permission.

25. Garcia, AM, Frank, EH, Grimshaw, PE, and Grodzinsky, AJ, *Contributions of fluid convection and electrical migration to transport in cartilage: relevance to loading.* Arch Biochem Biophys, 1996. **333**(2): p. 317-25.

26. Maroudas, AI, *Balance between swelling pressure and collagen tension in normal and degenerate cartilage.* Nature, 1976. **260**(5554): p. 808-9.

27. Grodzinsky, AJ, Lipshitz, H, and Glimcher, MJ, *Electromechanical properties of articular cartilage during compression and stress relaxation.* Nature, 1978. **275**(5679): p. 448-50.

28. Tucker, SA, *Multiphase continuum modeling of articular cartilage*, in *Mechanical Engineering.* 2003, Colorado State University: Fort Collins. p. 116.

29. Eyre, DR, *Cartilage-specific Collagens: Structural studies*, in *Articular Cartilage and Osteoarthritis*, Kuettner KE, S.R., Peyron JG, Hascall VC, Editor. 1995, Raven Press: New York. p. 119-131.

30. Kempson, GE, Muir, H, Pollard, C, and Tuke, M, *The tensile properties of the cartilage of human femoral condyles related to the content of collagen and glycosaminoglycans.* Biochim Biophys Acta, 1973. **297**(2): p. 456-72.

31. Woo, S, Akeson, W, and Jemmott, G, *Measurements of nonhomogeneous directional mechanical properties of articular cartilage in tension.* J. Biomechanics, 1976. **9**: p. 785-791.

32. Woo, S, Lubock, P, Gomez, M, Jemmott, F, Kuei, S, and Akeson, W, *Large deformation nonhomogeneous and directional properties of articular cartilage in uniaxial tension.* J. Biomechanics, 1979. **12**: p. 437-446.

33. Kempson, GE, *Relationship between the tensile properties of articular cartilage from the human knee and age.* Ann Rheum Dis, 1982. **41**(5): p. 508-11.

34. Akizuki, S, Mow, V, Muller, F, Pita, J, and Howell, D, *Tensile properties of human knee joint cartilage. II. Correlations between weight bearing and tissue pathology and the kinetics of swelling.* Journal of Orthopaedic Research, 1987. **5**(2): p. 173-186.

35. Kempson, G, *Age-related changes in the tensile properties of human articular cartilage: a comparative study between the femoral head of the hip joint and the talus of the ankle joint.* Biochimica et Biophysica Acta, 1991. **1075**: p. 223-230.

36. Zhu, W, Mow, VC, Koob, TJ, and Eyre, DR, *Viscoelastic shear properties of articular cartilage and the effects of glycosidase treatments.* J Orthop Res, 1993. **11**(6): p. 771-81.

Reproduced with permission of the copyright owner. Further reproduction prohibited without permission.

37. Buckwalter, JA and Mankin, HJ, *Articular cartilage: tissue design and chondrocyte-matrix interactions.* Instructional Course Lectures, 1998. **47**: p. 477-86.

38. Athanasiou, KA, Rosenwasser, MP, Buckwalter, JA, Malinin, TI, and Mow, VC, *Interspecies comparisons of in situ intrinsic mechanical properties of distal femoral cartilage.* Journal of Orthopaedic Research, 1991. **9**: p. 330-340.

39. Hunziker, E, *Articular cartilage structure in humans and experimental animals*, in *Articular Cartilage and Osteoarthritis*, Kuettner, K.E., Schleyerbach, R., Peyron, J.G., Hascall, V.C., Editor. 1992, Raven Press: New York. p. 183-199.

40. Maroudas, A, *Physicochemical properties of cartilage*, in *Adult Articular Cartilage*, Freeman, M.A.R., Editor. 1979, Pitman Medical: Tunbridge Well, England. p. 215-290.

41. Chen, SS, Falcovitz, YH, Schneiderman, R, Maroudas, A, and Sah, RL, *Depth-dependent compressive properties of normal aged human femoral head articular cartilage: relationship to fixed charge density.* Osteoarthritis Cartilage, 2001. **9**(6): p. 561-9.

42. Schinagl, R, Gurskis, D, Chen, A, and Sah, R, *Depth-dependent confined compression modulus of full thickness bovine articular cartilage.* Journal of Orthopaedic Research, 1997. **15**(4): p. 499-506.

43. Wang, CC, Hung, CT, and Mow, VC, *An analysis of the effects of depth-dependent aggregate modulus on articular cartilage stress-relaxation behavior in compression.* J Biomech, 2001. **34**(1): p. 75-84.

44. Setton, LA, Zhu, W, and Mow, VC, *The biphasic poroviscoelastic behavior of articular cartilage: role of the surface zone in governing the compressive behavior.* J Biomech, 1993. **26**(4-5): p. 581-92.

45. Clarke, IC, *Articular cartilage: a review and scanning electron microscope study. 1. The interterritorial fibrillar architecture.* Journal of Bone & Joint Surgery - British Volume, 1971. **53**(4): p. 732-50.

46. Amir, G, Pirie, CJ, Rashad, S, and Revell, PA, *Remodelling of subchondral bone in osteoarthritis: a histomorphometric study.* Journal of Clinical Pathology, 1992. **45**(11): p. 990-2.

47. Dequeker, J, Mokassa, L, Aerssens, J, and Boonen, S, *Bone density and local growth factors in generalized osteoarthritis.* Microsc Res Tech, 1997. **37**(4): p. 358-71.

Reproduced with permission of the copyright owner. Further reproduction prohibited without permission.

48. Martinelli, MJ, Eurell, J, Les, CM, Fyhrie, D, and Bennett, D, *Age-related morphometry of equine calcified cartilage.* Equine Veterinary Journal, 2002. **34**(3): p. 274-278.

49. Norrdin, RW, Kawcak, CE, Capwell, BA, and McIlwraith, CW, *Calcified cartilage morphometry and its relation to subchondral bone remodeling in equine arthrosis.* Bone, 1999. **24**(2): p. 109-14.

50. Sokoloff, L, *Microcracks in the calcified layer of articular cartilage.* Arch Pathol Lab Med, 1993. **117**(2): p. 191-5.

51. Redler, I, Mow, VC, Zimny, ML, and Mansell, J, *The ultrastructure and biomechanical significance of the tidemark of articular cartilage.* Clin Orthop, 1975(112): p. 357-62.

52. Sokoloff, L, *Elasticity of aging cartilage.* Fed Proc, 1966. **25**(3): p. 1089-95.

53. Blankevoort, L, Kuiper, JH, Huiskes, R, and Grootenboer, HJ, *Articular Contact in a 3-Dimensional Model of the Knee.* Journal of Biomechanics, 1991. **24**(11): p. 1019-1031.

54. Haider, MA and Holmes, MH, *A mathematical approximation for the solution of a static indentation test.* Journal of Biomechanics, 1997. **30**(7): p. 747-751.

55. Hayes, W, *Some viscoelastic properties of human articular cartilage.* Acta Orthop Belg, 1972. **38 Suppl 1**: p. 23-31.

56. Hayes, WC and Bodine, AJ, *Flow-Independent Viscoelastic Properties of Articular-Cartilage Matrix.* Journal of Biomechanics, 1978. **11**(8-9): p. 407-419.

57. Woo, SL, Simon, BR, Kuei, SC, and Akeson, WH, *Quasi-linear viscoelastic properties of normal articular cartilage.* J Biomech Eng, 1980. **102**(2): p. 85-90.

58. Spirt, AA, Mak, AF, and Wassell, RP, *Nonlinear viscoelastic properties of articular cartilage in shear.* J Orthop Res, 1989. **7**(1): p. 43-9.

59. Guilak, F, *The deformation behavior and viscoelastic properties of chondrocytes in articular cartilage.* Biorheology, 2000. **37**(1-2): p. 27-44.

60. Trickey, TR, Lee, M, and Guilak, T, *Viscoelastic properties of chondrocytes from normal and osteoarthritic human cartilage.* Journal of Orthopaedic Research, 2000. **18**(6): p. 891-8.

61. Armstrong, CG, Lai, WM, and Mow, VC, *An analysis of the unconfined compression of articular cartilage.* Journal of Biomechanical Engineering, 1984. **106**(2): p. 165-73.

Reproduced with permission of the copyright owner. Further reproduction prohibited without permission.

62. Guilak, F, Best, BA, Ratcliffe, A, and Mow, VC. *Instrumentation for load and displacement controlled studies on soft connective tissues.* in *Biomechanics Symposium at ASCE/ASME Mechanics Conference.* 1989. University of California, San Diego, La Jolla, California.

63. Mow, VC, Gibbs, MC, Lai, WM, Zhu, WB, and Athanasiou, KA, *Biphasic indentation of articular cartilage--II. A numerical algorithm and an experimental study.* J Biomech, 1989. **22**(8-9): p. 853-61.

64. Kwan, M, Lai, W, and Mow, V, *A finite deformation theory for cartilage and other soft hydrated connective tissues - I. equilibrium results.* J. Biomechanics, 1990. **23**(2): p. 145-155.

65. Bachrach, N, Mow, V, and Guilak, F, *Incompressibility of the solid matrix of articular cartilage under high hydrostatic pressures.* Journal of Biomechanics, 1998. **31**: p. 445-451.

66. DiSilvestro, M and Suh, JF. *A cross-validation of the biphasic poroelastic model of articular cartilage in unconfined compression, indentation, and confined compression.* in *ORS.* 2001. San Francisco, CA.

67. Broom, ND and Marra, DL, *New Structural Concepts of Articular-Cartilage Demonstrated With a Physical Model.* Connective Tissue Research, 1985. **14**(1): p. 1-8.

68. Oloyede, A and Broom, ND, *A Physical Model For the Time-Dependent Deformation of Articular-Cartilage.* Connective Tissue Research, 1993. **29**(4): p. 251-261.

69. Buschmann, MD and Grodzinsky, AJ, *A Molecular-Model of Proteoglycan-Associated Electrostatic Forces in Cartilage Mechanics.* Journal of Biomechanical Engineering-Transactions of the Asme, 1995. **117**(2): p. 179-192.

70. Buschmann, MD and Grodzinsky, AJ, *A molecular model of proteoglycan-associated electrostatic forces in cartilage mechanics.* J Biomech Eng, 1995. **117**(2): p. 179-92.

71. Brown, TD, Radin, EL, Martin, RB, and Burr, DB, *Finite element studies of some juxtarticular stress changes due to localized subchondral stiffening.* J Biomech, 1984. **17**(1): p. 11-24.

72. Eberhardt, AW, Keer, LM, Lewis, JL, and Vithoontien, V, *An Analytical Model of Joint Contact.* Journal of Biomechanical Engineering-Transactions of the Asme, 1990. **112**(4): p. 407-413.

Reproduced with permission of the copyright owner. Further reproduction prohibited without permission.

73. Brown, T, Pope, D, Hale, J, Buckwalter, J, and Brand, R, *Effects of osteochondral defect size on cartilage contact stress.* Journal of Orthopaedic Research, 1991. **9**(4): p. 559-567.

74. Eberhardt, A, Lewis, J, and Keer, L, *Contact of layered elastic spheres as a model of joint contact: effect of tangential load and friction.* Journal of Biomechanical Engineering, 1991. **113**: p. 107-108.

75. Anderson, DD, Brown, TD, and Radin, EL, *Stress wave effects in a finite element analysis of an impulsively loaded articular joint.* Proc Inst Mech Eng [H], 1991. **205**(1): p. 27-34.

76. Ateshian, GA, Lai, WM, Zhu, WB, and Mow, VC, *An asymptotic solution for the contact of two biphasic cartilage layers.* J Biomech, 1994. **27**(11): p. 1347-60.

77. Jacobs, CR and Eckstein, F, *Computer simulation of subchondral bone adaptation to mechanical loading in an incongruous joint.* Anat Rec, 1997. **249**(3): p. 317-26.

78. Garcia, JJ, Altiero, NJ, and Haut, RC, *An approach for the stress analysis of transversely isotropic biphasic cartilage under impact load.* Journal of Biomechanical Engineering-Transactions of the Asme, 1998. **120**(5): p. 608-613.

79. Donzelli, P, Spilker, R, Ateshian, G, and Mow, V, *Contact analysis of biphasic transversely isotropic cartilage layers and correlations with tissue failure.* Journal of Biomechanics, 1999. **32**: p. 1037-1047.

80. Kelkar, R and Ateshian, GA, *Contact creep of biphasic cartilage layers.* Journal of Applied Mechanics-Transactions of the Asme, 1999. **66**(1): p. 137-145.

81. Hoch, DH, Grodzinsky, AJ, Koob, TJ, Albert, ML, and Eyre, DR, *Early changes in material properties of rabbit articular cartilage after meniscectomy.* J Orthop Res, 1983. **1**(1): p. 4-12.

82. Whipple, RR, Gibbs, MC, Lai, WM, Mow, VC, Mak, AF, and Wirth, CR. *Biphasic properties of repaired cartilage at the articular surface.* in *ORS.* 1985. Las Vegas, NV.

83. Athanasiou, KA, Agarwal, A, and Dzida, FJ, *Comparative study of the intrinsic mechanical properties of the human acetabular and femoral head cartilage.* J Orthop Res, 1994. **12**(3): p. 340-9.

84. Niederauer, GG, Stevens, DM, Korvick, DL, and Athanasiou, KA. *Biomechanical properties of adjacent articular cartilage in response to osteochondral defect treatment.* in *ORS.* 1995. Orlando, FL.

Reproduced with permission of the copyright owner. Further reproduction prohibited without permission.

85. Athanasiou, KA, Agarwal, A, Muffoletto, A, Dzida, FJ, Constantinides, G, and Clem, M, *Biomechanical properties of hip cartilage in experimental animal models.* Clin Orthop, 1995(316): p. 254-66.

86. Athanasiou, KA, Niederauer, GG, and Schenck, RC, Jr., *Biomechanical topography of human ankle cartilage.* Ann Biomed Eng, 1995. **23**(5): p. 697-704.

87. Mukherjee, N and Wayne, JS, *Load sharing between solid and fluid phases in articular cartilage: I - Experimental determination of in situ mechanical conditions in a porcine knee.* Journal of Biomechanical Engineering-Transactions of the Asme, 1998. **120**(5): p. 614-619.

88. Murray, RC, DeBowes, RM, Gaughan, EM, Zhu, CF, and Athanasiou, KA, *The effects of intra-articular methylprednisolone and exercise on the mechanical properties of articular cartilage in the horse.* Osteoarthritis Cartilage, 1998. **6**(2): p. 106-14.

89. Lyyra, T, Kiviranta, I, Vaatainen, U, Helminen, H, and Jurvelin, J, *In vivo characterization of indentation stiffness of articular cartilage in the normal human knee.* Journal of Biomedical Materials Research (Applied Biomaterials), 1999. **48**: p. 482-487.

90. Murray, RC, Zhu, CF, Goodship, AE, Lakhani, KH, Agrawal, CM, and Athanasiou, KA, *Exercise affects the mechanical properties and histological appearance of equine articular cartilage.* Journal of Orthopaedic Research, 1999. **17**(5): p. 725-31.

91. Jurvelin, J, Arokoski, J, Hunziker, E, and Helminen, H, *Topographical variation of the elastic properties of articular cartilage in the canine knee.* Journal of Biomechanics, 2000. **33**: p. 669-675.

92. Athanasiou, KA, Zhu, CF, Wang, X, and Agrawal, CM, *Effects of aging and dietary restriction on the structural integrity of rat articular cartilage.* Ann Biomed Eng, 2000. **28**(2): p. 143-9.

93. Korhonen, RK, Wong, M, Arokoski, J, Lindgren, R, Helminen, HJ, Hunziker, EB, and Jurvelin, JS, *Importance of the superficial tissue layer for the indentation stiffness of articular cartilage.* Medical Engineering & Physics, 2002. **24**(2): p. 99-108.

94. Bae, WC, Lewis, CW, and Sah, RL. *Intra-tissue strain distribution in normal human articular cartilage during clinical indentation testing.* in *Transactions of the ORS.* 2002. New Orleans, Louisiana.

95. Armstrong, CG, Bahrani, AS, and Gardner, DL, *Alteration with age in compliance of human femoral-head cartilage.* Lancet, 1977. **1**(8021): p. 1103-4.

Reproduced with permission of the copyright owner. Further reproduction prohibited without permission.

96. Armstrong, CG, Bahrani, AS, and Gardner, DL, *In vitro measurement of articular cartilage deformations in the intact human hip joint under load.* Journal of Bone & Joint Surgery - American Volume, 1979. **61**(5): p. 744-55.

97. Roth, V and Mow, VC, *The intrinsic tensile behavior of the matrix of bovine articular cartilage and its variation with age.* Journal of Bone & Joint Surgery - American Volume, 1980. **62**(7): p. 1102-17.

98. Akizuki, S, Mow, VC, Muller, F, Pita, JC, Howell, DS, and Manicourt, DH, *Tensile properties of human knee joint cartilage: I. Influence of ionic conditions, weight bearing, and fibrillation on the tensile modulus.* J Orthop Res, 1986. **4**(4): p. 379-92.

99. Setton, LA, Mow, VC, Muller, FJ, Pita, JC, and Howell, DS, *Mechanical behavior and biochemical composition of canine knee cartilage following periods of joint disuse and disuse with remobilization.* Osteoarthritis Cartilage, 1997. **5**(1): p. 1-16.

100. McCormack, T and Mansour, JM, *Reduction in tensile strength of cartilage precedes surface damage under repeated compressive loading in vitro.* Journal of Biomechanics, 1998. **31**(1): p. 55-61.

101. Elliott, DM, Guilak, F, Vail, TP, Wang, JY, and Setton, LA, *Tensile properties of articular cartilage are altered by meniscectomy in a canine model of osteoarthritis.* J Orthop Res, 1999. **17**(4): p. 503-8.

102. Chen, AC, Temple, MM, Ng, DM, Richardson, CD, DeGroot, J, Verzijl, N, teKoppele, JM, and Sah, RL. *Age-related crosslinking alters tensile properties of articular cartilage.* in *Trans. ORS.* 2001.

103. Huang, CY, Mow, VC, and Ateshian, GA, *The role of flow-independent viscoelasticity in the biphasic tensile and compressive responses of articular cartilage.* J Biomech Eng, 2001. **123**(5): p. 410-7.

104. Elliott, DM, Narmoneva, DA, and Setton, LA, *Direct measurement of the Poisson's ratio of human patella cartilage in tension.* J Biomech Eng, 2002. **124**(2): p. 223-8.

105. Ateshian, GA, Warden, WH, Kim, JJ, Grelsamer, RP, and Mow, VC, *Finite deformation biphasic material properties of bovine articular cartilage from confined compression experiments.* Journal of Biomechanics, 1997. **30**(11-12): p. 1157-64.

106. Bursac, P, Obitz, T, Eisenberg, S, and Stamenovic, D, *Confined and unconfined stress relaxation of cartilage: appropriateness of a transversely isotropic analysis.* Journal of Biomechanics, 1999. **32**: p. 1125-1130.

Reproduced with permission of the copyright owner. Further reproduction prohibited without permission.

107. Buschmann, MD, Soulhat, J, Shirazi-Adl, A, Jurvelin, JS, and Hunziker, EB, *Confined compression of articular cartilage: linearity in ramp and sinusoidal tests and the importance of interdigitation and incomplete confinement.* J Biomech, 1998. **31**(2): p. 171-8.

108. Kim, YJ, Bonassar, LJ, and Grodzinsky, AJ, *The role of cartilage streaming potential, fluid flow and pressure in the stimulation of chondrocyte biosynthesis during dynamic compression.* J Biomech, 1995. **28**(9): p. 1055-66.

109. Kwan, M, Hacker, S, Woo, S, and Wayne, J, *The effect of storage on the biomechanical behavior of articular cartilage - a large strain study.* Journal of Biomechanical Engineering, 1992. **114**: p. 149-153.

110. Mizrahi, J, Maroudas, A, Lanir, Y, Ziv, I, and Webber, TJ, *The "instantaneous" deformation of cartilage: effects of collagen fiber orientation and osmotic stress.* Biorheology, 1986. **23**(4): p. 311-30.

111. Quinn, TM, Dierickx, P, and Grodzinsky, AJ, *Glycosaminoglycan network geometry may contribute to anisotropic hydraulic permeability in cartilage under compression.* J Biomech, 2001. **34**(11): p. 1483-90.

112. Sah, RL, Yang, A, Chen, AC, Hant, J, Halili, R, Yoshioka, M, Amiel, D, and Coutts, R, *Physical properties of rabbit articular cartilage after transection of the anterior cruciate ligament.* Journal of Orthopaedic Research, 1997. **15**(2): p. 197-203.

113. Sah, RL, Kim, YJ, Doong, JY, Grodzinsky, AJ, Plaas, AH, and Sandy, JD, *Biosynthetic response of cartilage explants to dynamic compression.* J Orthop Res, 1989. **7**(5): p. 619-36.

114. Schinagl, RM, Ting, MK, Price, JH, and Sah, RL, *Video microscopy to quantitate the inhomogeneous equilibrium strain within articular cartilage during confined compression.* Annal of Biomedical Engineering, 1996. **24**: p. 500-512.

115. Soltz, MA and Ateshian, GA, *Experimental verification and theoretical prediction of cartilage interstitial fluid pressurization at an impermeable contact interface in confined compression.* Journal of Biomechanics, 1998. **31**(10): p. 927-934.

116. Suh, JK, Li, Z, and Woo, SL, *Dynamic behavior of a biphasic cartilage model under cyclic compressive loading.* J Biomech, 1995. **28**(4): p. 357-64.

117. Treppo, S, Koepp, H, Quan, EC, Cole, AA, Kuettner, KE, and Grodzinsky, AJ, *Comparison of biomechanical and biochemical properties of cartilage from human knee and ankle pairs.* Journal of Orthopaedic Research, 2000. **18**(5): p. 739-48.

Reproduced with permission of the copyright owner. Further reproduction prohibited without permission.

118. DiSilvestro, MR and Suh, JK, *A cross-validation of the biphasic poroviscoelastic model of articular cartilage in unconfined compression, indentation, and confined compression.* Journal of Biomechanics, 2001. **34**(4): p. 519-25.

119. Huang, CY, Soltz, MA, Kopacz, M, Mow, VC, and Ateshian, GA, *Experimental verification of the roles of intrinsic matrix viscoelasticity and tension-compression nonlinearity in the biphasic response of cartilage.* J Biomech Eng, 2003. **125**(1): p. 84-93.

120. Langelier, E and Buschmann, MD, *Increasing strain and strain rate strengthen transient stiffness but weaken the response to subsequent compression for articular cartilage in unconfined compression.* J Biomech, 2003. **36**(6): p. 853-9.

121. Li, LP, Buschmann, MD, and Shirazi-Adl, A, *A fibril reinforced nonhomogeneous poroelastic model for articular cartilage: inhomogeneous response in unconfined compression.* Journal of Biomechanics, 2000. **33**: p. 1533-1541.

122. Li, LP, Buschmann, MD, and Shirazi-Adl, A, *Strain-rate dependent stiffness of articular cartilage in unconfined compression.* J Biomech Eng, 2003. **125**(2): p. 161-8.

123. Wang, C, Soltz, M, Mauck, R, Valhmu, W, Ateshian, G, and Hung, C. *Comparison of equilibrium axial strain distribution in articular cartilage explants and cell seeded alginate disks under unconfined compression.* in *46th Annual Orthopaedic Research Society*. 2000. Orlando, Florida.

124. Wang, CCB, Chahine, NO, Hung, CT, and Ateshian, GA, *Optical determination of anisotropic material properties of bovine articular cartilage in compression.* Journal of Biomechanics, 2003. **36**(3): p. 339-353.

125. Wang, CCB, Deng, JM, Ateshian, GA, and Hung, CT, *An automated approach for direct measurement of two-dimensional strain distributions within articular cartilage under unconfined compression.* Journal of Biomechanical Engineering-Transactions of the Asme, 2002. **124**(5): p. 557-567.

126. Woo, SL, Kwan, MK, Lee, TQ, Field, FP, Kleiner, JB, and Coutts, RD, *Perichondrial autograft for articular cartilage. Shear modulus of neocartilage studied in rabbits.* Acta Orthop Scand, 1987. **58**(5): p. 510-5.

127. Setton, L, Tohyama, H, and Mow, V, *Swelling and curling behaviors of articular cartilage.* Journal of Biomechanical Engineering, 1998. **120**: p. 355-361.

128. Chen, AC, Bae, WC, Schinagl, RM, and Sah, RL, *Depth- and strain-dependent mechanical and electromechanical properties of full-thickness bovine articular cartilage in confined compression.* Journal of Biomechanics, 2001. **34**(1): p. 1-12.

Reproduced with permission of the copyright owner. Further reproduction prohibited without permission.

129. Korvick, D and Athanasiou, K, *Variations in the mechanical properties of cartilage from the canine scapulohumeral joint.* Am J Vet Res, 1997. **58**(9): p. 949-53.

130. Brama, PA, Barneveld, A, Karssenberg, D, Van Kampen, GP, and van Weeren, PR, *The application of an indenter system to measure structural properties of articular cartilage in the horse. Suitability of the instrument and correlation with biochemical data.* J Vet Med A Physiol Pathol Clin Med, 2001. **48**(4): p. 213-21.

131. Palmer, JL, Bertone, AL, Mansour, J, Carter, BG, and Malemud, CJ, *Biomechanical properties of third carpal articular cartilage in exercised and nonexercised horses.* J Orthop Res, 1995. **13**(6): p. 854-60.

132. Sah, RL, Kim, YJ, and Grodzinsky, A, *The effect of mechanical compression on cartilage metabolism*, in *Methods in cartilage research*, Maroudas, A. and Kuettner, K., Editors. 1990, Academic Press: New York. p. 116-119.

133. Patwari, P, Fay, J, Cook, MN, Badger, AM, Kerin, AJ, Lark, MW, and Grodzinsky, AJ, *In vitro models for investigation of the effects of acute mechanical injury on cartilage.* Clin Orthop, 2001(391 Suppl): p. S61-71.

134. Patwari, P, Kurz, B, Sandy, JD, and Grodzinsky, AJ, *Mannosamine inhibits aggrecanase-mediated changes in the physical properties and biochemical composition of articular cartilage.* Arch Biochem Biophys, 2000. **374**(1): p. 79-85.

135. Bank, RA, Soudry, M, Maroudas, A, Mizrahi, J, and TeKoppele, JM, *The increased swelling and instantaneous deformation of osteoarthritic cartilage is highly correlated with collagen degradation.* Arthritis & Rheumatism, 2000. **43**(10): p. 2202-10.

136. Kurz, B, Jin, M, Patwari, P, Cheng, DM, Lark, MW, and Grodzinsky, AJ, *Biosynthetic response and mechanical properties of articular cartilage after injurious compression.* J Orthop Res, 2001. **19**(6): p. 1140-6.

137. Bonassar, LJ, Jeffries, KA, Paguio, CG, and Grodzinsky, AJ, *Cartilage degradation and associated changes in biochemical and electromechanical properties.* Acta Orthop Scand Suppl, 1995. **266**: p. 38-44.

138. Askew, MJ and Mow, VC, *The biomechanical function of the collagen fibril ultrastructure of articular cartilage.* Journal of Biomechanical Engineering, 1978. **100**: p. 105-115.

139. Cohen, NP, Foster, RJ, and Mow, VC, *Composition and dynamics of articular cartilage: Structure, function, and maintaining healthy state.* Journal of Orthopaedic & Sports Physical Therapy, 1998. **28**(4): p. 203-215.

Reproduced with permission of the copyright owner. Further reproduction prohibited without permission.

140. Wang, CC, Chahine, NO, Hung, CT, and Ateshian, GA, *Optical determination of anisotropic material properties of bovine articular cartilage in compression.* J Biomech, 2003. **36**(3): p. 339-53.

141. Torzilli, P, *Measurement of the compressive properties of thin cartilage slices: evaluating tissue inhomogeneity*, in *Methods of Cartilage Research*. 1990, Academic Press: London, San Diego. p. 304-308.

142. Guilak, F, Ratcliffe, A, and Mow, V, *Chondrocyte Deformation and Local Tissue Strain in Articular Cartilage: A Confocal Microscopy Study.* Journal of Orthopaedic Research, 1995. **13**: p. 410-421.

143. Wang, CC, Deng, JM, Ateshian, GA, and Hung, CT, *An automated approach for direct measurement of two-dimensional strain distributions within articular cartilage under unconfined compression.* J Biomech Eng, 2002. **124**(5): p. 557-67.

144. Erne, OK, Reid, J, and Bottlang, M. *Offset-strain and depth-dependent strain distribution across articular cartilage.* in *49th Annual Meeting of the Orthopaedic Research Society*. 2003. New Orleans, Lousiana.

145. Muller-Gerbl, M, *The subchondral bone plate.* Advances in anatomy, embryology & cell biology. Vol. 141. 1998. 1-134.

146. Todhunter, RJ, *Anatomy and physiology of synovial joints*, in *Joint Disease In The Horse*, McIlwraith, C.W. and Trotter, G.W., Editors. 1996, W.B. Saunders Company: Philadelphia. p. 1-28.

147. Lajeunesse, D, Hilal, G, Pelletier, JP, and Martel-Pelletier, J, *Subchondral bone morphological and biochemical alterations in osteoarthritis.* Osteoarthritis & Cartilage, 1999. 7(3): p. 321-2.

148. Braidotti, P, Bemporad, E, D'Alessio, T, Sciuto, S, and Stagni, L, *Tensile experiments and SEM fractography on bovine subchondral bone.* Journal of Biomechanics, 2000. **33**: p. 1153-1157.

149. Radin, EL, Burr, DB, Fyhrie, D, Brown, TD, and Boyd, RD, *Characteristics of joint loading as it applies to osteoarthrosis*, in *Biomechanics of diarthrodial joints*. 1990, Springer-Verlag: New York. p. 369-384.

150. Carter, DR, *Mechanical loading histories and cortical bone remodeling.* Calcif Tissue Int, 1984. **36 Suppl 1**: p. S19-24.

151. Ding, M, *Age variations in the properties of human tibial trabecular bone and cartilage.* Acta Orthop Scand Suppl, 2000. **292**: p. 1-45.

Reproduced with permission of the copyright owner. Further reproduction prohibited without permission.

152. Eckstein, F, Jacobs, CR, and Merz, BR, *Mechanobiological adaptation of subchondral bone as a function of joint incongruity and loading.* Med Eng Phys, 1997. **19**(8): p. 720-8.

153. Frost, HM, *Wolff's Law and bone's structural adaptations to mechanical usage: an overview for clinicians.* Angle Orthodontist, 1994. **64**(3): p. 175-88.

154. Meyer, GH, *Die Architektur die Spongiosa.* Arch. Anat. Physiol. Wiss. Med., 1867. **34**: p. 160-169.

155. Wolff, J, *Uber die innere Architecktur der Knochen und ihre Bedeutung fur die Frage vom Knochenwachstum.* Virchows Arch. Pathol., 1870. **50**: p. 389-450.

156. Frost, HM, *Skeletal structural adaptations to mechanical usage (SATMU): 1. Redefining Wolff's law: the bone modeling problem.* Anatomical Record, 1990. **226**(4): p. 403-13.

157. Frost, HM, *Skeletal structural adaptations to mechanical usage (SATMU): 2. Redefining Wolff's law: the remodeling problem.* Anatomical Record, 1990. **226**(4): p. 414-22.

158. Kawcak, CE, McIlwraith, CW, Norrdin, RW, Park, RD, and James, SP, *The role of subchondral bone in joint disease: a review.* Equine Vet J, 2001. **33**(2): p. 120-6.

159. Burr, DB, Schaffler, MB, Yang, KH, Wu, DD, Lukoschek, M, Kandzari, D, Sivaneri, N, Blaha, JD, and Radin, EL, *The effects of altered strain environments on bone tissue kinetics.* Bone, 1989. **10**(3): p. 215-21.

160. Cowin, SC, *Wolff's law of trabecular architecture at remodeling equilibrium.* J Biomech Eng, 1986. **108**(1): p. 83-8.

161. Frost, HM, *Bone "mass" and the "mechanostat": a proposal.* Anatomical Record, 1987. **219**(1): p. 1-9.

162. Fyhrie, DP and Carter, DR, *A unifying principle relating stress to trabecular bone morphology.* J Orthop Res, 1986. **4**(3): p. 304-17.

163. Lanyon, LE, *Functional strain as a determinant for bone remodeling.* Calcified Tissue International, 1984. **36 Suppl 1**: p. S56-61.

164. Lanyon, LE, *Functional strain in bone tissue as an objective, and controlling stimulus for adaptive bone remodelling.* Journal of Biomechanics, 1987. **20**(11-12): p. 1083-93.

Reproduced with permission of the copyright owner. Further reproduction prohibited without permission.

165. Lanyon, LE, Paul, IL, Rubin, CT, Thrasher, EL, DeLaura, R, Rose, RM, and Radin, EL, *In vivo strain measurements from bone and prosthesis following total hip replacement. An experimental study in sheep.* J Bone Joint Surg Am, 1981. **63**(6): p. 989-1001.

166. O'Connor, JA, Lanyon, LE, and MacFie, H, *The influence of strain rate on adaptive bone remodelling.* Journal of Biomechanics, 1982. **15**(10): p. 767-81.

167. Rubin, CT, *Skeletal strain and the functional significance of bone architecture.* Calcified Tissue International, 1984. **36 Suppl 1**: p. S11-8.

168. Rubin, CT and Lanyon, LE, *Regulation of bone mass by mechanical strain magnitude.* Calcified Tissue International, 1985. **37**(4): p. 411-7.

169. Rubin, CT and Lanyon, LE, *Regulation of bone formation by applied dynamic loads.* Journal of Bone & Joint Surgery - American Volume, 1984. **66**(3): p. 397-402.

170. Rubin, CT, McLeod, KJ, and Bain, SD, *Functional strains and cortical bone adaptation: epigenetic assurance of skeletal integrity.* Journal of Biomechanics, 1990. **23 Suppl 1**: p. 43-54.

171. Turner, C, Anne, V, and Pidaparti, R, *A uniform strain criterion for trabecular bone adaption: do continuum-level strain gradients drive adaptation?* Journal of Biomechanics, 1997. **30**(6): p. 555-563.

172. van Harreveld, PD, Lillich, JD, Kawcak, CE, Turner, AS, and Norrdin, RW, *Effects of immobilization followed by remobilization on mineral density, histomorphometric features, and formation of the bones of the metacarpophalangeal joint in horses.* Am J Vet Res, 2002. **63**(2): p. 276-81.

173. Rubin, CT and Lanyon, LE, *Osteoregulatory nature of mechanical stimuli, function as a determinant for adaptive remodeling in bone.* Journal of Orthopaedic Research, 1987. **5**: p. 300-310.

174. Radin, EL and Rose, RM, *Role of subchondral bone in the initiation and progression of cartilage damage.* Clin Orthop, 1986(213): p. 34-40.

175. Eckstein, F, Lohe, F, Schulte, E, Muller-Gerbl, M, Milz, S, and Putz, R, *Physiological incongruity of the humero-ulnar joint: a functional principle of optimized stress distribution acting upon articulating surfaces?* Anat Embryol (Berl), 1993. **188**(5): p. 449-55.

176. Eckstein, F, Merz, B, and Jacobs, CR, *Effects of joint incongruity on articular pressure distribution and subchondral bone remodeling.* Adv Anat Embryol Cell Biol, 2000. **152**: p. iii-ix, 1-127.

Reproduced with permission of the copyright owner. Further reproduction prohibited without permission.

177. Eckstein, F, Merz, B, Muller-Gerbl, M, Holzknecht, N, Pleier, M, and Putz, R, *Morphomechanics of the humero-ulnar joint: II. Concave incongruity determines the distribution of load and subchondral mineralization.* Anat Rec, 1995. **243**(3): p. 327-35.

178. Les, CM, Stover, SM, Keyak, JH, Taylor, KT, and Kaneps, AJ, *Stiff and strong compressive properties are associated with brittle post-yield behavior in equine compact bone material.* J Orthop Res, 2002. **20**(3): p. 607-14.

179. Radin, E, Paul, I, and Lowy, M, *A comparison of the dynamic force transmitting properties of subchondral bone and articular cartilage.* The Journal of Bone and Joint Surgery, 1970. **52-A**(3): p. 444-456.

180. Day, JS, Ding, M, van der Linden, JC, Hvid, I, Sumner, DR, and Weinans, H, *A decreased subchondral trabecular bone tissue elastic modulus is associated with pre-arthritic cartilage damage.* J Orthop Res, 2001. **19**(5): p. 914-8.

181. Ding, M, Danielsen, CC, and Hvid, I, *Bone density does not reflect mechanical properties in early-stage arthrosis.* Acta Orthop Scand, 2001. **72**(2): p. 181-5.

182. Coats, AM, Zioupos, P, and Aspden, RM, *Material properties of subchondral bone from patients with osteoporosis or osteoarthritis by microindentation testing and electron probe microanalysis.* Calcif Tissue Int, 2003. **73**(1): p. 66-71.

183. Kawcak, CE, McIlwraith, CW, Norrdin, RW, Park, RD, and Steyn, PS, *Clinical effects of exercise on subchondral bone of carpal and metacarpophalangeal joints in horses.* Am J Vet Res, 2000. **61**(10): p. 1252-8.

184. Milz, S and Putz, R, *Quantitative morphology of the subchondral plate of the tibial plateau.* J Anat, 1994. **185 (Pt 1)**: p. 103-10.

185. Eckstein, F, Milz, S, Anetzberger, H, and Putz, R, *Thickness of the subchondral mineralised tissue zone (SMZ) in normal male and female and pathological human patellae.* J Anat, 1998. **192 (Pt 1)**: p. 81-90.

186. Simkin, PA, Graney, DO, and Fiechtner, JJ, *Roman arches, human joints, and disease: differences between convex and concave sides of joints.* Arthritis Rheum, 1980. **23**(11): p. 1308-11.

187. Simkin, PA, Heston, TF, Downey, DJ, Benedict, RS, and Choi, HS, *Subchondral architecture in bones of the canine shoulder.* J Anat, 1991. **175**: p. 213-27.

188. Genant, HK and van Kuijk, C, *Bone densiometry*, in *Orthopaedic Basic Science: Biology and Biomechanics of the Musculoskeletal System*, Simon, S.R., Editor. 2000, American Academy of Orthopaedic Surgeons. p. 279-288.

Reproduced with permission of the copyright owner. Further reproduction prohibited without permission.

189. Riggs, CM, Whitehouse, GH, and Boyde, A, *Structural variation of the distal condyles of the third metacarpal and third metatarsal bones in the horse.* Equine Vet J, 1999. **31**(2): p. 130-9.

190. Firth, EC, van Weeren, PR, Pfeiffer, DU, Delahunt, J, and Barneveld, A, *Effect of age, exercise and growth rate on bone mineral density (BMD) in third carpal bone and distal radius of Dutch Warmblood foals with osteochondrosis.* Equine Vet J Suppl, 1999(31): p. 74-8.

191. Firth, EC, Delahunt, J, Wichtel, JW, Birch, HL, and Goodship, AE, *Galloping exercise induces regional changes in bone density within the third and radial carpal bones of Thoroughbred horses.* Equine Vet J, 1999. **31**(2): p. 111-5.

192. van de Lest, CH, Brama, PA, and Van Weeren, PR, *The influence of exercise on the composition of developing equine joints.* Biorheology, 2002. **39**(1-2): p. 183-91.

193. Cantley, CE, Firth, EC, Delahunt, JW, Pfeiffer, DU, and Thompson, KG, *Naturally occurring osteoarthritis in the metacarpophalangeal joints of wild horses.* Equine Vet J, 1999. **31**(1): p. 73-81.

194. Ding, M, Dalstra, M, Linde, F, and Hvid, I, *Changes in the stiffness of the human tibial cartilage-bone complex in early-stage osteoarthrosis.* Acta Orthop Scand, 1998. **69**(4): p. 358-62.

195. Ewers, BJ, Weaver, BT, Sevensma, ET, and Haut, RC, *Chronic changes in rabbit retro-patellar cartilage and subchondral bone after blunt impact loading of the patellofemoral joint.* J Orthop Res, 2002. **20**(3): p. 545-50.

196. Fahlgren, A, Messner, K, and Aspenberg, P, *Meniscectomy leads to an early increase in subchondral bone plate thickness in the rabbit knee.* Acta Orthop Scand, 2003. **74**(4): p. 437-41.

197. Grynpas, MD, Alpert, B, Katz, I, Lieberman, I, and Pritzker, KP, *Subchondral bone in osteoarthritis.* Calcif Tissue Int, 1991. **49**(1): p. 20-6.

198. Matsui, H, Shimizu, M, and Tsuji, H, *Cartilage and subchondral bone interaction in osteoarthrosis of human knee joint: a histological and histomorphometric study.* Microscopy Research And Technique, 1997. **37**: p. 333-342.

199. McIlwraith, CW and Vachon, A, *Review of pathogenesis and treatment of degenerative joint disease.* Equine Vet J Suppl, 1988(6): p. 3-11.

200. Messner, K, Fahlgren, A, Ross, I, and Andersson, B, *Simultaneous changes in bone mineral density and articular cartilage in a rabbit meniscectomy model of knee osteoarthrosis.* Osteoarthritis and Cartilage, 2000. **8**(3): p. 197-206.

Reproduced with permission of the copyright owner. Further reproduction prohibited without permission.

201. Radin, EL, *Subchondral bone changes and cartilage damage.* Equine Vet J, 1999. **31**(2): p. 94-5.

202. Shimizu, M, Tsuji, H, Matsui, H, Katoh, Y, and Sano, A, *Morphometric analysis of subchondral bone of the tibial condyle in osteoarthrosis.* Clin Orthop, 1993(293): p. 229-39.

203. Smith, RL, Thomas, KD, Schurman, DJ, Carter, DR, Wong, M, and van der Meulen, MC, *Rabbit knee immobilization: bone remodeling precedes cartilage degradation.* J Orthop Res, 1992. **10**(1): p. 88-95.

204. Yamada, K, Healey, R, Amiel, D, Lotz, M, and Coutts, R, *Subchondral bone of the human knee joint in aging and osteoarthritis.* Osteoarthritis Cartilage, 2002. **10**(5): p. 360-9.

205. Pool, RR and Meagher, DM, *Pathologic findings and pathogenesis of racetrack injuries.* Vet Clin North Am Equine Pract, 1990. **6**(1): p. 1-30.

206. Norrdin, RW, Kawcak, CE, Capwell, BA, and McIlwraith, CW, *Subchondral bone failure in an equine model of overload arthrosis.* Bone, 1998. **22**(2): p. 133-9.

207. Pool, RR, *Traumatic injury and osteoarthritis.* Joint Disease in the Horse, ed. McIlwraith, C.W. and Trotter, G.W. 1996, Philadelphia: W.B. Saunders Co. 87-104.

208. Hanie, E, Sullins, K, Powers, B, and Nelson, P, *Healing of full thickness cartilage compared with full thickness cartilage and subchondral bone defects in the equine third carpal bone.* Equine Veterinary Journal, 1992. **24**(5): p. 382-386.

209. Jackson, WA, Stick, JA, Arnoczky, SP, and Nickels, FA, *The effect of compacted cancellous bone grafting on the healing of subchondral bone defects of the medial femoral condyle in horses.* Vet Surg, 2000. **29**(1): p. 8-16.

210. Nixon, AJ, Brower-Toland, BD, Bent, SJ, Saxer, RA, Wilke, MJ, Robbins, PD, and Evans, CH, *Insulinlike growth factor-I gene therapy applications for cartilage repair.* Clin Orthop, 2000(379 Suppl): p. S201-13.

211. Frisbie, DD, Oxford, JT, Southwood, L, Trotter, GW, Rodkey, WG, Steadman, JR, Goodnight, JL, and McIlwraith, CW, *Early events in cartilage repair after subchondral bone microfracture.* Clin Orthop, 2003(407): p. 215-27.

212. Hidaka, C, Goodrich, LR, Chen, CT, Warren, RF, Crystal, RG, and Nixon, AJ, *Acceleration of cartilage repair by genetically modified chondrocytes over expressing bone morphogenetic protein-7.* J Orthop Res, 2003. **21**(4): p. 573-83.

Reproduced with permission of the copyright owner. Further reproduction prohibited without permission.

213. Vachon, A, Bramlage, LR, Gabel, AA, and Weisbrode, S, *Evaluation of the repair process of cartilage defects of the equine third carpal bone with and without subchondral bone perforation.* Am J Vet Res, 1986. **47**(12): p. 2637-45.

214. Vachon, AM, McIlwraith, CW, and Keeley, FW, *Biochemical study of repair of induced osteochondral defects of the distal portion of the radial carpal bone in horses by use of periosteal autografts.* Am J Vet Res, 1991. **52**(2): p. 328-32.

215. Nixon, AJ, Hendrickson, DA, Lust, G, and Grande, DA. *Chondrocyte laden fibrin polymers effectively resurface large articular defects in horses.* in *ORS.* 1992. Washington, D.C.

216. Hough, AJ, *Pathology of osteoarthritis*, in *Arthritis and Allied Conditions: A Textbook of Rheumatology*, Koopman, W.J., Editor. 1997, Williams & Wilkins: Balitmore, MD. p. 1945-1984.

217. Arokoski, JP, Jurvelin, JS, Vaatainen, U, and Helminen, HJ, *Normal and pathological adaptations of articular cartilage to joint loading [In Process Citation].* Scand J Med Sci Sports, 2000. **10**(4): p. 186-98.

218. Burr, DB and Schaffler, MB, *The involvement of subchondral mineralized tissues in osteoarthrosis: Quantitative microscopic evidence.* Microscopy Research and Technique, 1997. **37**(4): p. 343-357.

219. Simon, SR, Radin, EL, Paul, IL, and Rose, RM, *The response of joints to impact loading. II. In vivo behavior of subchondral bone.* J Biomech, 1972. **5**(3): p. 267-72.

220. Armstrong, S, Read, R, and Ghosh, P, *The effects of intraarticular hyaluronan on cartilage and subchondral bone changes in an ovine model of early osteoarthritis.* Journal of Rheumatology, 1994. **21**(4): p. 680-8.

221. Armstrong, SJ, Read, RA, and Price, R, *Topographical variation within the articular cartilage and subchondral bone of the normal ovine knee joint: a histological approach.* Osteoarthritis & Cartilage, 1995. **3**(1): p. 25-33.

222. Broom, N and Oloyede, A, *Experimental-Determination of the Subchondral Stress-Reducing Role of Articular-Cartilage under Static and Dynamic Compression.* Clinical Biomechanics, 1993. **8**(2): p. 102-108.

223. Eckstein, F, Muller-Gerbl, M, and Putz, R, *Distribution of subchondral bone density and cartilage thickness in the human patella.* J Anat, 1992. **180 (Pt 3)**: p. 425-33.

224. Milz, S, Eckstein, F, and Putz, R, *Thickness distribution of the subchondral mineralization zone of the trochlear notch and its correlation with the cartilage*

Reproduced with permission of the copyright owner. Further reproduction prohibited without permission.

thickness: an expression of functional adaptation to mechanical stress acting on the humeroulnar joint? Anat Rec, 1997. **248**(2): p. 189-97.

225. Murray, RC, Vedi, S, Birch, HL, Lakhani, KH, and Goodship, AE, *Subchondral bone thickness, hardness and remodelling are influenced by short-term exercise in a site-specific manner.* J Orthop Res, 2001. **19**(6): p. 1035-42.

226. Oegema, TJ, Carpenter, R, Hofmeister, F, and Thompson, R, *The interaction of the zone of calcified cartilage and subchondral bone in osteoarthritis.* Microscopy Research And Technique, 1997. **37**: p. 324-332.

227. Pugh, JW, Radin, EL, and Rose, RM, *Quantitative studies of human subchondral cancellous bone. Its relationship to the state of its overlying cartilage.* J Bone Joint Surg Am, 1974. **56**(2): p. 313-21.

228. Radin, E, Ehrlich, M, Chernack, R, Abernethy, P, Paul, I, and Rose, R, *Effect of repetitive impulsive loading on the knee joints of rabbits.* Clinical Orthopaedics and Related Research, 1978. **131**: p. 288-292.

229. Lane, LB, Villacin, A, and Bullough, PG, *The vascularity and remodelling of subchondrial bone and calcified cartilage in adult human femoral and humeral heads. An age- and stress-related phenomenon.* J Bone Joint Surg Br, 1977. **59**(3): p. 272-8.

230. Farkas, T, Boyd, RD, Schaffler, MB, Radin, EL, and Burr, DB, *Early vascular changes in rabbit subchondral bone after repetitive impulsive loading.* Clin Orthop, 1987(219): p. 259-67.

231. Imhof, H, Breitenseher, M, Kainberger, F, and Trattnig, S, *Degenerative joint disease: cartilage or vascular disease?* Skeletal Radiol., 1997. **26**: p. 398-403.

232. Imhof, H, Breitenseher, M, Kainberger, F, Rand, T, and Trattnig, S, *Importance of subchondral bone to articular cartilage in health and disease.* Topics in Magnetic Resonance Imaging, 1999. **10**(3): p. 180-92.

233. Patel, N and Buckland-Wright, C, *Advancement in the zone of calcified cartilage in osteoarthritic hands of patients detected by high definition macroradiography.* Osteoarthritis Cartilage, 1999. **7**(6): p. 520-5.

234. Bullough, PG, *The geometry of diarthrodial joints, its physiologic maintenance, and the possible significance of age-related changes in geometry-to-load distribution and the development of osteoarthritis.* Clin Orthop, 1981(156): p. 61-6.

Reproduced with permission of the copyright owner. Further reproduction prohibited without permission.

235. Lane, LB and Bullough, PG, *Age-related changes in the thickness of the calcified zone and the number of tidemarks in adult human articular cartilage.* J Bone Joint Surg Br, 1980. **62**(3): p. 372-5.

236. von Rechenberg, B, Guenther, H, McIlwraith, CW, Leutenegger, C, Frisbie, DD, Akens, MK, and Auer, JA, *Fibrous tissue of subchondral cystic lesions in horses produce local mediators and neutral metalloproteinases and cause bone resorption in vitro.* Vet Surg, 2000. **29**(5): p. 420-9.

237. Radin, E, *Factors influencing the progression of osteoarthrosis*, in *Articular Cartilage and Knee Joint Function: Basic Science and Arthroscopy*, Ewing, J.W., Editor. 1990, Raven Press, Ltd.: New York. p. 301-309.

238. Radin, EL, Burr, DB, Caterson, B, Fyhrie, D, Brown, TD, and Boyd, RD, *Mechanical Determinants of Osteoarthrosis.* Seminars in Arthritis and Rheumatism, 1991. **21**(3): p. 12-21.

239. Kawcak, C, *Effects of loading on subchondral bone of equine carpal and metacarpophalangeal joints*, in *Department of Clinical Sciences*. 1998, Colorado State University: Fort Collins.

240. Young, D, Richardson, D, Markel, M, and Nunamaker, D, *Mechanical and morphometric analysis of the third carpal bone of thoroughbreds.* Am. J. Vet. Res., 1991. **52**(3): p. 402-409.

241. Kawcak, CE, Norrdin, RW, Frisbie, DD, Trotter, GW, and McIlwraith, CW, *Effects of osteochondral fragmentation and intra-articular triamcinolone acetonide treatment on subchondral bone in the equine carpus.* Equine Vet J, 1998. **30**(1): p. 66-71.

242. Brama, PA, Bank, RA, Tekoppele, JM, and Van Weeren, PR, *Training affects the collagen framework of subchondral bone in foals.* Vet J, 2001. **162**(1): p. 24-32.

243. Solomon, L, *Pathogenesis of osteoarthritis.* Lancet, 1972. **1**(7759): p. 1072.

244. Meachim, G, *Cartilage fibrillation at the ankle joint in Liverpool necropsies.* Journal of Anatomy, 1975. **119**(3): p. 601-10.

245. Bullough, PG and Walker, PS, *The distribution of load through the knee joint and its possible significance to the observed patterns of articular cartilage breakdown.* Bull Hosp Joint Dis, 1976. **37**(2): p. 110-23.

246. Burr, DB, *The importance of subchondral bone in osteoarthrosis.* Curr Opin Rheumatol, 1998. **10**(3): p. 256-62.

Reproduced with permission of the copyright owner. Further reproduction prohibited without permission.

247. Felson, DT, Lawrence, RC, Dieppe, PA, Hirsch, R, Helmick, CG, Jordan, JM, Kington, RS, Lane, NE, Nevitt, MC, Zhang, Y, Sowers, M, McAlindon, T, Spector, TD, Poole, AR, Yanovski, SZ, Ateshian, G, Sharma, L, Buckwalter, JA, Brandt, KD, and Fries, JF, *Osteoarthritis: new insights. Part 1: the disease and its risk factors.* Ann Intern Med, 2000. **133**(8): p. 635-46.

248. Dedrick, DK, Goulet, RW, O'Connor, BL, and Brandt, KD, *Preliminary report: increased porosity of the subchondral plate in an accelerated canine model of osteoarthritis.* Osteoarthritis Cartilage, 1997. **5**(1): p. 71-4.

249. Pool, RR, *Multidisciplinary investigation of the aetiopathogenesis of parasagittal fractures of the third metacarpal and metatarsal bones of Thoroughbreds.* Equine Vet J, 1999. **31**(2): p. 96.

250. Rick, MC, O'Brien, TR, Pool, RR, and Meagher, D, *Condylar fractures of the third metacarpal bone and third metatarsal bone in 75 horses: radiographic features, treatments, and outcome.* J Am Vet Med Assoc, 1983. **183**(3): p. 287-96.

251. Riggs, CM, Whitehouse, GH, and Boyde, A, *Pathology of the distal condyles of the third metacarpal and third metatarsal bones of the horse.* Equine Vet J, 1999. **31**(2): p. 140-8.

252. Boyde, A, Haroon, Y, Jones, SJ, and Riggs, CM, *Three dimensional structure of the distal condyles of the third metacarpal bone of the horse.* Equine Vet J, 1999. **31**(2): p. 122-9.

253. Mankin, HJ, Mow, VC, and Buckwalter, JA, *Articular Cartilage Repair and Osteoarthritis*, in *Orthopaedic Basic Science*, Simon, S.R., Editor. 2000, American Academy of Orthopaedic Surgeons. p. 471-488.

254. Sah, RL, Doong, JY, Grodzinsky, AJ, Plaas, AH, and Sandy, JD, *Effects of compression on the loss of newly synthesized proteoglycans and proteins from cartilage explants.* Arch Biochem Biophys, 1991. **286**(1): p. 20-9.

255. Sah, RL, Grodzinsky, A, Plaas, A, and Sandy, JD, *Effects of static and dynamic compression on matrix metabolism in cartilage explants*, in *Articular Cartilage and Osteoarthritis*, Kuettner, K.E., Editor. 1992, Raven Press: New York. p. 373-392.

256. Kim, Y, Sah, R, Grodzinsky, A, Plaas, A, and Sandy, J, *Mechanical regulation of cartilage biosynthetic behavior: physical stimuli.* Archives of Biochemistry and Biophysics, 1994. **311**(1): p. 1-12.

257. Sah, RL, Trippel, SB, and Grodzinsky, AJ, *Differential effects of serum, insulin-like growth factor-I, and fibroblast growth factor-2 on the maintenance of*

Reproduced with permission of the copyright owner. Further reproduction prohibited without permission.

cartilage physical properties during long-term culture. J Orthop Res, 1996. **14**(1): p. 44-52.

258. Bonassar, LJ, Stinn, JL, Paguio, CG, Frank, EH, Moore, VL, Lark, MW, Sandy, JD, Hollander, AP, Poole, AR, and Grodzinsky, AJ, *Activation and inhibition of endogenous matrix metalloproteinases in articular cartilage: effects on composition and biophysical properties.* Arch Biochem Biophys, 1996. **333**(2): p. 359-67.

259. Lafeber, F, Veldhuijzen, JP, Vanroy, JL, Huber-Bruning, O, and Bijlsma, JW, *Intermittent hydrostatic compressive force stimulates exclusively the proteoglycan synthesis of osteoarthritic human cartilage.* Br J Rheumatol, 1992. **31**(7): p. 437-42.

260. Mow, VC, Wang, CC, and Hung, CT, *The extracellular matrix, interstitial fluid and ions as a mechanical signal transducer in articular cartilage.* Osteoarthritis Cartilage, 1999. **7**(1): p. 41-58.

261. Patwari, P, Cook, MN, DiMicco, MA, Blake, SM, James, IE, Kumar, S, Cole, AA, Lark, MW, and Grodzinsky, AJ, *Proteoglycan degradation after injurious compression of bovine and human articular cartilage in vitro: interaction with exogenous cytokines.* Arthritis Rheum, 2003. **48**(5): p. 1292-301.

262. Setton, L, Elliott, D, and Mow, V, *Altered mechanics of cartilage with osteoarthritis: human osteoarthritis and an experimental model of joint degeneration.* Osteoarthritis and Cartilage, 1999. **7**: p. 2-14.

263. LeRoux, MA, Arokoski, J, Vail, TP, Guilak, F, Hyttinen, MM, Kiviranta, I, and Setton, LA, *Simultaneous changes in the mechanical properties, quantitative collagen organization, and proteoglycan concentration of articular cartilage following canine meniscectomy.* J Orthop Res, 2000. **18**(3): p. 383-92.

264. Elliott, DM, Jones, R, 3rd, Setton, LA, Scully, SP, Vail, TP, and Guilak, F, *Joint degeneration following meniscal allograft transplantation in a canine model: mechanical properties and semiquantitative histology of articular cartilage.* Knee Surg Sports Traumatol Arthrosc, 2002. **10**(2): p. 109-18.

2 ADULT EQUINE CARTILAGE AND SUBCHONDRAL BONE PROPERTIES: STIFLE AND METACARPOPHALANGEAL JOINT

Reproduced with permission of the copyright owner. Further reproduction prohibited without permission.

2.1 Introduction

There is a strong interdependency between the structure and function of articular cartilage. Changes in structure produce alterations in function and/or functional changes cause structural modifications often leading to pathologies [1]. For example, focal injuries to the structure of the joint lead to degradation of function through necrosis of articular cartilage and underlying bone often leading to chronic debilitating osteoarthritis (OA) [2]. Similarly, age or disease-associated structural changes in cartilage are correlated with a loss in function, ultimately leading to OA. OA is the most frequent musculoskeletal diagnosis and disability [3].

Animal models are often used to better understand the etiology of cartilage degeneration, healing, and treatment modalities for damaged cartilage. The equine (horse) model has proven to be an effective model for osteoarthritis, cartilage healing, and/or exercise effects on the musculoskeletal system [4-14]. The equine model has many advantages over other animal models including: similar articular cartilage thickness to human joints, large articular surface area, ability to apply controlled exercise treatments, and joint loading is comparable to the human.

Although many articular cartilage studies have been conducted using the equine model [7-9, 11, 15-26], minimal data exists on baseline structural and mechanical properties of equine cartilage. Joints of particular interest in the equine model include the

Reproduced with permission of the copyright owner. Further reproduction prohibited without permission.

stifle and metacarpophalangeal joints due to similarities in joint loading in humans and prevalence of naturally occurring OA, respectively.

The stifle joint (analogous to the human knee joint) is often used for cartilage healing studies [12, 17, 27, 28]. The stifle is comprised of two articulations, the femorotibial (condyles of the femur with the meniscus and tibia) and femoropatellar (femoral trochlea with the patella) joints. The femorotibial joint is a simple condylar articulation providing flexion and extension motion with predominant compression loading and minimal ad- and abduction motions, while simple gliding action (compression and shear) predominates within the femoropatellar joint [29]. The low weight-bearing medial trochlear ridge (MTR) of the femoropatellar joint and the high weight-bearing areas of the medial femoral condyle (MFC) of the femorotibial joint are often used for cartilage regeneration studies (Figure 2.1A) [9, 16, 21, 22, 30-33].

The metacarpophalangeal joint (MCP) (analogous to the human finger joint) is a composite hinge joint composed of the distal 3rd metacarpal, proximal phalanx, and proximal sesamoid bones [29]. The primary motions of the joint are flexion and extension [29] with both compression and shear loading. Within the MCP joint, the palmar aspect is the most vulnerable to osteochondral degeneration relative to its dorsal surface due to the high compression loading by the proximal sesamoid bones (Figure 2.1B) [2, 34]. Also, naturally occurring subchondral bone sclerosis has been noted in the dorsal aspect of the 1st phalanx within notably more cartilage degeneration over sclerotic bone regions [35]. The sesamoid bones are part of the equine's suspensory stay apparatus noted to provide elastic storage and propulsion during locomotion [34, 36].

Reproduced with permission of the copyright owner. Further reproduction prohibited without permission.

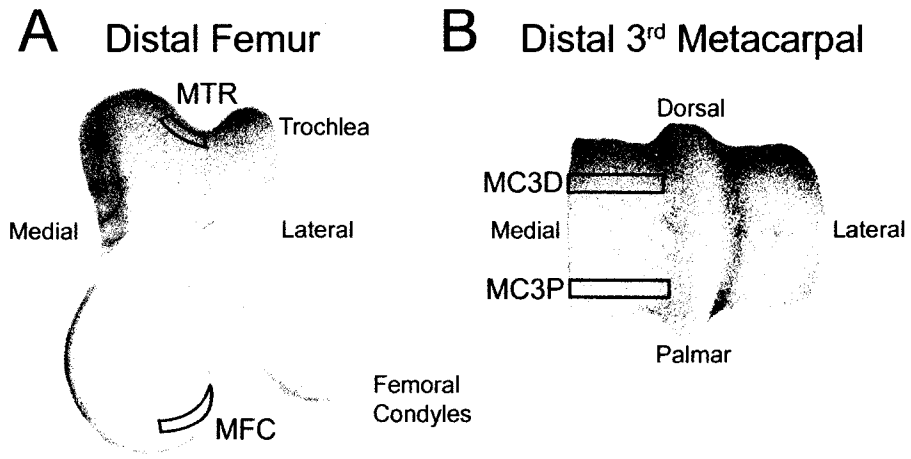

Figure 2.1: Articular surfaces of the distal femur (A) and distal 3rd metacarpal (MC3, B) bones. Distal femur samples were taken from the medial trochlear ridge (MTR) and medial femoral condyle (MFC), while distal 3rd metacarpal samples were taken from the medial dorsal (MC3D) and palmar (MC3P) aspects illustrated above. Note: Illustrations are not to scale.

Baseline or normal structural and material properties of stifle and MC3 could help to direct future veterinary/human research efforts in joint degeneration, cartilage healing, and tissue engineering. Based on the geometric differences and functional demands, it is hypothesized that the MC3 structural and material properties would differ from those of the stifle, as well as regionally. In addition, subarticular bone mineral density is hypothesized to correspond with articular cartilage properties [37-49]. To test these hypotheses, normal baseline structural and material properties of equine articular cartilage and underlying subarticular bone mineral density within the stifle (MFC/MTR) and MC3 (MC3P/MC3D) joints were quantified. Cartilage structure was characterized by cartilage thickness and surface degeneration, while *ex-vivo* material properties of cartilage were evaluated using static and dynamic tensile and compression loading.

Reproduced with permission of the copyright owner. Further reproduction prohibited without permission.

2.2 Materials and Methods

2.2.1 Sample Background

Tissue samples were acquired from an unrelated study involving three horses receiving carpal defects, while the remaining five received no defect. All horses underwent routine physical exams including lameness evaluations and blood panels before acceptance into the primary study. All horses were run on a high-speed treadmill 5 days/week for 3 weeks, 2 weeks off without running (defect created in carpal of treated horses), followed with 9 weeks of treadmill exercise 5 days/week. Daily exercise consisted of trotting (16-19km/hr) for two minutes, then two minutes of galloping (32 km/hr), and slowing down to a trot (16-19 km/hr) for the last two minutes. The influence of the carpal defect on the measured responses of the stifle and MC3 samples was statistically evaluated (see Appendix A for more sample history).

2.2.2 Tissue Acquisition

Bilateral MC3 and stifle samples were collected at necropsy from eight horses (age=2 years, weight=3190±418 Newtons (Mean±STD)) involved in the project described above. Tissues were collected within 4 hours of death. All structures were visually and manually inspected for normality (articular surfaces, ridges, synovial membranes, and superficial bone) before inclusion in the study. Joint areas of interest were harvested bilaterally (trochlear ridge, femoral condyles, and the 3rd metacarpal) using a band saw. The articular surface was kept hydrated during sample preparation using sterile phosphate buffered solution (PBS) mixed with proteinase inhibitors (PIs; 20mM disodium ethylenediamine tetraacetate, 10mM phenylmethanesulfonyl fluoride, 50mM benzamidine-HCl, and 10mM N-ethylmaleimide [50]). Osteochondral samples

Reproduced with permission of the copyright owner. Further reproduction prohibited without permission.

were wrapped with PBS+PIs soaked gauze and stored at -20°C until more precise sample preparation and record keeping were performed. Osteochondral blocks were thawed at room temperature, digital images were taken of all joint surfaces, and the samples were prepared to the desired geometry (10x10x10mm) using an Exakt® Cutting System (Exakt Technologies, Oklahoma City, OK) with PBS used as cooling fluid. Stifle samples from the medial femoral condyle were excised from a region, which predominately articulates with the tibia's medial condyle (medial femoral condyle (MFC), high-weight bearing, Figure 2.1A). Samples from the trochlear ridge were taken from the medial aspect of the trochlea (medial trochlear ridge (MTR), low-weight bearing, Figure 2.1A). The MFC and MTR regions were selected for their common use in cartilage regeneration studies [9, 16, 21, 22, 30-33]. Lastly, the MC3 samples were cut from the 3rd metacarpal, one centimeter palmar and dorsal from the transverse ridge (medial palmar (MC3P) and medial dorsal (MC3D), respectively (Figure 2.1B). The MC3 samples, MC3P and MC3D, were selected for their notable osteochondral changes during OA [2, 10, 51-57]. After samples were prepared, they were preserved in PBS+PIs soaked gauze at –20°C until testing.

2.2.3 Structural Properties of Cartilage

2.2.3.1 India Ink Staining

Samples were thawed to room temperature (~22°C) and the uptake of India ink was quantified as an indicator of surface degradation/fibrillation [58, 59]. Two pre-ink digital images of the articular surface were acquired prior to ink application with/without the template. The template was placed within the field of view to provide spatial and grayscale calibration targets to allow normalization between samples. India ink diluted with PBS+PIs (1:5) was painted on the cartilage surface and allowed to penetrate for ten

Reproduced with permission of the copyright owner. Further reproduction prohibited without permission.

seconds. Excess ink was carefully removed and a post-ink image was acquired. The pre- and post-ink images were evaluated for gray level intensity relative to the calibration standards using NIH Image (NIH, USA). The average gray levels were determined for the calibration targets (black (gray#19, $G19_{Mean}$), gray (gray#3, $G3_{Mean}$)) and post-ink region of interest (Ink_{Mean}, 25 mm^2 area) for each image. The reflectance score was calculated using the following formula:

$$RS = \frac{(G19_{Mean} - Ink_{Mean})}{(G19_{Mean} - G3_{Mean})} \qquad \textbf{Equation 2.1}$$

The RS score is inversely related to cartilage surface ink uptake, and thus cartilage fibrillation. As the mean gray value increases, the RS values decreases (↑ fibrillation = ↑ ink uptake = ↓ reflectance score).

2.2.3.2 Cartilage Thickness

Using a Nikon 920 digital camera (1600x1200 pixels), images of each sample with a spatial calibration template were taken to measure cartilage thickness. Using ImageJ (NIH, USA), cartilage thickness for each sample determined (average of five equally spaced locations perpendicular to the cartilage surface).

2.2.3.3 Water Content of Residual Cartilage

Cartilage samples were lyophilized and wet and dry weights (WW and DW, respectively) were taken from the tissue adjacent to the tested tensile and compression samples [60, 61]. Percent water content (WC) was determined using the following formula:

Reproduced with permission of the copyright owner. Further reproduction prohibited without permission.

$$WC = \frac{(WW - DW)}{WW} \times 100 \qquad \textbf{Equation 2.2}$$

2.2.4 Material Properties of Cartilage

2.2.4.1 Tensile Testing

Each 10x10x10mm osteochondral block sample was cut further to produce 3x10x10mm and 7x10x10mm blocks. Using the 3x10x10 portion, the first 300μm from the articular cartilage surface was sectioned from sample in predetermined tensile regions using a vise-equipped microtome. The superficial section was then cut into dumbbell-shaped specimens having a 0.8mm gage width and 4mm length using a custom-trephine. The long-axis of the tensile specimens was aligned perpendicular to the splitline direction. Stifle samples from unpublished work [62] were used to determine predominant splitline directions using the techniques similar to O'Connor [63] and all MC3 tensile samples were oriented perpendicular to joint motion. Each tensile gage thickness was determined (average of three measurements) in the unloaded state using a custom contact sensing micrometer (1μm resolution) to determine the cross-sectional area [60]. Using a micro-testing machine (Biosyntech, Quebec, Canada), all samples were tested using techniques previously published [60]. Briefly, the testing involved applying a tare load of 0.05N (0.2 MPa), followed by a constant displacement (0.25%/s) to a nominal strain of 10% and 20% (grip-to-grip distance, 4mm) while stress relaxation was monitored between each strain level until equilibrium (900 seconds). The samples were pulled to failure (5mm/min) following the 20% stress relaxation. Tensile equilibrium modulus was determined as the slope of the equilibrium stress-strain points via linear regression. Tensile dynamic stiffness was calculated as the slope of the stress-strain curve between 25-75% failure strain, while tensile strength and failure strain were

Reproduced with permission of the copyright owner. Further reproduction prohibited without permission.

taken as the maximum stress and strain at failure. All samples were tested under constant irrigation (tensile) or immersed (compression, below) in PBS at room temperature (~22°C).

2.2.4.2 Compression Testing

Only compression data was acquired for the MFC and MTR samples, since the articular cartilage thicknesses of the MC3 samples were less than 1mm and, thus too thin to determine accurate compression properties. Using a microtome and the 7x10x10mm portion of each sample, the first 1mm from the articular surface was sectioned off and stamped with a trephine to produce 4.8mm diameter disks. The average disk thickness was measured using a custom contact-sensing micrometer in six predetermined areas of the disk. Both static and dynamic compression tests perpendicular to the articular surface were performed at 15%, 30%, and 45% strain offsets [61]. Estimates of free swelling confined compression modulus (H_{A0}) were obtained using large deformation theory for soft hydrated connective tissue using a nonlinear least-squares regression (with d_1=0.9) [64]. The equilibrium modulus for each offset was estimated. Permeability (k_p) for each strain level was estimated by nonlinearly fitting the theoretical open-circuit stress solution with the amplitude and phase of the dynamic stiffness from experimental data [50, 65]. The estimated k_p values for each strain level were used to estimate the strain-dependent parameter, M [66]. Permeability and the strain-dependent parameter estimate the deformation dependent extracellular fluid flow behavior within cartilage.

Reproduced with permission of the copyright owner. Further reproduction prohibited without permission.

2.2.5 Subarticular Bone Mineral Density

Bone mineral density of subarticular bone was measured using a dual energy x-ray absorbtiometry scanner (DEXA, Hologic Delphi QDR; Bedford, MA) using the high-resolution settings and small animal software package. Subarticular scan area was set to 5.2 x 5.2 mm^2 in the plane perpendicular to the articular surface. The mean of three independent scans was used to quantify the area bone mineral density, μ_{BMD} ($grams/cm^2$). Subarticular volumetric bone mineral density (BMD, $grams/cm^3$) was calculated by dividing the area bone mineral density by the thickness of sample, *thickness*. Mean sample thickness was determined from five equally spaced locations along the scan plan with a micrometer with a 0.001mm resolution (Mitutoyo America Corporation, Aurora, IL, USA). In summary, volumetric BMD was calculated using the following formula:

$$BMD = \frac{\mu_{BMD}}{thickness} \qquad \text{Equation 2.3}$$

2.3 Statistical Analysis

The effects of side (R/L), sample location (MFC, MTR, MC3P, MC3D), and carpus treatment (unrelated study), along with two-way interactions were determined using a mixed model with SAS statistical software at a significance level of $\alpha = 0.05$ (SAS Institute Inc., Cary, NC, USA). Since some horses had a treatment on either the left or right carpus, the only random effect considered was horse within treatment. If significant effects were noted, Tukey's post-hoc comparisons were performed to determined differences within levels of the factor. Lastly, a mixed-model analysis of covariance determined if the subarticular bone mineral density had any effects on cartilage structural/material properties. When significant differences were noted between

Reproduced with permission of the copyright owner. Further reproduction prohibited without permission.

sample locations, separate plots were generated. See Appendix A for SAS algorithms used.

2.4 Results

Tensile equilibrium modulus, dynamic stiffness, and strength responses required a square-root transformation, while a $\log_{10}$ transformation was needed for cartilage thickness and failure strain to satisfy normal distribution assumptions. There was no significant effect from the unrelated earlier study's treatment (i.e. carpal defect) for all response variables (all $p>0.4$). Data for all response variables sorted by joint location are presented in Table 2.1.

2.4.1 Cartilage Structure

2.4.1.1 Thickness

The cartilage thickness measurement method had a variability of 9% (CV). Eight samples (8/64) were not imaged or analyzed since they were accidentally excluded. Differences between the right and left side for each location were not significantly different ($p=0.7$). There were significant differences between sample locations ($p<0.0001$, Figure 2.2A). The MFC had significantly thicker cartilage than all other locations ($p<0.0001$, Figure 2.2A). No significant differences were noted between the MC3 locations (MC3P vs. MC3D, $p=0.7$, Figure 2.2A). Taken together, the femoral regions (MFC and MTR) were more than 195% thicker than both MC3 regions ($p<0.001$, Figure 2.2A, see Appendix A for p-values).

Reproduced with permission of the copyright owner. Further reproduction prohibited without permission.

2.4.1.2 India Ink Staining

Wear lines were grossly observed on the articular surface of 25% (2/8) of the MC3 samples. One sample was taken out of the analysis due to substantial rigid body motions between the unstained and stained image, which made image analysis impossible. Surface staining was not significantly dependent on side (R/L) for each location ($p=0.4$), although there were significant differences between locations alone (Figure 2.2B). The reflectance scores for the stifle were generally greater (MTR), indicating less degeneration, than the MC3 locations ($p<0.005$, Figure 2.2B). However, there was no significant difference found between MFC and MTR ($p=0.2$) or between MC3P and MC3D ($p=0.5$, Figure 2.2B, see Appendix A for p-values).

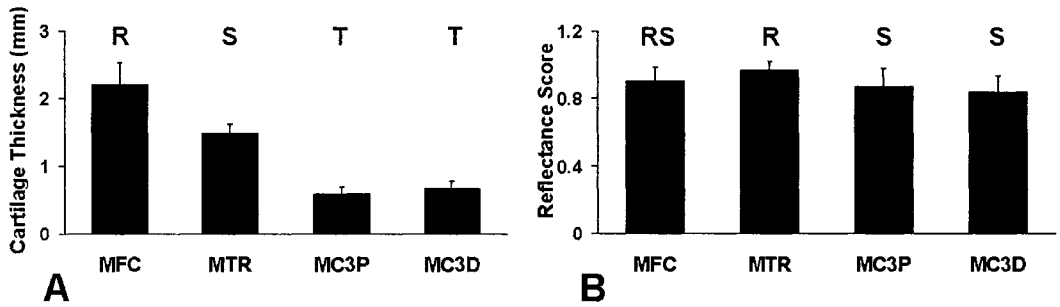

Figure 2.2: Cartilage structural properties (A) cartilage thickness (mm), and (B) reflectance score for each location. Significant differences ($p<0.05$) between areas are noted with different letters. Mean $\pm$ STD.

2.4.1.3 Water Content

Side and sample location showed very little influence on residual cartilage water content ($p=0.5$ and $p=0.9$, respectively). Therefore, the mean water content averaged over all regions and sides was: $70.8 \pm 2.4\%$.

Reproduced with permission of the copyright owner. Further reproduction prohibited without permission.

2.4.2 Cartilage Material Properties

2.4.2.1 Tensile

The average thickness of the prepared samples was 0.38±0.09mm. There were no significant differences in prepared sample thickness between locations ($p=0.4$). Two samples were not tested, due to testing system failure and sample preparation. Sample location was the only significant effect found for all tensile parameters ($p<0.005$). The tensile equilibrium modulus within the MC3 was significantly larger than stifle regions ($p<0.05$, Figure 2.3A), but sample locations within these regions were not significantly different (MC3P = MC3D, $p=0.17$; MFC = MTR, $p=0.41$).

Tensile dynamic stiffness showed similar differences (MC3>stifle, $p<0.05$). Additionally, MFC had a significantly smaller tensile dynamic stiffness compared to all other regions ($p<0.05$, Figure 2.3B). There were no tensile dynamic stiffness differences between MC3 locations (MC3P and MC3D). The MFC tensile strength at failure was significantly smaller than all other locations ($p<0.005$, Figure 2.3C). No tensile strength differences were noted between MTR, MC3P, and MC3D ($p>0.7$, Figure 2.3C). Lastly, MTR failed at a higher strain (grip-to-grip) than MC3P ($p<0.05$, Figure 2.3D). See Appendix A for p-values of all the statistical comparisons.

Reproduced with permission of the copyright owner. Further reproduction prohibited without permission.

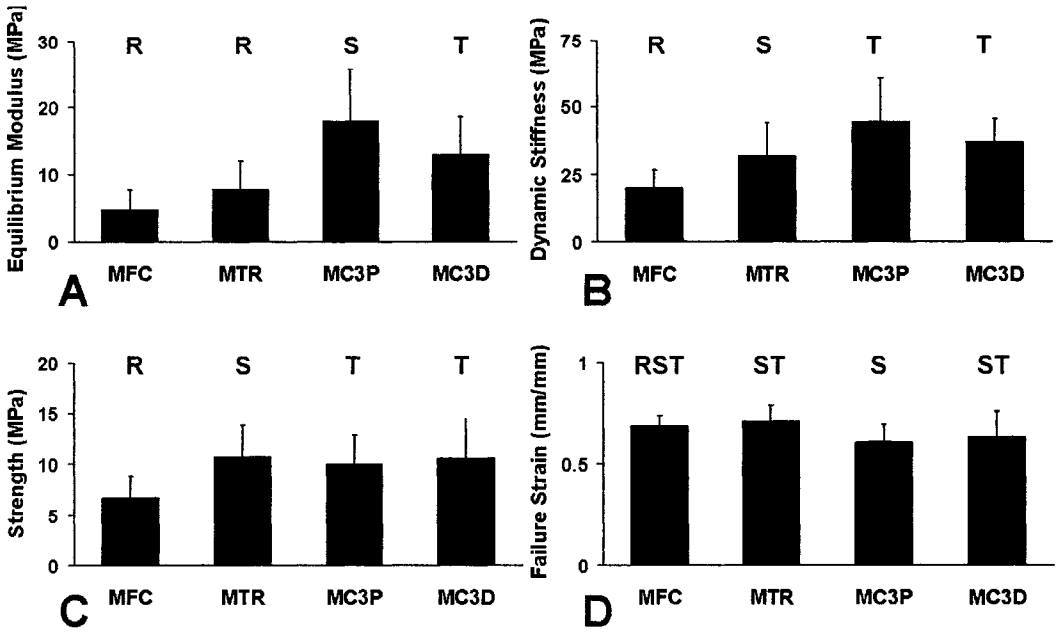

Figure 2.3: Tensile response parameters determined (A) tensile equilibrium modulus (B) tensile dynamic stiffness (C) tensile strength (D) tensile failure strain. Significant differences ($p<0.05$) between areas are noted with different letters. Mean $\pm$ STD.

2.4.2.2 Compression

Side did have a significant effect on compression responses ($p>0.4$). No compression modulus differences between MFC and MTR were detected ($p=0.8$, Figure 2.4A). While there was no interaction between location and strain for permeability ($p=0.6$), there was a difference between strain levels ($p<0.005$, Figure 2.4B). The depth-dependent parameter, M, was not significantly different between the two femoral locations ($p=0.3$, Figure 2.4C). See Appendix A for p-values of all the statistical comparisons.

Reproduced with permission of the copyright owner. Further reproduction prohibited without permission.

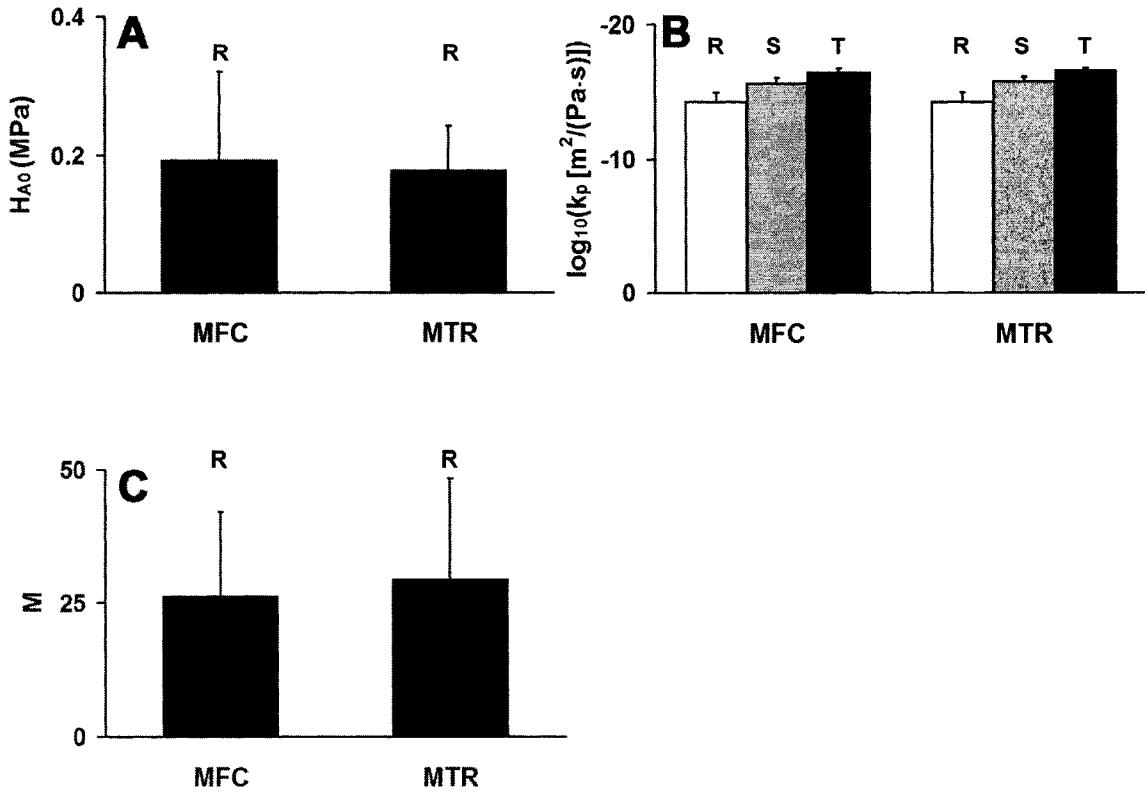

Figure 2.4: Confined compression response parameters for each stifle location (A) equilibrium confined compression modulus at free-swelling thickness; (B) hydraulic permeability, k_p (m^2/(Pa·s), at offset compression strain levels 15% (□), 30% (▒), and 45% (■) relative to the free-swelling thickness; (C) strain-dependent parameter, M. Significant differences ($p<0.05$) between areas are noted with different letters. Mean± STD.

2.4.3 Subarticular Bone Mineral Density

The determined intra-sample variability (CV) for the area-based BMD measurements from DEXA was less than 1%, but increased to 5% for volumetric BMD. Four samples were not scanned due to substantially unparallel faces. There were no significant interactions or side effect ($p>0.6$), but sample location had a significant effect on volumetric BMD ($p<0.005$, Figure 2.5). The MC3P region of the MC3 had the largest BMD ($p<0.005$), 85% more dense than the low-weight bearing region of the stifle joint, MTR (Figure 2.5). Also, the BMD was 21% greater in the palmar portion of the MC3 (MC3P) than its dorsal counterpart (MC3D, $p<0.005$, Figure 2.5). The high-weight

Reproduced with permission of the copyright owner. Further reproduction prohibited without permission.

bearing MFC region had a 26% larger BMD than the low-weight bearing MTR (Figure 2.5). See Appendix A for p-values of all the statistical comparisons.

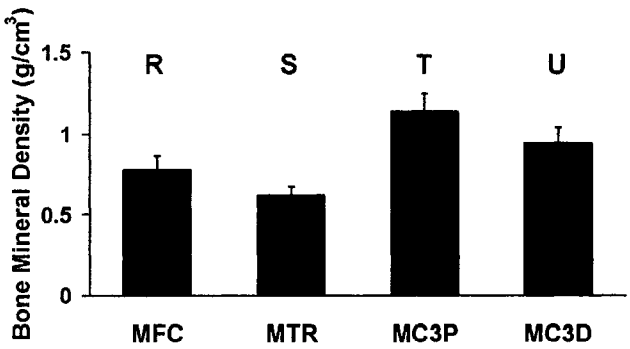

Figure 2.5: Subarticular bone mineral density for each location. Note: Regions were significantly different from each other. Significant differences ($p<0.05$) between areas are noted with different letters. Mean ± STD.

All the cartilage structural and material properties (*Section 2.4.2*) and subarticular bone mineral densities (*Section 2.4.3*) are summarized in Table 2.1.

2.4.4 Relationship between Cartilage Properties and Bone Mineral Density

The tensile equilibrium modulus had a significant positive relationship with BMD ($p=0.05$, Figure 2.6A), while dynamic stiffness ($p=0.5$), strength ($p=0.14$), failure strain ($p=0.4$), and cartilage thickness ($p=0.1$) were found to have non-significant relationships with underlying BMD (Figure 2.6B-E). A negative relationship was found between the reflectance score and BMD averaged over sample locations ($p=0.03$, Figure 2.6F). There were non-significant correlations between water content and BMD ($p=0.7$) and BMD with any of the compression responses (H_{A0}, k_p, and M; all $p>0.8$).

Reproduced with permission of the copyright owner. Further reproduction prohibited without permission.

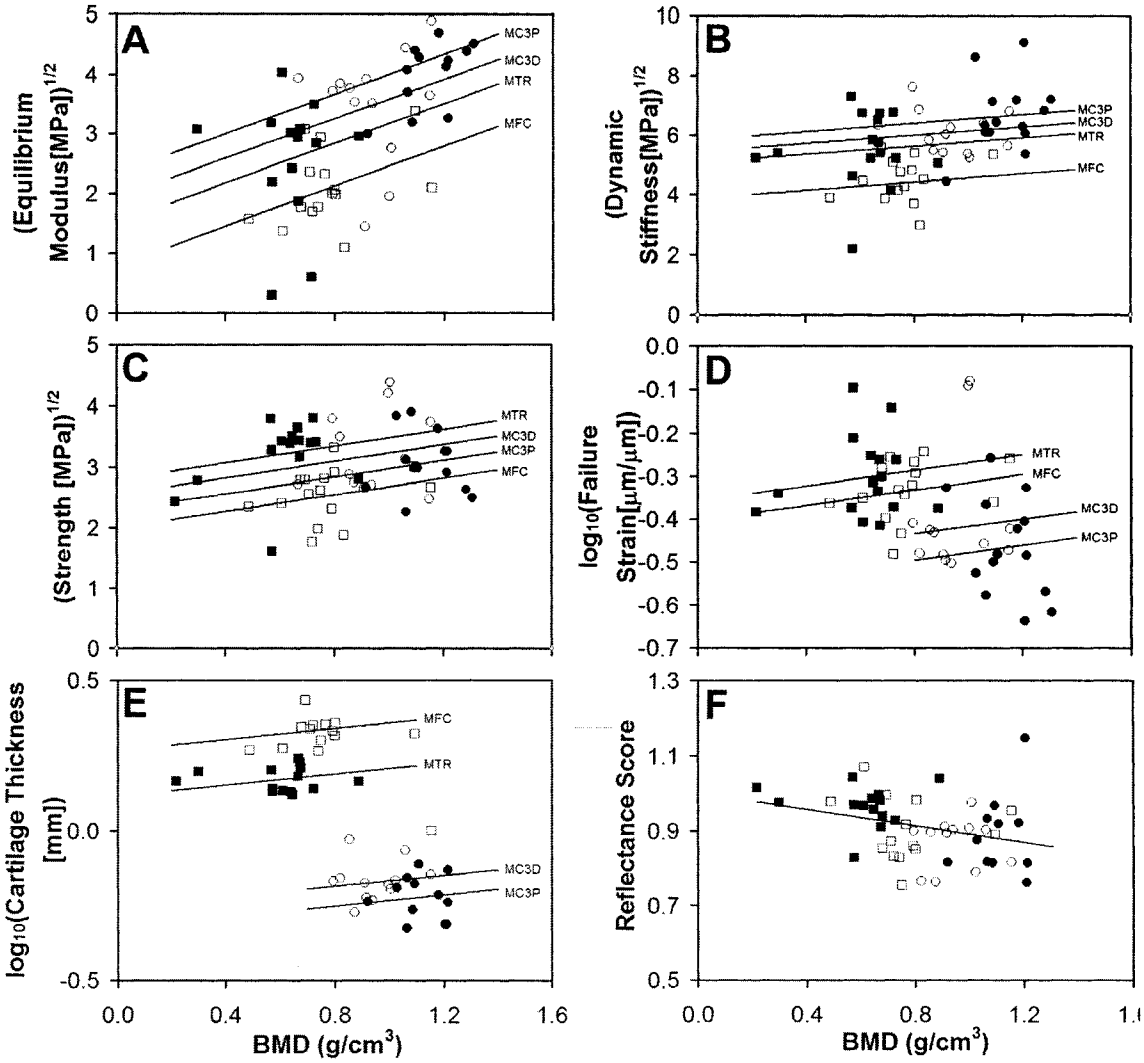

Figure 2.6: Linear relationships between overlying cartilage properties and underlying subchondral bone mineral density (BMD). Linear regressions are shown for (A) tensile equilibrium modulus, (B) tensile dynamics stiffness, (C) tensile strength, (D) tensile failure strain, (E) cartilage thickness, and (F) reflectance score versus BMD for the (□) MFC, (■) MTR, (○) MC3D, and (●) MC3P.

Reproduced with permission of the copyright owner. Further reproduction prohibited without permission.

Reproduced with permission of the copyright owner. Further reproduction prohibited without permission.

Dependent Responses				MFC	MTR	MC3D	MC3P
Cartilage	*Structure*	Cartilage Thickess (mm)		2.20 ± 0.33	1.48 ± 0.13	0.58 ± 0.11	0.67 ± 0.11
		Reflectance Score		0.90 ± 0.08	0.97 ± 0.06	0.87 ± 0.11	0.84 ± 0.10
				n = 14	n = 13	n = 14	n = 14
		Water Content (%)		68 ± 13%	73 ± 25%	70 ± 9%	73 ± 16%
	Tensile	Equilibrium Modulus (MPa)		4.76 ± 2.92	7.71 ± 4.25	17.88 ± 7.85	12.98 ± 5.57
		Dynamic Stiffness (MPa)		19.95 ± 6.75	31.72 ± 12.40	44.30 ± 16.43	36.90 ± 8.52
		Strength (MPa)		6.65 ± 2.19	10.68 ± 3.21	9.93 ± 2.89	10.58 ± 4.16
		Failure Strain (mm/mm)		0.68 ± 0.05	0.71 ± 0.08	0.60 ± 0.09	0.63 ± 0.13
				n = 15	n = 16	n = 15	n = 16
	Compression	Compression Modulus, H_{A0} (MPa)		0.19 ± 0.13	0.18 ± 0.07	Not Tested	Not Tested
		Permeability $\log_{10} k_p$ (m^2/(Pa*s))	15%	-14.28 ± 0.69	-14.26 ± 0.72		
			30%	-15.61 ± 0.43	-15.78 ± 0.32		
			45%	-16.41 ± 0.31	-16.59 ± 0.21		
		Strain-dependent parameter, M		26.20 ± 15.96	29.20 ± 19.21		
				n = 10	n = 10		
Bone		Bone Mineral Density (g/cm^3)		0.78 ± 0.16	0.62 ± 0.16	0.94 ± 0.14	1.14 ± 0.10
				n = 16	n = 16	n = 14	n = 14

Table 2.1: All responses for cartilage and subarticular bone are presented: sample mean ± standard deviation and sample sizes (n).

2.5 Discussion

Equine articular cartilage properties and subarticular bone mineral density varied between the MC3 and stifle locations demonstrating the importance of physiological loading history and joint geometry. The MC3 experiences tremendous stresses due to the small surface area and high loading (up to 2-3 times body weight during gait, [67]). On the contrary, the stifle joint withstands lower stresses and has a much larger articular contact surface area compared to the MC3. The MCP acts as the primary shock absorber within the forelimb, whereas the stifle and other joints (tarsal and fetlock) work in conjunction to absorb forces in the hind limb [36]. The MC3 surface has adapted to its environment with greater BMD and thin cartilage to minimize tissue strains. The patellofemoral joint (MTR) primarily accommodates shear loads applied by the patella (cartilage is thicker stiffer, and stronger than MFC), whereas the MFC is primarily in compression with the meniscus and tibial plateau (greater BMD, softer, and weaker than MTR) [29]. Also, the range of motion during physiological loading differs between these joints with the MCP (MC3) spanning ~88 degrees compared to the femorotibial joint (MFC) spanning 55 degrees [29, 36]. The lower reflectance scores (cartilage fibrillation) noted for the MC3 compared to the stifle probably are due to greater range of motion and stresses on the MCP. Furthermore, the higher MC3 tensile equilibrium moduli and dynamic moduli would accommodate these large tensile and shear stresses applied to the highly mobile joint. Interestingly, the palmar aspect of the MC3 only had greater BMD compared to the dorsal aspect, though the palmar aspect shows more degenerative changes clinically possibly due to higher contact stresses [51].

Reproduced with permission of the copyright owner. Further reproduction prohibited without permission.

Functional adaptations of the MC3 were also noted due to contrasting stress histories between the palmar and dorsal aspects (MC3P and MC3D). Higher loads are applied to the palmar aspect of the 3rd metacarpal compared to the dorsal aspect due to the equine's suspensory stay apparatus (connective tissue structures to lock joints during stance and are the main mechanism for locomotion) [29, 34]. The palmar aspect of the joint adapts to this physiological loading by increasing tensile properties (equilibrium modulus and stiffness) and subarticular bone mineral density. The presence of greater palmar bone mineral density coincides with regional loading estimates [34]. This study supports that adaptive mechanisms may take place within both cartilage and bone to withstand physiological demands *in-vivo* [68]. Similar possible adaptations and variations between joints have been documented for the human knee and ankle [44, 69]. The ankle joint (similar to the MC3) has thinner cartilage and appears to have more joint congruency than the knee (similar to the stifle) [70, 71]. Cartilage from the ankle is less compliant (stiffer) compared to the distal femur of the knee [69], possibly due to their differing stress environments.

Cartilage and bone properties have been found to vary by joint and location within the joint [44, 69, 72-74]. Therefore, differences in structure and function of articular tissues may be related to the "stress history" of each location [75, 76]. Comparing and contrasting the material properties at the MFC and MTR regions in the stifle joint supports this concept. Hypothetically, the MFC experiences primarily compression while the MTR experiences compression as well as shear and tension forces due to the sliding of the overlying patella. The larger BMD found in the MFC compared to the MTR may be related to greater applied MFC compressive loading (i.e.

Reproduced with permission of the copyright owner. Further reproduction prohibited without permission.

adaptation/remodeling). Similarly, the shear loading of the MTR by the patella provides impetus for the articular cartilage to have greater tensile modulus and strength compared to the MFC.

The effects of gender, animal breed, age, freeze-thaw cycles, and splitline direction (superficial collagen orientation) on cartilage material properties and/or bone mineral density are significant [77-85]. Gender, breed, and age were not controlled in this study and may have contributed to response variability. All tissues underwent two freeze-thaw cycles; therefore comparisons within the current study most likely would not be affected, but comparisons to other studies should consider the number of freeze-thaw cycles. Articular cartilage splitline direction has significant effects on the tensile properties [86]. In this study, the splitline direction was based on unpublished equine pilot data on a separate group of specimens and the assumption the MC3 splitline direction was aligned with the joint motion direction. These estimates of collagen orientation may have contributed to variability in tensile properties.

Human subarticular bone density has been correlated with overlying articular cartilage properties [40, 42, 87-90]. In this study, subarticular bone mineral density was positively related to tensile equilibrium modulus, extending this relationship to the equine species. Cartilage equilibrium modulus is independent of fluid exudation and dependent on collagen and collagen crosslink content. The same stress history initiating adaptation within the subarticular bone may also stimulate adaptation in articular cartilage by prompting chondrocytes to synthesize more collagen and crosslinks [91]. It must be noted that the samples were tested perpendicular to the splitline direction, therefore, the

Reproduced with permission of the copyright owner. Further reproduction prohibited without permission.

effects of collagen crosslinks were predominately tested, compared to collagen fibrils aligned with the splitline.

This positive trend between equilibrium modulus and underlying bone mineral density may start to become negative in early stages of OA. Although not found in this study, increasing the sample size of the compression samples may provide relationships between subarticular bone and overlying compression properties. Inconsistent with other reports, the cartilage water content did not correlate with tensile properties [60]. Systematic errors such as lengthy sample storage and/or the need to lyophilize samples twice may have caused these errors. There were large distinctions between trabecular (less dense) and subchondral bone (more dense) noted in the topographical bone mineral density profiles (Figure 2.7). The stifle regions (MFC/MTR) displayed very thin high-density subarticular plates, whereas the MC3 samples (MC3P/MC3D) had substantially thicker high-density subarticular plates (Figure 2.7). Therefore, the regional subarticular

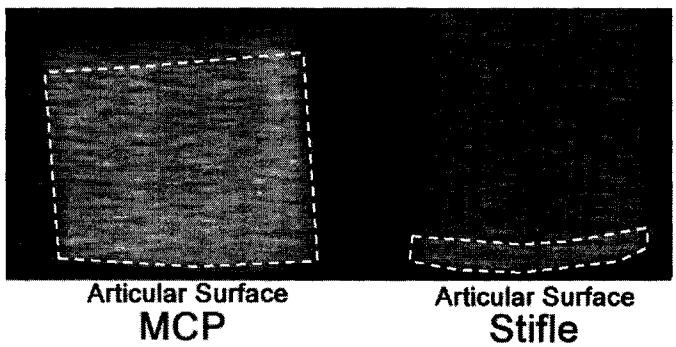

Figure 2.7: A typical DEXA scan topographical output (↑ intensity/white = ↑ density) is illustrated to note the visual difference between a MC3 and stifle sample bone mineral density distributions. MC3 samples have a thicker subchondral bone plate (highlighted dotted line), while the stifle samples have a markedly thinner subchondral bone plate.

bone mineral density differences found in this study may reflect differences in regional subchondral bone plate thicknesses due to the fixed area of analysis used for the bone mineral density measurement using DEXA. The BMD variations between joints found in

Reproduced with permission of the copyright owner. Further reproduction prohibited without permission.

this study was consistent with others showing subchondral bone variations with articular geometry and physiological loading [13, 38, 46, 47, 68, 89, 92-97].

2.6 Conclusion

This study presents the first comparative dataset of equine cartilage structural/material properties and the relationship between cartilage properties and underlying subchondral bone density for the palmar and dorsal aspect of the medial condyle of the 3rd metacarpal (MC3), medial trochlear ridge (MTR), and the medial femoral condyle (MFC). A positive correlation between cartilage tensile equilibrium modulus and underlying bone mineral density was found. Recommendations for future work include determining the effects of age, exercise, OA, sample orientation, subchondral bone thickness, and biochemical content on these properties and relationships.

2.7 References

1. Mankin, HJ, *The response of articular cartilage to mechanical injury.* J Bone Joint Surg [Am], 1982. **64**(3): p. 460-6.

2. Pool, RR, *Traumatic injury and osteoarthritis.* Joint Disease in the Horse, ed. McIlwraith, C.W. and Trotter, G.W. 1996, Philadelphia: W.B. Saunders Co. 87-104.

3. CDC&Prevention, *Targeting arthritis: The nation's leading cause of disability.* 1999, At-A-Glance, URL: www.cdc.gov/nccdphp/art-aag.htm.

4. Howard, RD, McIlwraith, CW, Trotter, GW, Powers, BE, McFadden, PR, Harwood, FL, and Amiel, D, *Long-term fate and effects of exercise on sternal cartilage autografts used for repair of large osteochondral defects in horses.* Am J Vet Res, 1994. **55**(8): p. 1158-67.

5. Howard, RD, McIlwraith, CW, and Trotter, GW, *Arthroscopic surgery for subchondral cystic lesions of the medial femoral condyle in horses: 41 cases (1988-1991).* J Am Vet Med Assoc, 1995. **206**(6): p. 842-50.

Reproduced with permission of the copyright owner. Further reproduction prohibited without permission.

6. Hurtig, M, Novak, K, McPherson, R, McFadden, S, McGann, L, Muldrew, K, and Schachar, N, *Osteochondral dowel transplantation for repair of focal defects in the knee: an outcome study using an ovine model.* Vet Surg, 1998. **27**: p. 5-16.

7. Hurtig, M, Pearce, S, Warren, S, Kalra, M, and Miniaci, A, *Arthroscopic mosaic arthroplasty in the equine third carpal bone.* Vet Surg, 2001. **30**(3): p. 228-39.

8. Hurtig, MB, *Experimental use of small osteochondral grafts for resurfacing the equine third carpal bone.* Equine Veterinary Journal. Supplement, 1988(6): p. 23-7.

9. Hurtig, MB, Fretz, PB, Doige, CE, and Schnurr, DL, *Effects of lesion size and location on equine articular cartilage repair.* Can J Vet Res, 1988. **52**(1): p. 137-46.

10. Kawcak, C, *Effects of loading on subchondral bone of equine carpal and metacarpophalangeal joints*, in *Department of Clinical Sciences*. 1998, Colorado State University: Fort Collins.

11. Frisbee, DD and Kawcak, CE, *Evaluation of early host response to tissue-engineered cartilage implants in mosaicplasty donor sites of the equine trochlear ridge.* In Preparation for Publication, 2000.

12. Frisbie, DD, Trotter, GW, Powers, BE, Rodkey, WG, Steadman, JR, Howard, RD, Park, RD, and McIlwraith, CW, *Arthroscopic subchondral bone plate microfracture technique augments healing of large chondral defects in the radial carpal bone and medial femoral condyle of horses.* Vet Surg, 1999. **28**(4): p. 242-55.

13. Murray, RC, Vedi, S, Birch, HL, Lakhani, KH, and Goodship, AE, *Subchondral bone thickness, hardness and remodelling are influenced by short-term exercise in a site-specific manner.* J Orthop Res, 2001. **19**(6): p. 1035-42.

14. Murray, RC, Zhu, CF, Goodship, AE, Lakhani, KH, Agrawal, CM, and Athanasiou, KA, *Exercise affects the mechanical properties and histological appearance of equine articular cartilage.* Journal of Orthopaedic Research, 1999. **17**(5): p. 725-31.

15. Brama, PA, Tekoppele, JM, Bank, RA, Karssenberg, D, Barneveld, A, and van Weeren, PR, *Topographical mapping of biochemical properties of articular cartilage in the equine fetlock joint.* Equine Vet J, 2000. **32**(1): p. 19-26.

16. Jackson, WA, Stick, JA, Arnoczky, SP, and Nickels, FA, *The effect of compacted cancellous bone grafting on the healing of subchondral bone defects of the medial femoral condyle in horses.* Vet Surg, 2000. **29**(1): p. 8-16.

Reproduced with permission of the copyright owner. Further reproduction prohibited without permission.

17. Hidaka, C, Goodrich, L, Quitoriano, M, Bent, S, Toland, B, Crystal, R, and Nixon, A. *Accelerated cartilage defect healing in horses by implantation of genetically modified chondrocytes expressing bone morphogenetic protein-7.* in *Trans. ORS.* 2001.

18. Little, C, Ghosh, P, and Rose, R, *The effect of strenuous versus moderate exercise on the metabolism of proteoglycans in articular cartilage from different weight-bearing regions of the equine third carpal bone.* Osteoarthritis and Cartilage, 1997. **5**: p. 161-172.

19. McIlwraith, CW and Vachon, A, *Review of pathogenesis and treatment of degenerative joint disease.* Equine Vet J Suppl, 1988(6): p. 3-11.

20. von Rechenberg, B, Guenther, H, McIlwraith, CW, Leutenegger, C, Frisbie, DD, Akens, MK, and Auer, JA, *Fibrous tissue of subchondral cystic lesions in horses produce local mediators and neutral metalloproteinases and cause bone resorption in vitro.* Vet Surg, 2000. **29**(5): p. 420-9.

21. Nixon, AJ, Hendrickson, DA, Lust, G, and Grande, DA. *Chondrocyte laden fibrin polymers effectively resurface large articular defects in horses.* in *ORS.* 1992. Washington, D.C.

22. Sams, AE, Minor, RR, Wootton, JA, Mohammed, H, and Nixon, AJ, *Local and remote matrix responses to chondrocyte-laden collagen scaffold implantation in extensive articular cartilage defects.* Osteoarthritis Cartilage, 1995. **3**(1): p. 61-70.

23. Vachon, AM, McIlwraith, CW, and Keeley, FW, *Biochemical study of repair of induced osteochondral defects of the distal portion of the radial carpal bone in horses by use of periosteal autografts.* Am J Vet Res, 1991. **52**(2): p. 328-32.

24. Hanie, E, Sullins, K, Powers, B, and Nelson, P, *Healing of full thickness cartilage compared with full thickness cartilage and subchondral bone defects in the equine third carpal bone.* Equine Veterinary Journal, 1992. **24**(5): p. 382-386.

25. Haugland, M, Collier, MA, Johnson, LL, Rohrer, MD, and Walls, RC, *Reparative and Degenerative Changes in Surgically Induced Articular-Cartilage Defects in the Horse During the Early Postoperative Period.* Journal of Equine Veterinary Science, 1994. **14**(9): p. 489-494.

26. Barr, A, Wotton, S, Dow, S, Waterman, A, Goodship, A, and Duance, V, *Effect of central or marginal location and post-operative exercise on the healing of osteochondral defects in the equine carpus.* Equine Veterinary Journal, 1994. **26**(1): p. 33-39.

Reproduced with permission of the copyright owner. Further reproduction prohibited without permission.

27. Nixon, AJ, Fortier, LA, Williams, J, and Mohammed, H, *Enhanced repair of extensive articular defects by insulin-like growth factor-I-laden fibrin composites.* J Orthop Res, 1999. **17**(4): p. 475-87.

28. Nixon, A. *Advances in promoting cartilage healing.* in *ACVS.* 1999.

29. Budras, KD, Sack, WO, and Rock, S, *Anatomy of the horse: an illustrated text.* Third ed. 2001, ?: Schlutersche.

30. Convery, FR, Meyers, M, and Akeson, WH, *Fresh osteochondral allografting of the femoral condyle.* Clin Orthop, 1991. **273**: p. 139-145.

31. Convery, FR, Akeson, WH, and Keown, GH, *The repair of large osteochondral defects. An experimental study in horses.* Clin Orthop, 1972. **82**: p. 253-62.

32. Hidaka, C, Goodrich, LR, Chen, CT, Warren, RF, Crystal, RG, and Nixon, AJ, *Acceleration of cartilage repair by genetically modified chondrocytes over expressing bone morphogenetic protein-7.* J Orthop Res, 2003. **21**(4): p. 573-83.

33. Frisbie, DD, Oxford, JT, Southwood, L, Trotter, GW, Rodkey, WG, Steadman, JR, Goodnight, JL, and McIlwraith, CW, *Early events in cartilage repair after subchondral bone microfracture.* Clin Orthop, 2003(407): p. 215-27.

34. Thomason, J, *The relationship of structure to mechanical function in the third metacarpal bone of the horse, Equus caballus.* Can. J. Zool., 1985. **63**: p. 1420-1428.

35. Cantley, CE, Firth, EC, Delahunt, JW, Pfeiffer, DU, and Thompson, KG, *Naturally occurring osteoarthritis in the metacarpophalangeal joints of wild horses.* Equine Vet J, 1999. **31**(1): p. 73-81.

36. Back, W, *Intro-limb coordination: the forelimb and hindlimb*, in *Equine Locomotion*, Back, W. and Clayton, H.M., Editors. 2001, W.B. Saunders: London. p. 95-133.

37. Radin, EL, *Subchondral bone changes and cartilage damage.* Equine Veterinary Journal, 1999. **31**(2): p. 94-95.

38. Dequeker, J, Mokassa, L, Aerssens, J, and Boonen, S, *Bone density and local growth factors in generalized osteoarthritis.* Microsc Res Tech, 1997. **37**(4): p. 358-71.

39. Imhof, H, Breitenseher, M, Kainberger, F, Rand, T, and Trattnig, S, *Importance of subchondral bone to articular cartilage in health and disease.* Topics in Magnetic Resonance Imaging, 1999. **10**(3): p. 180-92.

Reproduced with permission of the copyright owner. Further reproduction prohibited without permission.

40. Ding, M, *Age variations in the properties of human tibial trabecular bone and cartilage.* Acta Orthop Scand Suppl, 2000. **292**: p. 1-45.

41. Ding, M, Dalstra, M, Linde, F, and Hvid, I, *Changes in the stiffness of the human tibial cartilage-bone complex in early-stage osteoarthrosis.* Acta Orthop Scand, 1998. **69**(4): p. 358-62.

42. Eckstein, F, Putz, R, Muller-Gerbl, M, Steinlechner, M, and Benedetto, KP, *Cartilage degeneration in the human patellae and its relationship to the mineralisation of the underlying bone: a key to the understanding of chondromalacia patellae and femoropatellar arthrosis?* Surg Radiol Anat, 1993. **15**(4): p. 279-86.

43. Ewers, BJ, Weaver, BT, Sevensma, ET, and Haut, RC, *Chronic changes in rabbit retro-patellar cartilage and subchondral bone after blunt impact loading of the patellofemoral joint.* J Orthop Res, 2002. **20**(3): p. 545-50.

44. Meachim, G and Fergie, IA, *Morphological patterns of articular cartilage fibrillation.* Journal of Pathology, 1975. **115**(4): p. 231-40.

45. Pugh, JW, Radin, EL, and Rose, RM, *Quantitative studies of human subchondral cancellous bone. Its relationship to the state of its overlying cartilage.* J Bone Joint Surg Am, 1974. **56**(2): p. 313-21.

46. Shimizu, M, Tsuji, H, Matsui, H, Katoh, Y, and Sano, A, *Morphometric analysis of subchondral bone of the tibial condyle in osteoarthrosis.* Clin Orthop, 1993(293): p. 229-39.

47. Yamada, K, Healey, R, Amiel, D, Lotz, M, and Coutts, R, *Subchondral bone of the human knee joint in aging and osteoarthritis.* Osteoarthritis Cartilage, 2002. **10**(5): p. 360-9.

48. Radin, EL, Paul, IL, and Rose, RM, *Role of mechanical factors in pathogenesis of primary osteoarthritis.* Lancet, 1972. **1**(7749): p. 519-22.

49. Radin, EL and Rose, RM, *Role of subchondral bone in the initiation and progression of cartilage damage.* Clin Orthop, 1986(213): p. 34-40.

50. Frank, E and Grodzinsky, A, *Cartilage electromechanics - II. a continuum model of cartilage electrokinetics and correlation with experiments.* J. Biomechanics, 1987. **20**(6): p. 629-639.

51. Pool, RR and Meagher, DM, *Pathologic findings and pathogenesis of racetrack injuries.* Vet Clin North Am Equine Pract, 1990. **6**(1): p. 1-30.

Reproduced with permission of the copyright owner. Further reproduction prohibited without permission.

52. Riggs, CM, Whitehouse, GH, and Boyde, A, *Pathology of the distal condyles of the third metacarpal and third metatarsal bones of the horse.* Equine Vet J, 1999. **31**(2): p. 140-8.

53. Kawcak, CE, McIlwraith, CW, Norrdin, RW, Park, RD, and James, SP, *The role of subchondral bone in joint disease: a review.* Equine Vet J, 2001. **33**(2): p. 120-6.

54. Kawcak, CE, McIlwraith, CW, Norrdin, RW, Park, RD, and Steyn, PS, *Clinical effects of exercise on subchondral bone of carpal and metacarpophalangeal joints in horses.* Am J Vet Res, 2000. **61**(10): p. 1252-8.

55. Norrdin, RW, Kawcak, CE, Capwell, BA, and McIlwraith, CW, *Subchondral bone failure in an equine model of overload arthrosis.* Bone, 1998. **22**(2): p. 133-9.

56. Norrdin, RW, Kawcak, CE, Capwell, BA, and McIlwraith, CW, *Calcified cartilage morphometry and its relation to subchondral bone remodeling in equine arthrosis.* Bone, 1999. **24**(2): p. 109-14.

57. van Harreveld, PD, Lillich, JD, Kawcak, CE, Turner, AS, and Norrdin, RW, *Effects of immobilization followed by remobilization on mineral density, histomorphometric features, and formation of the bones of the metacarpophalangeal joint in horses.* Am J Vet Res, 2002. **63**(2): p. 276-81.

58. Chang, DG, Iverson, EP, Schinagl, RM, Sonoda, M, Amiel, D, Coutts, RD, and Sah, RL, *Quantitation and localization of cartilage degeneration following the induction of osteoarthritis in the rabbit knee.* Osteoarthritis & Cartilage, 1997. **5**(5): p. 357-72.

59. Temple, MM, Bae, WC, Rivard, D, Amiel, D, Coutts, R, and Sah, RL. *Age- and site-associated biomechanical weakening of human articular cartilage of the femoral condyle: relationship to cellularity and wear.* in *48th Annual Meeting of the Orthopaedic Research Society.* 2001. Dallas, Texas.

60. Williamson, AK, Chen, AC, Masuda, K, Thonar, EJ, and Sah, RL, *Tensile mechanical properties of bovine articular cartilage: variations with growth and relationships to collagen network components.* Journal of Orthopaedic Research, 2003. **21**: p. 872-880.

61. Williamson, AK, Chen, AC, and Sah, RL, *Compressive properties and function-composition relationships of developing bovine articular cartilage.* J Orthop Res, 2001. **19**(6): p. 1113-21.

62. Lewis, CW. *Articular cartilage preferential collagen fiber orientations within the equine stifle.* in *Phi Zeta Day.* 2003. Fort Collins, Colorado.

Reproduced with permission of the copyright owner. Further reproduction prohibited without permission.

63. O'Connor, P, Bland, C, Bjelle, A, and Gardner, DL, *Production of split patterns on the articular cartilage surfaces of rats.* Journal of Pathology, 1980. **130**(1): p. 15-21.

64. Kwan, M, Lai, W, and Mow, V, *A finite deformation theory for cartilage and other soft hydrated connective tissues - I. equilibrium results.* J. Biomechanics, 1990. **23**(2): p. 145-155.

65. Frank, E and Grodzinsky, A, *Cartilage electromechanics - I. electrokinetic transduction and the effects of electrolyte pH and ionic strength.* Journal of Biomechanics, 1987. **20**(6): p. 615-627.

66. Lai, WM, Mow, VC, and Roth, V, *Effects of nonlinear strain-dependent permeability and rate of compression on the stress behavior of articular cartilage.* Journal of Biomechanical Engineering, 1981. **103**: p. 61-66.

67. Biewener, AA, Thomason, J, Goodship, A, and Lanyon, LE, *Bone stress in the horse forelimb during locomotion at different gaits: a comparison of two experimental methods.* J Biomech, 1983. **16**(8): p. 565-76.

68. Arokoski, JP, Jurvelin, JS, Vaatainen, U, and Helminen, HJ, *Normal and pathological adaptations of articular cartilage to joint loading [In Process Citation].* Scand J Med Sci Sports, 2000. **10**(4): p. 186-98.

69. Treppo, S, Koepp, H, Quan, EC, Cole, AA, Kuettner, KE, and Grodzinsky, AJ, *Comparison of biomechanical and biochemical properties of cartilage from human knee and ankle pairs.* Journal of Orthopaedic Research, 2000. **18**(5): p. 739-48.

70. Athanasiou, KA, Niederauer, GG, and Schenck, RC, Jr., *Biomechanical topography of human ankle cartilage.* Ann Biomed Eng, 1995. **23**(5): p. 697-704.

71. Simon, SR, Radin, EL, Paul, IL, and Rose, RM, *The response of joints to impact loading. II. In vivo behavior of subchondral bone.* J Biomech, 1972. **5**(3): p. 267-72.

72. Athanasiou, KA, Rosenwasser, MP, Buckwalter, JA, Malinin, TI, and Mow, VC, *Interspecies comparisons of in situ intrinsic mechanical properties of distal femoral cartilage.* Journal of Orthopaedic Research, 1991. **9**: p. 330-340.

73. Athanasiou, KA, Agarwal, A, and Dzida, FJ, *Comparative study of the intrinsic mechanical properties of the human acetabular and femoral head cartilage.* J Orthop Res, 1994. **12**(3): p. 340-9.

74. Morgan, EF and Keaveny, TM, *Dependence of yield strain of human trabecular bone on anatomic site.* J Biomech, 2001. **34**(5): p. 569-77.

Reproduced with permission of the copyright owner. Further reproduction prohibited without permission.

75. Cowin, SC, *Wolff's law of trabecular architecture at remodeling equilibrium.* J Biomech Eng, 1986. **108**(1): p. 83-8.

76. Carter, DR, *Mechanical loading history and skeletal biology.* J Biomech, 1987. **20**(11-12): p. 1095-109.

77. van der Meulen, MC, Ashford, MW, Jr., Kiratli, BJ, Bachrach, LK, and Carter, DR, *Determinants of femoral geometry and structure during adolescent growth.* J Orthop Res, 1996. **14**(1): p. 22-9.

78. Armstrong, CG and Mow, VC, *Variations in the intrinsic mechanical properties of human articular cartilage with age, degeneration, and water content.* Journal of Bone & Joint Surgery - American Volume, 1982. **64**(1): p. 88-94.

79. Akizuki, S, Mow, V, Muller, F, Pita, J, and Howell, D, *Tensile properties of human knee joint cartilage. II. Correlations between weight bearing and tissue pathology and the kinetics of swelling.* Journal of Orthopaedic Research, 1987. **5**(2): p. 173-186.

80. Akizuki, S, Mow, VC, Muller, F, Pita, JC, Howell, DS, and Manicourt, DH, *Tensile properties of human knee joint cartilage: I. Influence of ionic conditions, weight bearing, and fibrillation on the tensile modulus.* J Orthop Res, 1986. **4**(4): p. 379-92.

81. Kwan, M, Hacker, S, Woo, S, and Wayne, J, *The effect of storage on the biomechanical behavior of articular cartilage - a large strain study.* Journal of Biomechanical Engineering, 1992. **114**: p. 149-153.

82. Ashizawa, N, Nonaka, K, Michikami, S, Mizuki, T, Amagai, H, Tokuyama, K, and Suzuki, M, *Tomographical description of tennis-loaded radius: reciprocal relation between bone size and volumetric BMD.* J Appl Physiol, 1999. **86**(4): p. 1347-51.

83. Carstanjen, B, Duboeuf, F, Detilleux, J, and Lepage, OM, *Equine third metacarpal bone assessment by quantitative ultrasound and dual energy X-ray absorptiometry: an ex vivo study.* Journal of Veterinary Medicine - Series A, 2003. **50**(1): p. 42-7.

84. Ding, M, Danielsen, CC, and Hvid, I, *Bone density does not reflect mechanical properties in early-stage arthrosis.* Acta Orthop Scand, 2001. **72**(2): p. 181-5.

85. Firth, EC, van Weeren, PR, Pfeiffer, DU, Delahunt, J, and Barneveld, A, *Effect of age, exercise and growth rate on bone mineral density (BMD) in third carpal bone and distal radius of Dutch Warmblood foals with osteochondrosis.* Equine Vet J Suppl, 1999(31): p. 74-8.

Reproduced with permission of the copyright owner. Further reproduction prohibited without permission.

86. Kempson, GE, Muir, H, Pollard, C, and Tuke, M, *The tensile properties of the cartilage of human femoral condyles related to the content of collagen and glycosaminoglycans.* Biochim Biophys Acta, 1973. **297**(2): p. 456-72.

87. Armstrong, SJ, Read, RA, and Price, R, *Topographical variation within the articular cartilage and subchondral bone of the normal ovine knee joint: a histological approach.* Osteoarthritis & Cartilage, 1995. **3**(1): p. 25-33.

88. Eckstein, F, Merz, B, Muller-Gerbl, M, Holzknecht, N, Pleier, M, and Putz, R, *Morphomechanics of the humero-ulnar joint: II. Concave incongruity determines the distribution of load and subchondral mineralization.* Anat Rec, 1995. **243**(3): p. 327-35.

89. Milz, S, Eckstein, F, and Putz, R, *Thickness distribution of the subchondral mineralization zone of the trochlear notch and its correlation with the cartilage thickness: an expression of functional adaptation to mechanical stress acting on the humeroulnar joint?* Anat Rec, 1997. **248**(2): p. 189-97.

90. van de Lest, CH, Brama, PA, and Van Weeren, PR, *The influence of exercise on the composition of developing equine joints.* Biorheology, 2002. **39**(1-2): p. 183-91.

91. Brama, PA, Tekoppele, JM, Bank, RA, Barneveld, A, and van Weeren, PR, *Functional adaptation of equine articular cartilage: the formation of regional biochemical characteristics up to age one year.* Equine Vet J, 2000. **32**(3): p. 217-21.

92. Burr, DB and Schaffler, MB, *The involvement of subchondral mineralized tissues in osteoarthrosis: Quantitative microscopic evidence.* Microscopy Research and Technique, 1997. **37**(4): p. 343-357.

93. Day, JS, Ding, M, van der Linden, JC, Hvid, I, Sumner, DR, and Weinans, H, *A decreased subchondral trabecular bone tissue elastic modulus is associated with pre-arthritic cartilage damage.* J Orthop Res, 2001. **19**(5): p. 914-8.

94. Eckstein, F, Jacobs, CR, and Merz, BR, *Mechanobiological adaptation of subchondral bone as a function of joint incongruity and loading.* Med Eng Phys, 1997. **19**(8): p. 720-8.

95. Eckstein, F, Merz, B, Schon, M, Jacobs, CR, and Putz, R, *Tension and bending, but not compression alone determine the functional adaptation of subchondral bone in incongruous joints.* Anat Embryol (Berl), 1999. **199**(1): p. 85-97.

96. Imhof, H, Sulzbacher, I, Grampp, S, Czerny, C, Youssefzadeh, S, and Kainberger, F, *Subchondral bone and cartilage disease - A rediscovered functional unit.* Investigative Radiology, 2000. **35**(10): p. 581-588.

Reproduced with permission of the copyright owner. Further reproduction prohibited without permission.

97. Radin, E, Ehrlich, M, Chernack, R, Abernethy, P, Paul, I, and Rose, R, *Effect of repetitive impulsive loading on the knee joints of rabbits.* Clinical Orthopaedics and Related Research, 1978. **131**: p. 288-292.

Reproduced with permission of the copyright owner. Further reproduction prohibited without permission.

3 REGIONAL SUBCHONDRAL BONE THICKNESS MEASUREMENT AND VALIDATION

3.1 Introduction

The structure of the synovial joint is consistent with its two primary functions: enabling motion and load transfer [1]. Osteochondral structures transmit load across the joint by means of the near-frictionless conforming articular cartilage and the energy absorbing abilities of underlying subchondral bone. These osteochondral structures include articular cartilage, calcified cartilage, cortical bone, and cancellous bone. The majority of energy dissipation is provided by the haversion systems of the cortical bone and the trabeculae systems of the cancellous bone [2, 3]. Subchondral bone can refer to some or all of the subarticular structures; however, for this study, the subchondral bone plate (ScBP) was defined as the radio-dense layer between the uncalcified articular cartilage and supportive trabecular system [2].

The subchondral bone plate consists of type-I collagen fibrils interwoven with inorganic calcium and phosphorus crystalline structures forming haversian systems similar to cortical bone [1]. The ScBP is organized parallel to the articular surface. The less dense underlying trabecular bone supports the ScBP with strut-like structures organized perpendicular to the articular surface [4-6]. This same structure is found across

Reproduced with permission of the copyright owner. Further reproduction prohibited without permission.

species.

For centuries, researchers have noted the strong relationship between bone morphology and mechanical stress history [7-12]. For example, the ScBP optimally remodels (densification and thickening) according to changes in the stress environment (e.g., exercise and aging) [2, 9, 13-16]. ScBP adaptation may contribute to the development of osteoarthritis by stiffening and reducing the shock absorption capabilities of the joint, producing higher cartilage strains [2, 13]. Subsequently, higher strains in the articular cartilage may lead to microfractures within the calcified cartilage and subsequent articular cartilage degradation (physical and metabolic) [13]. In summary, exercise and age can lead to ScBP microfractures requiring remodeling that increases the material stiffness, causing cartilage strains to increase leading to degradation and loss of joint conformity precipitating greater stresses and more ScBP microfractures [13].

Exercise-related osteoarthritis is a common condition in several species (e.g., human and horse), with the effects of loading on bone metabolism and bone structure being of particular interest. Understanding how osteochondral tissues change due to trauma and wear will unlock some new treatment modalities for the debilitating disease, osteoarthritis. Osteoarthritis has immense ramifications within the human population, as well as in the horse. For example, the equine metacarpophalangeal (MCP) joint is exposed to high mechanical loading and wear predisposing the joint to osteochondral fragmentation, subchondral lesions, articular/subarticular cysts, and articular surface fibrillations and erosion [17-25]. Distal lateral 3rd metacarpal bone fractures at the base of the sagittal ridge are very common in the equine athlete. An increase in subchondral bone

Reproduced with permission of the copyright owner. Further reproduction prohibited without permission.

thickness and bone mineral density have been noted with increased exercise and increased joint forces in the equine MCP joint, which may provide an explanation to the high incidence of fractures [17, 21, 22, 24, 26-28].

Subchondral bone structures/properties have been studied using several methods including, non-decalcified/decalcified histology [9, 24-32], high-resolution contact radiographs [33], and computed tomography [2, 26, 28]. Histological methods are very time consuming, costly, and can be very subjective. Computed tomography is very expensive, but comprehensive. Contact radiographs provide an economical means to determine subchondral bone thickness from samples ex-vivo, yet measurement variability has not been determined for this technique. Yamada et. al. used contact radiographs in combination with image processing to measure subchondral bone plate thickness, but neglected to comment on systematic errors contributing to a CV >34%. The purposes of this study were to develop a post-processing algorithm to measure ScBP thickness from digitized contact radiographs of thin osteochondral slabs from the equine MCP joint. The systemic errors of the method will also be assessed.

3.2 Materials and Methods

3.2.1 Sample Acquisition / Preparation

Three matched-pairs of equine MCP joints were collected within 4 hours of sacrifice to minimize tissue degradation (see Appendix B for sample history). After an arthrotomy was performed, the synovial fluid was flushed with phosphate buffered saline (PBS) and proteinase inhibitors (PIs; 10mM phenylmethanesulfonyl fluoride, 50mM

Reproduced with permission of the copyright owner. Further reproduction prohibited without permission.

benzamidine-HCl, and 10mM N-ethylmaleimide) [34]. Joints were wrapped with PBS+PIs soaked gauze and stored in sealed bags at –20°C until testing preparation.)

Samples were thawed in PBS for one hour at room temperature. The palmar and dorsal aspects of the joint were carefully opened to allow visualization of the articular margins. The joint was extended manually and rigidly fixed using a three-dimensional clamp (VWR, West Chester, PA, USA), maintained at full extension, and cut twice (6.5 mm apart, EXAKT Technologies, Inc., Oklahoma City, OK, USA) in the coronal plane to yield a flat 6.5 mm thick osteochondral specimens of mating cartilage surfaces (Figure 3.1)

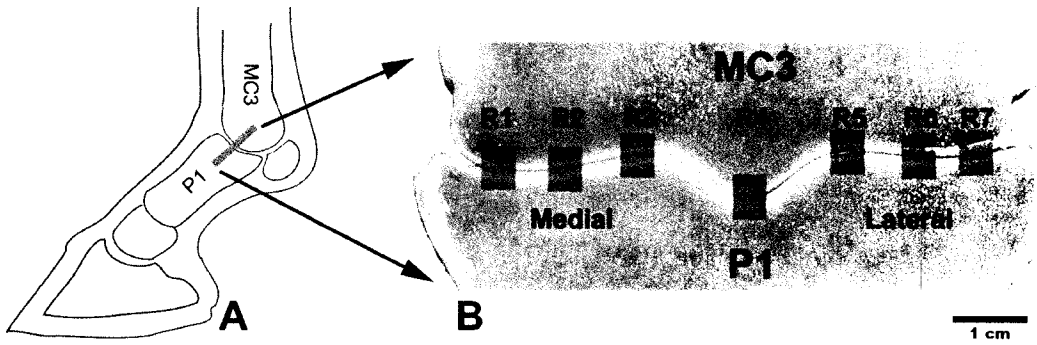

Figure 3.1: (A) Medial-lateral view of the anatomical position of the sample taken from the metacarpophalangeal (MCP) joint (B) Coronal view of the typical MCP sample, proximal 3rd metacarpal (MC3) and distal 1st phalanx (P1), with analyzed regions (R1-R7) highlighted.

3.2.2 Study Structure

Three matched-pair equine MCP joints (3-right, 3-left) were collected and analyzed. In summary, the study design involved: three horses (A, B, C), two sides (R/L), three x-rays (1,2,3), two bones (MC3/P1), and seven regions (R1-R7, Figure 3.2). Additionally, image analysis was repeated 5 independent times (i-v, Figure 3.2) for each radiograph.

Reproduced with permission of the copyright owner. Further reproduction prohibited without permission.

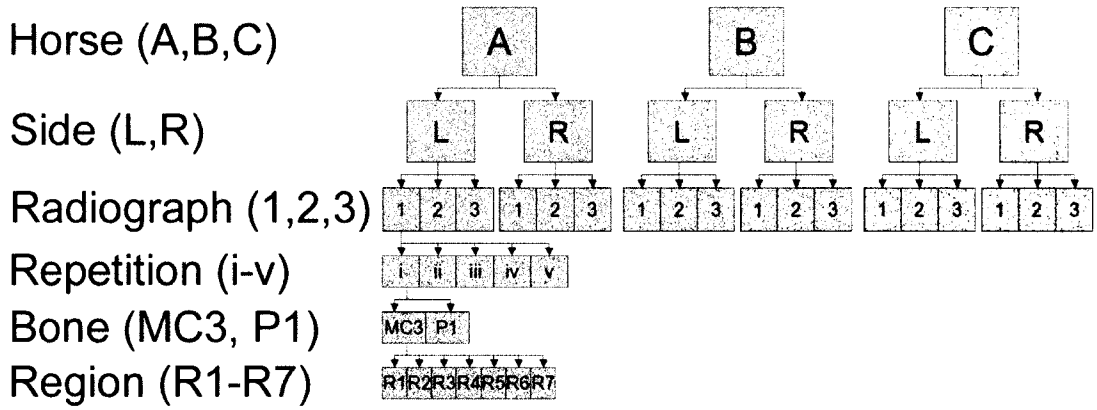

Figure 3.2: Study structure. Osteochondral slabs from bilateral (R, L) MCP joints from three horses (A, B, C) were exposed three consecutive times (1, 2, 3). ScBP thickness measurements were acquired for each region (R1-R7) within each bone (MC3, P1) five times (i-v) from each radiograph.

3.2.3 Contact radiographs

Osteochondral samples were thawed at room temperature and radiographed using a high-resolution cabinet x-ray machine (Faxitron® Cabinet X-ray System Model 43855A, Wheeling, IL) with high-resolution mammography film (X-OMAT film, Eastman Kodak, Rochester, NY). Three radiographs were taken of each joint sample with an aluminum calibration step wedge in view for each exposure (Dent-X Corporation, Elmsford, NY). A 2:15 minute exposure at 42 kVp was selected to allow visualization of all the step-wedge luminance intensities. Radiographs were developed and checked for consistency of step-wedge intensity graduations. Each film was converted to a digital image (LS75 digitizer, Eastman Kodak Company, Rochester, NY) at a resolution of 119.11 μm/pixel (Figure 3.3A).

3.2.4 Image processing and subchondral bone thickness measurement

Images were cropped and rotated to standard orientations using Image-Pro Plus (Media Cybernetics, Silverspring, MD). Each image was filtered using a local best-fit

Reproduced with permission of the copyright owner. Further reproduction prohibited without permission.

contrast enhancement to differentiate between pixel luminance values (Figure 3.3B) [35]. A custom semi-automatic analysis program was implemented to perform subchondral bone edge detection along the articular surfaces using articular landmarks (Figure 3.3B). Using the distance between the medial landmarks, the medial condyle regions were selected 30% (R1), 60% (R2), and 95% (R3) relative to the medial margin. Lateral condyle regions were selected 95% (R4), 60%(R5), and 30%(R7) between lateral landmarks relative to the lateral margin. The region R7 was selected at the sagittal ridge (See Appendix B more information on region selection). Briefly, ScBP thickness was determined by: (1) identifying luminance profiles at sites of interest (Figure 3.1) at a width of 25 pixels or 3mm; (2) inflection point recognition in the luminance profile determined the ScBP boundaries (Figure 3.3C); (3) linear distance determined between the subchondral bone boundaries (luminance inflection points) (Figure 3.3C); and (4) a visual confirmation of the measurement by the user. The ScBP thickness was quantified for all the regions (R1-R7) of each bone (MC3 and P1, Figure 3.1). All radiographs, including repeated measurements of the same radiograph, were analyzed in the same manner (see Appendix B for protocol and Image-Pro algorithm).

Reproduced with permission of the copyright owner. Further reproduction prohibited without permission.

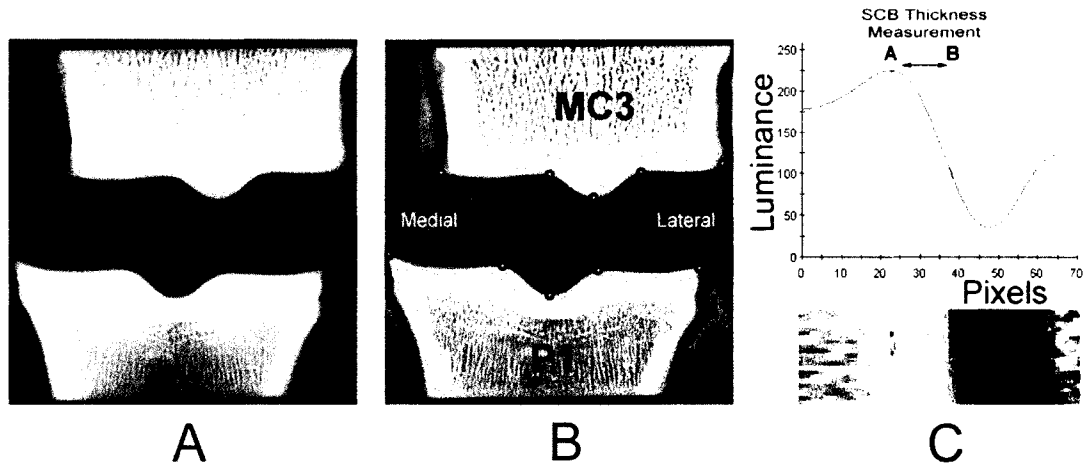

Figure 3.3: Image processing and subchondral bone (ScBP) thickness measurement: (A) raw radiograph image (B) filtered image with feature points used for ScBP thickness measurement locations for the distal 3rd metacarpal (MC3) and proximal 1st phalanx (P1) (C) an illustration of the ScBP thickness measurement using a line luminance profile to determine the ScBP margins, luminance peak (a) and largest negative gradient (b).

3.2.5 Statistics

Normality was checked and ScBP thickness was transformed to achieve a normal distribution. To determine systematic errors, a mixed-effects ANOVA using the Satterthwaite approximation for degrees of freedom (SAS Institute Inc., Cary, North Carolina, USA) was used with the following random effects, horse (e.g., subject), x-ray replication nested within horse, measurement replication nested within x-ray, and horse. Variance proportion of each random effect relative to the total systematic variance was used to determine the systematic error proportions.

3.3 Results

3.3.1 Systematic Error

The average overall osteochondral sample thickness was 6.30±0.24mm (Mean ± STD). A reciprocal transformation of ScBP thickness was required to achieve normality. The average error for ScBP thickness for the entire study was 23% of total error (CV). There was an insignificant source of error from the measurement algorithm (0.23% of

Reproduced with permission of the copyright owner. Further reproduction prohibited without permission.

total CV). The variability induced by the x-ray and digitizing (2.1% of total CV) was one-order of magnitude smaller than the error found between subjects (19.6% of total CV) and 2X smaller than the combined residual error of the entire process (4% of total CV). Precision was spatially dependent. The medial and lateral MC3 regions (R1 and R7) had a lower precision (meaning higher STD) than those centrally, contrasting the spatial dependency found for the P1 regions (R3 and R5 regions having the lowest precision, Figure 3.4). Processing algorithm precision was 0.045 $\pm$ 0.045 mm (37% of a pixel).

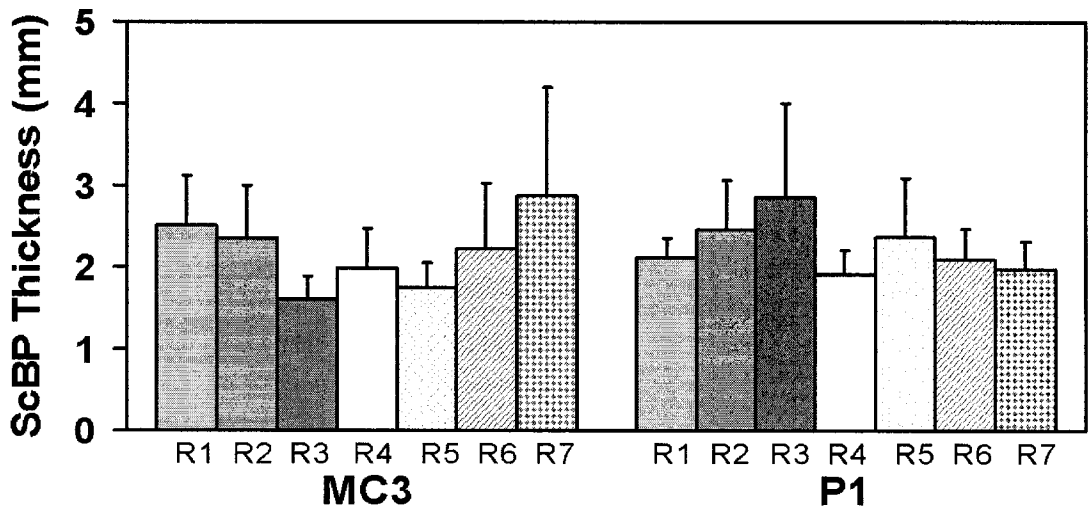

Figure 3.4: The subchondral bone (ScBP) thickness relationship between bones, distal 3rd metacarpal (MC3) and proximal 1st phalanx (P1), and regions (R1-R7).

3.4 Discussion

Contact radiographs proved to be a feasible method for assessment of ScBP thickness with the highest measurement variability associated with inherent sample differences and preparation. Variability caused by the radiographic procedure and digital conversion was negligible. Precision varied across the joint, possibly due to interference from the medial and lateral cortical edges and ScBP thickness variations at the base of the sagittal ridge (R4). Other research quantifying ScBP thickness has not assessed

Reproduced with permission of the copyright owner. Further reproduction prohibited without permission.

systematic errors making comparison to techniques used by others difficult, the current method had a 23%CV compared to >34%CV for Yamada et. al.'s method [33].

The inabilities to perform non-invasive three-dimensional analyses are fundamental limitations of contact radiographic methods to quantify ScBP thickness. Since radiographs are a two-dimensional representation of a three-dimensional object, an additional limitation is that as sample thickness increases, the possibility for measurement error also increases. Therefore, sample thickness must be relatively thin compared to the articular radius of curvature in order to obtain accurate results.

The radiograph digital scanning process limited the precision currently attained using the method described herein. The scanner in the present study had a resolution of 119.11 μm/pixel, which was significantly lower than the available resolution available to from high-resolution radiographic film (3-10μm/grain). Therefore, if the radiograph scanner resolution was comparable to the resolution of more economical radiographic film (>50μm/grain), it would be sufficient to use more economical radiographic film for the method presented in this study.

For this study, contact radiography has proven to be an effective and efficient means to measure subchondral bone plate thickness within planar osteochondral metacarpophalangeal joint samples. However, there are some drawbacks to using contact radiography to measure ScBP thickness. For example, it requires ex-vivo sample preparation and is a two-dimensional representation of a three-dimensional sample. Understanding these limitations are necessary to adequately prepare samples and interpret

Reproduced with permission of the copyright owner. Further reproduction prohibited without permission.

the results. Recommendations for future work include comparing radiographic, histological, and computed tomography methods for quantifying ScBP thickness.

3.5 Conclusion

The measurement of subchondral bone plate thickness is important to the study of osteoarthritis. A new subchondral bone plate thickness measurement technique that has minimal systematic error and repeatability using high-resolution contact radiographs and image processing has been developed in this study.

3.6 References

1. Todhunter, R.J., *Anatomy and physiology of synovial joints*, in *Joint Disease In The Horse*, C.W. McIlwraith and G.W. Trotter, Editors. 1996, W.B. Saunders Company: Philadelphia. p. 1-28.

2. Muller-Gerbl, M., *The subchondral bone plate.* Advances in anatomy, embryology & cell biology. Vol. 141. 1998. 1-134.

3. Radin, E.L., D.B. Burr, D. Fyhrie, T.D. Brown, and R.D. Boyd, *Characteristics of joint loading as it applies to osteoarthrosis*, in *Biomechanics of diarthrodial joints*. 1990, Springer-Verlag: New York. p. 369-384.

4. Redler, I., V.C. Mow, M.L. Zimny, and J. Mansell, *The ultrastructure and biomechanical significance of the tidemark of articular cartilage.* Clin Orthop, 1975(112): p. 357-62.

5. Lajeunesse, D., G. Hilal, J.P. Pelletier, and J. Martel-Pelletier, *Subchondral bone morphological and biochemical alterations in osteoarthritis.* Osteoarthritis & Cartilage, 1999. **7**(3): p. 321-2.

6. Braidotti, P., E. Bemporad, T. D'Alessio, S. Sciuto, and L. Stagni, *Tensile experiments and SEM fractography on bovine subchondral bone.* Journal of Biomechanics, 2000. **33**: p. 1153-1157.

7. Carter, D.R., *Mechanical loading histories and cortical bone remodeling.* Calcif Tissue Int, 1984. **36 Suppl 1**: p. S19-24.

8. Ding, M., *Age variations in the properties of human tibial trabecular bone and cartilage.* Acta Orthop Scand Suppl, 2000. **292**: p. 1-45.

Reproduced with permission of the copyright owner. Further reproduction prohibited without permission.

9. Eckstein, F., C.R. Jacobs, and B.R. Merz, *Mechanobiological adaptation of subchondral bone as a function of joint incongruity and loading.* Med Eng Phys, 1997. **19**(8): p. 720-8.

10. Frost, H.M., *Wolff's Law and bone's structural adaptations to mechanical usage: an overview for clinicians.* Angle Orthodontist, 1994. **64**(3): p. 175-88.

11. Meyer, G.H., *Die Architektur die Spongiosa.* Arch. Anat. Physiol. Wiss. Med., 1867. **34**: p. 160-169.

12. Wolff, J., *Uber die innere Architecktur der Knochen und ihre Bedeutung fur die Frage vom Knochenwachstum.* Virchows Arch. Pathol., 1870. **50**: p. 389-450.

13. Radin, E.L. and R.M. Rose, *Role of subchondral bone in the initiation and progression of cartilage damage.* Clin Orthop, 1986(213): p. 34-40.

14. Eckstein, F., F. Lohe, E. Schulte, M. Muller-Gerbl, S. Milz, and R. Putz, *Physiological incongruity of the humero-ulnar joint: a functional principle of optimized stress distribution acting upon articulating surfaces?* Anat Embryol (Berl), 1993. **188**(5): p. 449-55.

15. Eckstein, F., B. Merz, and C.R. Jacobs, *Effects of joint incongruity on articular pressure distribution and subchondral bone remodeling.* Adv Anat Embryol Cell Biol, 2000. **152**: p. iii-ix, 1-127.

16. Eckstein, F., B. Merz, M. Muller-Gerbl, N. Holzknecht, M. Pleier, and R. Putz, *Morphomechanics of the humero-ulnar joint: II. Concave incongruity determines the distribution of load and subchondral mineralization.* Anat Rec, 1995. **243**(3): p. 327-35.

17. Pool, R.R., *Traumatic injury and osteoarthritis.* Joint Disease in the Horse, ed. C.W. McIlwraith and G.W. Trotter. 1996, Philadelphia: W.B. Saunders Co. 87-104.

18. Pool, R.R., *Multidisciplinary investigation of the aetiopathogenesis of parasagittal fractures of the third metacarpal and metatarsal bones of Thoroughbreds.* Equine Vet J, 1999. **31**(2): p. 96.

19. Pool, R.R. and D.M. Meagher, *Pathologic findings and pathogenesis of racetrack injuries.* Vet Clin North Am Equine Pract, 1990. **6**(1): p. 1-30.

20. Rick, M.C., T.R. O'Brien, R.R. Pool, and D. Meagher, *Condylar fractures of the third metacarpal bone and third metatarsal bone in 75 horses: radiographic features, treatments, and outcome.* J Am Vet Med Assoc, 1983. **183**(3): p. 287-96.

Reproduced with permission of the copyright owner. Further reproduction prohibited without permission.

21. Riggs, C.M., G.H. Whitehouse, and A. Boyde, *Pathology of the distal condyles of the third metacarpal and third metatarsal bones of the horse.* Equine Vet J, 1999. **31**(2): p. 140-8.

22. Kawcak, C., *Effects of loading on subchondral bone of equine carpal and metacarpophalangeal joints*, in *Department of Clinical Sciences*. 1998, Colorado State University: Fort Collins.

23. Kawcak, C.E., C.W. McIlwraith, R.W. Norrdin, R.D. Park, and S.P. James, *The role of subchondral bone in joint disease: a review.* Equine Vet J, 2001. **33**(2): p. 120-6.

24. Norrdin, R.W., C.E. Kawcak, B.A. Capwell, and C.W. McIlwraith, *Subchondral bone failure in an equine model of overload arthrosis.* Bone, 1998. **22**(2): p. 133-9.

25. Norrdin, R.W., C.E. Kawcak, B.A. Capwell, and C.W. McIlwraith, *Calcified cartilage morphometry and its relation to subchondral bone remodeling in equine arthrosis.* Bone, 1999. **24**(2): p. 109-14.

26. Boyde, A., Y. Haroon, S.J. Jones, and C.M. Riggs, *Three dimensional structure of the distal condyles of the third metacarpal bone of the horse.* Equine Vet J, 1999. **31**(2): p. 122-9.

27. Cantley, C.E., E.C. Firth, J.W. Delahunt, D.U. Pfeiffer, and K.G. Thompson, *Naturally occurring osteoarthritis in the metacarpophalangeal joints of wild horses.* Equine Vet J, 1999. **31**(1): p. 73-81.

28. Riggs, C.M., G.H. Whitehouse, and A. Boyde, *Structural variation of the distal condyles of the third metacarpal and third metatarsal bones in the horse.* Equine Vet J, 1999. **31**(2): p. 130-9.

29. Milz, S., F. Eckstein, and R. Putz, *Thickness distribution of the subchondral mineralization zone of the trochlear notch and its correlation with the cartilage thickness: an expression of functional adaptation to mechanical stress acting on the humeroulnar joint?* Anat Rec, 1997. **248**(2): p. 189-97.

30. Matsui, H., M. Shimizu, and H. Tsuji, *Cartilage and subchondral bone interaction in osteoarthrosis of human knee joint: a histological and histomorphometric study.* Microscopy Research And Technique, 1997. **37**: p. 333-342.

31. Shimizu, M., H. Tsuji, H. Matsui, Y. Katoh, and A. Sano, *Morphometric analysis of subchondral bone of the tibial condyle in osteoarthrosis.* Clin Orthop, 1993(293): p. 229-39.

Reproduced with permission of the copyright owner. Further reproduction prohibited without permission.

32. Young, D., D. Richardson, M. Markel, and D. Nunamaker, *Mechanical and morphometric analysis of the third carpal bone of thoroughbreds.* Am. J. Vet. Res., 1991. **52**(3): p. 402-409.

33. Yamada, K., R. Healey, D. Amiel, M. Lotz, and R. Coutts, *Subchondral bone of the human knee joint in aging and osteoarthritis.* Osteoarthritis Cartilage, 2002. **10**(5): p. 360-9.

34. Frank, E. and A. Grodzinsky, *Cartilage electromechanics - II. a continuum model of cartilage electrokinetics and correlation with experiments.* J. Biomechanics, 1987. **20**(6): p. 629-639.

35. Media Cybernetics, I., *Local Best Fit Contrast Enhancement.* 2002: Silverspring, MD, USA.

Reproduced with permission of the copyright owner. Further reproduction prohibited without permission.

4 ERROR ASSESSMENT OF INTRA-TISSUE ARTICULAR CARTILAGE STRAIN WITHIN OPPOSING ARTICULAR SURFACES

4.1 Introduction

The structure and composition of articular cartilage has been found to vary by species, location within the organism and joint, and depth from the articular surface [1-3]. These variations in structure and composition contribute to depth-dependent mechanical properties [4-6]. For example, the collagen alignment relative to the articular surface changes from parallel in the superficial zone to more perpendicular at the cartilage/calcified cartilage interface creating depth-dependent compositional and mechanical characteristics [3]. The superficial fibers are primarily aligned in the direction of articulations to resist tensile forces, while the deep collagen orientation is designed primarily to resist shear forces between cartilage and calcified cartilage [7]. Proteoglycan content also varies as a function of cartilage depth resulting in depth-dependent fixed-charge densities and compressive properties [5, 6].

Characterization of articular cartilage physical properties has been performed using various methods. Experimental testing analyses using platen to platen strains, confined compression [8-11], and unconfined compression [12-14] assume articular cartilage intra-tissue deformation to be homogeneous, thereby neglecting its complex

Reproduced with permission of the copyright owner. Further reproduction prohibited without permission.

heterogeneous structure. Measurements of intra-tissue strains were needed to fully understand and characterize articular cartilage. Schinagl et al. [4, 5] found a depth-dependent compression modulus within articular cartilage using chondrocytes (cartilage cells) as fiducial markers to calculate depth-dependent strains during platen loading of the articular surface under confined compression. Articular cartilage's depth-dependent confined compression modulus was verified by taking serial sections along the articular depth [6, 15]. Other researchers soon followed, optimizing Schinagl et al.'s technique, by using chondrocytes as intra-tissue fiducial markers for deformation analysis [6, 15-17]. Recently, researchers used digital image correlation to facilitate tracking of chondrocyte positions between deformation states of indentation, confined, and unconfined compression via platens for intra-tissue strain analysis [15-18]. Until now, quantifying strain distributions within articular cartilage focused on compression behavior via an opposing platen only. Constitutive relationship determination is unproblematic for platen loading experiments due to the simplified boundary conditions, whereas determining constitutive relationships from articular surface loading is significantly more difficult due to geometry and uncontrollable articular surface displacements. Consequently, only strain distributions between articular surfaces are justifiably determined, but can offer considerable insight for certain situations. The study of articular cartilage intra-strain distribution under physiological loading conditions of opposing articular surfaces would provide a more physiologically appropriate simulation, and is the focus of this investigation.

Erne et. al. [19], using quantitative electronic speckle pattern interferometry, attempted to quantify articular cartilage intra-tissue strain distributions within unmatched

Reproduced with permission of the copyright owner. Further reproduction prohibited without permission.

opposing porcine osteochondral medial femoral and medial patellar specimens ($5x5x5mm^3$) under confined compression. These researchers were only able to capture one-dimensional infinitesimal strain fields within the small cubic femoral condyle section. To fully understand deformational changes occurring within articular cartilage during articular loading, two-dimensional strain field quantification in various regions along the width of matched joint surfaces are needed. Therefore, the objectives of this study were to develop a custom-designed loading system and associated sample preparation procedure, and to quantify two-dimensional strain fields between two opposing articular cartilage surfaces (MC3 and P1) within the equine metacarpophalangeal joint (MCP) using video image correlation analysis (VIC). Systematic errors were quantified to validate the system. The methodology will provide a mechanism to evaluate articular cartilage strain fields of various regions along the articular surface of naturally opposing osteochondral surfaces (Chapter 5).

4.2 Methods and Materials

4.2.1 Experimental Testing Setup

The experimental testing setup consisted of a sample, custom-designed loading system, microscope, digital camera, computer, and digital image correlation analysis (Figure 4.1).

Reproduced with permission of the copyright owner. Further reproduction prohibited without permission.

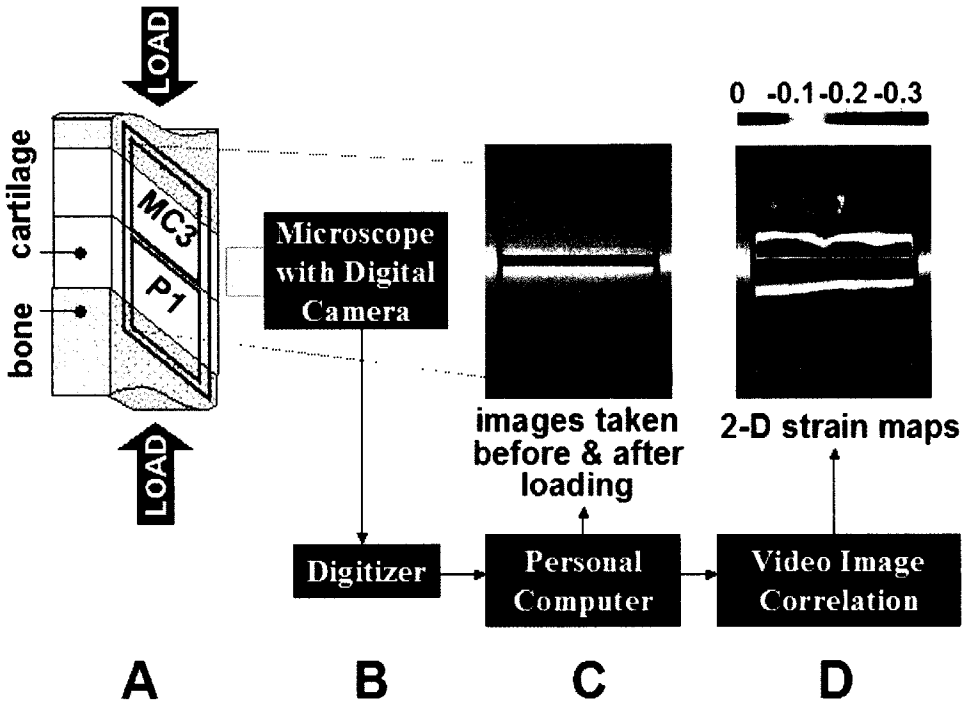

Figure 4.1: Schematic of testing setup (A) custom-designed loading system applies load to the osteochondral sample, (B) the epifluorescence microscope, digital camera, and digitizer capture a magnified view of fiducial markers (chondrocytes) within osteochondral sample's cartilage surfaces, (C) images are taken before and after loading and saved on a personal computer, (D) then digital image correlation is used to analyze the images to determine intra-tissue displacements and strains.

4.2.2 Sample Preparation

The equine metacarpophalangeal joint was chosen for analysis due to high clinical incidence of joint degeneration [20-23], simple two degrees-of-freedom motion [24], and prominent sagittal ridge to help maintain proper alignment during testing (R4 in Figure 4.2). An equine MCP joint (2-3yrs) was obtained within 4 hours of sacrifice and flushed with phosphate buffered saline (PBS) and proteinase inhibitors (PIs; 10mM phenylmethanesulfonyl fluoride, 50mM benzamidine-HCl, and 10mM N-ethylmaleimide) while keeping all support structures intact [10]. The joint sample was visually and manually inspected for normality prior to acceptance into the study. The joint was wrapped with PBS+PIs soaked gauze and stored in a sealed bag at –20°C until preparation and testing.

Reproduced with permission of the copyright owner. Further reproduction prohibited without permission.

The sample was thawed at room temperature and maintained at full extension during preparation using an adapted fixture (variable-clamp, cat#21572-658, VWR International; West Chester, PA). A 5.5mm slab was cut from the mounted specimen in the coronal plane using a precision bone saw (EXAKT Technologies, Inc., Oklahoma City, OK, USA) with constant irrigation of PBS during cutting. The parallel cuts were made through the aligned joint yielding mating osteochondral surfaces at full extension of the joint (Figure 4.2). Sample dimensions were quantified using the average of five thickness measurements of each bone portion (MC3/P1) using a micrometer ($\pm$1mm, Mitutoyo; Aurora, IL) and digital caliper to measure the whole sample height (proximal to distal, $\pm$10mm, Mitutoyo; Aurora, IL). Cell nuclei were stained in a solution of propidium iodide (0.02mg/ml) and PBS+PIs, overnight at 5°C prior to testing (see Appendix C for sample preparation protocol).

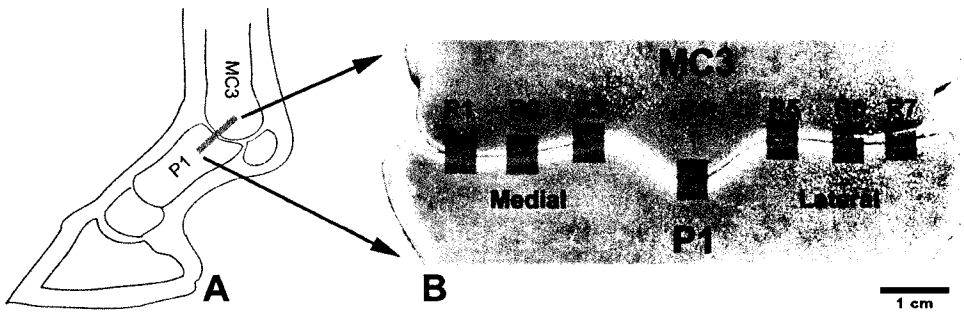

Figure 4.2: (A) Sagittal view of the metacarpophalangeal joint (MCP) showing the joint angle which the sample (gray area) prepared from the 1st phalanx (P1) and 3rd metacarpal bone (MC3). (B) Coronal view of a typical sample showing the P1 and MC3 articular surfaces and analysis regions (R1-R7). Note: The sagittal ridge restricts medial-to-lateral movement centrally (R4).

4.2.3 Custom-Designed Loading System

The loading system is diagrammatically presented in Figure 4.3. The system is comprised of a main hydration chamber (6061 aluminum) with a sample-viewing window (1/8 inch thick plate glass) at the base. The sample was mounted in the hydration

Reproduced with permission of the copyright owner. Further reproduction prohibited without permission.

chamber (filled with PBS+PIs) with palmar aspect of the sample against the viewing window. The sample was aligned centrally and stainless steel loading platens were installed. To minimize unbalanced sample loading, a self-alignment mechanism was used between the platens consisting of one stainless steel ball bearing centrally placed (relative to the sample) between two stainless steel platens (on both sides of the sample, Figure 4.3). To minimize friction and out-of-plane movement of the sample during compression, stainless steel rods (1/32"diameter) were placed parallel with the articular surface and perpendicular to applied displacement, between the dorsal bone surfaces (MC3 and P1) and a glass-lined confining plate (small 4N in the coronal plane) acting like linear bearings. Fluid flow in and around the tissue was allowed to flow freely, except for the surface against the viewing glass. The primary actuator (linear micrometer, 10μm resolution, Newport; Irvine, CA) applied load on the force cell (2.2kN, Model#51, Sensotec; Columbus, OH) located on the secondary actuator (Figure 4.3). An aluminum plate and two linear bearing guides (RSR9Z, 115mm, THK America; Schaumburg, IL) support the secondary actuator, which transfer load applied to the force cell to the stainless steel platen in the hydration reservoir, which in-turn applies load on the sample in the hydration reservoir (Figure 4.3). A 12-bit data acquisition system (LabView®, National Instruments; Austin, TX) was used to capture the force signal during loading at 4Hz (see Appendix C for more views of the system).

Reproduced with permission of the copyright owner. Further reproduction prohibited without permission.

Reproduced with permission of the copyright owner. Further reproduction prohibited without permission.

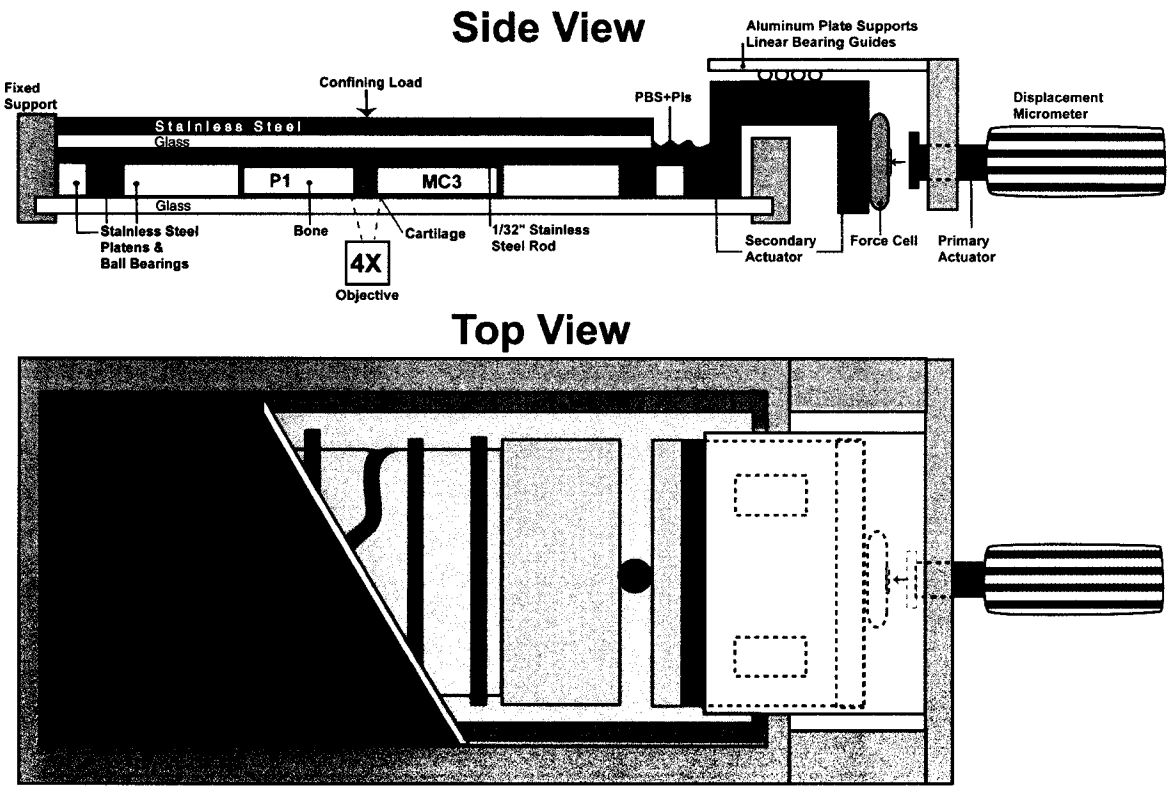

Figure 4.3: (TOP) Side view and (Bottom) top view schematic of the custom-designed loading system.

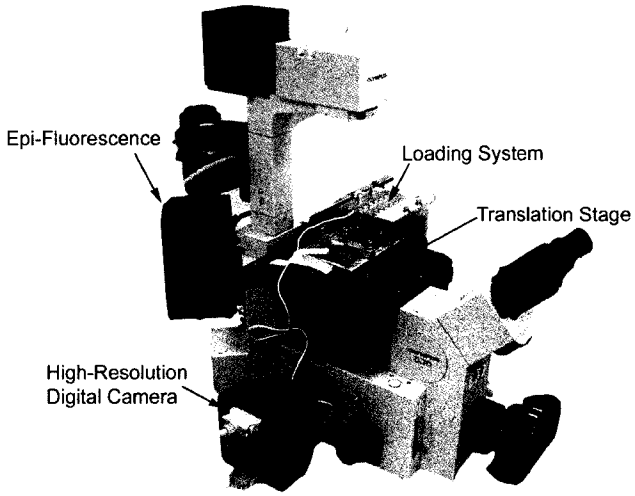

Figure 4.4: The custom-designed loading system within the translation stage on an epifluorescence equipped inverted microscope with a high-resolution digital camera.

4.2.4 Image Acquisition

The compression system was designed to fit securely on an xy-translation stage (±1μm, Microcode II, Boeckeler Inst.; Tucson, AZ) of an inverted microscope (Olylmpus IX-70, Melville, NY; 4X objective; Figure 4.4). The microscope was equipped with epifluorescence (WG filter, E_x570-550; E_m>590) and digital photography using a SpotRT camera (Diagnostic Instruments; Sterling Heights, MI) to capture high-resolution 16-bit grayscale images (FOV 2.2x3.0mm^2, 540 pixels/mm, aspect ratio=1.0; Figure 4.4).

4.2.5 Digital Image Correlation Analysis

Two-dimensional video image correlation (VIC) was performed on the image sets to determine displacements and displacement gradients of patterns (subsets) within the image. As discussed by Sutton et al. [25], VIC involves measurement of surface displacements by matching points on an undeformed object surface (undeformed image) to surface points of the deformed object (deformed image). This requires a one-to-one relationship between the two states of the object's images and a high-contrast random

Reproduced with permission of the copyright owner. Further reproduction prohibited without permission.

surface pattern. The imaging process converts the continuous light intensities *O(X,Y)* reflected off the sample surface to discrete quantities *I(X,Y)* using the charge coupled device array of the digital camera ([25], Figure 4.5).

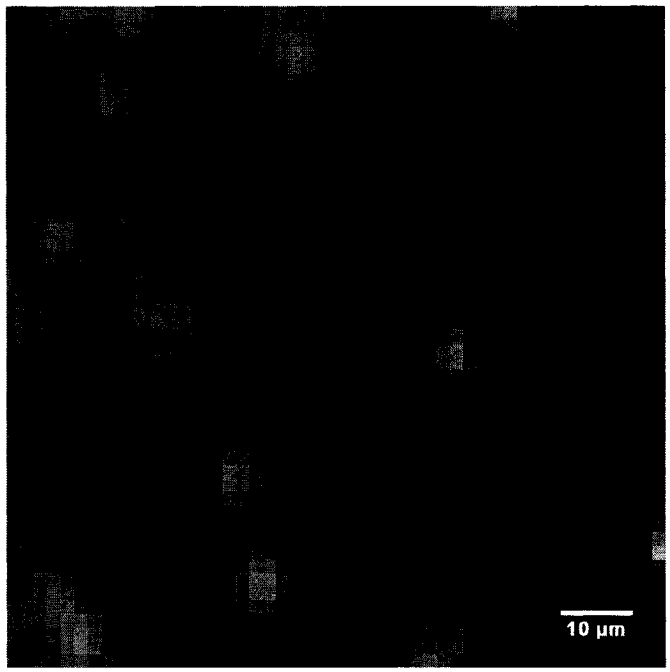

Figure 4.5: Typical subset pattern used for video image correlation (49x49 pixels, ~90x 90µm). The high intensity areas (white) are fluorescently stained chondrocytes.

The deformation process is illustrated in Figure 4.6 for a subset (intensity or pixel pattern). For the undeformed subset centered at (X,Y), the discrete sample location of point P is (X,Y) and the location of point Q is (X+dX, Y+dY) as presented in equations 4.1 and 4.2 below [25],

$$I(P) = I(X,Y) \qquad \text{Equation 4.1}$$

$$I(Q) = I(X+dX, Y+dY) \qquad \text{Equation 4.2}$$

Reproduced with permission of the copyright owner. Further reproduction prohibited without permission.

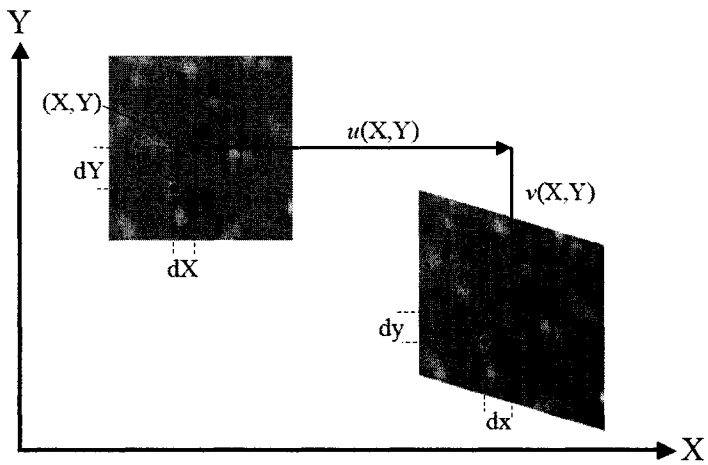

Figure 4.6: Two-dimensional deformation process of an image subset. Adapted from [25].

Displacements dX and dY between unloaded and loaded image captures are typically small distances. To accurately determine subset displacements quintic interpolation was used, in conjunction with a low-pass binomial filter to minimize interpolation error [26]. After deformation (Figure 4.6), points P and Q are transformed into the deformed points, p and q. Assuming a one-to-one relationship between the undeformed and deformed image sets, the displacement vector field was defined as $\{u(X,Y),\ v(X,Y)\}$ thereby $x = X + u(X,Y)$, $y = Y + v(X,Y)$ and discrete deformed intensity subset locations are defined by equations 4.3 and 4.4 [25],

$$I'(X_i, Y_j) = I(X_i + u(X_i, Y_j), Y_j + v(X_i, Y_j)) \qquad \text{Equation 4.3}$$

and

Reproduced with permission of the copyright owner. Further reproduction prohibited without permission.

$$I'\left[X_i + u\left(X_i, Y_j\right), Y_j + v\left(X_i, Y_j\right)\right]$$

$$= I\left[X_i + dX_i + u\left(X_i + dX_i, Y_j + dY_j\right), Y_j + dY_j + v\left(X_i + dX_i, Y_j + dY_j\right)\right]$$

$$= I\left[X_i + u\left(X_i, Y_j\right) + \left(1 + \frac{\partial u}{\partial X_i}\right) dX_i + \frac{\partial u}{\partial Y_j} dY_j, Y_j + v\left(X_i, Y_j\right) + \frac{\partial v}{\partial X_i} dX_i + \left(1 + \frac{\partial v}{\partial Y_j}\right) dY_j \right]$$

Equation 4.4

Constant displacement gradients within each pixel subset are assumed to achieve uniform strain within each subset. By, matching discrete pixel subsets between the undeformed and deformed images with a search method, the displacements and displacement gradients for each subset are determined. A normalized cross-correlation coefficient (C_l) was used to determine (u(P), v(P), $\partial u/\partial$X, $\partial v/\partial$X, $\partial u/\partial$Y, and $\partial v/\partial$Y) defined in equation 4.5 [25]:

$$1.0 - C_l\left(u, v, \frac{\partial u}{\partial X}, \frac{\partial u}{\partial Y}, \frac{\partial v}{\partial X}, \frac{\partial v}{\partial Y}\right) =$$

$$1.0 - \frac{\sum_{i=1}^{i=N} \sum_{j=1}^{j=M} I\left(X_i, Y_j\right) \cdot I'\left[X_i + u\left(X_i, Y_j\right), Y_j + v\left(X_i, Y_j\right)\right]}{\sum_{i=1}^{i=N} \sum_{j=1}^{j=M} \left\{I^2\left(X_i, Y_j\right) I'^2\left[X_i + u\left(X_i, Y_j\right), Y_j + v\left(X_i, Y_j\right)\right]\right\}^{\frac{1}{2}}} \qquad \text{Equation 4.5}$$

Initial user-defined estimates (u(P), v(P), $\partial u/\partial$X, $\partial v/\partial$X, $\partial u/\partial$Y, and $\partial v/\partial$Y) for a subset were selected using the undeformed and deformed images. Using optimization (Newton-Raphson), the values u(P), v(P), $\partial u/\partial$X, $\partial v/\partial$X, $\partial u/\partial$Y, and $\partial v/\partial$Y are selected to minimize the normalized correlation coefficient for that particular subset. The initial guess for the next subset uses the results from the previous subset for the next optimization step. This process repeats itself for the remaining subsets within the selected

Reproduced with permission of the copyright owner. Further reproduction prohibited without permission.

analysis region. After all the subsets have been correlated, a simple linear interpolation of the displacement gradients of selected pixel neighborhood size around each subset was used to calculate strain for each subset. Lagrangian strains were determined using the following equations (4.6-4.8) [27]:

$$E_{XX} = \frac{\partial u}{\partial X} + \frac{1}{2}\left[\left(\frac{\partial u}{\partial X}\right)^2 + \left(\frac{\partial v}{\partial X}\right)^2\right] \qquad \text{Equation 4.6}$$

$$E_{YY} = \frac{\partial v}{\partial Y} + \frac{1}{2}\left[\left(\frac{\partial v}{\partial Y}\right)^2 + \left(\frac{\partial u}{\partial Y}\right)^2\right] \qquad \text{Equation 4.7}$$

$$E_{XY} = \frac{1}{2}\left(\frac{\partial u}{\partial Y} + \frac{\partial v}{\partial X}\right) + \frac{1}{2}\left[\left(\frac{\partial u}{\partial X}\right)\left(\frac{\partial u}{\partial Y}\right) + \left(\frac{\partial v}{\partial X}\right)\left(\frac{\partial v}{\partial Y}\right)\right] \qquad \text{Equation 4.8}$$

Using the Lagrangian strains (Eqns 4.5-4.8), the maximum principal (E_{MAX}), minimum principal (E_{MIN}), and maximum shear (E_{SHEAR}) strains were calculated as detailed in equations 4.9-4.11 [27]:

$$P_{MAX} = \frac{1}{2}(E_{XX} + E_{YY}) + \frac{1}{2}\sqrt{(E_{XX} - E_{YY})^2 + 4E_{XY}^2} \qquad \text{Equation 4.9}$$

$$P_{MIN} = \frac{1}{2}(E_{XX} + E_{YY}) - \frac{1}{2}\sqrt{(E_{XX} - E_{YY})^2 + 4E_{XY}^2} \qquad \text{Equation 4.10}$$

$$P_{SHEAR} = \frac{1}{2}\sqrt{(E_{XX} - E_{YY})^2 + 4E_{XY}^2} = \frac{P_{MAX} - P_{MIN}}{2} \qquad \text{Equation 4.11}$$

The VIC program (VIC2D, Correlated Solutions; West Columbia, SC) output the following for each subset: displacement (u, v), correlation (C_l), Lagrangian strains (E_{xx},

Reproduced with permission of the copyright owner. Further reproduction prohibited without permission.

E_{yy}, E_{xy}), and principal strains (P_{MAX}, P_{MIN}, $\angle P_{MAX}$). See Appendix C for data reduction algorithms.

4.2.6 System Errors

4.2.6.1 Baseline Error

To determine the inherent error expected using the chondrocytes within the prepared MCP sample, two images (average of 1-20 images) were acquired five minutes apart without translating or deforming the sample. After the images were acquired and averaged, the images were analyzed using VIC to determine the displacement errors of u and v (standard deviation) using single images (no averaging) and averaged images.

4.2.6.2 Focusing Error

Since the focal plane is subjective and out-of-plane motion may be present requiring refocusing, focal plane selection and re-focusing errors were determined relative to a user-defined focal plane (set at 0μm). To determine how focal plane selection could affect VIC analysis, images (deformed) were taken 1-40 μm from the focal plane and analyzed with VIC with the user-defined focal plane image as the undeformed image. The error was defined as the u and v displacement standard deviations at each focal plane. To determine the effect refocusing had on VIC, focused (0μm, undeformed) and unfocused (1-40 μm from the optimal focal plane, deformed) images were acquired and analyzed. The error was defined as the u and v displacement standard deviation.

Reproduced with permission of the copyright owner. Further reproduction prohibited without permission.

4.2.6.3 Rigid Body Motion

Images were digitally transformed with a software plug-in (TransformJ, [28]) for ImageJ (NIH; Bethesda, MD) using quintic interpolation to mimic known u and v translations (0.001-100 pixels) and rotations (0.001-15 degrees). Using linear regression analysis with the applied motion as a predictor for the mean translation calculated by VIC, the pixel mean and standard deviations for all deformations were determined. [29-34]

In addition, known manual translations of the loading system on the microscope were applied in the xy-plane. Using linear regression analysis with the applied motion as a predictor for the mean translation calculated by VIC, the pixel mean and standard deviations for all translations were determined. [29-34]

4.2.6.4 Sample Friction Measurements

Friction induced by the upper and lower confining plates may have significant effects on the strain fields found during compression testing. To determine these possible systematic errors, a 4N-confining load was applied before translating the sample between the confining plate (upper plate) and viewing glass (lower confining plate), while the force (R) to translate the sample was acquired (see Figure 4.7). Epifluorescence images of the sample were captured before and after translating the sample 400μm. The mean and standard deviation of the two-dimensional strain fields were evaluated for both MC3 and PI of R1 only. In addition, the average static and dynamic friction forces were also determined assuming the measured force needed to translate the sample was solely due to friction (neglecting system friction within the linear bearings).

Reproduced with permission of the copyright owner. Further reproduction prohibited without permission.

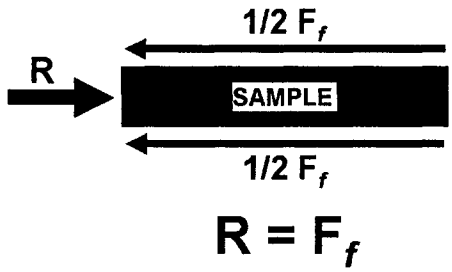

Figure 4.7: Rigid body diagram showing how the friction force (F_f) on the sample between the upper and lower confining plates was attained translating the sample by applying an unknown force (R).

4.2.6.5 System Compliance

The inherent compliance of the compression system was determined using the displacement rate of 0.01 mm/sec. Stiffness of the system was considered to be the average slope of the linear portion of the force-displacement curve of six consecutive compression tests of stainless steel.

4.3 Results

4.3.1 Sample Preparation

The prepared sample thickness was 5.415±0.070mm (mean±std). From medial to lateral the sample thickness was 5.403±0.063mm and 5.393±0.090mm, respectively. A 50μm saw curf loss was found for each cut.

4.3.2 System Errors

All images were analyzed using a subset size of 49 x 49 pixels with a five-pixel step size. The mean and standard deviations were determined using 30,222 points. A linear interpolation of a nine-pixel neighborhood of the displacement gradients was used for the strain calculations.

Reproduced with permission of the copyright owner. Further reproduction prohibited without permission.

4.3.2.1 Baseline Errors

There was a small benefit to averaging multiple images on the baseline error (Figure 4.8). Averaging greater than 10 images actually increased the error 1-3% for *u* and decreased the error by 20% in the *v*-direction (Figure 4.8). The expected error (STD) for acquiring single images was found to be 0.00025 and 0.00011 pixels for *u* and *v*, respectively. The calculated principal strains (P_{MAX}, P_{MIN}) were both 2 ± 6 μstrain (mean±std), respectively.

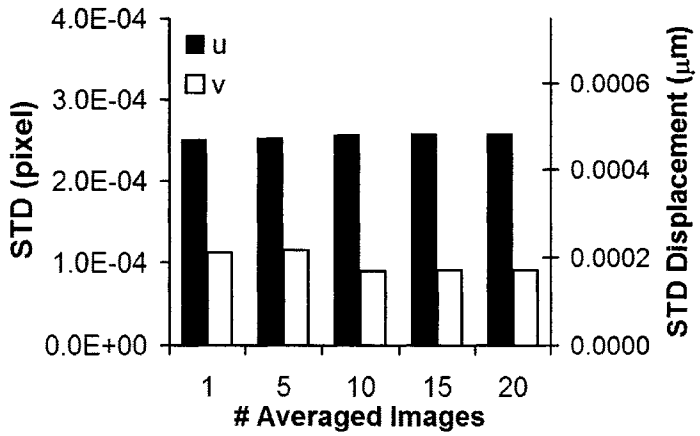

Figure 4.8: Baseline error of averaged images when no motion or deformation was applied.

4.3.2.2 Focusing Errors

When the second (deformed) image is not properly focused, the error expected is illustrated in Figure 4.9. The standard deviation of the displacement fields was about 0.04 pixels when ±20μm from the most favorable focal plane (minimum error). The displacement error increased in the *v*-direction only when the deviation was >20μm. In addition, the focal deviation was less severe into the tissue (negative) than out of the tissue surface (positive). The calculated P_{MAX} and P_{MIN} were 536 ± 545 and -501 ± 529 μstrain, respectively when within ±20μm from the focal plane.

Reproduced with permission of the copyright owner. Further reproduction prohibited without permission.

The refocus error results are illustrated in Figure 4.10. Using the current setup, the optimal focal range was found to be ±20μm. The *u*-direction had more displacement error than the *v*-direction (Figure 4.10). When within ±20μm from the focal plane, the calculated P_{MAX} and P_{MIN} were 459±490 and −474±504 μstrain, respectively.

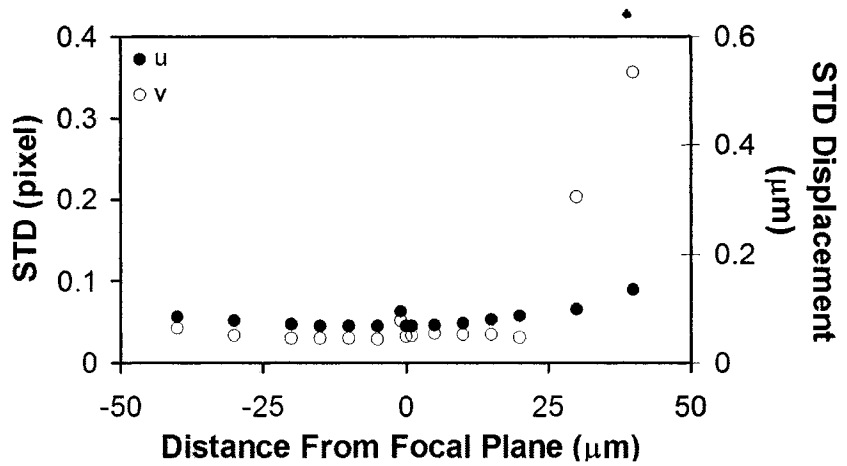

Figure 4.9: Focus error when correlating an optimally focused pattern with a pattern acquired a specified distance from the focal plane (0μm) without any deformation or translation.

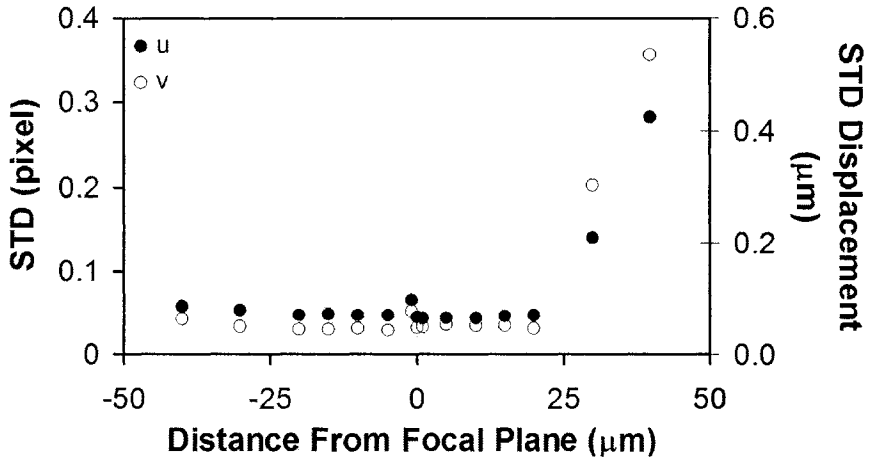

Figure 4.10: Refocus error when correlating two images acquired a specified distance from the focal plane (0μm) without any deformation or translation.

4.3.2.3 Rigid Body Motion Error

Artificially applied translations and calculated translations were strongly correlated (all r^2=1) (Figure 4.11ABC). The largest coefficient of variations (CV)

Reproduced with permission of the copyright owner. Further reproduction prohibited without permission.

occurred at the smallest applied translations (0.001 pixels) with 72% and 12% for *u* and *v* translation, respectively. Similarly, the largest CV for rigid body rotation was 62% at the smallest rotation increment of 0.001 degrees (Figure 4.11C). The calculated P_{MAX} and P_{MIN} strains for all artificial translations were both within 17±31 μstrain.

The manual translation calibration was highly correlated in the *v*-direction only (Figure 4.12). Similar to the artificial translations, the smallest increment (1μm) had a 68% CV error. The u-direction calibration poorly correlated. Both manual rigid body two-dimensional strain fields were continuous and homogeneous. The calculated P_{MAX} strains were 100±275 μstrain and the P_{MIN} strains were –410±270 μstrain for manually translating the sample across the stage.

4.3.2.4 Friction Errors

Static and dynamic friction forces were 88±13 N and 67±9 N, respectively. The static friction was 23% greater than the dynamic friction. The homogeneous strain patterns were consistent between repetitions. The calculated friction-induced strain was 4565±3257 and -8500±6136 μstrain for P_{MAX} and P_{MIN}, respectively (both CV=71%, Figure 4.13).

4.3.2.5 System Compliance

The average system compliance was 0.24±0.03 μm/N. Therefore for an applied load of 500N, the system is expected to have 119±15μm compliance. A linear relationship between force and displacement at all loading levels was assumed for system compliance calculations.

Reproduced with permission of the copyright owner. Further reproduction prohibited without permission.

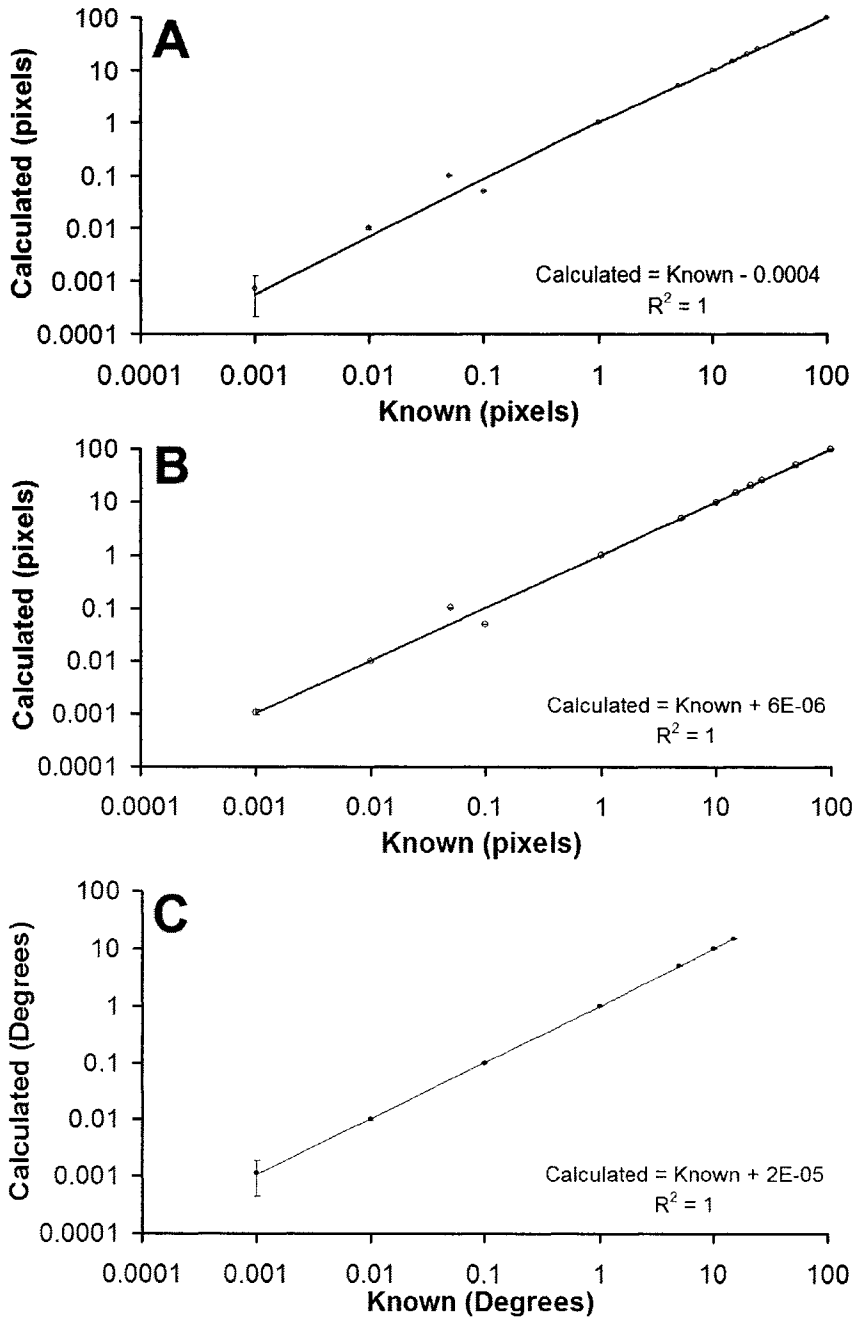

Figure 4.11: Artificial rigid body calibration. Linear regressions between VIC calculated and known (A) *u* translation (B) *v* translation (C) Z-axis rotation. Mean ± STD.

Reproduced with permission of the copyright owner. Further reproduction prohibited without permission.

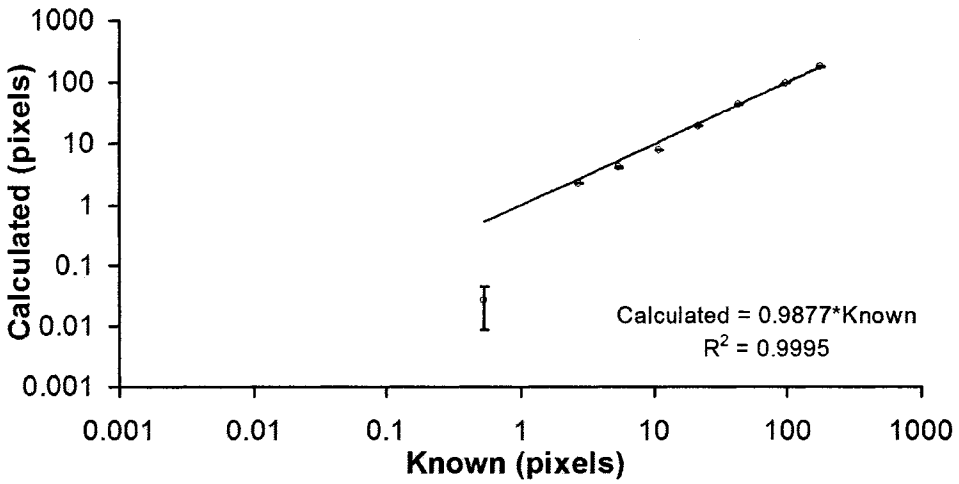

Figure 4.12: Manual rigid body calibration results in the *v*-direction. Mean ± STD.

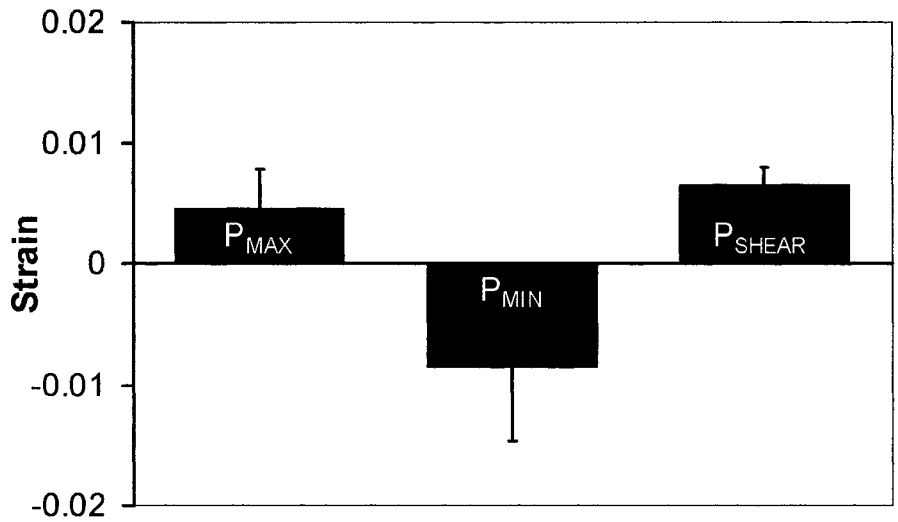

Figure 4.13: Expected principal strain and maximum shear strain errors caused by friction only. Mean ± STD.

4.4 Discussion

The strain error calculations associated with mating osteochondral specimen preparation, the custom-designed loading system, image acquisition, and VIC analysis methods have been quantified and documented. This system validation and error quantification has proven feasibility for testing planar osteochondral tissues and measurement of intra-tissue strains within opposing surfaces of cartilage loaded in compression. Baseline, focal, and rigid body motion errors are similar to those found in previous studies [16, 18, 31, 34]. The expected error involved in this process including

Reproduced with permission of the copyright owner. Further reproduction prohibited without permission.

the image acquisition system, data analysis, and friction is on the order of **7600 μstrain (0.76%)**. The equation, precision (%) = 0.0076 / Strain (%), represents the relationship between precision and the measured strain magnitude. For example, to achieve a tissue strain accurate within 5%, strain within the tissue must be greater than 15%.

The largest source of error was associated with friction induced on the sample, accounting for over 90% of the measured error. The next largest estimated errors were focal plane position and manually translating the sample having 0.23% and 0.13% of the total measured error, respectively. Ideas to minimize the systematic error associated with friction in future experiments include: reducing the confining load applied by using better prepared samples (sample thickness consistency and radius of curvature centrally placed within the sample), synovial fluid within the hydration chamber, coating the glass with a protein (e.g. bovine serum albumin), or adding stainless steel rods between the viewing glass and sample.

The benefit of taking multiple images filter noise during the image acquisition process, but the current system showed little benefit of taking multiple images and averaging them. Therefore, for future experiments, single image acquisition will be used which has the advantage of capturing quickly changing events (e.g. stress relaxation). The disparity between the estimated u and v baseline errors may be caused by slight errors in the digital timing of the CCD chip, similar errors are found using analog cameras [34]. The magnitudes of the baseline error were equivalent to researchers using similar systems [16, 18].

Reproduced with permission of the copyright owner. Further reproduction prohibited without permission.

The induced focus errors estimated in this study were also found to be very similar to previous research [31]. In the current study, an outlier at –1μm was noted and possibly caused by human or stage error when manipulating the focal length. The manual applied *u*-translations proved to be difficult and caused by the insecure attachment between the translation stage and the loading device permitting slip in the *u*-direction only. Therefore, the calculated and applied displacements in the *v*-direction correlated better than the *u*-direction translations. There were homogeneous strain fields for all translations, therefore the sample was parallel to the focal plane and lens aberration errors were not a systematic concern for the translations tested.

The system stiffness will have significant effects on testing osteochondral samples, given that a desired displacement to achieve a certain strain level will not be achieved. System compliance will cause errors in total applied strain and will depend on the forces being applied to the system. For example, a desired 20% compression strain is applied to a sample, but the sample was actually only compressed 17% at 200N or 13% at 400N due to system compliance. Increasing the stiffness of the system using more robust linear bearings would decrease system compliance to be negligible for expected loads.

Thorough evaluation of sample preparation error was not performed in this study, other than within sample thickness consistency (<2%CV). Uninvestigated sample preparation errors include: joint angle, sample location, and sagittal radius of curvature and articular surface placement within the sample. In particular, the radius of curvature placement could have significant effects on out-of-plane motion of the articular surfaces

Reproduced with permission of the copyright owner. Further reproduction prohibited without permission.

during loading. Orientation of the osteochondral sample within the testing chamber was not investigated and is recommended in future experiments.

Though not investigated, subset size and image contrast have an affect on the correlation results. Wang and researchers [35] determined a pixel subset size of 40x40 was sufficient for measuring intra-tissue strain within bovine cartilage at a magnification of 0.683μm/pixel (subset area = 1093μm^2). This is comparable to the current study's subset area of 1273μm^2 with a magnification of 0.530μm/pixel and a pixel subset size of 49x49. The optimization routine used for the correlation process has been found to minimize errors due to image contrast [36, 37], but image quality should be researched further in the future for this particular application.

It must be noted that the tissue in the current loading system will likely react to stresses/strains differently than it would if it were *in-vivo*, since this system represents only a snapshot of the joint dynamics during a gait-cycle. Also, the unconstrained tissue planes due to sample preparation most likely changed the normal fluid flow between the articular surfaces and surrounding tissues. In addition, the applied loads by the loading system are minimal compared to true physiological loads (whole joint loads of 4700N, [38]), and higher applied loads are limited by the current force cell and hardware.

The errors associated with specimen preparation, loading system, data acquisition, and analyses are rarely reported in the literature. The thorough analysis of error has validated the feasibility of using this unique system to load mating osteochondral surfaces and quantify strain within the cartilage matrix. The largest source of systematic error for the system was friction between the sample and the viewing glass. Additionally,

Reproduced with permission of the copyright owner. Further reproduction prohibited without permission.

specimen preparation could possibly exacerbate system error. The current work was concurrently performed with the work performed in Chapter 5; therefore knowledge of the large systematic error caused by friction was not addressed. Based on this study, this system can be used to investigate cartilage strain in opposing osteochondral surfaces with confidence. Future work will involve the use of this system to evaluate the effects of subchondral bone density, subchondral bone thickness, cartilage damage, age, joint angle, species, and tissue engineered cartilage replacement constructs on strain distributions and strain magnitudes within the cartilage matrix.

4.5 Conclusion

A custom-designed loading system and associated sample preparation procedure were developed and validated to quantify two-dimensional strain fields using video image correlation analysis (VIC) between two loaded opposing articular cartilage surfaces (MC3 and P1) within the equine metacarpophalangeal joint (MCP). The expected error involved in this process including the image acquisition system, data analysis, and friction is on the order of 7600 μstrain (0.76%), which is less than 23% of the average measured strain under low (relative to *in-vivo*) loads.

4.6 References

1. Maroudas, A., *Physicochemical properties of cartilage*, in *Adult Articular Cartilage*, M.A.R. Freeman, Editor. 1979, Pitman Medical: Tunbridge Well, England. p. 215-290.

2. Athanasiou, K.A., M.P. Rosenwasser, J.A. Buckwalter, T.I. Malinin, and V.C. Mow, *Interspecies comparisons of in situ intrinsic mechanical properties of distal femoral cartilage.* Journal of Orthopaedic Research, 1991. **9**: p. 330-340.

Reproduced with permission of the copyright owner. Further reproduction prohibited without permission.

3. Hunziker, E., *Articular cartilage structure in humans and experimental animals*, in *Articular Cartilage and Osteoarthritis*, K.E. Kuettner, Schleyerbach, R., Peyron, J.G., Hascall, V.C., Editor. 1992, Raven Press: New York. p. 183-199.

4. Schinagl, R.M., M.K. Ting, J.H. Price, and R.L. Sah, *Video microscopy to quantitate the inhomogeneous equilibrium strain within articular cartilage during confined compression.* Annal of Biomedical Engineering, 1996. **24**: p. 500-512.

5. Schinagl, R., D. Gurskis, A. Chen, and R. Sah, *Depth-dependent confined compression modulus of full thickness bovine articular cartilage.* Journal of Orthopaedic Research, 1997. **15**(4): p. 499-506.

6. Chen, S.S., Y.H. Falcovitz, R. Schneiderman, A. Maroudas, and R.L. Sah, *Depth-dependent compressive properties of normal aged human femoral head articular cartilage: relationship to fixed charge density.* Osteoarthritis Cartilage, 2001. **9**(6): p. 561-9.

7. Akizuki, S., V.C. Mow, F. Muller, J.C. Pita, D.S. Howell, and D.H. Manicourt, *Tensile properties of human knee joint cartilage: I. Influence of ionic conditions, weight bearing, and fibrillation on the tensile modulus.* J Orthop Res, 1986. **4**(4): p. 379-92.

8. Lee, R.C., E.H. Frank, A.J. Grodzinsky, and D.K. Roylance, *Oscillatory compressional behavior of articular cartilage and its associated electromechanical properties.* J Biomech Eng, 1981. **103**(4): p. 280-92.

9. Armstrong, C.G. and V.C. Mow, *Variations in the intrinsic mechanical properties of human articular cartilage with age, degeneration, and water content.* Journal of Bone & Joint Surgery - American Volume, 1982. **64**(1): p. 88-94.

10. Frank, E. and A. Grodzinsky, *Cartilage electromechanics - II. a continuum model of cartilage electrokinetics and correlation with experiments.* J. Biomechanics, 1987. **20**(6): p. 629-639.

11. Williamson, A.K., A.C. Chen, and R.L. Sah, *Compressive properties and function-composition relationships of developing bovine articular cartilage.* J Orthop Res, 2001. **19**(6): p. 1113-21.

12. Armstrong, C.G., W.M. Lai, and V.C. Mow, *An analysis of the unconfined compression of articular cartilage.* Journal of Biomechanical Engineering, 1984. **106**(2): p. 165-73.

13. Jurvelin, J.S., M.D. Buschmann, and E.B. Hunziker, *Optical and mechanical determination of Poisson's ratio of adult bovine humeral articular cartilage.* Journal of Biomechanics, 1997. **30**(3): p. 235-41.

Reproduced with permission of the copyright owner. Further reproduction prohibited without permission.

14. Wong, M., M. Ponticiello, V. Kovanen, and J.S. Jurvelin, *Volumetric changes of articular cartilage during stress relaxation in unconfined compression.* J Biomech, 2000. **33**(9): p. 1049-54.

15. Wang, C.C., C.T. Hung, and V.C. Mow, *An analysis of the effects of depth-dependent aggregate modulus on articular cartilage stress-relaxation behavior in compression.* J Biomech, 2001. **34**(1): p. 75-84.

16. Wang, C.C., J.M. Deng, G.A. Ateshian, and C.T. Hung, *An automated approach for direct measurement of two-dimensional strain distributions within articular cartilage under unconfined compression.* J Biomech Eng, 2002. **124**(5): p. 557-67.

17. Wang, C.C.B., N.O. Chahine, C.T. Hung, and G.A. Ateshian, *Optical determination of anisotropic material properties of bovine articular cartilage in compression.* Journal of Biomechanics, 2003. **36**(3): p. 339-353.

18. Bae, W.C., C.W. Lewis, and R.L. Sah. *Intra-tissue strain distribution in normal human articular cartilage during clinical indentation testing.* in *Transactions of the ORS.* 2002. New Orleans, Louisiana.

19. Erne, O.K., J. Reid, and M. Bottlang. *Offset-strain and depth-dependent strain distribution across articular cartilage.* in *49th Annual Meeting of the Orthopaedic Research Society.* 2003. New Orleans, Lousiana.

20. Pool, R.R. and D.M. Meagher, *Pathologic findings and pathogenesis of racetrack injuries.* Vet Clin North Am Equine Pract, 1990. **6**(1): p. 1-30.

21. Kawcak, C., *Effects of loading on subchondral bone of equine carpal and metacarpophalangeal joints*, in *Department of Clinical Sciences.* 1998, Colorado State University: Fort Collins.

22. Kawcak, C.E., C.W. McIlwraith, R.W. Norrdin, R.D. Park, and P.S. Steyn, *Clinical effects of exercise on subchondral bone of carpal and metacarpophalangeal joints in horses.* Am J Vet Res, 2000. **61**(10): p. 1252-8.

23. Norrdin, R.W., C.E. Kawcak, B.A. Capwell, and C.W. McIlwraith, *Subchondral bone failure in an equine model of overload arthrosis.* Bone, 1998. **22**(2): p. 133-9.

24. Budras, K.D., W.O. Sack, and S. Rock, *Anatomy of the horse: an illustrated text.* Third ed. 2001, ?: Schlutersche.

25. Sutton, M.A., S.R. McNeill, J.D. Helm, and Y.J. Chao, *Advances in two-dimensional and three-dimensional computer vision*, in *Photo-Mechanics.* 2000. p. 323-372.

Reproduced with permission of the copyright owner. Further reproduction prohibited without permission.

26. Schreier, H.W., J.R. Braasch, and M.A. Sutton, *Systematic errors in digital image correlation caused by intensity interpolation.* Optical Engineering, 2000. **39**(11): p. 2915-2921.

27. Eringen, A.C., *Mechanics of Continua.* 2nd ed. 1980, Huntington, NY: Robert E. Krieger Publishing Company.

28. Meijering, E.H., W.J. Niessen, and M.A. Viergever, *Quantitative evaluation of convolution-based methods for medical image interpolation.* Med Image Anal, 2001. **5**(2): p. 111-26.

29. Lu, H. and P.D. Cary, *Deformation measurements by digital image correlation: Implementation of a second-order displacement gradient.* Experimental Mechanics, 2000. **40**(4): p. 393-400.

30. Maddux, G.A., C.M. Horton, S.R. McNeil, and M.D. Lansing, *Field Methods to Measure Surface Displacement and Strain with the Video Image Correlation Method.* 1994, University of Alabama: Huntsville, Alabama. p. 33.

31. Smith, B.W., X. Li, and W. Tong, *Error assessment for strain mapping by digital image correlation.* Experimental Techniques, 1998. **22**(4): p. 19-21.

32. Vendroux, G., *Correlation : A digital image correlation program for displacement and displacement gradient measurements.* 1990, Graduate Aeronautical Laboratories, California Institute of Technology: Pasadena, CA. p. 1-32.

33. Bay, B., S. Yerby, R. McLain, and E. Toh, *Measurement of strain distributions within vertebral body sections by texture correlation.* Spine, 1999. **24**(1): p. 10-17.

34. Sun, Z.L., J.S. Lyons, and S.R. McNeill, *Measuring microscopic deformations with digital image correlation.* Optics and Lasers in Engineering, 1997. **27**(4): p. 409-428.

35. Wang, C.C.B., J.M. Deng, G.A. Ateshian, and C.T. Hung, *An automated approach for direct measurement of two-dimensional strain distributions within articular cartilage under unconfined compression.* Journal of Biomechanical Engineering-Transactions of the Asme, 2002. **124**(5): p. 557-567.

36. Sutton, M.A., S.R. McNeill, J.S. Jang, and M. Babai, *Effects of Subpixel Image-Restoration on Digital Correlation Error-Estimates.* Optical Engineering, 1988. **27**(10): p. 870-877.

Reproduced with permission of the copyright owner. Further reproduction prohibited without permission.

37. Bruck, H.A., S.R. McNeill, M.A. Sutton, and W.H. Peters, *Digital Image Correlation Using Newton-Raphson Method of Partial-Differential Correction.* Experimental Mechanics, 1989. **29**(3): p. 261-267.

38. Les, C.M., S.M. Stover, K.T. Taylor, J.H. Keyak, and N.H. Willits, *Ex vivo simulation of in vivo strain distributions in the equine metacarpus.* Equine Vet J, 1998. **30**(3): p. 260-6.

Reproduced with permission of the copyright owner. Further reproduction prohibited without permission.

5 MEASUREMENT OF ARTICULAR CARTILAGE INTRA-TISSUE STRAIN DISTRIBUTIONS AND UNDERLYING SUBCHONDRAL BONE THICKNESS AND BONE MINERAL DENSITY IN A NORMAL ARTICULATING JOINT

5.1 Introduction

The primary cause of osteoarthritis (OA) is unknown, but may be secondary to injury, joint infection, or a variety of genetic disorders [1, 2]. Usually, OA affects all joint tissues including the articular cartilage, subchondral bone, trabecular bone, synovial capsule, and ligaments [3]. Commonly, connective tissue changes related to OA include articular cartilage fibrillation and subchondral bone remodeling [2-8]. Though the roles of mechanical factors (e.g. trauma, repetitive movements, and joint laxity) on OA development and progression have been studied extensively, the role of subchondral bone in OA progression is less clear with conflicting reports in the literature [4, 6, 9-28].

Subchondral bone can refer to some or all of the subarticular structures. For this study, the subchondral bone plate (ScBP) was defined as the radio-dense layer between the uncalcified articular cartilage and supportive trabecular system [29]. The ScBP plays an integral part in the physiological function of the synovial joint by supporting the articular surface and dissipating applied joint energy [4, 30]. For centuries, researchers have noted the strong relationship between bone morphology and mechanical stress

Reproduced with permission of the copyright owner. Further reproduction prohibited without permission.

history [15, 31-35]. For example, research determined that the ScBP remodels (densification and thickening) according to its stress environment (e.g., exercise and aging) [15, 26, 29, 36-38]. Pauwels and later, Kummer proposed that subchondral bone remodeling is determined by applied localized stress [39-42]. This theory implies that subchondral bone remodels to create a structure (densification and/or thickening) capable of withstanding physiologically applied stresses in order to maintain optimal tissue strains [39-42].

The ScBP thickness is different between and within joints and is dependent on the function of the joint [29, 43, 44]. The geometric concavity of the surface (convex/concave) has been noted to have an effect on ScBP thickness as well [38, 45, 46]. The convex shaped surface is found to be much thinner than its concave counterpart due in part to greater tensile stresses acting on the concave surface [45]. Using computer simulations, the concave curvature has been noted to augment joint incongruity, providing a more even stress distribution across the joint, while enhancing cartilage nutrition and lubrication [38]. Bone mineral density (BMD) also varies between and within joints and is routinely found elevated under areas of predominately-loaded regions [29, 47]. Two factors, age and exercise, have been found to significantly affect the magnitude and distribution of bone mineral density [48-51]. Investigations have drawn conflicting conclusions about the relationship between ScBP thickness and BMD under areas of cartilage degradation [2, 4, 7, 14, 17-19, 27, 28, 52-57]

According to some theories, ScBP adaptation may contribute to the development of osteoarthritis by becoming thicker and denser after remodeling, thus reducing the

Reproduced with permission of the copyright owner. Further reproduction prohibited without permission.

shock absorption of the joint and causing greater physiological strains to be applied to the articular cartilage [26, 55]. The proposed increased applied strains may be related to uncalcified cartilage degradation (superficial fibrillation and erosion) and/or microfractures in the underlying calcified cartilage [22, 26, 58, 59]. The mechanical environment within articular cartilage is an important regulator of tissue metabolism during normal and pathological conditions. The effects of loading on metabolism and the structure of bone and cartilage are of particular interest.

Exercise-associated OA is common in human, equine, and canine species [2, 4, 24, 28, 60-71]. The equine metacarpophalangeal (MCP) joint is exposed to high mechanical loading and wear, predisposing the joint to osteochondral fragmentation, subchondral bone lesions, articular/subarticular cysts, and articular surface fibrillations and erosion [4, 22, 66-68, 72-75]. An increase in subchondral bone thickness and bone mineral density with exercise has been noted in the equine MCP joint, which may be associated with a high incidence of fractures and articular lesions in this joint [47, 53, 66, 67, 74-76]. The structural OA manifestations in the equine MCP joint are very similar to the human condition, possibly making the MCP joint an excellent model for the study of OA progression.

The analysis of cartilage contact between articular surfaces is crucial to study the etiology of osteoarthritis. Recent experimental methods, such as stereophotogrammetry magnetic resonance imaging have been used to analyze synovial joint contact behavior [77-80]. Though these methods are effective in observing overall strain, they are insensitive to cartilage's depth-dependent properties related to the zonal structure from

Reproduced with permission of the copyright owner. Further reproduction prohibited without permission.

the articular surface (superficial (0-20%), middle (20-50%), and deep (50-100%), [81-89]. Quantification of compression strains using either unconfined or confined boundary conditions under platen loading neglects the interaction between articular surfaces and geometrical effects on strain across the articular surface. To date, experimental data is only available for depth-dependent strains induced by contact of naturally opposing cartilage surfaces ($5x5x5mm^3$) for one articular surface, under infinitesimal strain conditions, and the tested cartilage specimens were not physiologically adjacent articular surfaces [90].

Though inhomogeneous deformation within cartilage using platen loading and subchondral thickness and bone mineral density have been studied extensively, intra-tissue cartilage strains within compressed opposing articular surfaces and their relationship with underlying subchondral bone properties (thickness and bone mineral density) have not. The ability to quantify intra-tissue cartilage strains and underlying subchondral bone characteristics between physiologically opposing surfaces is needed to help understand the etiology and progression of OA. Therefore, the purpose of this study was to experimentally determine and relate regional intra-tissue cartilage strain distributions to underlying regional subchondral bone properties of opposing osteochondral surfaces from normal equine MCP joints. Regional intra-tissue cartilage principal (P_{MAX} and P_{MIN}) and maximum shear (P_{SHEAR}) strains and their gradients (∇P_{MAX}, ∇P_{MIN}, and ∇P_{SHEAR}), will be experimentally determined for each cartilage zone (superficial, middle, and deep) across the articular surfaces of the MCP joint using digital image correlation (Chapter 4). The underlying regional subchondral bone properties (ScBP thickness and BMD) of each region will be determined using validated methods

Reproduced with permission of the copyright owner. Further reproduction prohibited without permission.

from Chapters 2 and 3, respectively. The hypotheses for this study include: superficial cartilage strains will be larger than deeper zones, ScBP thickness and bone mineral density will correlate, and cartilage strains (P_{MAX}, P_{MIN}, and P_{SHEAR}) will be greater over areas of greater ScBP thickness and greater BMD.

5.2 Materials and Methods

5.2.1 Sample Acquisition and Preparation

Six equine MCP joints (2-3yrs) were obtained within 4 hours of sacrifice and prepared as described in Chapter 4 (see Appendix D for sample history).

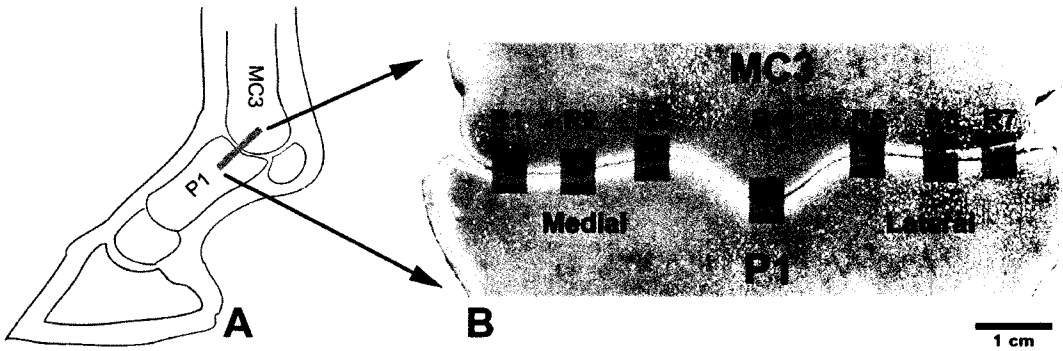

Figure 5.1: (A) Sagittal view of the metacarpophalangeal joint (MCP) showing the joint angle which the sample (gray area) prepared from the 1st phalanx (P1) and 3rd metacarpal bone (MC3). (B) Coronal view of a typical sample showing the P1 and MC3 articular surfaces and analysis regions (R1-R7). A benefit using the MCP joint is the sagittal ridge helped restrict medial-to-lateral movement centrally (R4) during loading.

5.2.2 Experimental Testing Setup

The experimental testing setup (Figure 5.2) is described and validated to provide accurate quantification of strain within mating osteochondral specimens in Chapter 4.

Reproduced with permission of the copyright owner. Further reproduction prohibited without permission.

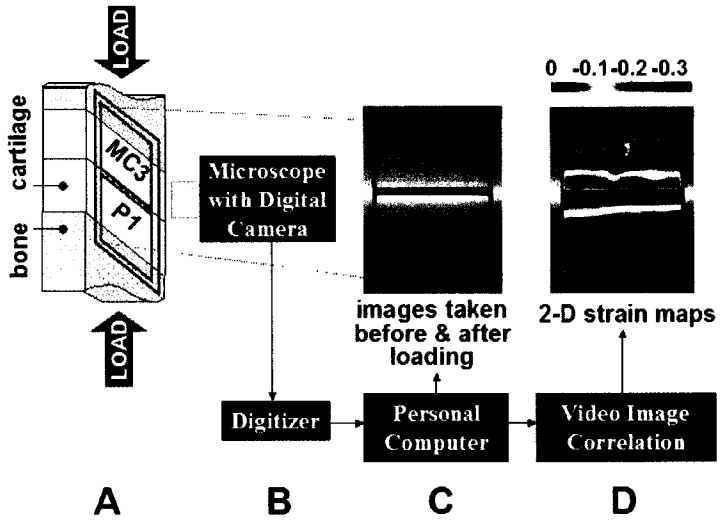

Figure 5.2: Schematic of testing setup (A) custom-designed loading system applies load to the osteochondral sample, (B) the epifluorescence microscope, digital camera, and digitizer capture a magnified view of fiducial markers (chondrocytes) within osteochondral sample's cartilage surfaces, (C) images are taken before and after loading and saved on a personal computer, (D) then digital image correlation is used to analyze the images to determine intra-tissue displacements and strains.

5.2.3 Compression Testing

Using the testing setup and image acquisition system described in Chapter 4, a 100N preload was applied at 0.01 mm/sec to the MC3 (proximal). The preload was allowed to equilibrate until the slope was less than 10 N/min, the images were acquired for each region of interest (Figure 5.1). Tidemark-to-tidemark (T-T) distances of the mating articular surfaces of each region were measured to determine the average regional gauge length using ImageJ software (NIH, Bethesda, MD). Based on the system compliance (Chapter 4) and gauge length, a 20% strain was applied to the osteochondral sample at 0.01mm/sec to obtain 12% T-T sample strain. Images of the compressed state were acquired for all regions after equilibrium. The testing protocol and an example of the datasheet used for each sample can be found in Appendix D.

Reproduced with permission of the copyright owner. Further reproduction prohibited without permission.

5.2.4 Strain Analysis and Post-Processing

Two-dimensional video image correlation (VIC) was performed with software (VIC2D, Correlated Solutions; West Columbia, SC) to determine the intra-tissue Lagrangian principal (P_{MAX} and P_{MIN}) and the maximum shear ($P_{SHEAR} = [P_{MAX} - P_{MIN}]/2$) strain maps between the equilibrium preload and equilibrium 12% strain condition. VIC used a 49x49 pixel subset (36μm x 36μm) with a step size of 5 pixels (specimen resolution=2.7μm). The subset pixel size (49x49) provided good tracking, given the fiducial density of the tissue tested. A binomial filter was applied to the image sets before VIC was performed to minimize displacement errors using quintic interpolation [91].

The axial spatial coordinates of each strain map (P_{MAX}, P_{MIN}, and P_{SHEAR}) were normalized to the regional cartilage thickness and their gradients were determined over 1% increments of the normalized thickness (∇P_{MAX}, ∇P_{MIN}, and ∇P_{SHEAR}). For each region, the strains (P_{MAX}, P_{MIN}, P_{SHEAR}, ∇P_{MAX}, ∇P_{MIN}, and ∇P_{SHEAR}) were divided into three zones corresponding to the superficial zone at 0-30% of the cartilage thickness (S), middle zone at 30-70% (M), and deep zone at 30-100% (D). Strains for each zone were averaged over an area having the width of 2-10 data points (Figure 5.3, see Appendix D for post-processing algorithms).

5.2.5 Subchondral Bone Mineral Density (BMD)

Bone mineral density of subchondral bone was measured using a dual energy x-ray absorbtiometry scanner (DEXA, Hologic Delphi QDR; Bedford, MA) using high-

Reproduced with permission of the copyright owner. Further reproduction prohibited without permission.

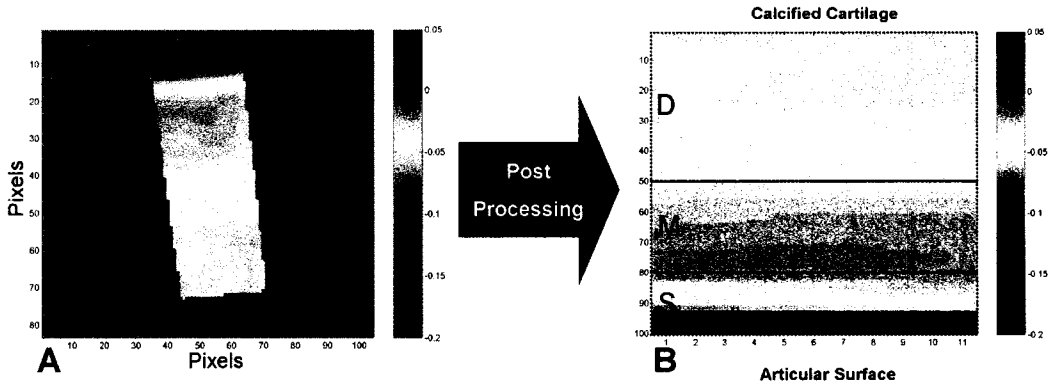

Figure 5.3: Post-processing schematic (A) region of interest is selected for a typical strain map from the articular surface to the tidemark (calcified cartilage) (B) after post-processing, the selected strain map is rotated, cartilage thickness is normalized, and responses for each zone (S, M, and D) are determined.

Reproduced with permission of the copyright owner. Further reproduction prohibited without permission.

resolution settings and small animal software. Subchondral scan regions were $3.1x3.1mm^2$ in the plane perpendicular to the articular surface. The mean of three independent scans was used to quantify the area bone mineral density, μ_{BMD} ($grams/cm^2$). Subchondral volumetric bone mineral density (BMD, $grams/cm^3$) was calculated by dividing the area bone mineral density ($grams/cm^2$) by the region thickness (cm) of sample. BMD measurement precision was determined previously to be within 5% of the mean (Chapter 2).

5.2.6 Subchondral Bone Thickness (ScBP thickness)

Osteochondral samples were radiographed using a high-resolution cabinet x-ray machine (Faxitron® Cabinet X-ray System Model 43855A, Wheeling, IL) with high-resolution mammography film (X-OMAT film, Eastman Kodak, Rochester, NY). Three radiographs were taken of each joint sample with an aluminum calibration step wedge in view for each exposure (Dent-X Corporation, Elmsford, NY). A 2:15 minute exposure at 42 kVp was selected to allow visualization of all the step-wedge luminance intensities. Radiographs were developed and checked for consistency of step-wedge intensity graduations. Each film was converted to a digital image (LS75 digitizer, Eastman Kodak Company, Rochester, NY) at a resolution of 119.11 μm/pixel (Figure 5.4A).

Images were cropped and rotated to standard orientations using Image-Pro Plus (Media Cybernetics, Silverspring, MD). Each image was filtered using a local best-fit contrast enhancement to differentiate between pixel luminance values (Figure 5.4B) [92]. A custom semi-automatic analysis program was implemented to perform subchondral bone edge detection along the articular surfaces using articular landmarks (Figure 5.4B).

Reproduced with permission of the copyright owner. Further reproduction prohibited without permission.

Briefly, ScBP thickness was determined by: (1) identifying luminance profiles at sites of interest (Figure 5.1) at a width of 25 pixels or 3mm; (2) inflection point recognition in the luminance profile determined the ScBP boundaries (Figure 5.4C); (3) linear distance between the subchondral bone boundaries (luminance inflection points) determination (Figure 5.4C); and (4) visual confirmation of the measurement by the user. The ScBP thickness was quantified for all the regions (R1-R7, coinciding with strain measurements of R1-R7) of each bone (MC3 and P1, Figure 5.1). Each measurement was repeated five times to provide a mean ScBP thickness (mm) across both MC3 and P1 articular surfaces (R1-R7). The measurement precision was quantified previously to be 0.045mm (Chapter 3). For more information on regional selection, see Appendix B.

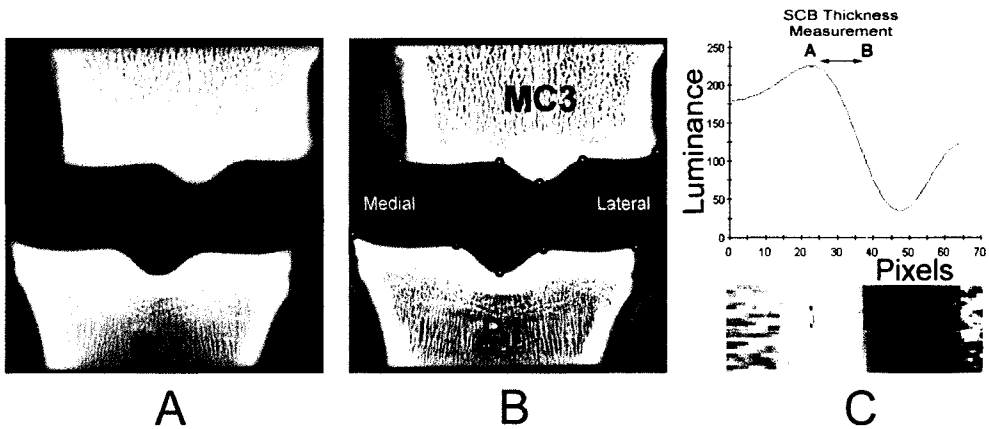

Figure 5.4: Image processing and subchondral bone (ScBP) thickness measurement: (A) raw radiograph image (B) filtered image with feature points used for ScBP thickness measurement locations for the distal 3rd metacarpal (MC3) and proximal 1st phalanx (P1) (C) an illustration of the ScBP thickness measurement using a line luminance profile to determine the ScBP margins, luminance peak (a) and largest negative gradient (b).

5.2.7 Statistical Analysis

Random error normality for each response was checked and transformed if needed for parametric statistical analysis. The effects and interactions of bone (MC3 and P1), region (R1-R7), and cartilage zone (S, M, and D) on P_{MAX}, P_{MIN}, P_{SHEAR}, ∇P_{MAX},

Reproduced with permission of the copyright owner. Further reproduction prohibited without permission.

∇P_{MIN}, and ∇P_{SHEAR} were determined with repeated measures mixed ANOVA using the Satterthwaite degrees of freedom approximation. Effects on ScBP thickness and BMD were also determined using the same model without considering cartilage zone. For only the ScBP thickness regional and bone comparisons, the ScBP measurement data (from Chapter 2) was combined with the current data to increase power. The random effect was considered as each sample. Post-hoc comparisons were determined using Tukeys-adjusted least squares means. Linear regressions were performed to determine the relationship between strain (P_{MAX}, P_{MIN}, and P_{SHEAR}) and subchondral bone properties (ScBP thickness and BMD) within each sample by cartilage zone (S, M, and D). The regression slopes (β) were compared using Student t-tests. All statistical tests were performed used SAS statistical software (SAS Institute Inc., Cary, NC, USA) at a significance level of α=0.05 (SAS algorithms are available in Appendix D)

5.3 Results

All samples were visually inspected and without any gross OA changes (superficial cartilage degradation and marginal osteophytes). Prepared osteochondral samples had uniform height (5.28±0.11mm, thickness, palmar-dorsal) and length (17.9±1.0mm, proximal-distal). From medial to lateral, the sample height varied from 5.26±0.22mm to 5.29±0.22mm, respectively. The width of the sample (joint breadth) was different between animals, but was accommodated by the testing setup. Opposing cartilage surfaces had a T-T gauge length of 1.47±0.13mm and were compressed (T-T, tidemark to tidemark) an average of 11.3±2.3% in the loaded state. Applied strains varied by region along the cartilage surface, thus region was considered a covariate for all statistical strain analyses. VIC pixel subset correlation between preload and loaded

Reproduced with permission of the copyright owner. Further reproduction prohibited without permission.

images for both mating cartilage surfaces was successful for 60% (8.4/14) of the regions on average of each sample or 60% (50/84) of the total attempted analyzed regions. Consequently, 40% of the data was not analyzed due to poor image quality (i.e. fiducial chondrocytes had moved into a different focal plane). For majority of the samples, R4 remained unloaded (i.e. unstrained) even after the preload was applied and all other regions were strained. Many response variables required transformations to satisfy normality conditions: $(P_{MAX})^{-0.3}$, $(P_{MIN})^{0.3}$, $\log_{10}(P_{SHEAR})$, $(\text{ScBP thickness})^{-1}$, and $\log_{10}(\text{BMD})$.

5.3.1 Principal and Maximum Shear Strains: P_{MAX}, P_{MIN}, and P_{SHEAR}

No significant differences between MC3 and P1 were found for P_{MAX}, P_{MIN}, and P_{SHEAR} strains (all $p>0.5$). Region and cartilage zone significantly influenced P_{MAX} ($p<0.0005$ and $p<0.05$), P_{MIN} ($p<0.005$ and $p<0.0001$), and P_{SHEAR} ($p<0.0001$ and $p<0.0001$ respectively). Regional T-T strain adjustment (covariate) was found to be significant for only P_{MAX} comparisons ($p<0.05$). P_{MAX} in R4 was significantly less than R1-R3, R5 and R7 regions (all $p<0.005$, Figure 5.5). P_{MAX} within R7 was found to be significantly greater than R3-R6 (all $p<0.05$, Figure 5.5). P_{MIN} regional differences were only detected between R4 and R7 (R7>R4, $p<0.005$, Figure 5.5). P_{SHEAR} at R4 was significantly less than adjacent regions (R1-R3, R5, and R7, all $p<0.05$, Figure 5.5).

Reproduced with permission of the copyright owner. Further reproduction prohibited without permission.

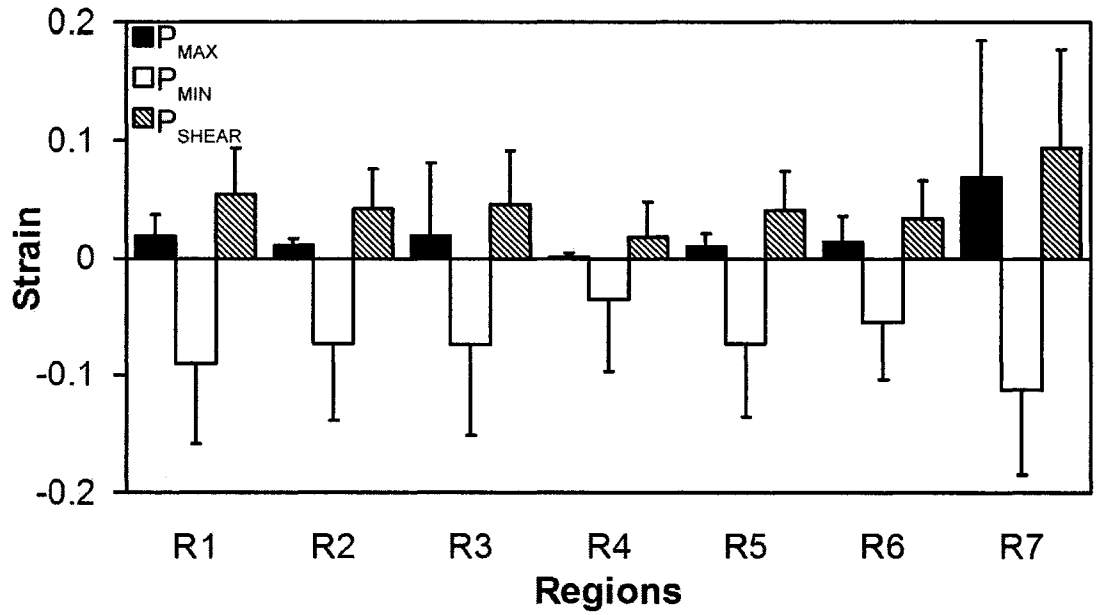

Figure 5.5: The effects of region on depth-averaged P_{MAX} (■), P_{MIN} (□), and P_{SHEAR} (▒) strains for 12% compression sample. Mean±STD.

When averaging over region, the superficial cartilage zone had slightly greater P_{MAX} strains than the middle zone ($p<0.051$, Figure 5.6). P_{MAX} directions were primarily parallel to the articular surface in the superficial zone with random orientation in the deeper zones, though tensile strains were noted in the deeper zones in some samples (Figure 5.7). P_{MIN} within the superficial (S) zone was greater than the deeper zones (M, $p<0.005$; D, $p<0.0005$; Figure 5.6). P_{MIN} orientation was perpendicular to the articular surface for all cartilage zones. P_{SHEAR} in the superficial cartilage zone was significantly greater than middle and deep zones ($p<0.05$ and $p<0.0001$ respectively, Figure 5.6). Generally, the measured regional averaged strains increased abaxially with distance from the sagittal ridge (R4). The medial/lateral edges had the largest strains, while the sagittal ridge (R4) had the least (Figure 5.5). Also, there was a decrease in all three strain components with decrease in cartilage depth (Figure 5.6). An example strain map is illustrated in Figures 5.7-5.9. P-values for all comparisons are available in Appendix D.

Reproduced with permission of the copyright owner. Further reproduction prohibited without permission.

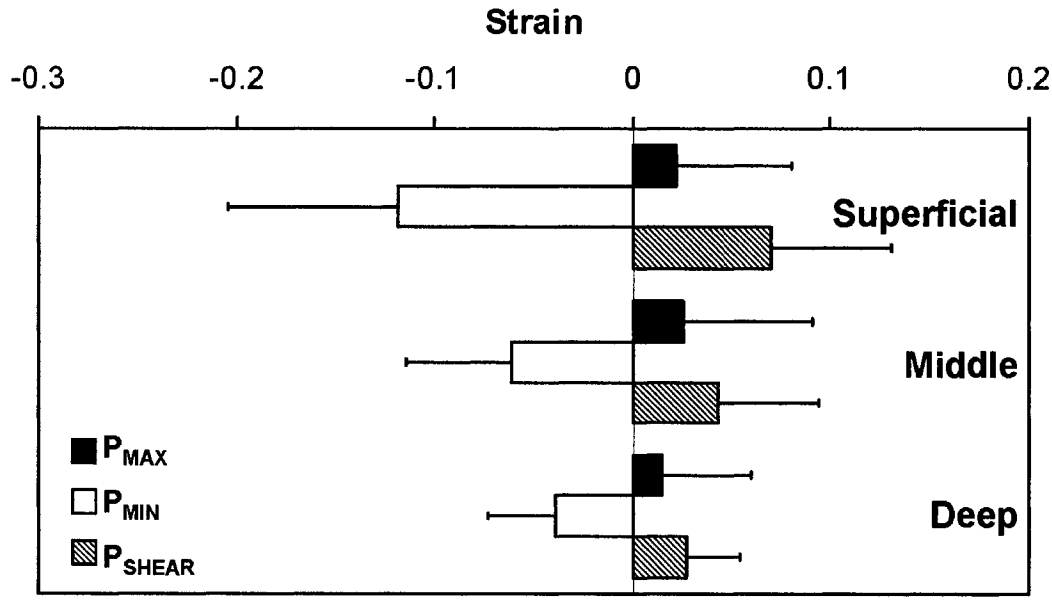

Figure 5.6: The effect of cartilage zone on region-averaged P_{MAX} (■), P_{MIN} (□), and P_{SHEAR} (▒) strains for 12% sample compression. Mean ± STD.

5.3.2 Strain Gradients (∇P_{MAX}, ∇P_{MIN}, and ∇P_{SHEAR})

Bone, region, or cartilage zone did not significantly affect ∇P_{MAX} results (Figure 5.10A). ∇P_{MIN} and ∇P_{SHEAR} had significant influences from bone, zone, and region (all $p<0.001$). ∇P_{MIN} in the P1 superficial cartilage zone were greater than the ∇P_{MIN} of the MC3 superficial cartilage zone ($p<0.05$, Figure 5.10B). P_{MIN} (-) strains have opposite signs compared with P_{MAX} & P_{SHEAR} (+) strains, therefore a negative ∇P_{MIN} and positive ∇P_{MAX} or ∇P_{SHEAR} represent the same phenomenon, the average strain change within 1% increments. The ∇P_{MIN} in the superficial cartilage zones of MC3 and P1 were both greater than the ∇P_{MIN} in the MC3 and P1 deep zones ($p<0.005$, Figure 5.10B). The

Reproduced with permission of the copyright owner. Further reproduction prohibited without permission.

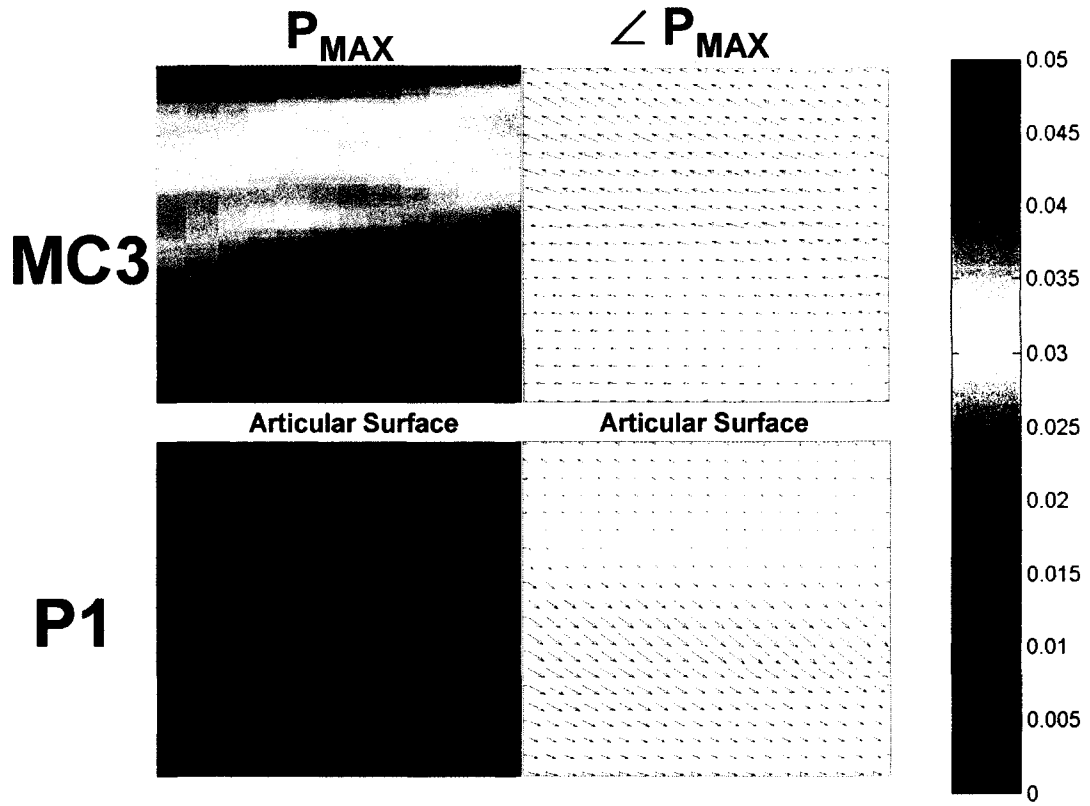

Figure 5.7: Example P_{MAX} strain and $\angle P_{MAX}$ maps for MC3 and P1. Notice the tensile strains are larger in the deeper zone and may coincide with collagen fiber direction in the zone (MC3-R2 of sample #5).

Reproduced with permission of the copyright owner. Further reproduction prohibited without permission.

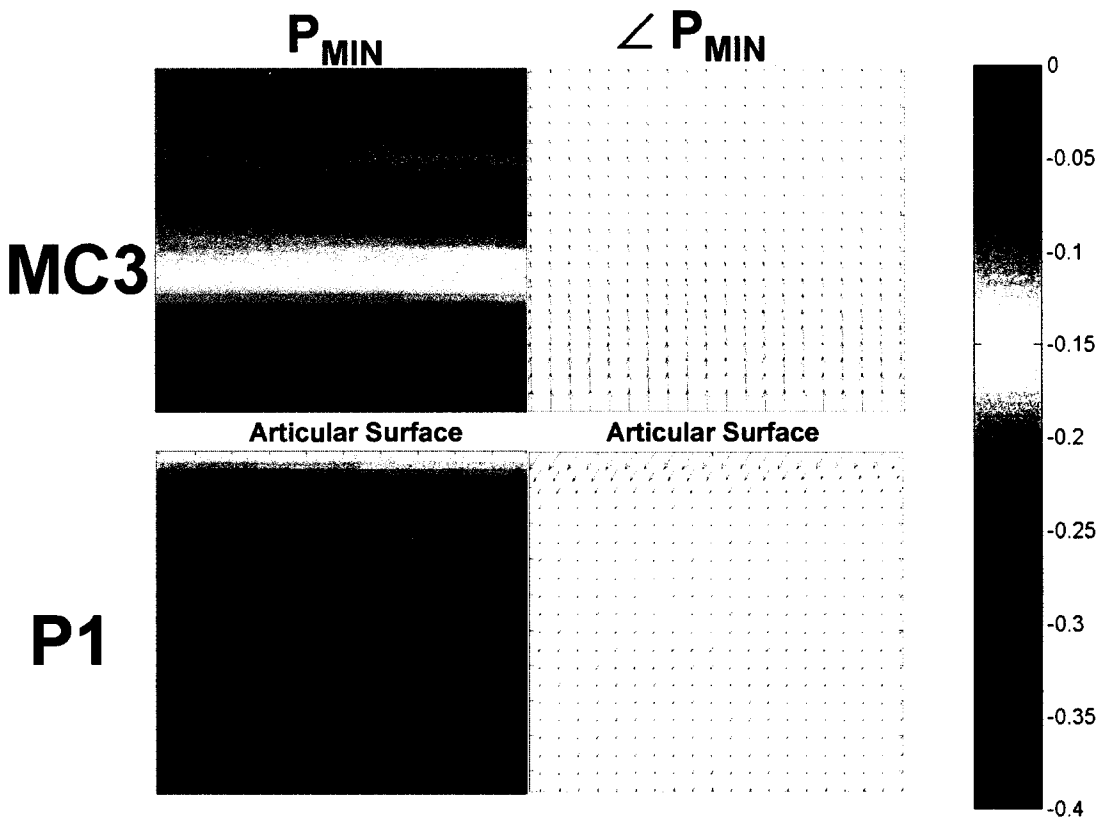

Figure 5.8: Example P_{MIN} strain and $\angle P_{MIN}$ maps for MC3 and P1. For this sample (MC3-R2 of sample #5), the tensile strains are larger in the deeper zone and may coincide with collagen fiber direction in this zone.

Reproduced with permission of the copyright owner. Further reproduction prohibited without permission.

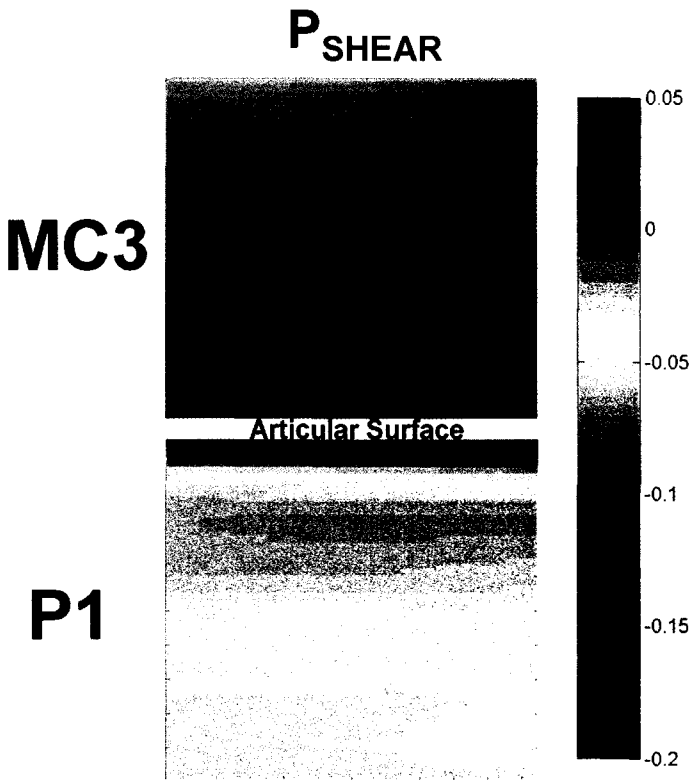

Figure 5.9: Example P_{SHEAR} strain and $\angle P_{SHEAR}$ maps for MC3 and P1 (MC3-R2 of sample #5).

Reproduced with permission of the copyright owner. Further reproduction prohibited without permission.

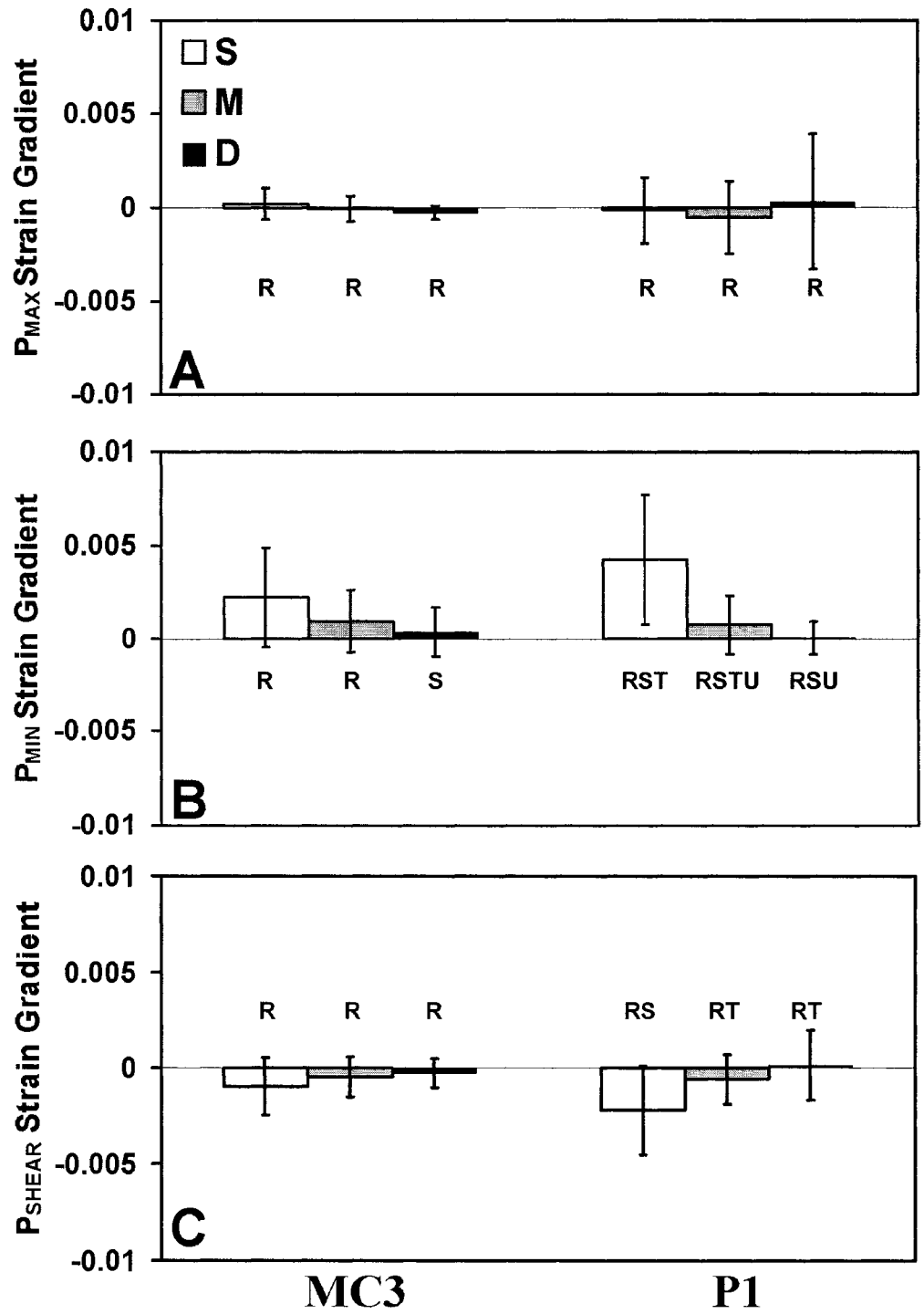

Figure 5.10: Depth-averaged strain gradients ([A] ∇P_{MAX}, [B] ∇P_{MIN}, and [C] ∇P_{SHEAR}) for cartilage zone (S[■], M[▒], D[□]), and bone (MC3, P1). A negative ∇P_{MIN} and positive ∇P_{SHEAR} and ∇P_{MAX} represent the same phenomenon, a decrease in strain with articular depth. Mean $\pm$ STD. Significant differences ($p<0.05$) are noted with different letters.

Reproduced with permission of the copyright owner. Further reproduction prohibited without permission.

superficial ∇P_{MIN} was greater than the deep zone at R2, greater than middle and deep zones at R5, and greater than deep zone at R6 (see Appendix D, $p<0.05$). In general, ∇P_{MIN} decreased with articular depth with few exceptions in the deep or middle cartilage zones of regions R1, R2, R4, and R6. P-values for all comparisons are noted in Appendix D. Briefly, the following trends were noted: superficial ∇P_{MIN} within P1 was greater than superficial ∇P_{MIN} in MC3, and superficial cartilage zone gradients were larger than deep zone gradients in all regions. P-values for all comparisons are noted in Appendix D.

5.3.3 Subchondral Properties (ScBP thickness and BMD)

Subchondral bone plate (ScBP) thickness was dependent on both region and bone ($p<0.0001$). There was both a visual and statistical trend found between regions within MC3 and P1 (Figure 5.11A). Opposing regions (e.g. R1 of MC3 and P1) were found to have significantly different ScBP thickness for R1, R3-R5, and R7 ($p<0.0005$, Figure 5.11A). These ScBP thickness differences support an increasing abaxial trend (concave) within the MC3 and decreasing trend (convex) within the P1 from R4 (sagittal ridge, Figure 5.11A). There were significant differences between regional cumulative (across the MC3 and P1) ScBP thicknesses; consequently there was not a common ScBP thickness across the joint surface in the coronal plane (Figure 5.11B). P-values for all comparisons are noted in Appendix D.

Reproduced with permission of the copyright owner. Further reproduction prohibited without permission.

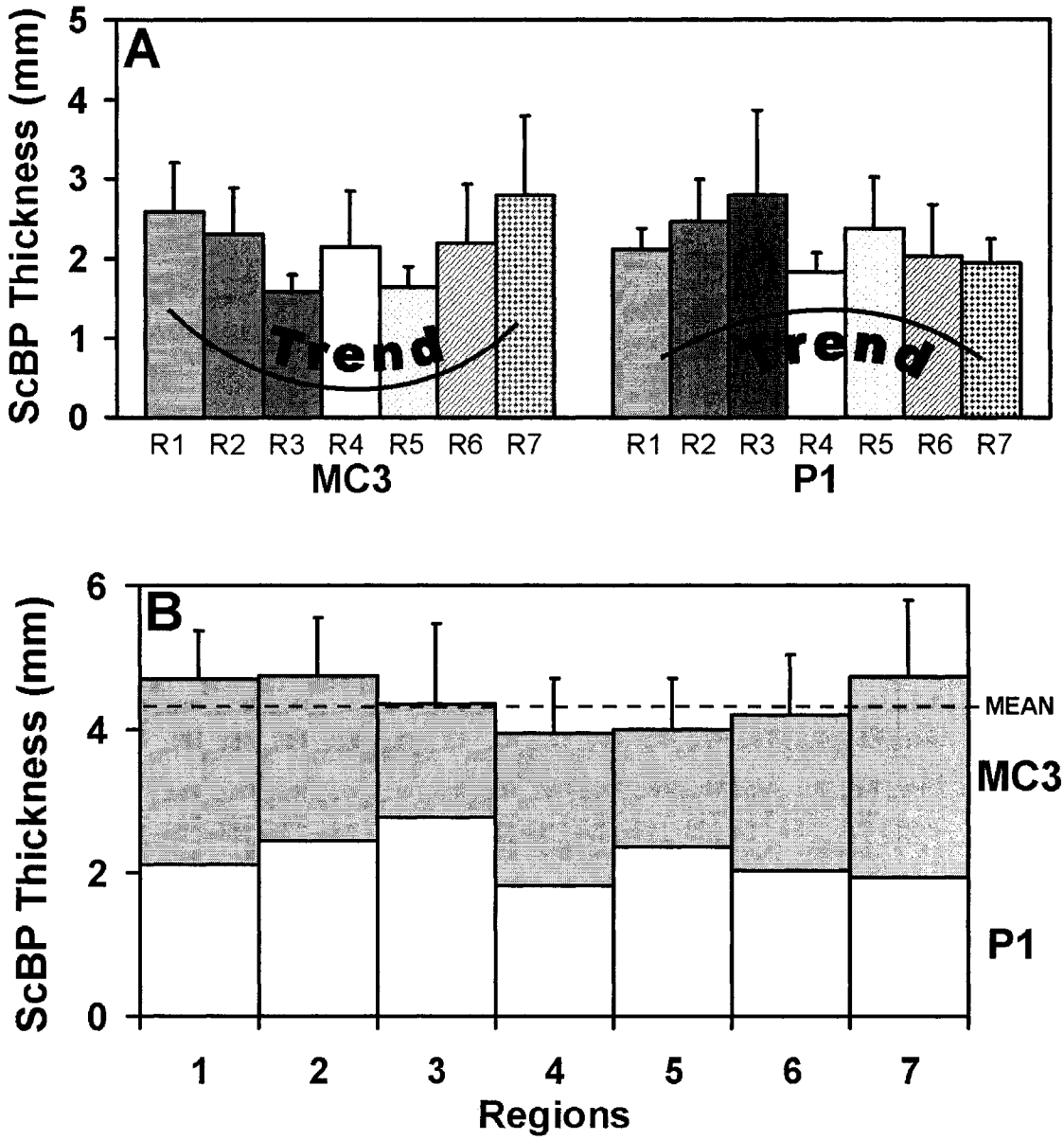

Figure 5.11: ScBP thickness: (A) Effects of bone (MC3/P1) and region (R1-R7) (B) cumulative (MC3 and P1, e.g. MC3 R1 is summed with R1 of P1) ScBP thickness over region. There are interesting trends of subchondral bone thickness within each bone. Mean cumulative thickness was 4.39±0.34mm. Mean ± STD. Statistical significant differences ***p<0.0005, **p<0.005, and *p<0.05.

Reproduced with permission of the copyright owner. Further reproduction prohibited without permission.

Region (R1-R7) and bone (MC3 and P1) had significant effects on the BMD response ($p<0.0001$). Unlike ScBP thickness, the only significant differences found between bones of the same region were R3 and R5 (both P1>MC3, $p<0.001$ and $p<0.0001$ respectively; Figure 5.12A, see Appendix for all comparisons). In general, BMD within P1 was greater than MC3 and abaxial trends relative to the sagittal ridge (R4) were similar to those found for ScBP thickness, across the articular surface for both MC3 and P1 were apparent (concave and convex, respectively; Figure 5.12A). There were significant differences between regional cumulative (across the MC3 and P1) BMD; consequently there was not a common BMD across the joint surface in the coronal plane (Figure 5.12B). There was a significant positive correlation between ScBP thickness and BMD ($p<0.0001$) over all regions and bones. P-values for all comparisons are noted in Appendix D.

5.3.4 Relationship Between Cartilage Strains and Subchondral Bone Properties

Cartilage strain was not correlated with subchondral properties (ScBP thickness and BMD). The regression slopes, change in cartilage strain with change in subchondral bone properties, were not significantly different than zero ($p>0.05$, Figure 5.13AB). Only trends ($p<0.15$) were noted for greater P_{MIN} over thicker ScBP and less BMD and P_{SHEAR} over thinner ScBP and greater BMD (Figure 5.13AB). A power analysis was performed since there was lack of significance. The highest observed power was 37% between the superficial P_{SHEAR} and P_{MIN} and ScBP thickness. Increasing the sample size to twelve (12) would increase their powers to 73%.

Reproduced with permission of the copyright owner. Further reproduction prohibited without permission.

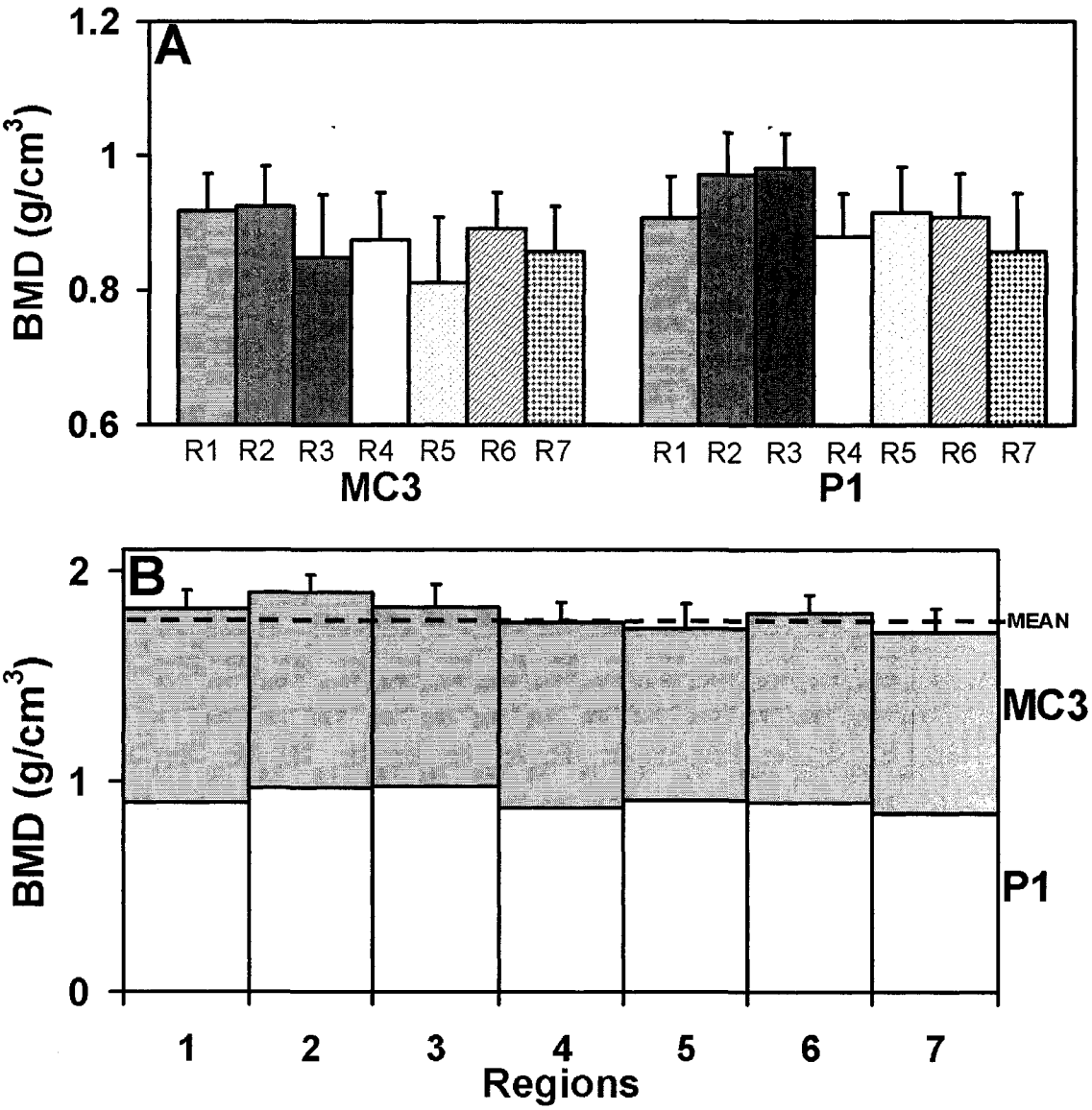

Figure 5.12: BMD (g/cm^3) (A) Effects of bone (MC3/P1) and region (R1-R7) (B) cumulative (MC3+P1) BMD over region. Mean cumulative BMD was 1.79±0.07 g/cm^3. Statistical comparisons are noted in Appendix. Mean ± STD.

Reproduced with permission of the copyright owner. Further reproduction prohibited without permission.

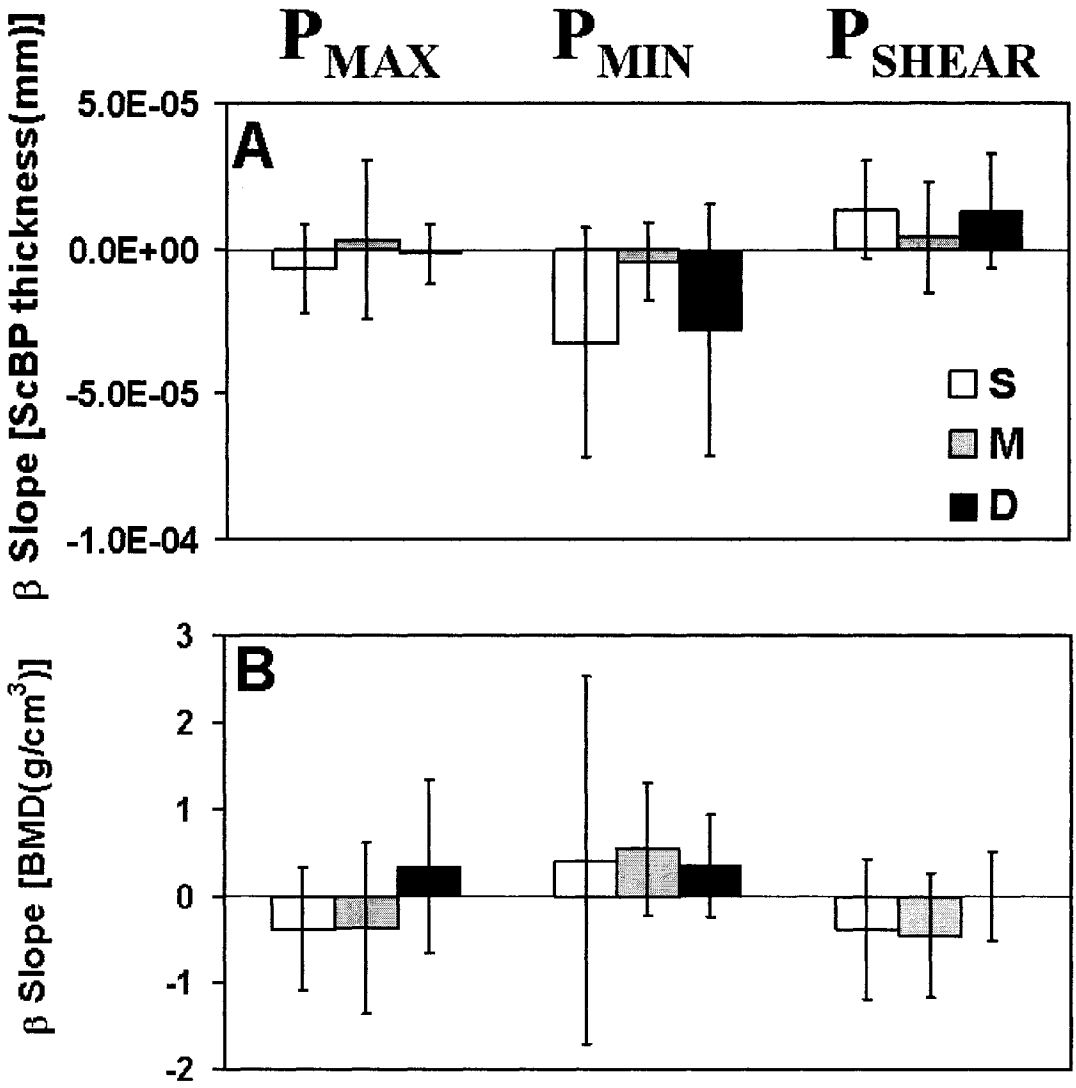

Figure 5.13: Regression slope means between overlying strain (P_{MAX}, P_{MIN}, and P_{SHEAR}) and subchondral bone properties by cartilage zone (S[■], M[▒], D[□]), (A) ScBP thickness and (B) BMD. Mean±STD.

Reproduced with permission of the copyright owner. Further reproduction prohibited without permission.

5.4 Discussion

This is the first experimental measurement of intra-tissue principal and maximum shear strains during contact of naturally opposing cartilage surfaces. The results demonstrate intra-tissue strains (P_{MIN}, P_{SHEAR}, ∇P_{MIN}, and ∇P_{SHEAR}) were depth dependent for both surfaces (Figures 5.6-5.7). Also, the P_{MAX} principal directions coincided with the cartilage structural organization (predominant collagen alignment). When considering the gauge length encompassed in the present study and applied strain level (12%), the P_{MIN} results were similar to previous reports of inhomogeneous cartilage strains using porous platen loading [83, 84, 86, 87]. Using an 8% platen-to-platen compression on adult bovine patellofemoral groove cartilage samples (dissected from underlying bone), Schinagl *et. al.* found the superficial strains were 6 times larger than strains found in the middle and deeper zones [84]. The present study found depth-dependent strains also, using a 12% T-T strain (an average 6% compression was applied to each cartilage surface assuming equal cartilage thickness and overall deformation for each surface); the superficial strains were 2.2 and 1.6 times larger than strains in the middle and deep zones. The depth-dependent disparity with Schinagl et al. [84] could be due to sample structural, preparation, and testing differences between the studies. Schingl et. al [84] used patellofemoral cartilage (similar to MTR location in Chapter 2) from bovine specimens, while the current study used osteochondral tissue from the equine MCP. Extrapolating the results from Chapter 2, the two locations have considerably different material properties and cartilage thicknesses producing different depth-dependent strain behavior. Also, the cartilage behavior without underlying bone versus with underlying bone could be another factor, along with platen vs. articular surface

Reproduced with permission of the copyright owner. Further reproduction prohibited without permission.

loading. Therefore, a direct comparison of platen loading and articular surface loading using the same tissue is recommended for future work. Unlike platen loading experiments, the current testing system is capable of detecting depth-dependent strain variations across complex surface geometry. These marked strain variations between regions and cartilage zones (Figures 5.5-5.6) were likely due to MCP regional variations in cartilage mechanical [93] and biochemical [94] properties, along with a complex joint geometry. The regional strain responses were similar between the opposing surfaces (MC3≅P1), even though the surface geometry (Figure 5.1) and possibly biochemical content [94] were different between them.

Though grossly congruent, increasing strain (compressive, tensile, and shear) magnitudes away from the sagittal ridge (Figure 5.5) is evidence that the MCP joint is incongruent in the tested configuration (joint angle and location). These larger condylar strains may be related to articular scoring lines (superficial degradation or fibrillation), parallel with the sagittal plane, most commonly found on the medial and lateral condyles [67, 68]. The most lateral margin (R7) notably experienced more strain, perhaps due to differences in regional biomechanical/biochemical properties, the lateral condyle having less curvature than the medial in the transverse plane, and/or the samples being consistently loaded unevenly across the joint surface. The large strains noted on the lateral condyle may be related to greater incidence of lateral condylar fractures [67, 68].

The present study demonstrates the subchondral bone responses (both ScBP thickness and BMD) across the articular surfaces were positively correlated and increased for the MC3 and decreased in the P1 from the sagittal ridge (Figures 5.8-5.9). These

Reproduced with permission of the copyright owner. Further reproduction prohibited without permission.

inverse ScBP regional relationships between bone (MC3/P1) and region (Figures 5.8-5.9) may coincide with theories on subchondral bone adaptation within incongruous joints [15, 63]. Bi-centric loading found within incongruous joints occurs between the seemingly congruent surfaces of the MCP. As the joint is initially loaded, the R4 region (apex of sagittal ridge) is minimally loaded and the contact stress is concentrated on the condyles and the inflections of the sagittal ridge. As higher loads are applied, the joint load is distributed across the entire medial-to-lateral surface creating a larger contact surface area, thus reducing contact stresses, similar to those found in the human humeroulnar joint [63]. The postulated benefits of incongruent joint surfaces include facilitating of articular cartilage nutritional demands and minimizing aberrant strains applied to bone and cartilage [63].

Unfortunately the current subchondral bone results were difficult to compare to previous work [47, 74-76, 95] of the MC3 due to analysis planes and animal age. Though analyzing different tissue planes using computed tomography; Riggs *et al.* [47] reported similar low radiodensity region (sagittal ridge) between the medial and lateral MC3 condyles for the palmar aspect and less pronounced dorsal radiodensity.

The distal 3rd metacarpal of the MCP joint has a convex articular surface and is thought to withstand primarily compression strains [63]. In contrast, the proximal 1st phalanx, with a concave surface, most likely experiences both compression and tensile strains. The combination of compressive and tensile strains have been shown to induce bone remodeling in human and other species [96-99]. Consistent with this theory, the concave 1st phalanx tended to have thicker ScBP to resist both compression and tensile

Reproduced with permission of the copyright owner. Further reproduction prohibited without permission.

loading history of an incongruent joint (Figure 5.8). On the other hand, the convex MC3 joint surface tended to have thinner ScBP and lower BMD (R3 and R5) possibly caused by stress shielding from the medullary cortex (R1 and R7, Figure 5.8). The thinner and less dense ScBP may predispose the equine MC3 joint surface to catastrophic failure, which is often seen clinically at the base of the sagittal ridge (R3 and R5) [53, 66, 74-76].

The present study also demonstrated that quantified cartilage strains were not related to underlying ScBP thickness or BMD variations using physiologically normal specimens and a sample size of six (Figure 5.13). Since the 2-3 year old equine specimens were without noticeable OA changes (superficial cartilage degradation and marginal osteophytes), the relationship between cartilage strains and underlying bone properties are expected to be less apparent, thus requiring high precision estimates of the measured responses. The expected systematic errors of the intra-tissue strain ($\pm$7600μstrain, Chapter 4), ScBP thickness ($\pm$45μm, Chapter 3), and BMD (0.01g/cm^3, Chapter 2) measurement methods were not precise enough for the sample size used. The small sample population (6), in conjunction with missing datasets, produced minimal statistical power for analyses. Even though the study had low statistical power, there were many relevant statistically significant comparisons (regions and zones). Increasing the sample size to twelve (12) and examining specimens with OA for future work will increase the power by 50% to possibly expose significant relationships between cartilage strains and underlying subchondral bone properties.

The differential distance used for the strain gradient probably had a significant effect on the outcome, and therefore, was a possible limitation of the present study. Using

Reproduced with permission of the copyright owner. Further reproduction prohibited without permission.

a 1% of total articular thickness was insensitive to the changes actually occurring within the zones studied. If the differential distance were larger (e.g. zone thickness) than 1% increments, perhaps intra-tissue strain patterns could perhaps be more diagnostic.

In the current study, only one strain level was applied; therefore, consecutive increasing strain levels are recommended for future studies. Another limitation was the poor correlation at the articular surface caused by the dense population of chondrocytes in the superficial zone. Staining each articular surface with different fluorescent stains (emitting different wavelengths) before testing could possibly minimize the problem by taking images using different fluorescence filters. The use of confocal microscopy could alleviate focal plane limitations in future endeavors. Another reason the present study had missing data points was the significant loss of information for certain regions due to out-of-plane movement. Out-of-plane movement seemed to coincide with misalignment of the articular surfaces (sagittal plane) during the sample preparation procedure. To possibly overcome this variability, two images (for each articular surface) could be taken at different focal lengths and separately analyzed coinciding with the proposed superficial chondrocyte density solution above. The current testing configuration (coronal view) limiting relative movement in one plane and the low levels of applied loads were other limitations of the current study, since relative 3-D relative motion between articular surfaces at physiological loads is also important to understanding intra-tissue cartilage strains and their relationship with underlying subchondral bone properties. Metacarpal loads as large as 15kN have been estimated to induce bone strains similar to those found in-vivo [100]. Also, instead of using the T-T strain to adjust for variability in regional

Reproduced with permission of the copyright owner. Further reproduction prohibited without permission.

applied strain, regional overall cartilage strains for each articular surface would be a more reliable adjustment in future works.

In conjunction with the limitation solutions suggested above, increasing the sample size to >12 is recommended for future studies. Although there are some limitations, testing opposing osteochondral surfaces in compression has tremendous benefits: (1) strain distributions across articular surfaces with complex geometry can be obtained, (2) the capability to relate depth-dependent strains with underlying subchondral bone properties or abnormal pathology, and (3) it emulates physiological boundary conditions better than platen loading experiments. Due to these benefits, the current method could be applied to a variety of applications where opposing articular surface loading would be important, such as, determining osteochondral implant discontinuities with surrounding host tissue, determining the effects of cartilage and/or bone defects on overlying cartilage strain distributions, and determining the effects of dynamic loading on strain distributions between articular cartilage strains. Also, the testing method can easily be extended to other joints and joints of other species.

This was the first experimental study to quantify intra-tissue cartilage strain distributions along/between compressed opposing articular surfaces. Thus, new findings were ascertained, such as, depth-dependent strain distributions between articular surfaces are similar, but depth-dependent strain gradients are different between articular surfaces. Additionally, attempts were made to determine a relationship of the measured intra-tissue strain distributions with underlying subchondral bone properties. The abaxial regional

Reproduced with permission of the copyright owner. Further reproduction prohibited without permission.

strains were not related with underlying subchondral bone properties, although increasing the sample size may elucidate these relationships.

5.5 Conclusion

The present study found that superficial cartilage strains were larger than strains of deeper zones, subchondral bone plate thickness and volumetric bone mineral density across the articular surfaces were positively correlated, and larger cartilage strains were not related to areas of thicker subchondral bone plate or greater volumetric bone mineral density in the normal equine metacarpophalangeal joint. In addition, the regional subchondral bone properties (both ScBP thickness and BMD) increased with distance away from the sagittal ridge for the MC3 and decreased with distance from the sagittal ridge in the P1.

5.6 References

1. Buckwalter, JA and Mankin, HJ, *Articular cartilage: degeneration and osteoarthritis, repair, regeneration, and transplantation.* Instructional Course Lectures, 1998. **47**: p. 487-504.

2. McIlwraith, CW and Vachon, A, *Review of pathogenesis and treatment of degenerative joint disease.* Equine Vet J Suppl, 1988(6): p. 3-11.

3. Hough, AJ, *Pathology of osteoarthritis*, in *Arthritis and Allied Conditions: A Textbook of Rheumatology*, Koopman, W.J., Editor. 1997, Williams & Wilkins: Balitmore, MD. p. 1945-1984.

4. Kawcak, CE, McIlwraith, CW, Norrdin, RW, Park, RD, and James, SP, *The role of subchondral bone in joint disease: a review.* Equine Vet J, 2001. **33**(2): p. 120-6.

5. Arokoski, JP, Jurvelin, JS, Vaatainen, U, and Helminen, HJ, *Normal and pathological adaptations of articular cartilage to joint loading [In Process Citation].* Scand J Med Sci Sports, 2000. **10**(4): p. 186-98.

Reproduced with permission of the copyright owner. Further reproduction prohibited without permission.

6. Burr, DB and Schaffler, MB, *The involvement of subchondral mineralized tissues in osteoarthrosis: Quantitative microscopic evidence.* Microscopy Research and Technique, 1997. **37**(4): p. 343-357.

7. Radin, EL, *Subchondral bone changes and cartilage damage.* Equine Vet J, 1999. **31**(2): p. 94-5.

8. Simon, SR, Radin, EL, Paul, IL, and Rose, RM, *The response of joints to impact loading. II. In vivo behavior of subchondral bone.* J Biomech, 1972. **5**(3): p. 267-72.

9. Armstrong, S, Read, R, and Ghosh, P, *The effects of intraarticular hyaluronan on cartilage and subchondral bone changes in an ovine model of early osteoarthritis.* Journal of Rheumatology, 1994. **21**(4): p. 680-8.

10. Armstrong, SJ, Read, RA, and Price, R, *Topographical variation within the articular cartilage and subchondral bone of the normal ovine knee joint: a histological approach.* Osteoarthritis & Cartilage, 1995. **3**(1): p. 25-33.

11. Broom, N and Oloyede, A, *Experimental-Determination of the Subchondral Stress-Reducing Role of Articular-Cartilage under Static and Dynamic Compression.* Clinical Biomechanics, 1993. **8**(2): p. 102-108.

12. Coats, AM, Zioupos, P, and Aspden, RM, *Material properties of subchondral bone from patients with osteoporosis or osteoarthritis by microindentation testing and electron probe microanalysis.* Calcif Tissue Int, 2003. **73**(1): p. 66-71.

13. Day, JS, Ding, M, van der Linden, JC, Hvid, I, Sumner, DR, and Weinans, H, *A decreased subchondral trabecular bone tissue elastic modulus is associated with pre-arthritic cartilage damage.* J Orthop Res, 2001. **19**(5): p. 914-8.

14. Ding, M, Dalstra, M, Linde, F, and Hvid, I, *Changes in the stiffness of the human tibial cartilage-bone complex in early-stage osteoarthrosis.* Acta Orthop Scand, 1998. **69**(4): p. 358-62.

15. Eckstein, F, Jacobs, CR, and Merz, BR, *Mechanobiological adaptation of subchondral bone as a function of joint incongruity and loading.* Med Eng Phys, 1997. **19**(8): p. 720-8.

16. Eckstein, F, Muller-Gerbl, M, and Putz, R, *Distribution of subchondral bone density and cartilage thickness in the human patella.* J Anat, 1992. **180 (Pt 3)**: p. 425-33.

17. Ewers, BJ, Weaver, BT, Sevensma, ET, and Haut, RC, *Chronic changes in rabbit retro-patellar cartilage and subchondral bone after blunt impact loading of the patellofemoral joint.* J Orthop Res, 2002. **20**(3): p. 545-50.

Reproduced with permission of the copyright owner. Further reproduction prohibited without permission.

18. Matsui, H, Shimizu, M, and Tsuji, H, *Cartilage and subchondral bone interaction in osteoarthrosis of human knee joint: a histological and histomorphometric study.* Microscopy Research And Technique, 1997. **37**: p. 333-342.

19. Messner, K, Fahlgren, A, Ross, I, and Andersson, B, *Simultaneous changes in bone mineral density and articular cartilage in a rabbit meniscectomy model of knee osteoarthrosis.* Osteoarthritis and Cartilage, 2000. **8**(3): p. 197-206.

20. Milz, S, Eckstein, F, and Putz, R, *Thickness distribution of the subchondral mineralization zone of the trochlear notch and its correlation with the cartilage thickness: an expression of functional adaptation to mechanical stress acting on the humeroulnar joint?* Anat Rec, 1997. **248**(2): p. 189-97.

21. Murray, RC, Vedi, S, Birch, HL, Lakhani, KH, and Goodship, AE, *Subchondral bone thickness, hardness and remodelling are influenced by short-term exercise in a site-specific manner.* J Orthop Res, 2001. **19**(6): p. 1035-42.

22. Norrdin, RW, Kawcak, CE, Capwell, BA, and McIlwraith, CW, *Calcified cartilage morphometry and its relation to subchondral bone remodeling in equine arthrosis.* Bone, 1999. **24**(2): p. 109-14.

23. Oegema, TJ, Carpenter, R, Hofmeister, F, and Thompson, R, *The interaction of the zone of calcified cartilage and subchondral bone in osteoarthritis.* Microscopy Research And Technique, 1997. **37**: p. 324-332.

24. Pugh, JW, Radin, EL, and Rose, RM, *Quantitative studies of human subchondral cancellous bone. Its relationship to the state of its overlying cartilage.* J Bone Joint Surg Am, 1974. **56**(2): p. 313-21.

25. Radin, E, Ehrlich, M, Chernack, R, Abernethy, P, Paul, I, and Rose, R, *Effect of repetitive impulsive loading on the knee joints of rabbits.* Clinical Orthopaedics and Related Research, 1978. **131**: p. 288-292.

26. Radin, EL and Rose, RM, *Role of subchondral bone in the initiation and progression of cartilage damage.* Clin Orthop, 1986(213): p. 34-40.

27. Shimizu, M, Tsuji, H, Matsui, H, Katoh, Y, and Sano, A, *Morphometric analysis of subchondral bone of the tibial condyle in osteoarthrosis.* Clin Orthop, 1993(293): p. 229-39.

28. Yamada, K, Healey, R, Amiel, D, Lotz, M, and Coutts, R, *Subchondral bone of the human knee joint in aging and osteoarthritis.* Osteoarthritis Cartilage, 2002. **10**(5): p. 360-9.

29. Muller-Gerbl, M, *The subchondral bone plate.* Advances in anatomy, embryology & cell biology. Vol. 141. 1998. 1-134.

Reproduced with permission of the copyright owner. Further reproduction prohibited without permission.

30. Radin, EL, Burr, DB, Fyhrie, D, Brown, TD, and Boyd, RD, *Characteristics of joint loading as it applies to osteoarthrosis*, in *Biomechanics of diarthrodial joints*. 1990, Springer-Verlag: New York. p. 369-384.

31. Carter, DR, *Mechanical loading histories and cortical bone remodeling.* Calcif Tissue Int, 1984. **36 Suppl 1**: p. S19-24.

32. Ding, M, *Age variations in the properties of human tibial trabecular bone and cartilage.* Acta Orthop Scand Suppl, 2000. **292**: p. 1-45.

33. Frost, HM, *Wolff's Law and bone's structural adaptations to mechanical usage: an overview for clinicians.* Angle Orthodontist, 1994. **64**(3): p. 175-88.

34. Meyer, GH, *Die Architektur die Spongiosa.* Arch. Anat. Physiol. Wiss. Med., 1867. **34**: p. 160-169.

35. Wolff, J, *Uber die innere Architecktur der Knochen und ihre Bedeutung fur die Frage vom Knochenwachstum.* Virchows Arch. Pathol., 1870. **50**: p. 389-450.

36. Eckstein, F, Lohe, F, Schulte, E, Muller-Gerbl, M, Milz, S, and Putz, R, *Physiological incongruity of the humero-ulnar joint: a functional principle of optimized stress distribution acting upon articulating surfaces?* Anat Embryol (Berl), 1993. **188**(5): p. 449-55.

37. Eckstein, F, Merz, B, and Jacobs, CR, *Effects of joint incongruity on articular pressure distribution and subchondral bone remodeling.* Adv Anat Embryol Cell Biol, 2000. **152**: p. iii-ix, 1-127.

38. Eckstein, F, Merz, B, Muller-Gerbl, M, Holzknecht, N, Pleier, M, and Putz, R, *Morphomechanics of the humero-ulnar joint: II. Concave incongruity determines the distribution of load and subchondral mineralization.* Anat Rec, 1995. **243**(3): p. 327-35.

39. Pauwels, F, *Biomechanics of the locomotor apparatus*. 1980, Berlin: Springer.

40. Kummer, B, *[Mechanical stress and functional adaptation of bones].* Verh Anat Ges, 1978(72): p. 21-45.

41. Kummer, B, *Is the Pauwels' theory of hip biomechanics still valid? A critical analysis, based on modern methods.* Anat Anz, 1993. **175**(3): p. 203-10.

42. Kummer, B, *[Basics of Pauwels' theory of the functional adaptation of bones].* Orthopade, 1995. **24**(5): p. 387-93.

43. Milz, S and Putz, R, *Quantitative morphology of the subchondral plate of the tibial plateau.* J Anat, 1994. **185 (Pt 1)**: p. 103-10.

Reproduced with permission of the copyright owner. Further reproduction prohibited without permission.

44. Eckstein, F, Milz, S, Anetzberger, H, and Putz, R, *Thickness of the subchondral mineralised tissue zone (SMZ) in normal male and female and pathological human patellae.* J Anat, 1998. **192 (Pt 1)**: p. 81-90.

45. Simkin, PA, Graney, DO, and Fiechtner, JJ, *Roman arches, human joints, and disease: differences between convex and concave sides of joints.* Arthritis Rheum, 1980. **23**(11): p. 1308-11.

46. Simkin, PA, Heston, TF, Downey, DJ, Benedict, RS, and Choi, HS, *Subchondral architecture in bones of the canine shoulder.* J Anat, 1991. **175**: p. 213-27.

47. Riggs, CM, Whitehouse, GH, and Boyde, A, *Structural variation of the distal condyles of the third metacarpal and third metatarsal bones in the horse.* Equine Vet J, 1999. **31**(2): p. 130-9.

48. Kawcak, CE, McIlwraith, CW, Norrdin, RW, Park, RD, and Steyn, PS, *Clinical effects of exercise on subchondral bone of carpal and metacarpophalangeal joints in horses.* Am J Vet Res, 2000. **61**(10): p. 1252-8.

49. Firth, EC, van Weeren, PR, Pfeiffer, DU, Delahunt, J, and Barneveld, A, *Effect of age, exercise and growth rate on bone mineral density (BMD) in third carpal bone and distal radius of Dutch Warmblood foals with osteochondrosis.* Equine Vet J Suppl, 1999(31): p. 74-8.

50. Firth, EC, Delahunt, J, Wichtel, JW, Birch, HL, and Goodship, AE, *Galloping exercise induces regional changes in bone density within the third and radial carpal bones of Thoroughbred horses.* Equine Vet J, 1999. **31**(2): p. 111-5.

51. van de Lest, CH, Brama, PA, and Van Weeren, PR, *The influence of exercise on the composition of developing equine joints.* Biorheology, 2002. **39**(1-2): p. 183-91.

52. Amir, G, Pirie, CJ, Rashad, S, and Revell, PA, *Remodelling of subchondral bone in osteoarthritis: a histomorphometric study.* Journal of Clinical Pathology, 1992. **45**(11): p. 990-2.

53. Cantley, CE, Firth, EC, Delahunt, JW, Pfeiffer, DU, and Thompson, KG, *Naturally occurring osteoarthritis in the metacarpophalangeal joints of wild horses.* Equine Vet J, 1999. **31**(1): p. 73-81.

54. Dequeker, J, Mokassa, L, Aerssens, J, and Boonen, S, *Bone density and local growth factors in generalized osteoarthritis.* Microsc Res Tech, 1997. **37**(4): p. 358-71.

Reproduced with permission of the copyright owner. Further reproduction prohibited without permission.

55. Fahlgren, A, Messner, K, and Aspenberg, P, *Meniscectomy leads to an early increase in subchondral bone plate thickness in the rabbit knee.* Acta Orthop Scand, 2003. **74**(4): p. 437-41.

56. Grynpas, MD, Alpert, B, Katz, I, Lieberman, I, and Pritzker, KP, *Subchondral bone in osteoarthritis.* Calcif Tissue Int, 1991. **49**(1): p. 20-6.

57. Smith, RL, Thomas, KD, Schurman, DJ, Carter, DR, Wong, M, and van der Meulen, MC, *Rabbit knee immobilization: bone remodeling precedes cartilage degradation.* J Orthop Res, 1992. **10**(1): p. 88-95.

58. Eckstein, F, Putz, R, Muller-Gerbl, M, Steinlechner, M, and Benedetto, KP, *Cartilage degeneration in the human patellae and its relationship to the mineralisation of the underlying bone: a key to the understanding of chondromalacia patellae and femoropatellar arthrosis?* Surg Radiol Anat, 1993. **15**(4): p. 279-86.

59. Sokoloff, L, *Microcracks in the calcified layer of articular cartilage.* Arch Pathol Lab Med, 1993. **117**(2): p. 191-5.

60. Solomon, L, *Pathogenesis of osteoarthritis.* Lancet, 1972. **1**(7759): p. 1072.

61. Meachim, G, *Cartilage fibrillation at the ankle joint in Liverpool necropsies.* Journal of Anatomy, 1975. **119**(3): p. 601-10.

62. Bullough, PG and Walker, PS, *The distribution of load through the knee joint and its possible significance to the observed patterns of articular cartilage breakdown.* Bull Hosp Joint Dis, 1976. **37**(2): p. 110-23.

63. Bullough, PG, *The geometry of diarthrodial joints, its physiologic maintenance, and the possible significance of age-related changes in geometry-to-load distribution and the development of osteoarthritis.* Clin Orthop, 1981(156): p. 61-6.

64. Burr, DB, *The importance of subchondral bone in osteoarthrosis.* Curr Opin Rheumatol, 1998. **10**(3): p. 256-62.

65. Felson, DT, Lawrence, RC, Dieppe, PA, Hirsch, R, Helmick, CG, Jordan, JM, Kington, RS, Lane, NE, Nevitt, MC, Zhang, Y, Sowers, M, McAlindon, T, Spector, TD, Poole, AR, Yanovski, SZ, Ateshian, G, Sharma, L, Buckwalter, JA, Brandt, KD, and Fries, JF, *Osteoarthritis: new insights. Part 1: the disease and its risk factors.* Ann Intern Med, 2000. **133**(8): p. 635-46.

66. Norrdin, RW, Kawcak, CE, Capwell, BA, and McIlwraith, CW, *Subchondral bone failure in an equine model of overload arthrosis.* Bone, 1998. **22**(2): p. 133-9.

Reproduced with permission of the copyright owner. Further reproduction prohibited without permission.

67. Pool, RR, *Traumatic injury and osteoarthritis.* Joint Disease in the Horse, ed. McIlwraith, C.W. and Trotter, G.W. 1996, Philadelphia: W.B. Saunders Co. 87-104.

68. Pool, RR and Meagher, DM, *Pathologic findings and pathogenesis of racetrack injuries.* Vet Clin North Am Equine Pract, 1990. **6**(1): p. 1-30.

69. Dedrick, DK, Goulet, RW, O'Connor, BL, and Brandt, KD, *Preliminary report: increased porosity of the subchondral plate in an accelerated canine model of osteoarthritis.* Osteoarthritis Cartilage, 1997. **5**(1): p. 71-4.

70. Elliott, DM, Guilak, F, Vail, TP, Wang, JY, and Setton, LA, *Tensile properties of articular cartilage are altered by meniscectomy in a canine model of osteoarthritis.* J Orthop Res, 1999. **17**(4): p. 503-8.

71. Setton, LA, Mow, VC, Muller, FJ, Pita, JC, and Howell, DS, *Mechanical behavior and biochemical composition of canine knee cartilage following periods of joint disuse and disuse with remobilization.* Osteoarthritis Cartilage, 1997. **5**(1): p. 1-16.

72. Pool, RR, *Multidisciplinary investigation of the aetiopathogenesis of parasagittal fractures of the third metacarpal and metatarsal bones of Thoroughbreds.* Equine Vet J, 1999. **31**(2): p. 96.

73. Rick, MC, O'Brien, TR, Pool, RR, and Meagher, D, *Condylar fractures of the third metacarpal bone and third metatarsal bone in 75 horses: radiographic features, treatments, and outcome.* J Am Vet Med Assoc, 1983. **183**(3): p. 287-96.

74. Riggs, CM, Whitehouse, GH, and Boyde, A, *Pathology of the distal condyles of the third metacarpal and third metatarsal bones of the horse.* Equine Vet J, 1999. **31**(2): p. 140-8.

75. Kawcak, C, *Effects of loading on subchondral bone of equine carpal and metacarpophalangeal joints*, in *Department of Clinical Sciences*. 1998, Colorado State University: Fort Collins.

76. Boyde, A, Haroon, Y, Jones, SJ, and Riggs, CM, *Three dimensional structure of the distal condyles of the third metacarpal bone of the horse.* Equine Vet J, 1999. **31**(2): p. 122-9.

77. Ateshian, GA, Kwak, SD, Soslowsky, LJ, and Mow, VC, *A stereophotogrammetric method for determining in situ contact areas in diarthrodial joints, and a comparison with other methods.* J Biomech, 1994. **27**(1): p. 111-24.

Reproduced with permission of the copyright owner. Further reproduction prohibited without permission.

78. Ahmad, CS, Cohen, ZA, Levine, WN, Ateshian, GA, and Mow, VC, *Biomechanical and topographic considerations for autologous osteochondral grafting in the knee.* Am J Sports Med, 2001. **29**(2): p. 201-6.

79. Cohen, ZA, McCarthy, DM, Kwak, SD, Legrand, P, Fogarasi, F, Ciaccio, EJ, and Ateshian, GA, *Knee cartilage topography, thickness, and contact areas from MRI: in-vitro calibration and in-vivo measurements.* Osteoarthritis Cartilage, 1999. **7**(1): p. 95-109.

80. Herberhold, C, Faber, S, Stammberger, T, Steinlechner, M, Putz, R, Englmeier, KH, Reiser, M, and Eckstein, F, *In situ measurement of articular cartilage deformation in intact femoropatellar joints under static loading.* Journal of Biomechanics, 1999. **32**(12): p. 1287-1295.

81. Hunziker, E, *Articular cartilage structure in humans and experimental animals*, in *Articular Cartilage and Osteoarthritis*, Kuettner, K.E., Schleyerbach, R., Peyron, J.G., Hascall, V.C., Editor. 1992, Raven Press: New York. p. 183-199.

82. Kempson, GE, *Relationship between the tensile properties of articular cartilage from the human knee and age.* Ann Rheum Dis, 1982. **41**(5): p. 508-11.

83. Schinagl, RM, Ting, MK, Price, JH, and Sah, RL, *Video microscopy to quantitate the inhomogeneous equilibrium strain within articular cartilage during confined compression.* Annal of Biomedical Engineering, 1996. **24**: p. 500-512.

84. Schinagl, R, Gurskis, D, Chen, A, and Sah, R, *Depth-dependent confined compression modulus of full thickness bovine articular cartilage.* Journal of Orthopaedic Research, 1997. **15**(4): p. 499-506.

85. Chen, AC, Bae, WC, Schinagl, RM, and Sah, RL, *Depth- and strain-dependent mechanical and electromechanical properties of full-thickness bovine articular cartilage in confined compression.* Journal of Biomechanics, 2001. **34**(1): p. 1-12.

86. Chen, SS, Falcovitz, YH, Schneiderman, R, Maroudas, A, and Sah, RL, *Depth-dependent compressive properties of normal aged human femoral head articular cartilage: relationship to fixed charge density.* Osteoarthritis Cartilage, 2001. **9**(6): p. 561-9.

87. Wang, CC, Hung, CT, and Mow, VC, *An analysis of the effects of depth-dependent aggregate modulus on articular cartilage stress-relaxation behavior in compression.* J Biomech, 2001. **34**(1): p. 75-84.

88. Wang, CCB, Deng, JM, Ateshian, GA, and Hung, CT, *An automated approach for direct measurement of two-dimensional strain distributions within articular cartilage under unconfined compression.* Journal of Biomechanical Engineering-Transactions of the Asme, 2002. **124**(5): p. 557-567.

Reproduced with permission of the copyright owner. Further reproduction prohibited without permission.

89. Bae, WC, Lewis, CW, and Sah, RL. *Intra-tissue strain distribution in normal human articular cartilage during clinical indentation testing.* in *Transactions of the ORS.* 2002. New Orleans, Louisiana.

90. Erne, OK, Reid, J, and Bottlang, M. *Offset-strain and depth-dependent strain distribution across articular cartilage.* in *49th Annual Meeting of the Orthopaedic Research Society.* 2003. New Orleans, Lousiana.

91. Schreier, HW, Braasch, JR, and Sutton, MA, *Systematic errors in digital image correlation caused by intensity interpolation.* Optical Engineering, 2000. **39**(11): p. 2915-2921.

92. Media Cybernetics, I, *Local Best Fit Contrast Enhancement.* 2002: Silverspring, MD, USA.

93. Brama, PA, Barneveld, A, Karssenberg, D, Van Kampen, GP, and van Weeren, PR, *The application of an indenter system to measure structural properties of articular cartilage in the horse. Suitability of the instrument and correlation with biochemical data.* J Vet Med A Physiol Pathol Clin Med, 2001. **48**(4): p. 213-21.

94. Brama, PA, Tekoppele, JM, Bank, RA, Karssenberg, D, Barneveld, A, and van Weeren, PR, *Topographical mapping of biochemical properties of articular cartilage in the equine fetlock joint.* Equine Vet J, 2000. **32**(1): p. 19-26.

95. van Harreveld, PD, Lillich, JD, Kawcak, CE, Turner, AS, and Norrdin, RW, *Effects of immobilization followed by remobilization on mineral density, histomorphometric features, and formation of the bones of the metacarpophalangeal joint in horses.* Am J Vet Res, 2002. **63**(2): p. 276-81.

96. Carter, DR, Orr, TE, and Fyhrie, DP, *Relationships between loading history and femoral cancellous bone architecture.* J Biomech, 1989. **22**(3): p. 231-44.

97. Bailey, AJ and Mansell, JP, *Do subchondral bone changes exacerbate or precede articular cartilage destruction in osteoarthritis of the elderly?* Gerontology, 1997. **43**(5): p. 296-304.

98. Eckstein, F, Merz, B, Schon, M, Jacobs, CR, and Putz, R, *Tension and bending, but not compression alone determine the functional adaptation of subchondral bone in incongruous joints.* Anat Embryol (Berl), 1999. **199**(1): p. 85-97.

99. Putz, R, Milz, S, Maier, M, and Boszczyk, A, *[Functional morphology of the elbow joint].* Orthopade, 2003. **32**(8): p. 684-90.

100. Les, CM, Stover, SM, Taylor, KT, Keyak, JH, and Willits, NH, *Ex vivo simulation of in vivo strain distributions in the equine metacarpus.* Equine Vet J, 1998. **30**(3): p. 260-6.

Reproduced with permission of the copyright owner. Further reproduction prohibited without permission.

6 SUMMARY AND CONCLUSION

The overall goal of this study was to examine the relationship between the properties of articular cartilage and its underlying subchondral bone using an equine model. The objectives of this study were: (1) to determine the structural and mechanical properties of equine articular cartilage, (2) to determine the bone mineral density of the underlying subchondral bone, (3) to determine the relationship between these articular cartilage and bone properties in different joint regions, (4) to develop a method for measuring the thickness of the subchondral bone plate, (5) to develop experimental protocols and novel equipment for loading opposing osteochondral surfaces and quantify the intra-tissue articular cartilage strains within the loaded samples, and (6) to determine any regional relationships between the articular cartilage strains and underlying subchondral bone plate thicknesses and bone mineral densities.

In Chapter 2, the first comparative body of data was presented for equine articular cartilage structural/material properties and the relationship between articular cartilage properties and underlying subchondral bone density for the palmar and dorsal aspects of the medial condyle of the 3rd metacarpal bone (MC3), medial trochlear ridge (MTR), and the medial femoral condyle (MFC). A positive correlation between articular cartilage tensile equilibrium modulus and underlying bone mineral density was found.

Reproduced with permission of the copyright owner. Further reproduction prohibited without permission.

Recommendations for future work include determining the effects of age, exercise, OA, sample orientation, subchondral bone thickness, and biochemical content on these properties and relationships.

Since there is a strong relationship between bone morphology and mechanical stress history, subchondral bone plate thickness is an important indicator of mechanical stress history acting on the bone within the synovial joint. In Chapter 3, a new subchondral bone plate thickness measurement technique was developed. This technique has minimal systematic error and a high level of repeatability and uses high-resolution contact radiographs and image processing. This research provides the understanding of the limitations of this method that is crucial to minimizing experimental errors due to surface curvature and sample plane selection. Recommendations for future work include quantitatively compare/contrast radiographic, histological, and computed tomography methods for quantifying ScBP thickness.

The ability to quantify intra-tissue articular cartilage strains and underlying subchondral bone characteristics between physiologically opposing surfaces is obviously needed to help elucidate the progression of OA. For this reason, in Chapter 4, a custom-designed loading system and the associated sample preparation procedures were developed and validated to quantify two-dimensional strain fields using video image correlation analysis (VIC) between two loaded opposing articular cartilage surfaces (MC3 and P1) within the equine metacarpophalangeal joint (MCP). The expected error involved in this process including the image acquisition system, data analysis, and friction was shown to be on the order of 7600 μstrain (0.76%). This error is less than 23%

Reproduced with permission of the copyright owner. Further reproduction prohibited without permission.

of the average strain measured in the experiments under low (relative to *in-vivo*) loads. Friction was the largest known error in the methodology; therefore it is imperative to minimize the interaction of friction on the quantified strain fields in future work.

In Chapter 5, the methodologies used in Chapters 2-4 were used to show that superficial cartilage strains were larger than strains of deeper layers; that subchondral bone plate thickness and volumetric bone mineral density across the articular surfaces were positively correlated; and that larger articular cartilage strains were not related to areas of thicker subchondral bone plate or greater volumetric bone mineral density in the normal equine metacarpophalangeal joint. In addition, the regional subchondral bone properties (both ScBP thickness and BMD) were found to increase with distance away from the sagittal ridge for the MC3 and found to decrease with distance from the sagittal ridge in the P1. The regional subchondral bone variations, found in this study, may be related to a common distal lateral 3rd metacarpal bone fracture injury originating at the base of the sagittal ridge (R5) in the equine athlete population.

Out-of-plane motion proved to be difficult to eliminate causing more than a third of the possible data regions to be dropped from the analysis. In addition to the proposed techniques to minimize bad images, increasing the sample size is recommended for future work. The proposed bone mineral density limitation of Chapter 2 had little if any affect on bone mineral density measurements in Chapter 5, because the DEXA region of analysis encompassed only the subchondral bone plate. Since articular cartilage mechanical properties have been found to vary across the articular surface (Chapter 2) within the metacarpophalangeal joint, it is expected that the strain distributions measured

Reproduced with permission of the copyright owner. Further reproduction prohibited without permission.

were dependent not only on the boundary conditions of the sample, but also the location of sample acquisition and joint angle. It must be noted that the prominent sagittal ridge geometry of the metacarpophalangeal joint in the coronal plane played an important role in maintaining physiologic joint alignment during compression loading, therefore testing samples from other joints would be dependent on joint geometry. Recommendations for future work include determining the effects of joint, age, gender, exercise, joint angle, strain level, pathology, healing state, lubrication, stress relaxation, impact loading, and osteochondral sample thickness on articular cartilage strains and subchondral bone plate thickness and bone mineral density.

Although there are some limitations, testing opposing osteochondral surfaces in compression has tremendous benefits: (1) strain distributions across articular surfaces with complex geometry can be obtained, (2) the capability to relate depth-dependent overlying strains within subchondral bone properties or pathology changes, and (3) it emulates physiological boundary conditions better than platen loading experiments. Due to these benefits, the current method could be applied to a variety of applications where opposing articular surface loading would be important, such as, determining osteochondral implant discontinuities with surrounding host tissue, determining the effects of articular cartilage and/or bone defects on overlying articular cartilage strain distributions, and determining the effects of impact loading on strain distributions between articular cartilage strains.

Reproduced with permission of the copyright owner. Further reproduction prohibited without permission.

7 Appendix A

7.1 Chapter 2 Sample history

Table 7.1: Sample history

Horse ID#	Approx. Age (yrs)	Weight (#)	Tall (cm)	Gender	Treatment (OCF: Osteochondral Fragment) All treatments occurred within the intercarpal joint (Distal Radial Carpal Bone). Horses were exercised 5days/week for 3 weeks prior to surgery and 8 weeks postoperatively.)	Location	Aspect (R/L)	Surface Area Dimensions (mm)
F9	2	735	148	Female	Right OCF	MFC	R	3 x >10 Long
F11	2	744	142	Male	Right OCF	MFC	R	3 x >10 Long
F12	2	840	156	Male	Control	MFC	R	3 x >10 Long
F14	2	656	142	Female	Control	MFC	R	10 x >10 Long
F15	2	880	146	Female	Control	MFC	R	10 x >10 Long
F16	2	700	140	Female	Left OCF	MFC	R	10 x >10 Long
F17	2	625	136	Female	Control	MFC	R	10 x >10 Long
F18	2	625	140	Female	Left OCF	MFC	R	10 x >10 Long

Reproduced with permission of the copyright owner. Further reproduction prohibited without permission.

7.2 Raw Tensile Data

Table 7.2: Raw tensile data

ID	Horse#	Joint	RL	Treatment	Region	Tensile thickness (mm)	Tensile MaxLoad (KN)	Tensile Elongation (mm)	Tensile Failure Stress (MPa)	Tensile Failure Strain (mm/mm)	Tensile Stiffness @ Failure (MPa)	Tensile Equilibrium Modulus (MPa)	Tensile Dynamic Stiffness (MPa)
1	14	S	R	noTRT	MFC	0.462	0.248	2.390	6.581	0.554	11.879	5.535	15.130
2	14	S	R	noTRT	MTR	0.249	0.292	1.758	14.351	0.424	33.883	10.091	53.265
3	14	S	L	noTRT	MTR	0.476	0.300	1.955	7.717	0.458	16.858	9.396	29.040
4	14	S	L	noTRT	MFC	0.466	0.209	1.850	5.507	0.433	12.704	2.451	20.349
5	14	F	R	noTRT	MC3D	0.465	0.270	1.303	7.122	0.319	22.353	15.391	36.163
6	14	F	R	noTRT	MC3P	0.376	0.298	1.789	9.703	0.431	22.504	16.581	39.907
7	14	F	L	noTRT	MC3D	0.433	0.267	1.529	7.549	0.369	20.441	12.468	29.826
8	14	F	L	noTRT	MC3P	0.465	0.323	1.332	8.508	0.328	25.975	17.829	36.542
9	12	S	L	noTRT	MFC	0.601	0.171	2.850	3.484	0.571	6.106	1.189	8.926
10	12	S	L	noTRT	MTR	0.420	0.396	3.059	11.572	0.720	16.077	0.359	17.136
11	12	F	L	noTRT	MC3D	0.408	0.202	1.496	6.070	0.337	17.988	13.229	31.595
12	12	F	L	noTRT	MC3P	0.452	0.255	1.111	6.916	0.269	25.699	19.212	46.431
13	12	S	R	noTRT	MFC	.	.	.	.	.	.	.	.
14	12	S	R	noTRT	MTR	0.359	0.341	2.287	11.632	0.547	21.277	8.072	27.048
15	12	F	R	noTRT	MC3P	0.427	0.215	0.985	6.184	0.241	25.633	20.292	51.759
16	12	F	R	noTRT	MC3D	0.324	0.195	0.767	7.390	0.180	40.953	15.464	39.948
17	15	S	L	noTRT	MFC	0.450	0.260	2.344	7.084	0.552	12.837	4.347	19.970
18	15	S	L	noTRT	MTR	0.465	0.380	2.124	10.028	0.501	20.023	9.380	29.086
19	15	F	L	noTRT	MC3P	0.411	0.238	2.045	7.091	0.471	15.050	8.922	19.743
20	15	F	L	noTRT	MC3D	0.398	0.231	1.380	7.100	0.329	21.595	2.104	29.210
21	17	S	L	noTRT	MTR	0.447	0.286	1.764	7.846	0.421	18.644	8.714	25.492
22	17	S	L	noTRT	MFC	0.397	0.187	1.964	5.770	0.445	12.954	1.868	18.263
23	17	F	L	noTRT	MC3P	0.382	0.279	1.314	8.955	0.316	28.316	19.282	50.648
24	17	F	L	noTRT	MC3D	0.364	0.416	1.549	14.003	0.378	37.015	23.930	46.080
25	16	S	L	TRT	MFC	0.377	0.243	1.928	7.904	0.454	17.421	5.365	23.231
26	16	S	L	TRT	MTR	0.307	0.334	1.936	13.350	0.464	28.782	8.651	42.336
27	16	S	R	TRT	MFC	0.391	0.170	2.037	5.334	0.478	11.167	3.983	15.020
28	16	S	R	TRT	MTR	0.353	0.340	1.644	11.824	0.385	30.731	9.455	45.358
29	16	F	L	TRT	MC3P	0.300	0.322	1.583	13.165	0.377	34.886	21.919	51.354
30	16	F	L	TRT	MC3D	.	.	.	.	.	.	.	.
31	16	F	R	TRT	MC3P	0.545	0.228	1.102	5.136	0.264	19.434	13.641	37.006
32	16	F	R	TRT	MC3D	0.357	0.285	1.483	9.791	0.350	27.978	19.685	40.865
33	18	S	L	TRT	MFC	0.332	0.211	1.838	7.805	0.400	19.527	9.445	29.053
34	18	S	L	TRT	MTR	0.339	0.318	2.328	11.507	0.559	20.591	9.052	27.153
35	18	S	R	TRT	MFC	0.351	0.246	2.169	8.578	0.510	16.807	3.901	22.524
36	18	S	R	TRT	MTR	0.379	0.362	1.623	11.723	0.391	29.952	16.252	45.332
37	18	F	L	TRT	MC3P	0.301	0.362	1.240	14.759	0.299	49.399	35.313	73.901
38	18	F	L	TRT	MC3D	0.493	0.334	1.555	8.297	0.375	22.097	14.145	33.815
39	18	F	R	TRT	MC3P	0.352	0.256	1.373	8.914	0.330	26.985	18.352	41.288
40	18	F	R	TRT	MC3D	0.277	0.324	1.625	14.359	0.391	36.765	13.816	58.150
41	9	S	L	TRT	MFC	0.346	0.194	1.597	6.874	0.369	18.643	8.606	25.866
42	9	S	L	TRT	MTR	0.228	0.201	2.855	10.792	0.615	17.558	4.757	21.349
43	9	F	L	TRT	MC3D	0.230	0.229	1.328	12.223	0.332	36.821	14.743	46.881
44	9	F	L	TRT	MC3P	0.324	0.281	0.990	10.643	0.231	46.129	33.038	82.595
45	9	S	R	TRT	MFC	0.470	0.119	1.601	3.104	0.331	9.385	2.851	13.681
46	9	S	R	TRT	MTR	0.323	0.068	4.254	2.595	0.802	3.236	0.091	4.856
47	9	F	R	TRT	MC3D	0.508	0.304	1.331	7.326	0.315	23.281	12.337	39.221
48	9	F	R	TRT	MC3P	0.289	0.251	1.579	10.629	0.395	26.926	17.014	39.373
49	11	S	L	TRT	MFC	0.316	0.285	2.430	11.044	0.541	20.408	4.201	28.416
50	11	S	L	TRT	MTR	0.255	0.256	2.054	12.317	0.485	25.382	5.777	34.109
51	11	F	L	TRT	MC3D	0.305	0.477	3.422	19.193	0.830	23.135	7.545	27.266
52	11	F	L	TRT	MC3P	0.269	0.334	2.290	15.235	0.552	27.597	10.149	36.901
53	11	S	R	TRT	MFC	0.365	0.269	1.745	9.045	0.436	20.730	11.437	31.132
54	11	S	R	TRT	MTR	0.279	0.301	2.341	13.226	0.548	24.140	3.482	33.113
55	11	F	R	TRT	MC3D	0.328	0.473	3.388	17.701	0.808	21.894	3.780	28.622
56	11	F	R	TRT	MC3P	0.497	0.432	1.983	10.653	0.472	22.565	10.569	28.592
57	15	S	R	noTRT	MFC	0.158	0.100	3.179	7.798	0.525	14.853	3.132	17.099
58	15	S	R	noTRT	MTR	0.329	0.159	1.659	5.920	0.415	14.278	.	27.269
59	15	F	R	noTRT	MC3D	0.400	0.270	1.325	8.290	0.331	25.037	16.047	35.162
60	15	F	R	noTRT	MC3P	0.371	0.330	2.683	10.907	0.637	17.132	5.587	22.975
61	17	S	R	noTRT	MFC	0.552	0.176	2.075	3.901	0.467	8.355	3.115	10.655
62	17	S	R	noTRT	MTR	0.141	0.167	1.975	14.499	0.425	34.141	12.163	45.634
63	17	F	R	noTRT	MC3D	0.508	0.507	2.296	12.231	0.574	21.311	9.951	30.704
64	17	F	R	noTRT	MC3P	0.418	0.393	1.458	11.529	0.348	33.145	18.403	49.815

Reproduced with permission of the copyright owner. Further reproduction prohibited without permission.

7.3 Structural Raw Data

Table 7.3: Raw structural data

ID	Horse#	Joint	RL	Treatment	Region	Reflectance Score	Cartilage Thickness (mm)	Volumetric Bone Mineral Density (g/cm^3)
1	14	S	R	noTRT	MFC	0.871	2.184	0.7103
2	14	S	R	noTRT	MTR	1.043	1.590	0.5695
3	14	S	L	noTRT	MTR	0.977	1.575	0.2995
4	14	S	L	noTRT	MFC	0.978	1.858	0.4893
5	14	F	R	noTRT	MC3D	0.893	0.596	0.9172
6	14	F	R	noTRT	MC3P	0.816	0.473	1.0650
7	14	F	L	noTRT	MC3D	0.763	0.533	0.8734
8	14	F	L	noTRT	MC3P	0.813	0.738	1.2147
9	12	S	L	noTRT	MFC	.	.	0.8360
10	12	S	L	noTRT	MTR	.	.	0.7159
11	12	F	L	noTRT	MC3D	.	.	1.1489
12	12	F	L	noTRT	MC3P	.	.	1.2851
13	12	S	R	noTRT	MFC	.	.	0.8237
14	12	S	R	noTRT	MTR	.	.	0.7343
15	12	F	R	noTRT	MC3P	.	.	1.3076
16	12	F	R	noTRT	MC3D	.	.	0.6688
17	15	S	L	noTRT	MFC	0.954	3.047	1.1553
18	15	S	L	noTRT	MTR	0.940	1.616	0.6774
19	15	F	L	noTRT	MC3P	0.815	0.580	0.9201
20	15	F	L	noTRT	MC3D	0.912	0.667	0.9100
21	17	S	L	noTRT	MTR	1.040	1.460	0.8897
22	17	S	L	noTRT	MFC	1.070	1.882	0.6112
23	17	F	L	noTRT	MC3P	0.967	0.665	1.0929
24	17	F	L	noTRT	MC3D	0.815	0.714	1.1541
25	16	S	L	TRT	MFC	0.917	2.261	0.7654
26	16	S	L	TRT	MTR	0.997	1.521	0.6662
27	16	S	R	TRT	MFC	0.859	2.145	0.7932
28	16	S	R	TRT	MTR	0.910	1.691	0.6744
29	16	F	L	TRT	MC3P	0.921	0.610	1.1812
30	16	F	L	TRT	MC3D	0.788	0.680	1.0229
31	16	F	R	TRT	MC3P	0.932	0.694	1.0661
32	16	F	R	TRT	MC3D	0.903	0.859	1.0594
33	18	S	L	TRT	MFC	0.995	2.711	0.6944
34	18	S	L	TRT	MTR	0.986	1.348	0.6415
35	18	S	R	TRT	MFC	0.981	2.300	0.8042
36	18	S	R	TRT	MTR	0.967	1.362	0.6105
37	18	F	L	TRT	MC3P	0.874	0.643	1.0286
38	18	F	L	TRT	MC3D	0.896	0.936	0.8571
39	18	F	R	TRT	MC3P	0.918	0.770	1.1082
40	18	F	R	TRT	MC3D	0.900	0.677	0.7955
41	9	S	L	TRT	MFC	0.754	2.000	0.7515
42	9	S	L	TRT	MTR	0.969	1.355	0.5735
43	9	F	L	TRT	MC3D	0.765	0.690	0.8214
44	9	F	L	TRT	MC3P	0.761	0.487	1.2102
45	9	S	R	TRT	MFC	0.831	2.250	0.7212
46	9	S	R	TRT	MTR	0.827	1.382	0.5738
47	9	F	R	TRT	MC3D	0.903	0.586	0.9379
48	9	F	R	TRT	MC3P	1.147	0.488	1.2064
49	11	S	L	TRT	MFC	0.850	2.076	0.8004
50	11	S	L	TRT	MTR	0.957	1.320	0.6476
51	11	F	L	TRT	MC3D	0.976	0.637	1.0071
52	11	F	L	TRT	MC3P	0.813	0.545	1.0846
53	11	S	R	TRT	MFC	0.891	2.101	1.0943
54	11	S	R	TRT	MTR	0.981	1.741	0.6702
55	11	F	R	TRT	MC3D	0.906	0.661	0.9993
56	11	F	R	TRT	MC3P	.	0.577	1.2148
57	15	S	R	noTRT	MFC	0.852	2.221	0.6798
58	15	S	R	noTRT	MTR	1.015	1.463	0.2162
59	15	F	R	noTRT	MC3D	0.660	0.618	.
60	15	F	R	noTRT	MC3P	0.784	0.541	.
61	17	S	R	noTRT	MFC	0.828	1.843	0.7416
62	17	S	R	noTRT	MTR	0.927	1.383	0.7249
63	17	F	R	noTRT	MC3D	0.636	0.517	.
64	17	F	R	noTRT	MC3P	0.760	0.360	.

Reproduced with permission of the copyright owner. Further reproduction prohibited without permission.

7.4 Compression Raw Data

Table 7.4: Raw compression data

ID	Horse#	RL	Treatment	Region	Thickness (mm)	Ha-0% (MPa)	M	log_{10} (Perm-0% [m^2/Pa*s])	log_{10} (Perm-15% [m^2/Pa*s])	log_{10} (Perm-30% [m^2/Pa*s])	log_{10} (Perm-45% [m^2/Pa*s])
2	14	R	noTRT	MTR	1.214	0.235	16.52	-13.52	-14.50	-15.84	-16.66
3	14	L	noTRT	MTR	0.995	0.133	20.74	-12.59	-13.77	-15.63	-16.47
18	15	L	noTRT	MTR	1.105	0.143	25.41	-12.09	-13.54	-15.81	-16.85
21	17	L	noTRT	MTR	1.335	0.262	10.76	-14.60	-15.29	-16.01	-16.70
26	16	L	TRT	MTR	1.061	0.102	14.57	-13.79	-14.61	-15.93	-16.51
28	16	R	TRT	MTR	1.028	0.168	8.41	-14.84	-15.38	-15.97	-16.47
34	18	L	TRT	MTR	1.121	0.264	25.20	-12.22	-13.62	-16.00	-16.90
36	18	R	TRT	MTR	1.062	0.218	17.71	-13.36	-14.38	-15.92	-16.69
58	15	R	noTRT	MTR	1.373	0.109	22.78	-11.83	-13.24	-14.95	-16.21
62	17	R	noTRT	MTR	1.296	0.122	16.83	-13.29	-14.26	-15.72	-16.45
1	14	R	noTRT	MFC	1.118	0.069	19.49	-12.24	-13.41	-14.96	-15.95
4	14	L	noTRT	MFC	1.103	0.124	14.98	-13.35	-14.22	-15.53	-16.17
17	15	L	noTRT	MFC	1.121	0.093	21.34	-12.30	-13.61	-15.22	-16.39
22	17	L	noTRT	MFC	1.139	0.112	12.19	-14.10	-14.82	-15.83	-16.41
25	16	L	TRT	MFC	1.201	0.136	19.81	-12.66	-13.79	-15.56	-16.37
27	16	R	TRT	MFC	1.143	0.209	15.12	-13.95	-14.85	-16.09	-16.82
33	18	L	TRT	MFC	1.151	0.400	11.90	-14.32	-15.04	-15.97	-16.59
35	18	R	TRT	MFC	1.086	0.338	12.53	-14.52	-15.29	-16.25	-16.92
57	15	R	noTRT	MFC	1.189	0.055	19.48	-12.33	-13.50	-15.07	-16.04
61	17	R	noTRT	MFC	1.099	0.152	16.83	-13.29	-14.26	-15.72	-16.45

Reproduced with permission of the copyright owner. Further reproduction prohibited without permission.

7.5 SAS programs

```
data compression;
input id h RL $ trt $ region $ strain Ha0 kp M;
cards;
1       14      R       noTRTMFC  0       0.0692 28.17276179  19.4936
...
...
...
62      17      R       noTRTMTR  0       0.122  30.5908              16.826
;
proc mixed;
   class h RL region;
        model M=RL|region @2 /ddfm=satterth;
        random h;
        lsmeans region/pdiff cl adjust=tukey;
        lsmeans RL/pdiff adjust=tukey;
run;
proc mixed;
   class h RL region;
        model Ha0=RL|region @2 /ddfm=satterth;
        random h;
        lsmeans region/pdiff cl adjust=tukey;
        lsmeans RL/pdiff adjust=tukey;
run;
proc means;
        class region;
        var Ha0 M;
run;
```


Reproduced with permission of the copyright owner. Further reproduction prohibited without permission.

```
data cwl2003;
input id H      Joint$ RL$ trt$ location$ Tensile_thickness Tensile_MaxLoad
Tensile_Elongation Tensile_Failure_StressTensile_Failure_Strain
Tensile_failure_stiffness Tensile_EM Tensile_DS Tensile_Bestfit_DS mPre mInk stdPre
stdInk mG19 stdG19 mG3 stdG3 CDI stdCDI cartthick std_thickness BoneThick BMD1
BMD2 BMD3 meanBMD volBMD WC compthick Ha0 M lnkp0 lnkp15 lnkp30 lnkp45
logkp0 logkp15 logkp30 logkp45;

/*response scaling*/
sqrt_tensile_EM = sqrt(tensile_EM);
sqrt_tensile_failure_stress = sqrt(tensile_failure_stress);
sqrt_tensile_failure_strain = sqrt(tensile_failure_strain);
sqrt_tensile_failure_stiffness = sqrt(tensile_failure_stiffness);
sqrt_tensile_EM = sqrt(tensile_EM);
sqrt_tensile_DS = sqrt(tensile_DS);
log_tensile_bestfit_DS = log(tensile_Bestfit_DS);
cards;
...
...
...
64      17      F       R       noTRTMC3P 0.418   0.393   1.458   11.529 0.348   33.145
        18.403 49.815 49.877 46.920 80.365 7.389   11.806 241.470        5.391   29.606
        3.301   0.760   0.056   0.360   0.012   .       .       .       .       .       .
        72.76051188  .       .       .       .       .       .       .       .       .
        .       .
;
proc mixed;
        class h location RL trt;
        model sqrt_tensile_EM=trt|location|RL @2 /ddfm=satterth;
        random h(trt);
        lsmeans location /pdiff cl adjust=tukey;
run;
proc mixed;
        class h location RL trt;
        model sqrt_tensile_EM=trt|location|RL @2 tensile_thickness/ddfm=satterth;
        random h(trt);
        lsmeans location /pdiff cl adjust=tukey;
run;
proc mixed;
        class h location RL trt;
        model sqrt_tensile_failure_stress=trt|location|RL @2 tensile_thickness
/ddfm=satterth;
        random h(trt);
        lsmeans location/pdiff cl adjust=tukey;
        run;
proc mixed;
```


Reproduced with permission of the copyright owner. Further reproduction prohibited without permission.

```
        class h location RL trt;
        model sqrt_tensile_failure_strain=trt|location|RL @2 /ddfm=satterth;
        random h(trt);
        lsmeans location/pdiff cl adjust=tukey;
proc mixed;
        class h location RL trt;
        model sqrt_tensile_DS=trt|location|RL @2 tensile_thickness/ddfm=satterth;
        random h(trt);
        lsmeans location/pdiff cl adjust=tukey;
run;
proc mixed;
        class h location RL trt;
        model sqrt_tensile_DS=trt|location|RL @2 /ddfm=satterth;
        random h(trt);
        lsmeans location/pdiff cl adjust=tukey;
run;
proc mixed;
        class h location RL trt;
        model log_tensile_bestfit_DS=trt|location|RL @2 /ddfm=satterth;
        random h(trt);
        lsmeans location/pdiff cl adjust=tukey;
proc mixed;
        class h location RL trt;
        model CDI=trt|location|RL @2/ddfm=satterth;
        random h(trt);
        lsmeans location*trt/pdiff adjust=tukey;
        lsmeans location/pdiff adjust=tukey;
run;
proc mixed;
        class h location RL trt;
        model cartthick=trt|location|RL @2 /ddfm=satterth;
        random h(trt);
        lsmeans location/pdiff adjust=tukey;
run;
proc mixed;
        class h location RL trt;
        model volBMD=trt|location|RL @2/ddfm=satterth;
        random h(trt);
        lsmeans location/pdiff adjust=tukey;
run;
proc mixed;
        class h location RL trt;
        model WC=trt|location|RL @2/ddfm=satterth;
        random h(trt);
        lsmeans location/pdiff adjust=tukey;
run;
```


Reproduced with permission of the copyright owner. Further reproduction prohibited without permission.

```
proc sort;
        by location;
proc corr;
        by location;
        var Tensile_EM        Tensile_DS Tensile_Failure_stress cartthick CDI WC
volBMD Ha0  kp M ;
run;
proc corr;
var sqrt_Tensile_EM sqrt_Tensile_DS sqrt_Tensile_Failure_stress
sqrt_Tensile_Failure_strain cartthick CDI WC volBMD Ha0 kp M ;
run;

proc corr;
var sqrt_Tensile_EM sqrt_Tensile_Failure_stress sqrt_Tensile_Failure_strain
sqrt_Tensile_DS  M kp Ha0 WC volBMD cartthick CDI;
run;
proc means;
        by location;
        var cartthick volBMD  CDI Tensile_Failure_stress Tensile_DS Tensile_EM WC;
run;
proc sort;
        by location;
proc means;
        by location;
        var logkp0 logkp15 logkp30 logkp45;
run;
```


Reproduced with permission of the copyright owner. Further reproduction prohibited without permission.

7.6 Statistical Comparisons

Location Comparison	Cartilage Thickness	Reflectance Score	Tensile Equilibrium Modulus	Tensile Dynamic Stiffness	Tensile Strength	Tensile Failure Strain	Bone Mineral Density
MC3D vs. MC3P	0.2658	0.544	**0.0416**	0.1416	0.3458	0.4735	**0.0005**
MC3D vs. MFC	**<.0001**	0.0795	**<.0001**	**<.0001**	0.1206	**<.0001**	**0.0076**
MC3D vs. MTR	**<.0001**	**0.0002**	**0.0049**	**0.046**	**0.0217**	0.3183	**<.0001**
MC3P vs. MFC	**<.0001**	0.6969	**<.0001**	**<.0001**	**0.0138**	**0.0002**	**<.0001**
MC3P vs. MTR	**<.0001**	**0.0143**	**<.0001**	**0.0009**	**0.0014**	0.7571	**<.0001**
MFC vs. MTR	**<.0001**	0.1637	0.0859	0.0133	0.4463	**0.0009**	**0.0028**

A

Location Comparison	Equilibrium Confined Compression Modulus	Hydraulic Permeability	Strain-Dependent Parameter
MFC vs. MTR	0.8335	**0.0495**	0.3032

B

Tables 7.5 and 7.6: Statistical comparisons (p-values) for (A) structural and tensile responses (B) compression responses.

Reproduced with permission of the copyright owner. Further reproduction prohibited without permission.

8 Appendix B

8.1 Chapter 3 Sample history

Table 8.1: Sample history

Horse ID#	Approx. Age (yrs)	Weight (#)	Treatment (OCF: Osteochondral Fragment) All treatments occurred within the intercarpal joint (Distal Radial Carpal Bone). Horses were exercised 5days/week for 3 weeks prior to surgery and 9 weeks postoperatively.)
1	2.5	804	Right OCF
2	2	994	Left OCF
3	2	798	Left OCF

Reproduced with permission of the copyright owner. Further reproduction prohibited without permission.

8.2 SCBP Thickness Measurement Protocol

- Scan x-ray in VTH multimedia center
- Save image to zip disk (*see example below*)

Example: sample_ID#.jpg

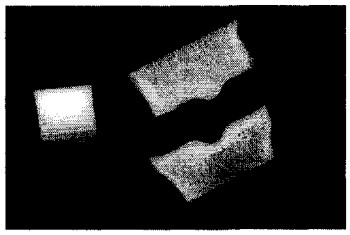

- Transfer images on to image analysis computer
- Open Image Pro Plus
- Open image to be analyzed
- Apply macro to image: MINMAX
- Macro applies a local best fit contrast enhancement filter
- (see example image below)

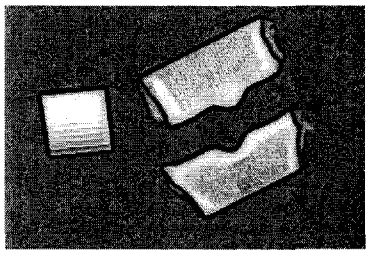

- Rotate image so articular surfaces are horizontal (*see example below*)

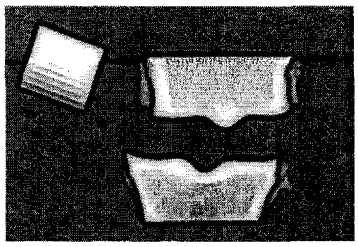

Reproduced with permission of the copyright owner. Further reproduction prohibited without permission.

- Run Macro: SCBthickness
- Uses optimal settings for smoothness and thickness
- Uses calipers to measure thickness and sends data to Excel spreadsheet
- Asks user to select points to outline sample geometry
- Calipers measure the rising and falling points of inflection based on changes in pixel value (direction of measurement tool: trabecular bone to articular cartilage)
- Six (6) regions are analyzed from both the surfaces of MC3 and P1, and their coordinates are recorded in the data table (*see example below*)

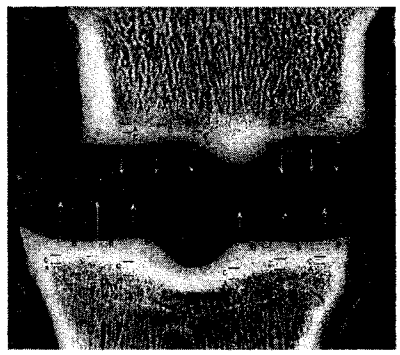

- Luminance (pixel intensity) profile for each region (arrow) are is analyzed to determine SCB thickness (*see example below*)
- Each vertical line represents either the rising or falling point of inflection, which determine the SCB boundaries
- The line in between the two vertical lines represents the subchondral bone thickness

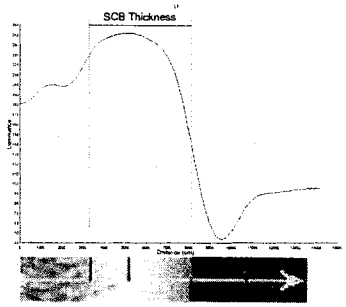

- Arrange data in Excel and perform statistical operations

Reproduced with permission of the copyright owner. Further reproduction prohibited without permission.

8.3 Region Selection

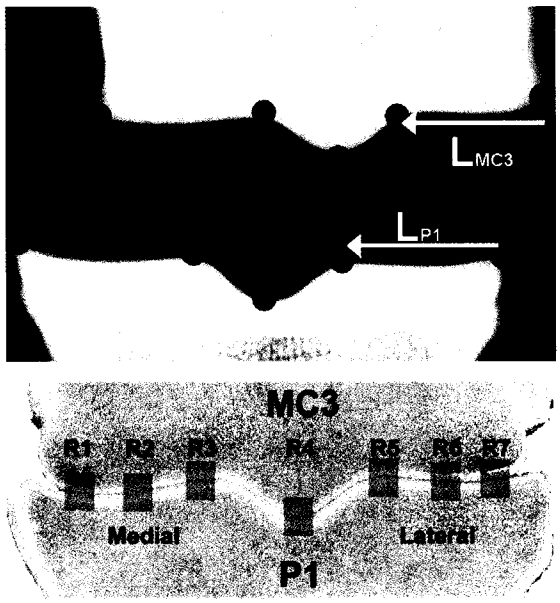

Proportions of M_{MC3} and M_{P1} lengths are used to determine R1-R3 locations relative to the medial articular margin:

R1: 30%

R2: 60%

R3: 95%

R4 is always at the apex of the sagittal ridge.

Proportions of L_{MC3} and L_{P1} lengths are used to determine R5-R7 locations relative to the lateral articular margin :

R5: 95%

R6: 60%

R7: 30%

Figure 8.1: Region selection for ScBP measurement and strain analysis (Chapter5).

Reproduced with permission of the copyright owner. Further reproduction prohibited without permission.

8.4 Image-Pro Algorithm

```
Option Explicit
Sub SCBthickness()

'*************************************************************************
***************
'
'   SCBthickness MACRO
'   Used within IMAGE PRO PLUS
'
'     Function: Determines subchondral bone thickness In various
regions according
'                  changes in greyscale values of high resolution
radiograph for the MC3 and P1
'
'     Input: Digitally scanned high resolution radiograph of MC3 and P1
'                 Digitally Rotated so articular surface is horizontal
'                 Rotated Image filtered using MINMAX macro filter
(found on IPPRO website)
'                 Orientation:
'                       Medial aspects - Right
'                       Lateral aspects - Left
'
'     Output: Excel DDE
'                 xy coordinates for all the 7 features for MC3 and P1
'                 Subchondral bone thickness
'                       Medial MC3 (3 regions)
'                       Lateral MC3 (3 regions)
'                       Medial P1 (3 regions)
'                       Lateral P1 (3 regions)
'
'     Chad W Lewis
'     Colorado State University
'     Date: 02.25.2003
'*************************************************************************
*****************

Dim numpoints As Integer
Dim numobj As Integer
Dim num_MC3 As Integer
Dim num_P1 As Integer
Dim measType As Integer
Dim i As Integer
Dim mc3org1(2) As pointapi
Dim mc3org2(2) As pointapi
Dim mc3org3(2) As pointapi
Dim mc3org4(2) As pointapi
Dim mc3org5(2) As pointapi
Dim mc3org6(2) As pointapi
Dim p1org1(2) As pointapi
Dim p1org2(2) As pointapi
Dim p1org3(2) As pointapi
Dim p1org4(2) As pointapi
Dim p1org5(2) As pointapi
Dim p1org6(2) As pointapi
Dim fValues(15) As Single
```


Reproduced with permission of the copyright owner. Further reproduction prohibited without permission.

```
Dim mc3x1 As Integer
Dim mc3y1 As Integer
Dim mc3x2 As Integer
Dim mc3y2 As Integer
Dim mc3x3 As Integer
Dim mc3y3 As Integer
Dim mc3x4 As Integer
Dim mc3y4 As Integer

Dim p1x1 As Integer
Dim p1y1 As Integer
Dim p1x2 As Integer
Dim p1y2 As Integer
Dim p1x3 As Integer
Dim p1y3 As Integer
Dim p1x4 As Integer
Dim p1y4 As Integer


ipoutputclear

'Ask user for geometry points for MC3 portion
'-----------------------------------------
tryagain:
ret = IpMeasShow(MEAS_SHOWADVANCED)
ret = IpMeasDelete(MEAS_ALL)
ret = IpMeasShow(MEAS_SHOWADVANCED)
ret = IpMeasTool(MEAS_POINT)

'Asks user to use point tool to select point of interest
ret = ipmacrostop("Using The Point Tool: Select the geometry points for
the MC3 (SEE protocol for specifics)",0)
ret = IpMeasGet (GETNUMOBJ,1,num_MC3)
ReDim MC3pt(num_MC3) As pointapi

For i=0 To num_MC3 - 1
      ret = IpMeasGet(GETFEATVALUES, i, fValues (0))
      MC3pt(i).x = fValues(-MDATA_POS)  'MC3  point X coordinate
      MC3pt(i).y= fValues(-MDATA_POSY)  'MC3  point Y coordinate
Next i

mc3x1 = MC3pt(0).x  'MC3  point X coordinate
mc3y1 = MC3pt(0).y  'MC3  point Y coordinate
mc3x2 = MC3pt(1).x  'MC3  point X coordinate
mc3y2 = MC3pt(1).y  'MC3  point Y coordinate
mc3x3 = MC3pt(3).x  'MC3  point X coordinate
mc3y3 = MC3pt(3).y 'MC3  point Y coordinate
mc3x4 = MC3pt(4).x  'MC3  point X coordinate
mc3y4 = MC3pt(4).y 'MC3  point Y coordinate

'Asks user to confirm points are correct
ret = ipmacrostop("Are the " & num_MC3 & " points
correct?",ms_modal+ms_yesno)  'Confirm coordinates are correct
If ret = 0 Then GoTo tryagain

'Save the feature data to Excel
```


Reproduced with permission of the copyright owner. Further reproduction prohibited without permission.

```
'------------------------------
Dim direc As String * 255
Dim filen As String * 255
direc = GetFilePath$("xydata","",,"Save Excel File As:", 2)
ret = ipdocgetstr(inf_name, docsel_active, filen)
ret = IpMeasSaveData(filen, S_DATA + S_DDE)


'Ask user for geometry points for P1 portion'
'-------------------------------------------
tryagain2:
ret = IpMeasDelete(MEAS_ALL)
ret = IpMeasShow(MEAS_SHOWADVANCED)
ret = IpMeasTool(MEAS_POINT)

'Ask user to use point tool to select points of interest
ret = ipmacrostop("Using The Point Tool: Select the geometry points for
the P1 (SEE protocol for specifics)",0)
ret = IpMeasGet (GETNUMOBJ,1,num_P1)
ReDim P1pt(num_P1) As pointapi

For i=0 To num_P1 - 1
      ret = IpMeasGet(GETFEATVALUES, i, fValues (0))
      P1pt(i).x = fValues(-MDATA_POS)  'P1  point X coordinate
      P1pt(i).y= fValues(-MDATA_POSY)  'P1  point Y coordinate
Next i

p1x1 = P1pt(0).x  'P1  point X coordinate
p1y1 = P1pt(0).y  'P1  point Y coordinate
p1x2 = P1pt(1).x  'P1  point X coordinate
p1y2 = P1pt(1).y  'P1  point Y coordinate
p1x3 = P1pt(3).x  'P1  point X coordinate
p1y3 = P1pt(3).y  'P1  point Y coordinate
p1x4 = P1pt(4).x  'P1  point X coordinate
p1y4 = P1pt(4).y  'P1  point Y coordinate

'Ask user to make sure points are correct
ret = ipmacrostop("Are the " & num_P1 & " selected points
correct?",ms_modal+ms_yesno)  'Confirm coordinates are correct
If ret = 0 Then GoTo tryagain2

'Save correct data points
ret = IpMeasSaveData(filen, S_DATA + S_DDE)


'Calculations to determine reference line coordinates for MC3 and P1
'For MC3
Dim mmc3y As Integer
Dim lmc3y As Integer
mmc3y = (MC3y1 + MC3y2)/2
lmc3y = (MC3y3 + MC3y4)/2

'For P1
Dim mp1y As Integer
Dim lp1y As Integer
mp1y = (P1y1 + P1y2)/2
lp1y = (P1y3 + P1y4)/2
```


Reproduced with permission of the copyright owner. Further reproduction prohibited without permission.

```
'Proportions to analyze
Const A=0.30
Const B=0.60
Const C=0.95

Const E=0.05
Const F=0.40
Const G=0.70

'Lengths of articular surface to be analyzed
'For MEDIAL MC3
Dim Dmedial_mc3 As Integer
Dmedial_mc3 = mc3x2 - mc3x1

'x and y coordinates for caliper tool lines
mc3org1(1).x = mc3x1 + (A * Dmedial_mc3)
mc3org1(1).y = mmc3y + 35
mc3org1(0).x = mc3x1 + (A * Dmedial_mc3)
mc3org1(0).y = mmc3y - 80
mc3org2(1).x = mc3x1 + (B * Dmedial_mc3)
mc3org2(1).y = mmc3y + 35
mc3org2(0).x = mc3x1 + (B * Dmedial_mc3)
mc3org2(0).y = mmc3y - 30
mc3org3(1).x = mc3x1 + (C * Dmedial_mc3)
mc3org3(1).y = mmc3y + 35
mc3org3(0).x = mc3x1 + (C * Dmedial_mc3)
mc3org3(0).y = mmc3y - 30

'For LATERAL MC3
Dim Dlateral_mc3 As Integer
Dlateral_mc3 = mc3x4 - mc3x3

'x and y coordinates for caliper tool lines
mc3org4(1).x = mc3x3 + (E * Dlateral_mc3)
mc3org4(1).y = lmc3y + 35
mc3org4(0).x = mc3x3 + (E * Dlateral_mc3)
mc3org4(0).y = lmc3y - 30
mc3org5(1).x = mc3x3 + (F * Dlateral_mc3)
mc3org5(1).y = lmc3y + 35
mc3org5(0).x = mc3x3 + (F * Dlateral_mc3)
mc3org5(0).y = lmc3y - 30
mc3org6(1).x = mc3x3 + (G * Dlateral_mc3)
mc3org6(1).y = lmc3y + 35
mc3org6(0).x = mc3x3 + (G * Dlateral_mc3)
mc3org6(0).y = lmc3y - 80

'For MEDIAL P1
Dim Dmedial_p1 As Integer
Dmedial_p1 = p1x2 - p1x1

'x and y coordinates for caliper tool lines
plorg1(0).x = p1x1 + (A * Dmedial_p1)
plorg1(0).y = mp1y + 50
plorg1(1).x = p1x1 + (A * Dmedial_p1)
plorg1(1).y = mp1y - 5
plorg2(0).x = p1x1 + (B * Dmedial_p1)
```


Reproduced with permission of the copyright owner. Further reproduction prohibited without permission.

```
p1org2(0).y = mp1y + 50
p1org2(1).x = p1x1 + (B * Dmedial_p1)
p1org2(1).y = mp1y - 5
p1org3(0).x = p1x1 + (C * Dmedial_p1)
p1org3(0).y = mp1y + 50
p1org3(1).x = p1x1 + (C * Dmedial_p1)
p1org3(1).y = mp1y - 5

'For LATERAL P1
Dim Dlateral_p1 As Integer
Dlateral_p1 = p1x4 - p1x3

'x and y coordinates for caliper tool lines
p1org4(0).x = p1x3 + (E * Dlateral_p1)
p1org4(0).y = lp1y + 50
p1org4(1).x = p1x3 + (E * Dlateral_p1)
p1org4(1).y = lp1y - 15
p1org5(0).x = p1x3 + (F * Dlateral_p1)
p1org5(0).y = lp1y + 50
p1org5(1).x = p1x3 + (F * Dlateral_p1)
p1org5(1).y = lp1y - 15
p1org6(0).x = p1x3 + (G * Dlateral_p1)
p1org6(0).y = lp1y + 50
p1org6(1).x = p1x3 + (G * Dlateral_p1)
p1org6(1).y = lp1y - 15

'Caliper Analysis
'Caliper Settings
Dim ID(12) As Integer
ret = IpClprSet(CLPR_AUTOREFRESH, 1)
ret = IpClprSet(CLPRO_SMOOTHING, 34)
ret = IpClprSet(CLPRO_THICKNESS, 21)
ret = IpClprSet(CLPRO_APPLY_SCAL,1)
ret = IpClprSet(CLPRO_SHOW_LABEL,1)
ret = IpClprSet(CLPRO_SHOW_NUMBER,1)
ret = IpClprSet(CLPRO_PRECISION,4)
ret = IpClprSet(CLPR_AUTOREFRESH, 0)

ret = IpClprShow(1)

'Set Edge Detectors
ret = IpClprDeleteMeas(-1, "", "")
ret = IpClprCreateDerivativeEdge("Falling","A", 255, 0, CLPR_FALLING)
ret = IpClprCreateDerivativeEdge("Peak","B", 1234523, 0, CLPR_PEAK)
ret = IpClprCreateMeas(CLPR_MEAS_DIST2, "Peak", "Falling")

'Create Line Samplers
'For LATERAL MC3
'Deletes samplers from previous analysis
ID(1) = IpClprCreateSampler(CLPR_LINE, "mc3_L1", mc3org1(0), 0)
ID(2) = IpClprCreateSampler(CLPR_LINE, "mc3_L2", mc3org2(0), 0)
ID(3) = IpClprCreateSampler(CLPR_LINE, "mc3_L3", mc3org3(0), 0)
ID(4) = IpClprCreateSampler(CLPR_LINE, "mc3_L4", mc3org4(0), 0)
ID(5) = IpClprCreateSampler(CLPR_LINE, "mc3_L5", mc3org5(0), 0)
ID(6) = IpClprCreateSampler(CLPR_LINE, "mc3_L6", mc3org6(0), 0)
ID(7) = IpClprCreateSampler(CLPR_LINE, "p1_L1", p1org1(0), 0)
ID(8) = IpClprCreateSampler(CLPR_LINE, "p1_L2", p1org2(0), 0)
```


Reproduced with permission of the copyright owner. Further reproduction prohibited without permission.

```
ID(9) = IpClprCreateSampler(CLPR_LINE, "p1_L3", p1org3(0), 0)
ID(10) = IpClprCreateSampler(CLPR_LINE, "p1_L4", p1org4(0), 0)
ID(11) = IpClprCreateSampler(CLPR_LINE, "p1_L5", p1org5(0), 0)
ID(12) = IpClprCreateSampler(CLPR_LINE, "p1_L6", p1org6(0), 0)

'Confirm calipers are collecting the correct information
ret = ipmacrostop("Make sure all calipers are capturing the CORRECT
edges. Use the caliper tool to correct if necessary. Are All calipers
CORRECT?",0)  'Confirm coordinates are correct

For i=1 To 12
      ret = IpClprSelectSampler(ID(i))
      ret = IpClprSave(filen, S_DATA2 + S_DDE)
Next i

ret = IpClprShow(0)
ret = IpMeasShow(0)

'Remind user to save excel spreadsheet
ret = ipmacrostop("SAVE EXCEL SPREADSHEET corresponding to SAMPLE
ID",0)


End Sub
```


Reproduced with permission of the copyright owner. Further reproduction prohibited without permission.

9 Appendix C

9.1 Sample preparation protocol

Materials Required

- Propidium Iodide (1 mg/ml Solution)
- Benzamidine (100X Stock Solution, 5mM)
- N-Ethylmalemide (100X Stock Solution, 10mM)
- PMSF (100X Stock Solution, 1mM)
- Phosphate Buffered Solution
- Phosphate Buffered Solution Packets (#5)
- 10% Formalin
- Pipette to deliver volume of 100µl
- Pipette tips for 100µl volume
- Superglue
- Sharpie Marker
- VWR Sample Cups and Lids (4oz and 8oz)
- Exakt Macro 0.2mm Blade Rollers
- Exakt Macro 0.2mm Blade
- Exakt Acrylic Vacuum Slides
- Exakt Saw
- Exakt Vacuum Plate
- Custom 90 degree Exakt fixture
- Scalpel Handle
- Scalpel Blades
- Rat Tooth Forceps
- Exakt Laser Positioning Guide
- Blue Absorbent Pad
- Sample Worksheet
- Micrometer (0.001mm resolution)
- Non-sterile Gauze
- Digital Camera (Nikon 900)
- Camera Tripod
- 3-D Mounting Bracket
- Stainless Steel Pins (3/8" diameter, 1" long)-Mounting Pins

Reproduced with permission of the copyright owner. Further reproduction prohibited without permission.

- 4.6mm Stainless Steel Drill Bit (sharp point)
- 7/16 HSS Drill Bit
- 3/8" Electric Drill
- Latex Gloves

Procedure

- Remove Specimen (Whole Joint in Freezer Bag) from Freezer
- Place Specimen in Refrigerator until thawed (~1hr)
- Prepare Exakt Cutting System (See Exakt Users Manual)
- Attach Rollers
- Rollers should be dismantled and rebuilt for every samples prepared
- Place Cutting Band on Wheels
- Make sure band is placed correctly into rollers before Tensioning
- Manually Turn Wheels while Band Tensioning
- Test Band for Proper Tension (See Exakt Users Manual)
- Properly Align Band and Rollers (See Exakt Users Manual)
- Place Top and Bottom Plates into position using Nylon covered nuts
- Make sure Exakt Drain is CLOSED
- ADD 8 Liters of Unsterile Phosphate Buffered Saline to the Exakt's Water Coolant Basin
- Attach Laser Guide to Top Plate Mount
- Align Laser to Band Cutting Path (See Exakt Users Manual)
- Setup Preparation Area
- Layout blue absorbent pad
- Layout the following items on pad
    - Scalpel Blade + Handle
    - Forceps
    - Three-Dimensional Mounting Bracket
    - Drill Bits
    - Electric Drill
    - Gauze Pads
    - Box of Gloves
    - Mounting Pins
    - Alignment Pins
- Prepare Solution of PBS + Proteinase Inhibitors (PBS+PIs)
- Add 96ml of PBS to 8oz VWR Specimen Cup
- Using a pipette, add the following to the 96ml of PBS
    - 1ml of 100X 1mM PMSF
    - 1ml of 100X 5mM Benzamidine
    - 1ml of 100X 10mM N-Ethylmalemide
- Gently Mix Solution
- Setup Camera
- Attach Portable Nikon Digital Camera to Tripod
- Make Labels for the Sample
    - Sample ID#

Reproduced with permission of the copyright owner. Further reproduction prohibited without permission.

Medial
Lateral

- Properly position background mat (black foam pad, 1/8" thick)

Joint Dissection

- Soak Gauze with PBS+PIs
- NOTE: At All Times Keep Articular Surfaces Hydrated with PBS+PIs soaked gauze
- DO NOT CUT / Dissect Medial/Lateral Ligaments
- Remove Soft Tissue from
- Palmar Aspect
- Dorsal Aspect
- SEE Figure 9.1
- Using Exakt and Manual Cutting Plate Add-on
- Remove Excess Bone from MC3/P1 to allow proper cutting clearance for Cut #1
- SEE Figure 9.2
- Take DIGITAL picture
- Instructions for CUT #1
- Drill hole into P1 3cm below dorsal AC margin
- Place 5/8" Pin into hole (SEE Figure 9.2)
- Attach 3-D clamp to P1 pin
- Extend joint so dorsal AC margins are in contact
- Manipulate clamp to assure proper joint angle when MC3 pin is placed
- While holding the joint at the proper angle, drill hole into MC3 using a 4.8mm SS bit with SS alignment barrel (5/8" barrel + 4.8mm barrel)
- Replace 4.8mm drill bit with 5/8" SS bit
- Take out 4.8mm barrel from SS alignment barrel
- Drill hole for 5/8" pin
- Place pin into MC3
- Tighten clamp to both pins. (Figure 9.3)
- NOTE: Make sure dorsal margin AC surfaces are in
- contact (medial to lateral).

Instructions for CUT#1

- Attach vise clamp (using small jaws) to Exakt (Figure 9.4)
- Using the vise, clamp onto P1 pin using wet gauze to increase the friction between the pin and the vise
- Turn ON Laser
- Align sample so the long axis of the palmer side of P1 is parallel with the cutting axis (planar area on the palmer side)(Figure 9.5)
- Align the sample so 1cm of tissue (from the planar palmar P1) will be cut (CUT#1)
- Perform CUT #1 (Figure 9.6)
- Carefully remove clamp and sample from Exakt System

Reproduced with permission of the copyright owner. Further reproduction prohibited without permission.

- Remove Clamp and Pins
- Take DIGITAL picture (medial/lateral view)
- Super Glue Slide to CUT#1 Surface
- Remove paper from ONE side of an Exakt slide
- Using a Permanent Marker, draw a minor axis line in the middle of the slide (perpendicular to the long axis)
- Using a scalpel, carefully cut away soft tissue (not articular cartilage) from the medial and lateral aspects of the joint, only near CUT#1 to allow visibility of the articular cartilage when gluing sample to slide
- Place a nominal amount of SUPERGLUE to the slide
- Carefully press the sample on to the slide WHILE assuring articular surface is parallel to the marker line (Figure 9.7, Figure 9.8)
- Hold in place for 10 seconds and allow to dry
- Setup additional slide (remove protecting paper from both sides of slide)
- Setup vacuum plate on slide table of Exakt
- Turn on vacuum pump
- Place new slide on vacuum plate and apply vacuum to plate
- Make sure there is vacuum being applied
- Place a small amount of SUPER GLUE on vacuum plate slide
- Remove remaining paper from sample slide
- Inspect perpendicularity of the articular surface to the long axis of the glued slide. If not correct, compensate when gluing to vacuum slide. (Figure 9.10)
- Place the glued slide/sample on vacuum slide (Figure 9.9)
- Make sure both edges of slides (sample and vacuum) match up
- Allow glue to setup for >10min
- REMINDER: MAKE SURE CARTILAGE IS HYDRATED WITH PBS + Protease Inhibitors
- Remove sample from vacuum plate
- Take DIGITAL pictures of sample (cut surface, dorsal view, side view)

Instructions for CUT#2

- Attach vacuum plate so vacuum surface is parallel with cutting path of blade on Exakt system
- Vacuum plate the sample
- Align table so ONLY the MC3 portion is cut
- Perform CUT #2 (Figure 9.11)

Instructions for CUT #3 (Figure 9.12 - Figure 9.15)

- Remove vacuum plate
- Attach 90 degree cutting jig (make sure it is somewhat level)
- Attach vacuum plate to 90 degree jig (see figure)
- Fix sample to vacuum plate using vacuum (make sure the slide is under max vacuum)
- Plan CUTS#3 & 4 (1.5cm proximal/distal from AC surface) using MagicMarker

Reproduced with permission of the copyright owner. Further reproduction prohibited without permission.

- Make sure automatic translation stepper is fully extended or contained
- Align sample for CUT#3 by adjusting table (proximal or distal) depending on stepper translation position (Figure 9.12)
- Before starting, NOTE: WATCH CUT TO PREVENT CUTTING INTO VACUUM PLATE
- Perform CUT#3 (Figure 9.13)

Instructions for CUT#4

- Using the automatic translation stage (manually translate if needed), translate 3cm to properly align sample for CUT #4
- Perform CUT#4 (Figure 9.14,Figure 9.15)
- Remove Sample, Vacuum Plate, and 90 degree attachment in reverse order of installation

Instructions for CUT#5

- Attach vacuum plate to translation table (long axis parallel to blade axis) (Figure 9.16)
- Determine where sample will be taken from sample
- Make sure curvature of surface is in the middle of sample
- Very Important
- Make alignment marks using a MagicMarker
- Fix sample to vacuum plate (using vacuum of course) (Figure 9.16)
- Adjust table to align sample for CUT#5
- Make sure there is nothing that will disrupt the travel of the table during these cuts, i.e. vacuum hoses, plates, sample.. Very Important
- Check alignment AGAIN
- Perform CUT#5 (FIGURE 17)
- Take DIGITAL picture of remnants (Figure 9.17)

Instructions for CUT#6

- Carefully translate the sample stage 7.5mm
- 7mm AUTO + 0.5mm MANUAL
- Check Alignment
- DoubleCheck thickness
- Perform CUT#6 (Figure 9.18)
- Carefully watch for sample to be cut free and immediately place into PBS+PI solution basin
- Stop Exakt

Perform Sample Measurements

- Using 0.001mm resolution micrometer, measure/record the thickness at the 9 points noted in the sample worksheet
- Using a 0.01mm resolution caliper, measure/record the height of the sample on the sample worksheet
- Take DIGITAL picture of the FINAL sample with (Figure 9.19)
- Labels

Reproduced with permission of the copyright owner. Further reproduction prohibited without permission.

- Spatial scale
- Take out memory card
- Promptly tear down camera setup and store in appropriate site
- Place sample in PBS+PI solution basin (50ml PBS+PI Total Volume)

Stain Sample

- NOTE PROPIDIUM IODIDE IS KNOWN TO BE A POTENTIAL MUTAGEN
- CAREFULLY: Add 1ml of Propidium Iodide Solution (1mg/ml) to the solution basin
- Carefully place container cover of basin
- Transport the sample to be stored in a 5° C refrigerator
- Store sample in stain for >8 hours

CLEAN UP:

- PLACE SHARPS IN PROPER CONTAINER
- CLEAN Exakt Saw per protocol
- DISCARD excised tissue at VTH NECROPSY
- DISCARD paper/plastic trash in wastebasket
- CLEAN Tools
- Place Tools in storage box
- Clear of Table Surface
- Sanitize Table Surface and Wipe Clean

Reproduced with permission of the copyright owner. Further reproduction prohibited without permission.

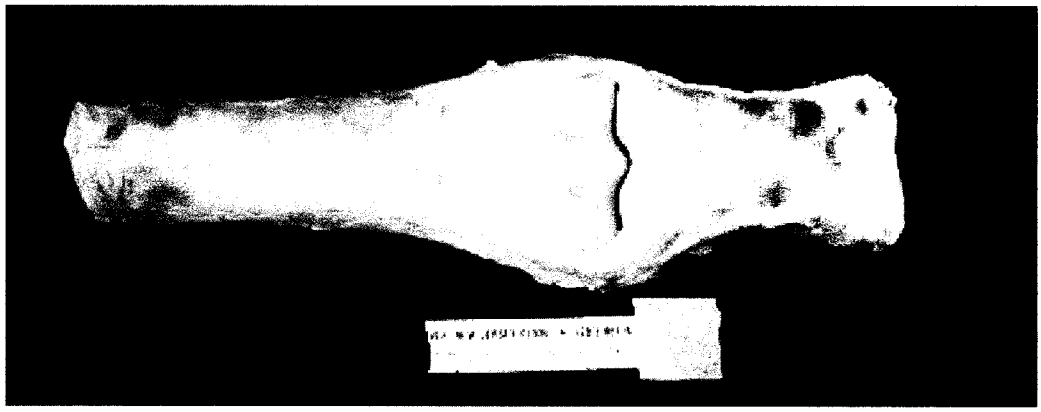

Figure 9.1: Coronal view of the initial MCP sample anatomy with synovial membrane removed.

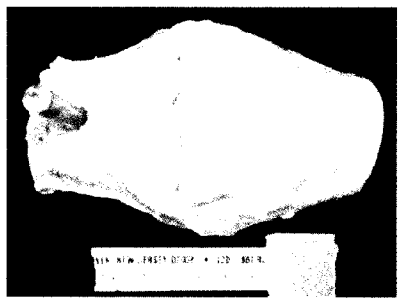

Figure 9.2: Sample after excess bone from the MC3 and P1 has been removed.

Figure 9.3: CUT#1 Sample fixed in angle clamp using fixation pins (5/8" diam)

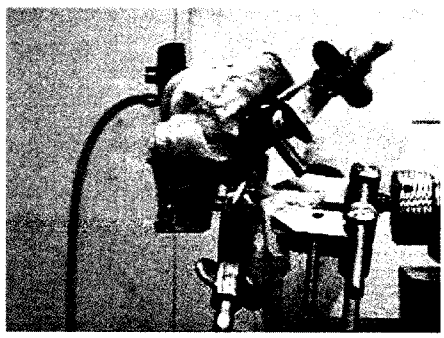

Figure 9.4: CUT#1 angle fixation using the small vise on the Exakt system.

Reproduced with permission of the copyright owner. Further reproduction prohibited without permission.

Figure 9.5: CUT#1 Alignment of laser to assure proper orientation of sample. This is the most important step of the whole process.

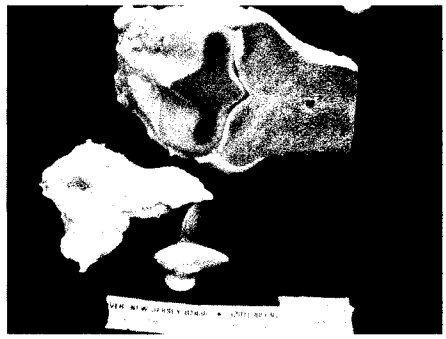

Figure 9.6: CUT#1 Results

Figure 9.7: Position of joint during gluing phase #1

Figure 9.8: Dorsal view of joint during gluing phase #1

Reproduced with permission of the copyright owner. Further reproduction prohibited without permission.

Figure 9.9: Gluing Phase #2

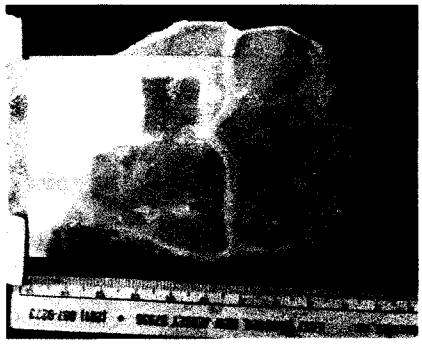

Figure 9.10: View of the cut surface #1 which has been glued to the acrylic surface

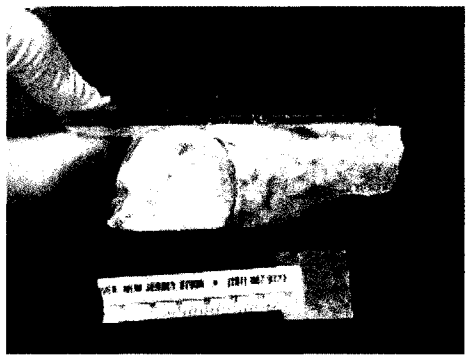

Figure 9.11: View after CUT #2

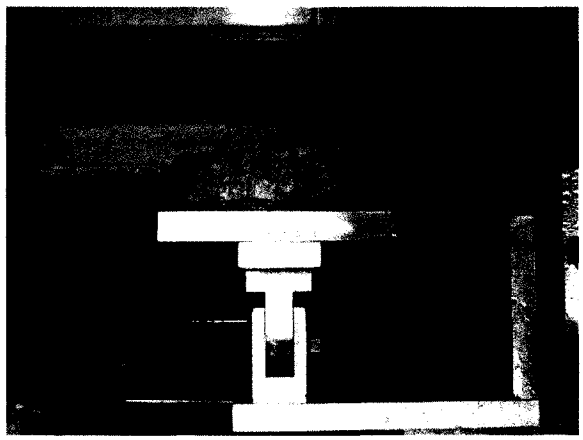

Figure 9.12: View of the laser aligning tool for CUTS# 3 & 4

Reproduced with permission of the copyright owner. Further reproduction prohibited without permission.

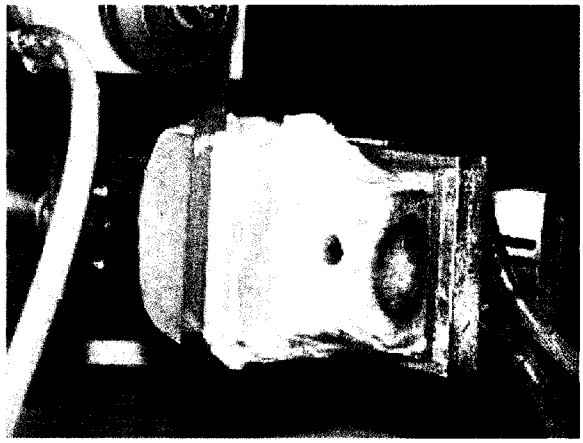

Figure 9.13: Dorsal view of CUTS#3 & 4 in ACTION

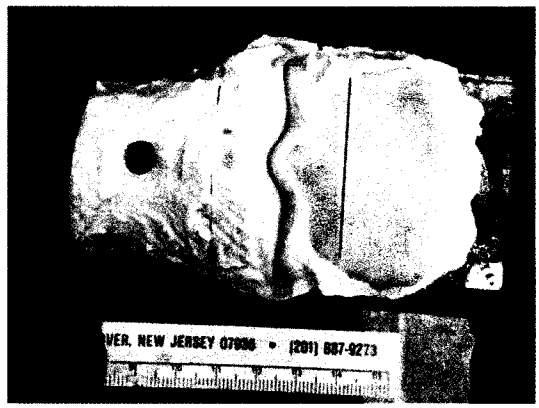

Figure 9.14: Dorsal view of CUTS# 3 & 4 FINAL

Figure 9.15: Medial-Lateral View of CUTS # 3 & 4

Reproduced with permission of the copyright owner. Further reproduction prohibited without permission.

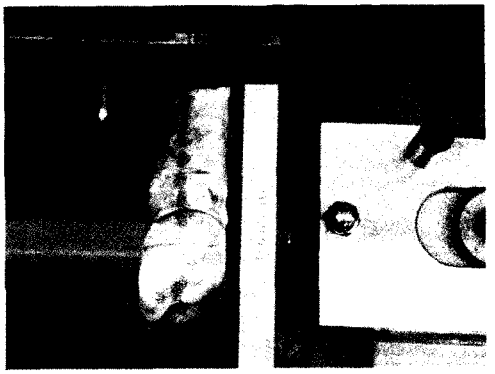

Figure 9.16: Setting up for CUT#5

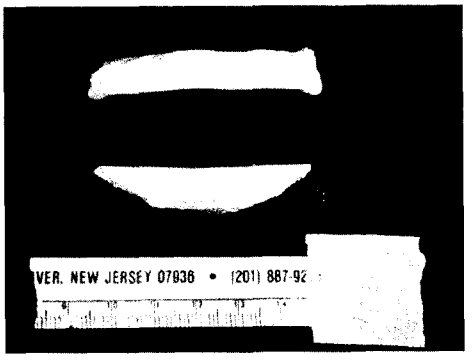

Figure 9.17: Remnants of CUT #5

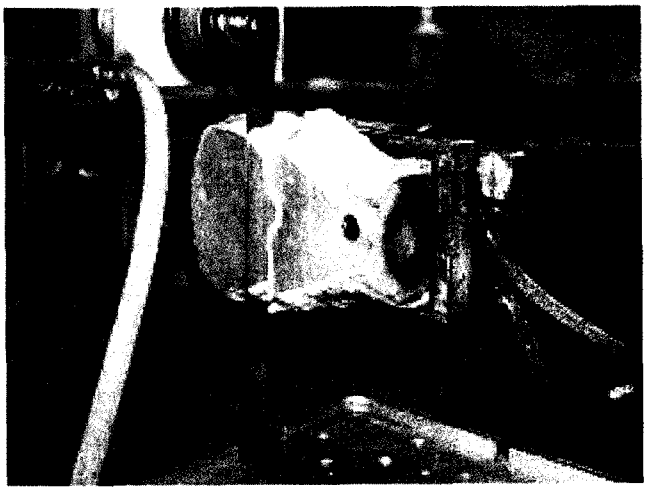

Figure 9.18: CUT #6 in progress (NOTE: The sample needs to be rotated 90 degrees relative to the blade to minimize out of plane motion).

Reproduced with permission of the copyright owner. Further reproduction prohibited without permission.

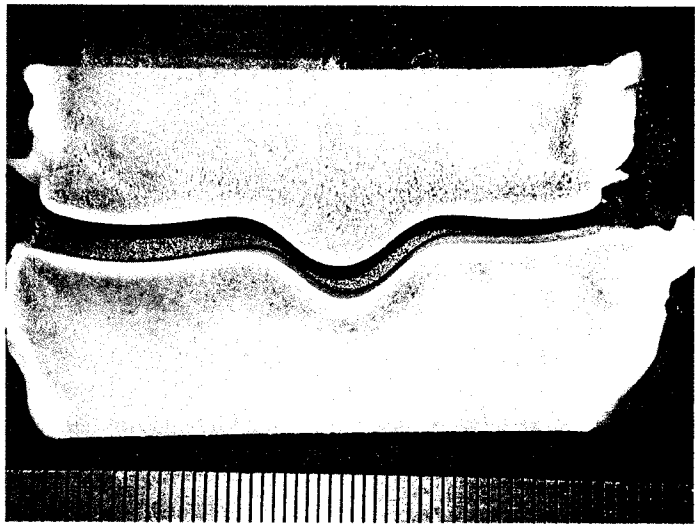

Figure 9.19: Final Sample with millimeter scale (below)

Reproduced with permission of the copyright owner. Further reproduction prohibited without permission.

9.2 *Illustrations of custom loading system*

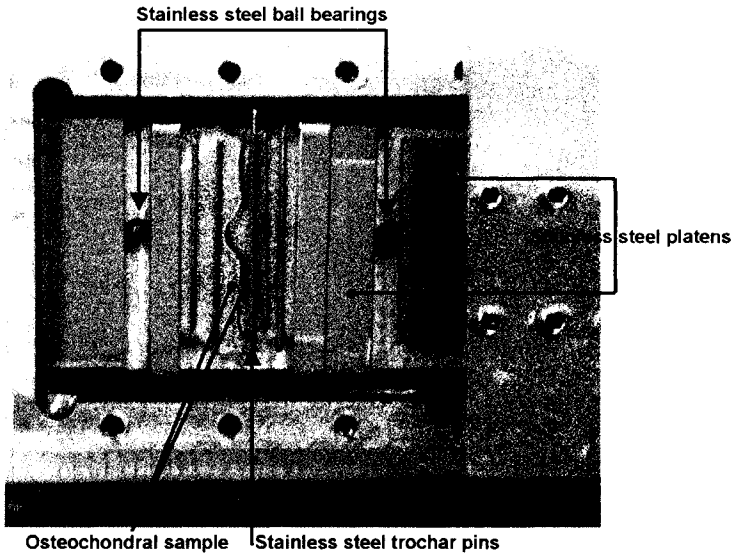

Figure 9.20: Top-view of the compression chamber with the osteochondral sample, stainless steel ball bearing (alignment), and stainless steel trochar pins in position before the confining compression plate is placed on top.

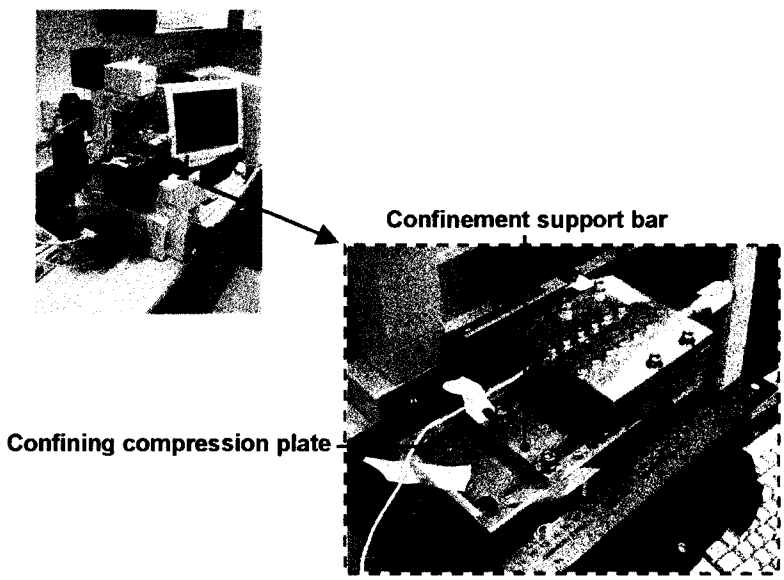

Figure 9.21: View of the custom-loading system on the inverted microscope with a close-up view showing the confining compression plate and confinement support bar.

Reproduced with permission of the copyright owner. Further reproduction prohibited without permission.

9.3 Matlab m-file for data reduction

9.3.1 getstats.m

```
function [stats] = getstats(fname,fpath)

filespec = fullfile(fpath,fname);

% %Extract the first two lines of the data header
% fid = fopen(filespec,'r');
% variables = fgetl(fid);
% param = fgetl(fid);
% fclose(fid);
%
% %Number of rows and columns in data set #1
% rows1 = param1(1,:);
% columns1 = param1(2,:);
% rc=rows1*columns1;


%Extract 8 columns of data from *.dat files
Z= dlmread(filespec,',',2,0);

%Divide up columns for datasets 1 & 2
%x and y coordinates (pixels) = coords
x= Z(:,1);
y= Z(:,2);

%u displacements
u = Z(:,3);

%v displacements
v = Z(:,4);

%correlation coefficients
corr = Z(:,5);

%Strain Components
Exx=Z(:,6);
Eyy=Z(:,7);
Exy=Z(:,8);

E1=Z(:,9);
E2=Z(:,10);
theta=Z(:,11);

clear Z;
```


Reproduced with permission of the copyright owner. Further reproduction prohibited without permission.

```
num=size(u(:,1));

% for i=1:num
%    if u(i)==0;
%       u(i)=nan;
%    end
%    if v(i)==0;
%       v(i)=nan;
%    end
%    if corr(i)==-1;
%       corr(i)=nan;
%    end
%    if Exx(i)==0;
%       Exx(i)=nan;
%    end
%    if Eyy(i)==0;
%       Eyy(i)=nan;
%    end
%    if Exy(i)==0;
%       Exy(i)=nan;
%    end
%    if E1(i)==0;
%       pMax(i)=nan;
%    end
%    if E2(i)==0;
%       pMin(i)=nan;
%    end
%    if theta(i)==0;
%       pMin(i)=nan;
%    end
% end

mean_u = nanmean(u);
std_u = nanstd(u);
mean_v = nanmean(v);
std_v = nanstd(v);
mean_corr = nanmean(corr);
std_corr = nanstd(corr);
mean_Exx = nanmean(Exx);
std_Exx = nanstd(Exx);
mean_Eyy = nanmean(Eyy);
std_Eyy = nanstd(Eyy);
mean_Exy = nanmean(Exy);
std_Exy = nanstd(Exy);
```


Reproduced with permission of the copyright owner. Further reproduction prohibited without permission.

```
mean_E1 = nanmean(E1);
std_E1 = nanstd(E1);
mean_E2 = nanmean(E2);
std_E2 = nanstd(E2);
mean_theta = nanmean(theta);
std_theta = nanstd(theta);

stats=[mean_u std_u mean_v std_v mean_corr std_corr mean_Exx std_Exx mean_Eyy
std_Eyy mean_Exy std_Exy mean_E1 std_E1 mean_E2 std_E2 mean_theta std_theta];
```

9.3.2 rgbstats.m

```
clear;

[fname1,fpath1] = uigetfile('*.dat','Choose 1st data file');
[fname2,fpath2] = uigetfile('*.dat','Choose 2nd data file');
[fname3,fpath3] = uigetfile('*.dat','Choose 3rd data file');
[fname4,fpath4] = uigetfile('*.dat','Choose 4th data file');
[fname5,fpath5] = uigetfile('*.dat','Choose 5th data file');
[fname6,fpath6] = uigetfile('*.dat','Choose 6th data file');
[fname7,fpath7] = uigetfile('*.dat','Choose 7yh data file');
% [fname8,fpath8] = uigetfile('*.dat','Choose 8th data file');
% [fname9,fpath9] = uigetfile('*.dat','Choose 9th data file');
% [fname10,fpath10] = uigetfile('*.dat','Choose 10th data file');
% [fname11,fpath11] = uigetfile('*.dat','Choose 11th data file');
% [fname12,fpath12] = uigetfile('*.dat','Choose 12th data file');
% [fname13,fpath13] = uigetfile('*.dat','Choose 13th data file');
% [fname14,fpath14] = uigetfile('*.dat','Choose 14th data file');
% [fname15,fpath15] = uigetfile('*.dat','Choose 15th data file');
% [fname16,fpath16] = uigetfile('*.dat','Choose 16th data file');
% [fname17,fpath17] = uigetfile('*.dat','Choose 17th data file');

row1 = getstats(fname1,fpath1);
row2 = getstats(fname2,fpath2);
row3 = getstats(fname3,fpath3);
row4 = getstats(fname4,fpath4);
row5 = getstats(fname5,fpath5);
row6 = getstats(fname6,fpath6);
row7 = getstats(fname7,fpath7);
% row8 = getstats(fname8,fpath8);
% row9 = getstats(fname9,fpath9);
% row10 = getstats(fname10,fpath10);
% row11 = getstats(fname11,fpath11);
% row12 = getstats(fname12,fpath12);
% row13 = getstats(fname13,fpath13);
% row14 = getstats(fname14,fpath14);
```


Reproduced with permission of the copyright owner. Further reproduction prohibited without permission.

```
% row15 = getstats(fname15,fpath15);
% row16 = getstats(fname16,fpath16);
% row17 = getstats(fname17,fpath17);

M=[row1; row2; row3; row4; row5; row6; row7];

[newfile,newpath] = uiputfile('data.txt','Save file name');
newfilespec = fullfile(newpath,newfile);
dlmwrite(newfilespec,M);

rotation.m
clear;

[fname,fpath] = uigetfile('*.dat','Choose 1st data file');

filespec = fullfile(fpath,fname);

% %Extract the first two lines of the data header
% fid = fopen(filespec,'r');
% variables = fgetl(fid);
% param = fgetl(fid);
% fclose(fid);
%
% %Number of rows and columns in data set #1
% rows1 = param1(1,:);
% columns1 = param1(2,:);
% rc=rows1*columns1;


%Extract 8 columns of data from *.dat files
Z= dlmread(filespec,',',2,0);

%Divide up columns for datasets 1 & 2
%x and y coordinates (pixels) = coords
x= Z(:,1);
y= Z(:,2);

%u displacements
u = Z(:,3);

%v displacements
v = Z(:,4);

%correlation coefficients
corr = Z(:,5);
```


Reproduced with permission of the copyright owner. Further reproduction prohibited without permission.

```
%Strain Components
Exx=Z(:,6);
Eyy=Z(:,7);
Exy=Z(:,8);

E1=Z(:,9);
E2=Z(:,10);
theta=Z(:,11);

clear Z;

num=size(u(:,1));

midx = 600;
midy = 800;

for i=1:num-1
   x0 = x(i);
   y0 = y(i);
   x1 = x(i+1);
   y1 = y(i+1);
   x0f = x(i) + u(i);
   y0f = y(i) + v(i);
   x1f = x(i+1) + u(i+1);
   y1f = y(i+1) + v(i+1);
   Rx0 = x1 - x0;
   Ry0 = y1 - y0;
   Rx1 = x1f - x0f;
   Ry1 = y1f - y0f;
   d0 = sqrt((x0-x1)^2 + (y0-y1)^2);
   d1 = sqrt((x0f-x1f)^2 + (y0f-y1f)^2);
   alpha(i) = acos((Rx0*Rx1+Ry0*Ry1)/(d0*d1));
end

plot (alpha)

mean(alpha)*(180/pi)
```


Reproduced with permission of the copyright owner. Further reproduction prohibited without permission.

10 Appendix D

10.1 Chapter 5 Sample history

Table 10.1: Sample history

Sample ID#	Horse ID#	Side	Approx. Age (yrs)	Weight (lbs)	Treatment (OCF: Osteochondral Fragment) All treatments occurred within the intercarpal joint (Distal Radial Carpal Bone). Horses were exercised 5days/week for 3 weeks prior to surgery and 9 weeks postoperatively.)
1	A	Right	2.5	965	Right OCF
2	A	Left	2.5	965	Right OCF
3	B	Right	2.5	935	Left OCF
4	B	Left	2.5	935	Left OCF
5	C	Right	2.5	744	Left OCF
6	D	Left	3.5	745	Right OCF

Reproduced with permission of the copyright owner. Further reproduction prohibited without permission.

10.2 Opposing osteochondral sample testing protocol

Materials Required

- Propidium Iodide (1 mg/ml Solution)
- Benzamidine (100X Stock Solution, 5mM)
- N-Ethylmalemide (100X Stock Solution, 10mM)
- PMSF (100X Stock Solution, 1mM)
- Phosphate Buffered Solution pH=7.5
- Pipette to deliver volume of 100µl
- Pipette tips for 100µl volume
- Rat Tooth Forceps
- Sample Worksheet
- Non-sterile Gauze
- Latex Gloves
- Lens Cleaning Supplies
- Fluorescence equipped Olympus IX-70 with translation stage digital readout
- SpotRT digital camera
- Computer system with latest SpotRT camera capture software
- 133Mhz Computer system with Labview software and hardware
- Force Cell Amplifier
- Osteochondral Testing System
- 500# Sensotec Force Cell
- Clean Plate Glass level within Base Structure
- Trochar pins (0.067")
- Stainless steel platens
- ¼" Stainless steel ball bearings
- Top plate (plate glass mounted on stainless steel)
- Aluminum compression vise

Procedure

- Make sure Fluorescent Source is ADJUSTED
- Clean all lenses
- Data acquisition computer and software open
- Labview File:cwl2003.vi
- Force Amplifier: Make sure force cell is CALIBRATED and Turned ON
- Add 50ml of PBS with PI solution into testing chamber
- Label Cryovial for DMMB sample solution analysis
- Make sure all software and sample worksheets are ready
- Load Sample in to Chamber
- Take sample out of 50ml Falcon Tube with tweezers
- Using lenses paper, clean imaged surface (palmar) of sample
- Make sure P1 is place on the stationary end
- Align sample between stainless steel platens

Reproduced with permission of the copyright owner. Further reproduction prohibited without permission.

- Make sure SS ball bearings are in the correct position by gently compressing the sample and assuring sample is stable. Release any compression applied to sample.
- Make sure sample is at free swelling state with AC surfaces aligned
- Place trochar pins on sample bone regions (parallel to AC surface)
- Carefully place SSplate/glass support on top of sample and pins (see image)
- Add compression arm – tighten side bolts
- Carefully place Testing Chamber on microscope
- Remove round silver plate above objectives from IX-70
- Slide chamber into translation stage bracket
- Assure chamber/stage fixation using label tape at both ends of chamber setup.
- Place brass shim under back right side of fixture to stabilize during loading.
- Camera Software setup
- Multi-image capture
- Linked to correct directory structure
- Correct Acquisition Rate
- Correct Camera Shutter Speed and Gamma Updated in Camera Settings
- Perform pilot translation test using VIC2D to make sure shutter speed and gamma settings are correct (good correlation output)
- Correct Focal Plane
- Position objective at maximum distance away from sample
- Slowly bring in objective closer to sample
- Correct Focal plane is considered to be when osteocytes(bone) and chondrocytes(cartilage) are both in sharp focus.

Setup Translation Stage Reference System

- While viewing the image output, translate stage to LATERAL side of sample.
- Position POINT A (see worksheet) on the edge of the image.
- Reset Translation Stage Coordinates (0,0)
- Translate to POINT B using the same side of the image as in A, Record Coordinates on Worksheet
- Perform Step Above for POINTS C and D.
- Open Excel Spreadsheet (NAME?)
- Enter Translation Coordinates for A, B, C, and D.
- Record Translation Stage Coordinates for Regions
- #0, #1, #2
- #4, #5, #6
- Region #3 is the Sagittal Ridge, which will be centered in the image and position will be recorded.
- Image File Name Structure:

Reproduced with permission of the copyright owner. Further reproduction prohibited without permission.

- SampleID_Side_%_state_#.tif

Preloading Sequence (Time Required: 1.5hrs)

- Capture Preloading Equilibrium Images for ALL REGIONS
- Use the above calculated coordinates for each region
- Make sure to use the correct image file labeling system
- Record z-axis values for each region
- Last Image taken should be over Region #6
- Make sure CAMERA SETTINGS are the same as LIVE SETTINGS
- Setup Mulitple Image Acquisition Parameters
- Frame Rate = 5min
- Number of Images = 12
- Link Preload/SR Directory
- Starting Image # = 0
- Start Force Data Acquisition Program (Labview)
- Name File: SampleID_Side_0%
- Load Sample (10um/sec) to a Voltage = 0.230 Volts (100N)

0% Sequence (Time Required: 1.5 hrs)

- Acquire/Save 0% Equilibrium Images for ALL REGIONS
- Record z-axis for each Region's Image
- Last Image taken should be over Region #6
- Using Image Pro Plus and IX70-4X spatial calibration, measure WHOLE cartilage thickness (tidemark – tidemark) for ALL regions (2 measurements/image)
- Average the 12 thickness measurements, Record on Worksheet
- Using Excel Spreadsheet (STRAIN.XLS), calculate micrometer position for offset compression levels, Record on Worksheet

20% Sequence (Time Required: 4.5hrs)

- Last Image taken should be over Region #6
- Load Sample (10um/sec) to Mean 20% Calculated Offset Level
- Allow sample to relax for 3hrs
- Turn ON UV Source, Allow to warmup for 15minutes
- Acquire/Save 2% Equilibrium Images for ALL REGIONS
- Record z-axis for each Region's Image

Post Test Procedures

- Turn OFF UV Light Power
- Turn Off Camera
- Unload Sample
- Safely Remove Sample
- Clean Testing System with GAUZE and PBS

Reproduced with permission of the copyright owner. Further reproduction prohibited without permission.

- Prepare for System for NEXT TEST
- Record All Data/Images on to CDROM IMMEDIATELY!
- VIC2D Strain Analysis
- Copy Directory Structure with Images to Computer
- Create Analysis Directory Structure
- VIC2D Parameters
- Subset=45
- Step = 5
- Guess = Use 4 Points with Complete Guess
- Quintic Spline Interpolation
- Binomial Pre Filter
- Strain Window Size (45/5) = 9
- Check Principals Box
- Output Directory (.dat files) for each offset in Analysis Dir
- Equilibrium
- For Each Region
- Analyze all equilibrium images at all offsets
- Check for Acceptable Correlation
- Export All Data Files (TecPlot Format)
- Note Any Concerns

Reproduced with permission of the copyright owner. Further reproduction prohibited without permission.

10.3 Blank sample testing sheet

Sample ID: **Left Right** **Date:**_____

Gross Anatomical Notes:

Digital Images: 1 2 3 4 5 6 **Exakt Speed**_____

Test Sample Measurement

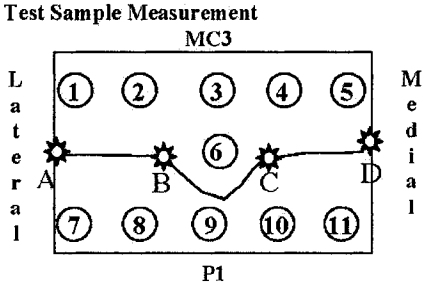

1-_____mm 7-_____
2-_____ 8-_____
3-_____ 9-_____
4-_____ 10-_____
5-_____ 11-_____
6-_____
Height_____mm

Histology Label:_____

Add 1.6ml of Propidium to 40ml PBS+PIs (0.04mg/ml) **Vial Label:**_____

Translation Stage Coordinates (um)
A-_____ B-_____ C-_____ D-_____

Cartilage Thickness _____**mm**

	Micro Position												
Coordinates	z-axis					Preload		0%	2%		4%		8%	
Image	P	0	2	4	8	SR	Eq	Eq	SR	Eq	SR	Eq	SR	Eq
0-						☐	☐	☐	☐	☐	☐	☐	☐	☐
1-							☐	☐		☐		☐		☐
2-							☐	☐		☐		☐		☐
3-							☐	☐		☐		☐		☐
4-							☐	☐		☐		☐		☐
5-							☐	☐		☐		☐		☐
6-							☐	☐		☐		☐		☐

NOTES:

Reproduced with permission of the copyright owner. Further reproduction prohibited without permission.

10.4 Matlab m-files

10.4.1 main.m

```
% Clear All Variables
clear;

%Ask user location and name to save statistics data
[fpath] = uigetdir('Select Directory Where Datafiles Are Located');

%Ask user location and name to save statistics data
[newpath2] = uigetdir('Select Directory for Matrix Datafiles');

files=dir(fpath)
R=size(files);
n=R(1)-2;
count=0;

for i=1:n
   % Ask User to Select *.out file
   fname=files(i+2).name;
   filespec = fullfile(fpath,fname);

   %Read Data
   A= csvread(filespec);
   figure(1);
   imagesc(A)
   axis image
   colorbar

   if i==1
   button = questdlg('Is the image for MC3 or P1?','MC3','P1','MC3');
   if strcmp(button,'MC3')
      [S, M, D, Sstd, Mstd, Dstd, width, P, Sgy, Mgy, Dgy, Sstdgy, Mstdgy,
Dstdgy]=analyzeMC3(A);
      temp = ['MC3' fname S M D Sstd Mstd Dstd Sgy Mgy Dgy Sstdgy Mstdgy Dstdgy
width];
      j = length(temp);
      data(i,j) = cellstr(temp);
      matrix = P;
      newfilespec2 = fullfile(newpath2, fname);
      csvwrite(newfilespec2,matrix);

   elseif strcmp(button,'P1')
      [S, M, D, Sstd, Mstd, Dstd, width, P, Sgy, Mgy, Dgy, Sstdgy, Mstdgy,
Dstdgy]=analyzeP1(A);
```


Reproduced with permission of the copyright owner. Further reproduction prohibited without permission.

```
      temp = ['P1' fname S M D Sstd Mstd Dstd Sgy Mgy Dgy Sstdgy Mstdgy Dstdgy
width];
      j = length(temp);
      data(i,j) = cellstr(temp)
      matrix = P;
      newfilespec2 = fullfile(newpath2, fname);
      csvwrite(newfilespec2,matrix);
   end

   elseif i > 1

   button = questdlg('Is the image for MC3 or P1?','MC3','P1','MC3');
   if strcmp(button,'MC3')
      [S, M, D, Sstd, Mstd, Dstd, width, P, Sgy, Mgy, Dgy, Sstdgy, Mstdgy,
Dstdgy]=analyzeMC3(A);
      temp = [fname S M D Sstd Mstd Dstd Sgy Mgy Dgy Sstdgy Mstdgy Dstdgy width];
      j = length(temp);
      data(i,j) = cellstr(temp)
      matrix = P;
      csvwrite(newfilespec,data,i,0);
      csvwrite(newfilespec2,matrix);

   elseif strcmp(button,'P1')
      [S, M, D, Sstd, Mstd, Dstd, width, P, Sgy, Mgy, Dgy, Sstdgy, Mstdgy,
Dstdgy]=analyzeP1(A);
      temp = [fname S M D Sstd Mstd Dstd Sgy Mgy Dgy Sstdgy Mstdgy Dstdgy width];
      j = length(temp);
      data(i,j) = cellstr(temp)
      matrix = P;
      newfilespec2 = fullfile(newpath2, fname);
      csvwrite(newfilespec2,matrix);
   end
end
end

%Ask user location and name to save statistics data
[name, fpath] = uiputfile('*.txt','Save Statistics File As');
newfilespec = fullfile(fpath,name);
csvwrite(newfilespec,data);
```


Reproduced with permission of the copyright owner. Further reproduction prohibited without permission.

10.4.2 analyze.m

```
function [S, M, D, Sstd, Mstd, Dstd, width, P, Sgy, Mgy, Dgy, Sstdgy, Mstdgy,
Dstdgy]=analyze(A)

A = shrink(A);

figure(1)
imagesc(A);

%Determine group element locations
for k = 1:length(A(1,:))
   group(k,:) = groupfind(A(:,k));
end

dif = group(:,2) - group(:,1);
grad2=gradient(gradient(dif));
tempdiff2= diff(grad2,2);
temp=find(tempdiff2 >= max(tempdiff2)/1.2);

d1 = group(1,1) - group(temp(end),1);
d2 = group(1,2) - group(temp(end),2);

if abs(d1) < abs(d2)
   dd1 = abs(d1);
elseif abs(d1) > abs(d2)
   dd1 = abs(d2);
elseif abs(d1) == abs(d2)
   dd1 = abs(d2);
end

if dd1 <4
   J=A;
   num = round((size(J,2))/3);
   J(:,1:num)=[];
   J(:,end-num:end)=[];
end

if dd1 >= 4

   %Determine Angle MAGNITUDE for which to rotate A
   %First determine boundaries where both the parallel lines match up (image
top/bottom)

   if length(temp) <= 2
      [S,IS] = sortrows(grad2);
```


Reproduced with permission of the copyright owner. Further reproduction prohibited without permission.

```
    s1 = IS(1);
    s2 = IS(end);
  end

  if length(temp) > 2
    [S,IS] = sortrows(grad2);
    s1 = IS(1);
    s2 = IS(2);
  end

  %Calcualte Angle(degrees)
  opposite = group(s1,2) - group(s2,2);
  adjacent = s2 - s1;
  theta = atan2(opposite,adjacent);
  degrees = theta*180/pi;
  angle = -degrees;

  %Rotate Image
  J = imrotate(A,angle,'bicubic','crop');

  % TRIM Image:  Trim the partial thickness data off the edges :) using the
  % indicies found for the common boundaries
  %First determine the boundaries
  num = round((size(J,2))/3);
  J(:,1:num)=[];
  J(:,end-num:end)=[];
end

%Trim TOP/BOTTOM to clean borders
J(1:5,:)=[];
J(end-2:end,:)=[];

% figure (3);
% imagesc(J);

%Interpolate data points to 100 (bicubic)
P = imresize(J,[100,size(J,2)]);

figure (4);
imagesc(P);

%Output Statistics
S= mean2(P(1:30,:));
M= mean2(P(31:70));
D= mean2(P(71:100,:));
width = size(P,2);
```


Reproduced with permission of the copyright owner. Further reproduction prohibited without permission.

```
Sstd = std2(P(1:30,:));
Mstd = std2(P(31:70,:));
Dstd = std2(P(71:100,:));

[gradx, grady] = gradient(P);
Sgx= mean2(gradx(1:30,:));
Mgx= mean2(gradx(31:70));
Dgx= mean2(gradx(71:100,:));
Sstdgx = std2(gradx(1:30,:));
Mstdgx = std2(gradx(31:70,:));
Dstdgx = std2(gradx(71:100,:));
Sgy= mean2(grady(1:30,:));
Mgy= mean2(grady(31:70));
Dgy= mean2(grady(71:100,:));
Sstdgy = std2(grady(1:30,:));
Mstdgy = std2(grady(31:70,:));
Dstdgy = std2(grady(71:100,:));
```


Reproduced with permission of the copyright owner. Further reproduction prohibited without permission.

10.5 Positive correlation results

		1	2	3	4	5	6	TOTAL
Region 1	MC3	+			+	+		n=3
	P1		+	+	+	+		4
Region 2	MC3	+	+		+			3
	P1		+			+		2
Region 3	MC3	+	+	+	+	+		5
	P1		+		+	+		3
Region 4	MC3	+	+		+	+		3
	P1	+	+		+	+	+	5
Region 5	MC3				+	+	+	3
	P1			+	+	+	+	4
Region 6	MC3	+				+	+	3
	P1	+		+		+	+	4
Region 7	MC3			+			+	2
	P1	+	+	+		+	+	5

Table 10.2: Positive image correlation results (+) for each sample (top, 1-6) and the total number of samples used for each region (R1-R7) of each bone (MC3 and P1).

Reproduced with permission of the copyright owner. Further reproduction prohibited without permission.

10.6 Raw Data

ID	Horse	Side	Bone	Region	Zone	Pmax Mean	Pmax STD	Pmax Gradient Mean	Pmax Gradient STD
2L	2	L	MC3	1	S	-0.0706	0.0260	0.0024	0.0016
2L	2	L	MC3	1	M	-0.0213	0.0027	0.0002	0.0003
2L	2	L	MC3	1	D	-0.0098	0.0089	0.0005	0.0019
2L	2	L	MC3	2	S	-0.2162	0.0337	0.0036	0.0017
2L	2	L	MC3	2	M	-0.0752	0.0358	0.0032	0.0032
2L	2	L	MC3	2	D	-0.0248	0.0068	0.0008	0.0011
2L	2	L	MC3	3	S	-0.0255	0.0402	-0.0036	0.0096
2L	2	L	MC3	3	M	-0.0882	0.0145	0.0011	0.0032
2L	2	L	MC3	3	D	-0.0121	0.0256	0.0022	0.0074
2L	2	L	MC3	4	S	-0.2605	0.0322	0.0025	0.0031
2L	2	L	MC3	4	M	-0.1238	0.0621	0.0042	0.0027
2L	2	L	MC3	4	D	-0.0245	0.0112	-0.0003	0.0021
2L	2	L	MC3	5	S	-0.2091	0.0531	0.0056	0.0029
2L	2	L	MC3	5	M	-0.0823	0.0229	0.0010	0.0029
2L	2	L	MC3	5	D	-0.0853	0.0165	0.0007	0.0031
2L	2	L	P1	1	S	-0.0312	0.0081	0.0008	0.0029
2L	2	L	P1	1	M	-0.0381	0.0036	0.0001	0.0007
2L	2	L	P1	1	D	-0.0197	0.0045	0.0006	0.0011
2L	2	L	P1	3	S	-0.2548	0.0495	0.0024	0.0051
2L	2	L	P1	3	M	-0.0914	0.0695	0.0054	0.0067
2L	2	L	P1	3	D	-0.0076	0.0033	0.0004	0.0006
2L	2	L	P1	4	S	-0.0808	0.0548	0.0036	0.0086
2L	2	L	P1	4	M	-0.0155	0.0052	0.0003	0.0005
2L	2	L	P1	4	D	-0.0096	0.0010	0.0001	0.0003
2L	2	L	P1	5	S	-0.1055	0.0591	0.0054	0.0042
2L	2	L	P1	5	M	-0.0374	0.0067	-0.0003	0.0008
2L	2	L	P1	5	D	-0.0346	0.0019	0.0003	0.0005
2R	2	R	MC3	3	S	-0.2527	0.0290	0.0034	0.0017
2R	2	R	MC3	3	M	-0.1211	0.0383	0.0030	0.0022
2R	2	R	MC3	3	D	-0.0623	0.0084	0.0006	0.0011
2R	2	R	MC3	7	S	-0.2742	0.0433	0.0011	0.0020
2R	2	R	MC3	7	M	-0.2016	0.0495	0.0049	0.0026
2R	2	R	MC3	7	D	-0.0608	0.0232	0.0022	0.0041
2R	2	R	P1	1	S	-0.2276	0.0478	0.0038	0.0110
2R	2	R	P1	1	M	-0.1566	0.0121	0.0006	0.0028
2R	2	R	P1	1	D	-0.1223	0.0209	0.0013	0.0040
2R	2	R	P1	5	S	-0.1585	0.0449	0.0041	0.0051
2R	2	R	P1	5	M	-0.0837	0.0256	0.0019	0.0014
2R	2	R	P1	5	D	-0.0130	0.0068	0.0008	0.0008
2R	2	R	P1	6	S	-0.1682	0.0666	0.0053	0.0078
2R	2	R	P1	6	M	-0.0340	0.0189	0.0015	0.0027

Reproduced with permission of the copyright owner. Further reproduction prohibited without permission.

ID	Horse	Side	Bone	Region	Zone	Pmin Mean	Pmin STD	Pmin Gradient Mean	Pmin Gradient STD	T-T strain
2L	2	L	MC3	1	S	0.0082	0.0024	-0.0001	0.0003	-0.096
2L	2	L	MC3	1	M	0.0067	0.0016	-0.0001	0.0001	-0.096
2L	2	L	MC3	1	D	0.0018	0.0017	-0.0001	0.0003	-0.096
2L	2	L	MC3	2	S	0.0061	0.0075	0.0006	0.0006	-0.083
2L	2	L	MC3	2	M	0.0150	0.0048	0.0002	0.0008	-0.083
2L	2	L	MC3	2	D	0.0028	0.0033	-0.0003	0.0003	-0.083
2L	2	L	MC3	3	S	-0.0001	0.0023	0.0000	0.0003	-0.096
2L	2	L	MC3	3	M	-0.0043	0.0143	0.0000	0.0019	-0.096
2L	2	L	MC3	3	D	-0.0055	0.0040	-0.0001	0.0007	-0.096
2L	2	L	MC3	4	S	-0.0078	0.0152	0.0010	0.0014	-0.118
2L	2	L	MC3	4	M	0.0101	0.0041	0.0000	0.0006	-0.118
2L	2	L	MC3	4	D	0.0002	0.0026	-0.0001	0.0004	-0.118
2L	2	L	MC3	5	S	0.0252	0.0069	0.0007	0.0008	-0.149
2L	2	L	MC3	5	M	0.0221	0.0089	-0.0005	0.0005	-0.149
2L	2	L	MC3	5	D	0.0036	0.0026	-0.0002	0.0003	-0.149
2L	2	L	P1	1	S	-0.0005	0.0112	0.0011	0.0011	-0.124
2L	2	L	P1	1	M	0.0214	0.0025	0.0002	0.0006	-0.124
2L	2	L	P1	1	D	0.0090	0.0046	-0.0005	0.0003	-0.124
2L	2	L	P1	3	S	0.0029	0.0032	0.0002	0.0008	-0.1448
2L	2	L	P1	3	M	0.0022	0.0415	-0.0009	0.0067	-0.1448
2L	2	L	P1	3	D	0.3078	0.3937	0.0163	0.0233	-0.1448
2L	2	L	P1	4	S	-0.0049	0.0127	0.0006	0.0033	-0.1438
2L	2	L	P1	4	M	0.0031	0.0021	0.0001	0.0004	-0.1438
2L	2	L	P1	4	D	0.0073	0.0013	0.0000	0.0005	-0.1438
2L	2	L	P1	5	S	0.0118	0.0045	0.0004	0.0009	-0.1442
2L	2	L	P1	5	M	0.0214	0.0037	0.0002	0.0004	-0.1442
2L	2	L	P1	5	D	0.0119	0.0059	-0.0007	0.0005	-0.1442
2R	2	R	MC3	3	S	0.0137	0.0034	0.0002	0.0006	-0.119
2R	2	R	MC3	3	M	0.0073	0.0059	-0.0005	0.0007	-0.119
2R	2	R	MC3	3	D	-0.0032	0.0018	0.0002	0.0003	-0.119
2R	2	R	MC3	7	S	0.0832	0.1458	-0.0021	0.0064	-0.165
2R	2	R	MC3	7	M	0.0501	0.0360	-0.0027	0.0025	-0.165
2R	2	R	MC3	7	D	0.0078	0.0149	-0.0001	0.0014	-0.165
2R	2	R	P1	1	S	0.0068	0.0093	0.0011	0.0018	-0.124
2R	2	R	P1	1	M	0.0616	0.0095	0.0002	0.0022	-0.124
2R	2	R	P1	1	D	0.0153	0.0127	-0.0016	0.0020	-0.124
2R	2	R	P1	5	S	0.0163	0.0085	0.0009	0.0015	-0.145
2R	2	R	P1	5	M	0.0439	0.0112	-0.0004	0.0016	-0.145
2R	2	R	P1	5	D	0.0074	0.0048	-0.0006	0.0006	-0.145
2R	2	R	P1	6	S	0.0963	0.1140	-0.0042	0.0187	-0.162
2R	2	R	P1	6	M	0.0188	0.0144	-0.0014	0.0023	-0.162

Reproduced with permission of the copyright owner. Further reproduction prohibited without permission.

ID	Horse	Side	Bone	Region	Zone	Pmax Mean	Pmax STD	Pmax Gradient Mean	Pmax Gradient STD
2R	2	R	P1	6	D	-0.0096	0.0038	0.0001	0.0010
2R	2	R	P1	7	S	-0.2721	0.0583	0.0057	0.0048
2R	2	R	P1	7	M	-0.1460	0.0515	0.0045	0.0040
2R	2	R	P1	7	D	-0.0272	0.0156	0.0014	0.0011
3L	3	L	MC3	1	S	-0.1836	0.0167	0.0000	0.0030
3L	3	L	MC3	1	M	-0.1494	0.0616	-0.0014	0.0094
3L	3	L	MC3	1	D	-0.1514	0.1079	-0.0010	0.0013
3L	3	L	MC3	3	S	-0.1902	0.0465	0.0050	0.0035
3L	3	L	MC3	3	M	-0.0956	0.0259	0.0006	0.0045
3L	3	L	MC3	3	D	-0.0815	0.0148	-0.0002	0.0032
3L	3	L	MC3	4	S	-0.0018	0.0005	0.0000	0.0001
3L	3	L	MC3	4	M	-0.0010	0.0006	0.0000	0.0001
3L	3	L	MC3	4	D	0.0003	0.0016	0.0000	0.0002
3L	3	L	MC3	7	S	-0.0818	0.0125	-0.0013	0.0007
3L	3	L	MC3	7	M	-0.1014	0.0037	0.0004	0.0015
3L	3	L	MC3	7	D	-0.1023	0.0241	0.0008	0.0058
3L	3	L	P1	2	S	-0.1981	0.1225	0.0126	0.0067
3L	3	L	P1	2	M	-0.0440	0.0088	-0.0004	0.0014
3L	3	L	P1	2	D	-0.0344	0.0102	0.0001	0.0025
3L	3	L	P1	3	S	-0.2101	0.1122	0.0130	0.0097
3L	3	L	P1	3	M	-0.0288	0.0157	0.0014	0.0011
3L	3	L	P1	3	D	-0.0041	0.0023	-0.0001	0.0006
3L	3	L	P1	4	S	-0.0051	0.0005	0.0000	0.0001
3L	3	L	P1	4	M	-0.0040	0.0009	0.0001	0.0001
3L	3	L	P1	4	D	-0.0011	0.0009	-0.0001	0.0003
3L	3	L	P1	7	S	-0.1863	0.0244	0.0017	0.0027
3L	3	L	P1	7	M	-0.1661	0.0342	0.0018	0.0029
3L	3	L	P1	7	M	-0.1436	0.0448	-0.0026	0.0057
3R	3	R	MC3	1	S	-0.0449	0.0106	0.0006	0.0033
3R	3	R	MC3	1	M	-0.0732	0.0107	-0.0005	0.0023
3R	3	R	MC3	1	D	-0.0515	0.0118	0.0007	0.0036
3R	3	R	MC3	2	S	-0.0211	0.0096	0.0011	0.0021
3R	3	R	MC3	2	M	-0.0138	0.0038	-0.0001	0.0010
3R	3	R	MC3	2	D	-0.0604	0.0142	-0.0017	0.0020
3R	3	R	MC3	3	S	-0.0287	0.0419	0.0042	0.0075
3R	3	R	MC3	3	M	-0.0144	0.0037	-0.0002	0.0004
3R	3	R	MC3	3	D	-0.0225	0.0052	-0.0003	0.0007
3R	3	R	MC3	4	S	-0.0018	0.0012	-0.0001	0.0003
3R	3	R	MC3	4	M	-0.0015	0.0007	0.0000	0.0002
3R	3	R	MC3	4	D	-0.0014	0.0007	0.0000	0.0001
3R	3	R	MC3	6	S	-0.0948	0.0363	0.0038	0.0023

Reproduced with permission of the copyright owner. Further reproduction prohibited without permission.

ID	Horse	Side	Bone	Region	Zone	Pmin Mean	Pmin STD	Pmin Gradient Mean	Pmin Gradient STD	T-T strain
2R	2	R	P1	6	D	0.0028	0.0029	-0.0003	0.0006	-0.162
2R	2	R	P1	7	S	0.1863	0.1660	-0.0044	0.0133	-0.119
2R	2	R	P1	7	M	0.0525	0.0364	-0.0003	0.0061	-0.119
2R	2	R	P1	7	D	0.0145	0.0084	-0.0008	0.0007	-0.119
3L	3	L	MC3	1	S	0.0418	0.0208	0.0019	0.0010	-0.083
3L	3	L	MC3	1	M	0.0463	0.0460	-0.0008	0.0092	-0.083
3L	3	L	MC3	1	D	0.0070	0.0063	-0.0003	0.0004	-0.083
3L	3	L	MC3	3	S	0.0134	0.0022	0.0000	0.0004	-0.134
3L	3	L	MC3	3	M	0.0204	0.0050	0.0004	0.0009	-0.134
3L	3	L	MC3	3	D	0.0195	0.0096	-0.0007	0.0011	-0.134
3L	3	L	MC3	4	S	-0.0002	0.0007	0.0001	0.0001	-0.131
3L	3	L	MC3	4	M	0.0020	0.0011	0.0000	0.0001	-0.131
3L	3	L	MC3	4	D	0.0038	0.0016	0.0001	0.0002	-0.131
3L	3	L	MC3	7	S	0.0154	0.0094	0.0010	0.0005	-0.125
3L	3	L	MC3	7	M	0.0332	0.0080	-0.0003	0.0014	-0.125
3L	3	L	MC3	7	D	0.0084	0.0074	-0.0006	0.0008	-0.125
3L	3	L	P1	2	S	0.0179	0.0239	-0.0026	0.0050	-0.134
3L	3	L	P1	2	M	0.0122	0.0052	0.0002	0.0008	-0.134
3L	3	L	P1	2	D	0.0080	0.0050	-0.0004	0.0006	-0.134
3L	3	L	P1	3	S	0.0051	0.0139	-0.0018	0.0060	-0.113
3L	3	L	P1	3	M	0.0025	0.0030	0.0002	0.0004	-0.113
3L	3	L	P1	3	D	0.0008	0.0009	-0.0001	0.0001	-0.113
3L	3	L	P1	4	S	0.0005	0.0004	0.0000	0.0001	-0.144
3L	3	L	P1	4	M	-0.0004	0.0006	0.0000	0.0001	-0.144
3L	3	L	P1	4	D	0.0006	0.0006	0.0000	0.0002	-0.144
3L	3	L	P1	7	S	0.3417	0.1288	0.0041	0.0024	-0.119
3L	3	L	P1	7	M	0.4455	0.1450	-0.0079	0.0053	-0.119
3L	3	L	P1	7	M	0.0265	0.0584	-0.0050	0.0080	-0.119
3R	3	R	MC3	1	S	0.0090	0.0047	0.0006	0.0005	-0.083
3R	3	R	MC3	1	M	0.0336	0.0086	0.0003	0.0013	-0.083
3R	3	R	MC3	1	D	0.0142	0.0089	-0.0007	0.0009	-0.083
3R	3	R	MC3	2	S	0.0071	0.0035	0.0004	0.0004	-0.096
3R	3	R	MC3	2	M	0.0107	0.0024	-0.0001	0.0004	-0.096
3R	3	R	MC3	2	D	0.0106	0.0068	0.0004	0.0008	-0.096
3R	3	R	MC3	3	S	0.0096	0.0124	-0.0009	0.0022	-0.143
3R	3	R	MC3	3	M	0.0104	0.0019	0.0000	0.0003	-0.143
3R	3	R	MC3	3	D	0.0054	0.0028	-0.0002	0.0003	-0.143
3R	3	R	MC3	4	S	0.0013	0.0020	-0.0001	0.0003	-0.131
3R	3	R	MC3	4	M	0.0005	0.0007	0.0000	0.0002	-0.131
3R	3	R	MC3	4	D	0.0006	0.0009	0.0000	0.0003	-0.131
3R	3	R	MC3	6	S	0.0000	0.0069	-0.0007	0.0007	-0.183

Reproduced with permission of the copyright owner. Further reproduction prohibited without permission.

ID	Horse	Side	Bone	Region	Zone	Pmax Mean	Pmax STD	Pmax Gradient Mean	Pmax Gradient STD
3R	3	R	MC3	4	D	-0.0014	0.0007	0.0000	0.0001
3R	3	R	MC3	6	S	-0.0948	0.0363	0.0038	0.0023
3R	3	R	MC3	6	M	-0.0230	0.0052	0.0006	0.0017
3R	3	R	MC3	6	D	-0.0227	0.0100	-0.0001	0.0017
3R	3	R	P1	4	S	-0.0010	0.0015	0.0001	0.0004
3R	3	R	P1	4	M	-0.0014	0.0014	0.0000	0.0005
3R	3	R	P1	4	D	-0.0013	0.0009	-0.0001	0.0004
3R	3	R	P1	6	S	-0.1187	0.0685	0.0078	0.0045
3R	3	R	P1	6	M	-0.0233	0.0038	0.0002	0.0010
3R	3	R	P1	6	D	-0.0298	0.0090	-0.0005	0.0015
3R	3	R	P1	7	S	-0.1181	0.0226	0.0026	0.0017
3R	3	R	P1	7	M	-0.0579	0.0196	0.0017	0.0007
3R	3	R	P1	7	D	-0.0314	0.0071	-0.0004	0.0012
5R	5	R	MC3	3	S	-0.0142	0.0248	-0.0008	0.0085
5R	5	R	MC3	3	M	-0.0120	0.0214	-0.0019	0.0083
5R	5	R	MC3	3	D	-0.0164	0.0337	0.0023	0.0114
5R	5	R	MC3	4	S	-0.1490	0.0711	0.0078	0.0041
5R	5	R	MC3	4	M	-0.0419	0.0058	0.0004	0.0012
5R	5	R	MC3	4	D	-0.0440	0.0110	-0.0006	0.0017
5R	5	R	MC3	5	S	-0.0260	0.0297	0.0036	0.0048
5R	5	R	MC3	5	M	-0.0072	0.0020	-0.0002	0.0003
5R	5	R	MC3	5	D	-0.0331	0.0174	-0.0013	0.0018
5R	5	R	MC3	6	S	-0.1115	0.0346	0.0042	0.0023
5R	5	R	MC3	6	M	-0.0257	0.0134	0.0015	0.0021
5R	5	R	MC3	6	D	-0.0644	0.0468	-0.0020	0.0081
5R	5	R	P1	2	S	-0.0826	0.0359	0.0044	0.0041
5R	5	R	P1	2	M	-0.0537	0.0061	0.0000	0.0017
5R	5	R	P1	2	D	-0.0575	0.0137	-0.0004	0.0031
5R	5	R	P1	3	S	-0.0693	0.0461	0.0051	0.0042
5R	5	R	P1	3	M	-0.0281	0.0047	0.0000	0.0012
5R	5	R	P1	3	D	-0.0338	0.0090	-0.0003	0.0019
5R	5	R	P1	5	S	-0.1151	0.0700	0.0066	0.0041
5R	5	R	P1	5	M	-0.0319	0.0105	-0.0009	0.0024
5R	5	R	P1	5	D	-0.0673	0.0136	-0.0010	0.0018
5R	5	R	P1	6	S	-0.1325	0.0511	0.0059	0.0032
5R	5	R	P1	6	M	-0.0324	0.0192	0.0011	0.0024
5R	5	R	P1	6	D	-0.0531	0.0262	-0.0020	0.0032
5R	5	R	P1	7	S	-0.1313	0.0277	0.0031	0.0023
5R	5	R	P1	7	M	-0.0803	0.0068	0.0003	0.0012
5R	5	R	P1	7	D	-0.0771	0.0070	0.0006	0.0011
7L	7	L	MC3	5	S	-0.2291	0.0471	0.0048	0.0025
7L	7	L	MC3	5	M	-0.0945	0.0247	0.0023	0.0032
7L	7	L	MC3	5	D	-0.0593	0.0137	0.0015	0.0022
7L	7	L	MC3	7	S	-0.1644	0.0807	0.0005	0.0145
7L	7	L	MC3	7	M	-0.1325	0.0192	0.0011	0.0015
7L	7	L	MC3	7	D	-0.0698	0.0444	0.0031	0.0084
7L	7	L	P1	4	S	-0.0439	0.0201	0.0016	0.0025
7L	7	L	P1	4	M	-0.0126	0.0047	0.0005	0.0011
7L	7	L	P1	4	D	-0.0172	0.0054	-0.0011	0.0024
7L	7	L	P1	5	S	-0.0287	0.0351	0.0033	0.0037
7L	7	L	P1	5	M	-0.0082	0.0064	-0.0004	0.0010
7L	7	L	P1	5	D	-0.0204	0.0131	-0.0009	0.0018
7L	7	L	P1	6	S	-0.0339	0.0391	0.0044	0.0047
7L	7	L	P1	6	M	-0.0023	0.0014	-0.0001	0.0003
7L	7	L	P1	6	D	-0.0069	0.0013	-0.0001	0.0003
7L	7	L	P1	7	S	-0.0172	0.0244	-0.0016	0.0051
7L	7	L	P1	7	M	-0.0518	0.0211	0.0016	0.0058
7L	7	L	P1	7	D	-0.0158	0.0307	0.0019	0.0063

Reproduced with permission of the copyright owner. Further reproduction prohibited without permission.

ID	Horse	Side	Bone	Region	Zone	Pmin Mean	Pmin STD	Pmin Gradient Mean	Pmin Gradient STD	T-T strain
3R	3	R	MC3	4	D	0.0006	0.0009	0.0000	0.0003	-0.131
3R	3	R	MC3	6	S	0.0000	0.0069	-0.0007	0.0007	-0.183
3R	3	R	MC3	6	M	0.0117	0.0130	0.0007	0.0012	-0.183
3R	3	R	MC3	6	D	0.0138	0.0041	-0.0005	0.0003	-0.183
3R	3	R	P1	4	S	0.0015	0.0012	0.0000	0.0005	-0.1941
3R	3	R	P1	4	M	0.0010	0.0015	0.0000	0.0005	-0.1941
3R	3	R	P1	4	D	0.0007	0.0011	-0.0001	0.0004	-0.1941
3R	3	R	P1	6	S	0.0041	0.0027	0.0000	0.0005	-0.165
3R	3	R	P1	6	M	0.0110	0.0045	0.0002	0.0006	-0.165
3R	3	R	P1	6	D	0.0062	0.0046	-0.0004	0.0006	-0.165
3R	3	R	P1	7	S	.	.	.	.	-0.140
3R	3	R	P1	7	M	.	.	.	.	-0.140
3R	3	R	P1	7	D	.	.	.	.	-0.140
5R	5	R	MC3	3	S	0.0041	0.0071	0.0003	0.0024	-0.143
5R	5	R	MC3	3	M	0.0033	0.0090	0.0004	0.0039	-0.143
5R	5	R	MC3	3	D	0.0104	0.0242	-0.0008	0.0094	-0.143
5R	5	R	MC3	4	S	-0.0036	0.0020	0.0001	0.0002	-0.149
5R	5	R	MC3	4	M	-0.0055	0.0027	0.0000	0.0003	-0.149
5R	5	R	MC3	4	D	-0.0011	0.0017	0.0000	0.0002	-0.149
5R	5	R	MC3	5	S	-0.0044	0.0015	0.0001	0.0003	-0.150
5R	5	R	MC3	5	M	0.0036	0.0037	0.0002	0.0003	-0.150
5R	5	R	MC3	5	D	0.0069	0.0022	-0.0002	0.0003	-0.150
5R	5	R	MC3	6	S	0.0036	0.0036	-0.0004	0.0003	-0.183
5R	5	R	MC3	6	M	0.0042	0.0044	0.0005	0.0012	-0.183
5R	5	R	MC3	6	D	0.0040	0.0099	-0.0007	0.0024	-0.183
5R	5	R	P1	2	S	0.0038	0.0026	0.0002	0.0003	-0.145
5R	5	R	P1	2	M	0.0241	0.0074	0.0005	0.0008	-0.145
5R	5	R	P1	2	D	0.0162	0.0097	-0.0009	0.0009	-0.145
5R	5	R	P1	3	S	0.0032	0.0011	0.0001	0.0002	-0.113
5R	5	R	P1	3	M	0.0124	0.0045	0.0003	0.0005	-0.113
5R	5	R	P1	3	D	0.0124	0.0034	-0.0003	0.0005	-0.113
5R	5	R	P1	5	S	-0.0049	0.0026	0.0002	0.0004	-0.154
5R	5	R	P1	5	M	0.0120	0.0060	0.0000	0.0010	-0.154
5R	5	R	P1	5	D	0.0026	0.0027	0.0000	0.0003	-0.154
5R	5	R	P1	6	S	0.0249	0.0029	0.0003	0.0005	-0.146
5R	5	R	P1	6	M	0.0227	0.0070	-0.0005	0.0010	-0.146
5R	5	R	P1	6	D	0.0067	0.0059	-0.0005	0.0008	-0.146
5R	5	R	P1	7	S	-0.0044	0.0022	0.0000	0.0005	-0.140
5R	5	R	P1	7	M	0.0278	0.0180	0.0013	0.0008	-0.140
5R	5	R	P1	7	D	0.0473	0.0094	-0.0006	0.0012	-0.140
7L	7	L	MC3	5	S	0.0070	0.0061	-0.0003	0.0008	-0.116
7L	7	L	MC3	5	M	-0.0023	0.0024	-0.0001	0.0004	-0.116
7L	7	L	MC3	5	D	0.0008	0.0014	0.0000	0.0003	-0.116
7L	7	L	MC3	7	S	0.0156	0.0160	0.0015	0.0020	-0.125
7L	7	L	MC3	7	M	0.0486	0.0041	0.0002	0.0006	-0.125
7L	7	L	MC3	7	D	0.0238	0.0156	-0.0011	0.0028	-0.125
7L	7	L	P1	4	S	-0.0020	0.0017	0.0000	0.0004	-0.188
7L	7	L	P1	4	M	-0.0020	0.0030	0.0001	0.0004	-0.188
7L	7	L	P1	4	D	0.0089	0.0117	-0.0008	0.0043	-0.188
7L	7	L	P1	5	S	0.0063	0.0032	-0.0002	0.0008	-0.154
7L	7	L	P1	5	M	0.0076	0.0021	0.0000	0.0005	-0.154
7L	7	L	P1	5	D	0.0009	0.0020	-0.0001	0.0004	-0.154
7L	7	L	P1	6	S	0.0058	0.0054	0.0004	0.0008	-0.146
7L	7	L	P1	6	M	0.0055	0.0027	-0.0002	0.0005	-0.146
7L	7	L	P1	6	D	0.0051	0.0023	-0.0001	0.0004	-0.146
7L	7	L	P1	7	S	0.0004	0.0020	0.0002	0.0006	-0.079
7L	7	L	P1	7	M	0.0134	0.0154	-0.0001	0.0027	-0.079
7L	7	L	P1	7	D	0.0071	0.0139	-0.0008	0.0028	-0.079

Reproduced with permission of the copyright owner. Further reproduction prohibited without permission.

10.7 Statistical Comparisons

ScBP Thickness Comparisons

Region Comparison	R1	R2	R3	R4	R5	R6	R7
R1		1.0000	**0.0136**	**0.0092**	**0.0045**	0.2442	0.4800
R2			**0.0008**	**0.0005**	**0.0002**	**0.0223**	0.4824
R3				0.9036	0.7833	0.2656	**0.0073**
R4					0.8319	0.2177	**0.0051**
R5						0.1491	**0.0027**
R6							0.1103
R7							

Table 10.3: ScBP thickness p-values for comparisons between regions.

ScBP Thickness Comparisons

Location Comparison	MC3 R1	MC3 R2	MC3 R3	MC3 R4	MC3 R5	MC3 R6	MC3 R7
MC3 R1		0.9391	**<0.0001**	0.2303	**<0.0001**	0.3153	1.0000
MC3 R2			**<0.0001**	0.9952	**0.0006**	0.9988	0.8345
MC3 R3				**0.0067**	1.0000	**0.0038**	**<0.0001**
MC3 R4					**0.0412**	1.0000	0.1254
MC3 R5						**0.0254**	**<.0001**
MC3 R6							0.1824
MC3 R7							
P1 R1							
P1 R2							
P1 R3							
P1 R4							
P1 R5							
P1 R6							
P1 R7							

ScBP Thickness Comparisons

P1 R1	P1 R2	P1 R3	P1 R4	P1 R5	P1 R6	P1 R7
0.6746	1.0000	1.0000	**0.0021**	0.9962	0.2606	0.0521
1.0000	0.9981	0.9704	0.2718	1.0000	0.9971	0.8788
0.0005	**<0.0001**	**<0.0001**	**0.0137**	**<0.0001**	**<0.0001**	**0.0008**
1.0000	0.5672	0.3078	0.9585	0.9306	1.0000	1.0000
0.0043	**<.0001**	**<.0001**	**0.7975**	**<.0001**	**0.0344**	0.1935
1.0000	0.6790	0.4068	0.9153	0.9676	1.0000	1.0000
0.4860	0.9999	1.0000	**0.0007**	0.9764	0.1452	**0.0234**
	0.9405	0.7692	0.6213	0.9995	1.0000	0.9921
		1.0000	**0.0139**	1.0000	0.6102	0.2020
			0.0036	0.9990	0.3438	0.0782
				0.0961	0.9446	0.9996
					0.9470	0.6072
						1.0000

Table 10.4: ScBP thickness p-values for comparisons between region and bone.

Reproduced with permission of the copyright owner. Further reproduction prohibited without permission.

BMD Comparisons

Location Comparison	MC3 R1	MC3 R2	MC3 R3	MC3 R4	MC3 R5	MC3 R6	MC3 R7
MC3 R1		1.0000	**0.0144**	0.5656	**<.0001**	0.9928	0.0787
MC3 R2			**0.0040**	0.3223	**<.0001**	0.9423	**0.0272**
MC3 R3				0.9691	0.6263	0.4026	1.0000
MC3 R4					**0.0191**	0.9990	0.9996
MC3 R5						**0.0003**	0.2608
MC3 R6							0.7816
MC3 R7							
P1 R1							
P1 R2							
P1 R3							
P1 R4							
P1 R5							
P1 R6							
P1 R7							

BMD Comparisons

P1 R1	P1 R2	P1 R3	P1 R4	P1 R5	P1 R6	P1 R7
1.0000	0.2958	0.0971	0.7805	1.0000	1.0000	**0.0593**
0.9998	0.5331	0.2286	0.5366	1.0000	0.9999	**0.0196**
0.0798	**<.0001**	**<.0001**	0.8758	**0.0202**	0.0657	1.0000
0.8980	**0.0001**	**<.0001**	1.0000	0.6378	0.8689	0.9989
<.0001	**<.0001**	**<.0001**	0.0063	**<.0001**	**<.0001**	0.3178
1.0000	**0.0079**	**0.0013**	1.0000	0.9967	1.0000	0.7183
0.2921	**<.0001**	**<.0001**	0.9929	0.1032	0.2541	1.0000
	0.0802	**0.0184**	0.9771	1.0000	1.0000	0.2380
		1.0000	**0.0004**	0.2414	0.0967	**<.0001**
			<.0001	0.0739	0.0231	**<.0001**
				0.8363	0.9664	0.9858
					1.0000	0.0787
						0.2049

Table 10.5: BMD p-values for comparisons between bone and region.

Reproduced with permission of the copyright owner. Further reproduction prohibited without permission.

BMD Comparisons

Region Comparison	R1	R2	R3	R4	R5	R6	R7
R1		0.1536	1.0000	0.1216	**0.0023**	0.9803	**0.0006**
R2			0.1369	**<.0001**	**<.0001**	**0.0151**	**<.0001**
R3				0.1369	**0.0028**	0.9857	0.0007
R4					0.8599	0.5568	0.6650
R5						**0.0380**	0.9999
R6							**0.0131**
R7							

Table 10.6: BMD p-values for comparisons between regions.

P_{MIN} Comparisons

Region Comparison	R1	R2	R3	R4	R5	R6	R7
R1		1.0000	0.9331	0.3163	0.9997	0.9817	0.8928
R2			0.9753	0.3644	1.0000	0.9908	0.8133
R3				0.6237	0.9946	1.0000	0.1009
R4					0.1589	0.7347	**0.0007**
R5						0.9898	0.4812
R6							0.2897
R7							

A

Layer Comparison	S	M	D
S		**0.0002**	**<.0001**
M			0.1882
D			

B

Table 10.7: P_{MIN} p-values for comparisons between (A) region and (B) layer.

P_{MAX} Comparisons

Region Comparison	R1	R2	R3	R4	R5	R6	R7
R1		0.9967	0.3001	**<.0001**	0.2744	0.3383	0.9870
R2			0.7190	**0.0004**	0.5894	0.5656	0.8135
R3				**0.0022**	0.9985	0.9834	**0.0139**
R4					**0.0052**	0.0625	**<.0001**
R5						0.9993	**0.0053**
R6							**0.0160**
R7							

A

Layer Comparison	S	M	D
S		**0.051**	**0.9163**
M			0.1283
D			

B

Table 10.8: P_{MAX} p-values for comparisons between (A) region and (B) layer.

Reproduced with permission of the copyright owner. Further reproduction prohibited without permission.

P_{SHEAR} Comparisons

Region Comparison	R1	R2	R3	R4	R5	R6	R7
R1		1.0000	0.9540	**0.0057**	0.9173	0.8317	0.8678
R2			0.9910	**0.0072**	0.9680	0.8866	0.7477
R3				**0.0041**	0.9997	0.9797	0.1212
R4					**0.0059**	0.1006	**<.0001**
R5						0.9962	0.0693
R6							0.0752
R7							

A

Layer Comparison	S	M	D
S		**0.0104**	**<.0001**
M			0.2075
D			

B

Table 10.9: P_{SHEAR} p-values for comparisons between (A) region and (B) layer.

∇P_{MIN} Comparisons

Location Comparison	D R1	M R1	S R1	D R2	M R2	S R2	D R3	M R3	S R3
D R1		0.6160	0.2855	1.0000	1.0000	**0.0183**	1.0000	1.0000	0.1639
M R1			0.9914	1.0000	1.0000	**0.0036**	1.0000	0.9974	**0.0377**
S R1				0.9989	1.0000	0.2755	1.0000	1.0000	0.8746
D R2					1.0000	**0.0105**	1.0000	0.9997	0.0924
M R2						0.0924	1.0000	1.0000	0.5048
S R2							**0.0170**	0.0765	0.9994
D R3								1.0000	0.1154
M R3									0.4245
S R3									
D R4									
M R4									
S R4									
D R5									
M R5									
S R5									
D R6									
M R6									
S R6									
D R7									
M R7									
S R7									

Reproduced with permission of the copyright owner. Further reproduction prohibited without permission.

∇P_{MIN} Comparisons

D R4	M R4	S R4	D R5	M R5	S R5	D R6	M R6	S R6	D R7	M R7	S R7
1.0000	1.0000	0.9995	1.0000	1.0000	0.1087	1.0000	1.0000	0.1865	1.0000	1.0000	1.0000
1.0000	1.0000	0.9725	1.0000	1.0000	**0.0259**	1.0000	1.0000	**0.0596**	0.9989	0.9904	0.9995
0.9918	1.0000	1.0000	0.9989	1.0000	0.7342	0.9739	1.0000	0.7993	1.0000	1.0000	1.0000
1.0000	1.0000	0.9912	1.0000	1.0000	**0.0553**	1.0000	1.0000	0.0906	0.9999	0.9983	1.0000
1.0000	1.0000	1.0000	1.0000	1.0000	0.3406	0.9998	1.0000	0.4112	1.0000	1.0000	1.0000
0.0019	**0.0256**	0.3231	**0.0053**	**0.0187**	1.0000	**0.0031**	0.1049	1.0000	0.0979	0.1222	0.0610
1.0000	1.0000	0.9999	1.0000	1.0000	**0.0565**	0.9992	1.0000	0.1026	1.0000	1.0000	1.0000
0.9894	1.0000	1.0000	0.9993	1.0000	0.2383	0.9602	1.0000	0.3236	1.0000	1.0000	1.0000
0.0085	0.1363	0.8719	**0.0281**	0.1027	1.0000	**0.0132**	0.4133	1.0000	0.4973	0.5739	0.3600
	1.0000	0.7778	1.0000	1.0000	**0.0011**	1.0000	1.0000	0.0016	0.9938	0.9521	0.9968
		0.9994	1.0000	1.0000	**0.0297**	0.9989	1.0000	**0.0329**	1.0000	1.0000	1.0000
			0.9491	0.9979	0.5227	0.6267	1.0000	0.4890	1.0000	1.0000	1.0000
				1.0000	**0.0043**	1.0000	1.0000	**0.0082**	0.9996	0.9939	0.9999
					0.0206	0.9999	1.0000	**0.0322**	1.0000	1.0000	1.0000
						0.0013	0.1208	1.0000	0.2455	0.3029	0.1526
							0.9983	**0.0005**	0.9676	0.8879	0.9795
								0.0645	1.0000	1.0000	1.0000
									0.3130	0.3806	0.2124
										1.0000	1.0000
											1.0000

Table 10.10: ∇P_{MIN} p-values for comparisons between region and layer.

∇P_{MIN} Comparisons

Comparions	S MC3	M MC3	D MC3	S P1	M P1	D P1
S MC3		**0.0143**	**0.0007**	**0.0019**	**0.0042**	**0.0002**
M MC3			0.3177	**<.0001**	0.6169	0.6347
D MC3				**<.0001**	0.6332	0.1518
S P1					**<.0001**	**<.0001**
M P1						0.3108
D P1						

Table 10.11: ∇P_{MIN} p-values for comparisons between bone and layer.

Reproduced with permission of the copyright owner. Further reproduction prohibited without permission.

∇P_{SHEAR} Comparisons

Location Comparison	D R1	M R1	S R1	D R2	M R2	S R2	D R3	M R3	S R3
D R1		0.5492	0.9402	0.7223	0.9058	**0.0128**	0.2159	0.8381	0.0636
M R1			0.6002	0.8378	0.6587	**0.0025**	0.5512	0.3968	**0.0133**
S R1				0.7754	0.9615	**0.0106**	0.2485	0.7760	**0.0524**
D R2					0.8201	**0.0066**	0.4284	0.5597	**0.0316**
M R2						**0.0125**	0.2939	0.7456	**0.0576**
S R2							**0.0001**	**0.0115**	0.3293
D R3								**0.0917**	**0.0004**
M R3									**0.0519**
S R3									
D R4									
M R4									
S R4									
D R5									
M R5									
S R5									
D R6									
M R6									
S R6									
D R7									
M R7									
S R7									

∇P_{SHEAR} Comparisons

D R4	M R4	S R4	D R5	M R5	S R5	D R6	M R6	S R6	D R7	M R7	S R7
0.6501	0.9805	0.5914	0.8605	0.9564	**0.0545**	0.6521	0.9518	**0.0262**	0.4819	0.2002	0.9727
0.8892	0.5697	0.2597	0.6779	0.5922	**0.0126**	0.9450	0.5619	**0.0065**	0.1926	**0.0578**	0.5124
0.7042	0.9603	0.5412	0.9188	0.9846	**0.0464**	0.6987	0.9000	**0.0226**	0.4363	0.1739	0.9110
0.9396	0.7307	0.3725	0.8466	0.7557	**0.0264**	0.9039	0.6976	**0.0116**	0.3002	0.1096	0.6827
0.7480	0.9214	0.5174	0.9605	0.9456	**0.0471**	0.7340	0.8655	**0.0207**	0.4276	0.1776	0.8745
0.0027	**0.0094**	**0.0384**	**0.0067**	**0.0093**	0.4800	**0.0063**	**0.0245**	0.9194	**0.0556**	0.1364	**0.0093**
0.4048	0.1778	0.0442	0.2539	0.1982	**0.0004**	0.5130	0.2064	**0.0002**	**0.0346**	**0.0040**	0.1553
0.4378	0.7965	0.6738	0.6650	0.7733	**0.0393**	0.4626	0.9005	**0.0146**	0.5592	0.2085	0.8498
0.0094	**0.0360**	0.1516	**0.0256**	**0.0363**	0.7984	**0.0206**	**0.0847**	0.3883	0.2286	0.5129	0.0422
	0.5824	0.2059	0.7351	0.6267	**0.0041**	0.9448	0.5514	**0.0008**	0.1989	**0.0465**	0.5675
		0.4723	0.8529	0.9704	**0.0178**	0.5763	0.9154	**0.0039**	0.4209	0.1384	0.9464
			0.3849	0.4709	**0.0881**	0.2318	0.5933	**0.0227**	0.8623	0.4191	0.5535
				0.8843	0.0124	0.7116	0.7892	**0.0035**	0.3332	0.1030	0.8084
					0.0183	0.6165	0.8925	**0.0052**	0.4051	0.1356	0.9192
						0.0084	**0.0428**	0.5019	0.1629	0.3800	**0.0282**
							0.5210	**0.0010**	0.2313	0.0732	0.5740
								0.0071	0.5354	0.2320	0.9705
									0.0648	0.1567	**0.0104**
										0.5464	0.4503
											0.1508

Table 10.12: ∇P_{SHEAR} p-values for comparisons between region and layer.

Reproduced with permission of the copyright owner. Further reproduction prohibited without permission.

∇P_{SHEAR} Comparisons

Comparions	S MC3	M MC3	D MC3	S P1	M P1	D P1
S MC3		0.7399	0.5844	0.1434	0.8161	0.1362
M MC3			0.9999	**0.0034**	1.0000	0.8500
D MC3				**0.0015**	0.9994	0.9358
S P1					**0.0021**	**<.0001**
M P1						0.7580
D P1						

Table 10.13: ∇P_{SHEAR} p-values for comparisons between bone and layer.

Reproduced with permission of the copyright owner. Further reproduction prohibited without permission.